Non-singular black holes beyond General Relativity and their characteristic image features

Delaporte, Héloïse

DOI:
10.21996/bfy9-tm22

Publication date:
2024

Document version:
Final published version

UNIVERSITY OF SOUTHERN DENMARK

DOCTORAL THESIS

Non-singular black holes beyond General Relativity and their characteristic image features

Author:
Héloïse DELAPORTE

Supervisor:
Prof. Astrid EICHHORN

A thesis submitted in fulfilment of the requirements for the degree of Doctor of Philosophy

in the

Quantum Gravity group at CP3-Origins
Department of Physics, Chemistry and Pharmacy
Faculty of Science

October 14, 2024

Declaration of Authorship

I, Héloïse DELAPORTE, declare that this thesis titled "Non-singular black holes beyond General Relativity and their characteristic image features" and the work presented in it are my own. Apart from the introductory Chapters 1 to 3, this thesis is based on the following publications:

- Chapter 4: **H. Delaporte**, A. Eichhorn and A. Held, "Parameterizations of black-hole spacetimes beyond circularity", Class.Quant.Grav. 39 (2022) 13, 134002, arXiv:2203.00105 [DEH22]

  R. Carballo-Rubio, **H. Delaporte**, A. Eichhorn and A. Held, "Disentangling photon rings beyond General Relativity with future radio-telescope arrays", JCAP 05 (2024) 103, arXiv:2312.11351 [CR+24]

- Chapter 5: **H. Delaporte** and A. Eichhorn, "The principled-parameterized approach to gravitational collapse", Submitted to JCAP (2024), arXiv:2407.07862 [DE24]

- Chapter 6: **H. Delaporte**, A. Eichhorn and A. Held, "Parameterizations of black-hole spacetimes beyond circularity", Class.Quant.Grav. 39 (2022) 13, 134002, arXiv:2203.00105 [DEH22].

Although this thesis reflects the aforementioned collaborative work carried out by the author during her Ph.D., the author decided to use the more impersonal pronoun "we" to refer to her contributions. The author apologises in advance for any potential confusion this choice may cause regarding authorship attribution.

"Between two worlds life hovers like a star,
Twixt night and morn, upon the horizon's verge.
How little do we know that which we are!
How less what we may be! [...]"

Lord Byron, *Don Juan* (poem), 1819

"Suppose I was to tell you that it's just beauty that's calling me, the beauty of the far off and unknown, the mystery and spell which lures me, the need of freedom of great wide spaces, the joy of wandering on and on—-in quest of the secret which is hidden over there—-beyond the horizon?"

Eugene O'Neill, *Beyond the horizon* (play), 1920

"[...] There is a crack, a crack in everything
That's how the light gets in [...]"

Leonard Cohen, *Anthem* (song), 1992

Abstract

This thesis centres on non-singular black-hole spacetimes derived in all three different approaches to black holes beyond General Relativity and their characteristic image features. This topic has sparked considerable interest in past years with the tremendous development of observational tests of General Relativity in the strongest gravitational fields induced by neutron stars and black holes.

The thesis begins with a brief overview of the current classical theory of gravity, General Relativity, and its main black-hole solutions. We then elaborate on the successes and flaws of General Relativity for different gravitational field strengths, which motivate the proliferation of both classical gravity and quantum gravity theories beyond General Relativity within the *fundamental approach*. We shortly describe two complementary and largely theory-agnostic approaches to black holes beyond General Relativity, the *parameterised approach* and the *principled-parameterised approach*, and review horizonless compact objects as alternatives to black holes.

We then move on to describe the principles and outcomes of imaging compact objects and apply them to non-singular black holes, horizonless spacetimes and parameterised black holes. We find that spacetimes beyond General Relativity generically exhibit peculiar image features, especially imprinted in photon rings, which distinguish them from the classical black holes. This serves as a motivation to analyse the detectability of a second thin photon ring in synthetic image data produced with a simple flux density profile by current and future radio telescope arrays. We find that we can only tell apart two thin photon rings with the current array if we use super-resolution techniques, while we can do so without restrictions with planned extensions of the array on Earth and in space.

Next, we review a simple scenario of spherically symmetric gravitational collapse in General Relativity and build on its shortcomings to perform a regular upgrade of the classical dynamical spacetime in the *fundamental approach* and in the *principled-parameterised approach*. We investigate their various properties which seem to indicate that the upgraded dynamical spacetimes are future null-geodesically complete and might allow (quantum) modifications to be visible by an asymptotic observer but may suffer from a mass-inflation instability in their interior.

In the final part, we discuss the existing axisymmetric and stationary black-hole metrics within the *parameterised approach* given their symmetry constraints and emphasise that circularity and an additional hidden constant of motion are superfluous. We thus put forward a new parametric spacetime which does not assume those superfluous symmetries while encompassing the existing parameterisations. We do so in two coordinate sets and examine their pros and cons. Finally, we highlight the connection between the absence of those two superfluous symmetries and the presence of peculiar image features, making a case for analyses of image data collected by future radio telescope arrays to consider our more general parameterisation.

Resumé

Denne afhandling omhandler ikke-singulære rumtider af sorte huller udledt i alle tre forskellige tilgange til sorte huller ud over den generelle relativitetsteori og deres karakteristiske billedtræk. Dette emne har vakt stor interesse i de seneste år med den enorme udvikling af observationelle tests af den generelle relativitetsteori i de stærkeste tyngdefelter skabt af neutronstjerner og sorte huller.

Afhandlingen begynder med en kort oversigt over den nuværende klassiske teori for tyngdekraft, generel relativitetsteori, og dens primære sorthuls løsninger. Derefter uddyber vi den generelle relativitetsteoris succeser og utilstrækkeligheder for forskellige tyngdefeltstyrker, hvilket motiverer udbredelsen af både klassisk tyngdekraft og kvantegravitationsteorier ud over den generelle relativitetsteori inden for den *fundamentale tilgang*. Vi beskriver kort to komplementære og stort set teori-agnostiske tilgange til sorte huller ud over den generelle relativitetsteori, den *parameteriserede tilgang* og *principiel-parameteriserede tilgang*, og gennemgår horisontløse kompakte objekter som alternativer til sorte huller.

Derefter går vi videre til at beskrive principperne og resultaterne af billeddannelse af kompakte objekter og anvender dem på ikke-singulære sorte huller, horisontløse rumtider og parametriserede sorte huller. Vi finder, at rumtider uden for den generelle relativitetsteori generelt udviser særlige billedegenskaber, især fotonringe, som adskiller dem fra de klassiske sorte huller. Dette giver motivation for at analysere muligheden for at opdage en anden tynd fotonring i syntetiske billeddata, der er produceret med en simpel fluxtæthedsprofil af nuværende og fremtidige radioteleskoparrays. Vi kommer frem til, at vi kun kan skelne mellem to tynde fotonringe med den nuværende opstilling, hvis vi bruger superopløsningsteknikker, mens vi kan gøre det uden sådanne begrænsninger med planlagte udvidelser af arrays på jorden og i rummet.

Dernæst gennemgår vi et simpelt scenarie med sfærisk symmetrisk gravitationelt kollaps i GR og bygger på dets mangler for at udføre en regelmæssig opgradering af den klassiske dynamiske rumtid i den *fundamentale tilgang* og i den *principiel-parameteriserede tilgang*. Vi undersøger deres forskellige egenskaber, som tilsyneladende indikerer, at de opgraderede dynamiske rumtider er fremtidige nulgeodætisk komplette og kan tillade at (kvante)modifikationer kan være synlige for en asymptotisk observatør, men kan have problemer med en masse-inflations ustabilitet i deres indre.

I den sidste del diskuterer vi de eksisterende aksesymmetriske og stationære sorte hul-metrikker inden for den *parameteriserede tilgang* i betragtning af deres symmetribegrænsninger og understreger, at cirkularitet og en ekstra skjult bevægelseskonstant er overflødig. Vi fremlægger derfor en ny parametrisk rumtid, som ikke antager disse overflødige symmetrier, mens den omfatter de eksisterende parametriseringer. Vi gør det i to koordinatsæt og undersøger deres fordele og ulemper. Endelig fremhæver vi forbindelsen mellem fraværet af de to overflødige symmetrier og tilstedeværelsen af særegne billedegenskaber, hvilket taler for, at analyser af billeddata indsamlet af fremtidige radioteleskoper skal tage vores mere generelle parameterisering i betragtning.

Acknowledgements

First and foremost, I would like to thank my supervisor Astrid Eichhorn for her intellectual stimulation, her guidance, for having understood that I needed to be thrown in at the deep end to make the most out of it and for having challenged me all along, all which shaped me as a capable researcher in theoretical physics.

Then, I would like to acknowledge physicists who have proofread chapters of this thesis: Astrid Eichhorn, Fabian Wagner, Aaron Held, Gustavo P. de Brito, Raúl Carballo-Rubio, Benjamin Knorr, Pedro G. S. Fernandes, Shouryya Ray and Rafael R. Lino dos Santos. A special thank to Mattias for having translated my English abstract to Danish. As you are the next one on the list, you will hopefully not need to do that again for others. I also thank Thomas Ryttov, Vitor Cardoso and Stefano Liberati for having accepted to form my PhD committee.

As a PhD journey is never completed alone, I would like to thank Martin Pauly and Alessia Platania for their mentoring during the whole course of my PhD. Their advice and experience were particularly valuable and I felt supported. Additionally, I address a special thank to Aaron and Alessia for having hosted me at Princeton University and Perimeter Institute, respectively, during my research visits to the American continent, and I thank Marc for having taken the time to help me rehearsing my seminar talk.

My everyday life's motivation, mood and work commitment were strongly enhanced by my colleagues and academic peers. Here is a customised list of all the credits and thanks you deserve.

To Gustavo or "the Mathematica master": I am particularly glad we came across and that I could met such a nice person. I will be more than happy to play again table tennis matches with you wherever in the world. To Rafael, my "PhD buddy": thank you for the endless hours we spent together listening to classical music out loud in our office, for the jokes about the different wrong ways Brasilians can make lasagna. I feel sorry that Palmeiras currently ranks second in the Brasilian football league but am here if you need comfort after reading this. To Juan or "the most German Colombian": thank you for having made me discover bouldering, for all the political and societal debates at lunch – I still think you can have a career as a lawyer – and for all the activities we spent together with the "Spanish-speaking mafia" in Odense. To Mattias or "the IT guy": I am glad you finally showed up in person at SDU so that I got to know you other than by your name; thank you for all the discussions about the pros and cons of Denmark, the cultural shocks and the Slavic politics. I wish you a future as colourful and sound as LEGO bricks. To Shouryya or "the polyglot": thank you for having embarked me on the journey to the subtleties of the Danish and Faroese languages and for having been supportive all along. I am happy that you ventured to the remote Faroe Islands to pursue your career. To Raúl: thank you for the wonderful paella you made in a traditional way and for your helpful career counselling. To Pedro or the "intellectual agitator": thank you for your energy, smile and spontaneity, and for having shown that there is more than one way of doing things. To Johanna, Eike, Atreya, Alex, Annamalai, Nikolaj, Mads, Asha, Fabian, Jan, Ludivine, Christopher and all the other physicists at CP3-Origins, I say a big thank you for filling our institute with joy, intellectual stimulation, sweets and cultural differences. I cherished all the moments we spent together.

I had the chance to live with great flatmates who facilitated my integration in Denmark, and to share “hygge” times with friends. Hence, I would like to thank my flatmates Tobias, Tue, Guy, and all the others I do not have space to name, for the movies, discussions, parties and common cleaning meetings we shared. It is to a great extent through you that I could improve my understanding of spoken Danish, the Danish way of life and enjoy these three years in a new country. To my Swiss and French friends Louise, Mathis, Benjamin, to my danish class fellows Tim, Jose and Lucas, to my PAUSD mates and those with whom I played beachvolley, to Maryna, to all enthusiastic early-career researchers I met during conferences and PhD schools, thank you for your support and the necessary breaks our activities provided in my work.

Last but not least, I would like to express my profound gratitude and my attachment to my family, and in particular to my three grandparents who left when I was flying the nest, to Mamiriche who always makes sure I am fed with the best food I could wish for, and to my parents Papa, Maman, my sisters Isaure, Florence and her husband Leon. I am eternally indebted to you for your protean support and love, which may drive me up to the Moon. *Merci !*

I could not end without thanking you, Martin – yet another one – for having embarked with me to this journey to the unknown, having overcome together all the obstacles that appeared on our route and for all the great discoveries and trips we made during these last years. Thank you, Manje, for your continuous support during the ups and downs, for your love and for believing in me more than I will probably ever will.

Contents

List of Figures

List of Tables

List of Abbreviations

ADM	**A**rnowitt-**D**eser-**M**isner
ALMA	**A**tacama **L**arge **M**illimeter/Submillimeter **A**rray
APEX	**A**tacama **P**athfinder **EX**periment
ASQG	**A**symptotically **S**afe **Q**uantum **G**ravity
BH	**B**lack **H**ole
(SM)BHB	(**S**upermassive) **B**lack **H**ole **B**inary
BHEX	**B**lack **H**ole **EX**plorer
BL	**B**oyer-**L**indquist
CE	**C**osmic **E**xplorer
CMB	**C**osmic **M**icrowave **B**ackground
DE	**D**ark **E**nergy
DES	**D**ark **E**nergy **S**urvey
DESI	**D**ark **E**nergy **S**pectroscopic **I**nstrument
DM	**D**ark **M**atter
DPFU	**D**egree **P**er **F**lux density **U**nit
EFT	**E**ffective **F**ield **T**heory
EHT	**E**vent **H**orizon **T**elescope
EM	**E**lectromagnetic
ESGB	**E**instein **S**calar **G**auss **B**onnet
ET	**E**instein **T**elescope
FOV	**F**ield **O**f **V**iew
FWHM	**F**ull **W**idth at **H**alf **M**aximum
GLT	**G**reenland **T**elescope
GR	**G**eneral **R**elativity
GRMHD	**G**eneral **R**elativity **M**agnetohydro **D**ynamics
GW	**G**ravitational **W**ave
(N)IR	(**N**ear) **I**nfrared
INTEGRAL	**INTE**rnational **G**amma-**R**ay **A**strophysics **L**aboratory
IRAM	**I**nstitut de **R**adio **A**stronomie **M**illimétrique
ISCO	**I**nnermost **S**table **C**ircular **O**rbit
JCMT	**J**ames **C**lerk **M**axwell **T**elescope
JP	**J**ohannsen-**P**saltis
KAGRA	**KA**mionka **GRA**vitational wave detector
KP	**K**itt **P**eak
KRZ	**K**onoplya-**R**ezzolla-**Z**hidenko
KS	**K**olmogorov-**S**mirnov
LHS	**L**eft **H**and **S**ide
LIGO	**L**aser **I**nterferometer **G**ravitational wave **O**bservatory
LISA	**L**aser **I**nterferometer **S**pace **A**ntenna
LLA(MA)	**L**arge **L**atin **A**merican **M**illimeter **A**rray
LMT	**L**arge **M**illimeter **T**elescope
LVK	**L**IGO-**V**irgo-**K**AGRA

MAD	**M**agnetically **A**rrested **D**isk
MRI	**M**agnetorotational **I**nstability
ngEHT	**n**ext **g**eneration **E**vent **H**orizon **T**elescope
NJ	**N**ewman-**J**anis
NP	**N**ew **P**hysics
NS	**N**eutron **S**tars
NSB	**N**eutron **S**tar **B**inary
PM	**P**ost-**M**inkowskian
PP	**P**rincipled-**P**arameterised
PPN	**P**arameterised **P**ost-**N**ewtonian
QFT	**Q**uantum **F**ield **T**heory
QG	**Q**uantum **G**ravity
QM	**Q**uantum **M**echanics
QNM	**Q**uasi **N**ormal **M**ode
rDEC	**r**elative **DEC**lination
RG	**R**enormalisation **G**roup
RHS	**R**ight **H**and **S**ide
RMS	**R**oot **M**ean **S**quare
rRA	**r**elative **R**ight **A**scension
SANE	**S**tandard **A**nd **N**ormal **E**volution
SED	**S**pectral **E**nergy **D**ensity
SEFD	**S**ystem **E**quivalent **F**lux **D**ensity
SEP	**S**trong **E**quivalence **P**rinciple
SI	**I**nternational **S**ystem of units
SM	**S**tandard **M**odel
SMA	**S**ubmillimeter **A**rray
SMT	**S**ubmillimeter **T**elescope
SNe	**S**upernovae
SNR	**S**ignal to **N**oise **R**atio
SPT	**S**outh **P**ole **T**elescope
SR	**S**pecial **R**elativity
UG	**U**nimodular **G**ravity
VKP	**V**aidya-**K**uroda-**P**apapetrou
VLBI	**V**ery **L**ong **B**aseline **I**nterferometry
WEP	**W**eak **E**quivalence **P**rinciple
ZM	**Z**akhary-**M**cIntosh
ΛCDM	**Λ** **C**old **D**ark **M**atter

Conventions

We work in natural units in which reduced Planck's constant $\hbar$ and the speed of light c are set by $\hbar = c = 1$, but the Newton constant $G_0 \neq 1$ (unless explicitly stated). Also, we use the mostly-plus convention $(-,+,+,+)$ for the signature of Lorentzian spacetime metrics.

To my grandparents - Mechou, Pépé and Papy - whose light snuffed out while I was flying the nest, and to Mamiriche whose presence I cherish all the more.

À mes grands-parents - Mechou, Pépé et Papy, qui se sont envolés alors que je prenais mon envol, et à Mamiriche dont je chéris d'autant plus la présence.

Chapter 1

Introduction

Well ahead other fundamental forces, a first mathematical description of gravity was provided by I. Newton in the late 17th century [New87], dubbed *Newtonian gravity*. At that time, Newtonian's gravity accurately described the mutual attraction and motion of two massive bodies in the weak gravitational field of the Earth or the Sun. However, new observations of the motion of planets in the solar system, e.g. the precession of Mercury's perihelion [LV59], were at odds with Newtonian's gravity, thus shedding light on discrepancies. In 1915, A. Einstein came up with a new mathematical description of gravity, called *General Relativity* (GR) [Ein15b], which accurately explained the rate of precession of Mercury's perihelion [Ein15a] and the bending of light [Ein16; KKS97]. General Relativity extended Newtonian's gravity by including *Special Relativity* (SR) [Ein05], which postulates that the the laws of physics are identical in all inertial reference frames and that the speed of light in vacuum is the same for all observers. Furthermore, Einstein's original formulation of GR differed from Newtonian's gravity on the *nature* of gravity: while gravity was expressed as a force between two massive bodies for Newton, it corresponded, for Einstein, to a geometrical deformation of space and time – combined to form a four-dimensional (4D) curved *spacetime*. The geometrical nature of gravity was manifest in the Einstein tensorial field equations, whose left-hand side (LHS) involves the curved spacetime's geometry as sourced by matter fields in the right-hand side (RHS).

Since its derivation, GR has passed all observational tests [BCA24], from Earth scales (i.e. laboratory and solar-system tests, reviewed in [Ciu24]) all the way up to astronomical scales, e.g. in radio pulsars [FW24] and, more recently, in Neutron Stars (NSs) and Black Holes (BHs) via Electromagnetic (EM) waves [Psa08; Aki+19a; Aki+22a; AB24] and Gravitational Waves (GWs) [Abb+16a; Abb+17a; CY22; Afz+23].

The common denominator of tests on Earth scales is that they all probe weak gravitational fields. Contrary to that, pulsar tests probe stronger gravitational regimes, and NSs and BHs probe the strongest gravitational fields in the Universe.

The agreement of observations on cosmological scales with the current standard model of cosmology based on GR and the Standard Model (SM) of particles, namely ΛCDM, further strengthened GR to be *the* fundamental theory of gravity [Agh+20; Abb+22; Ada+24]. Those tests, which probed the formation and the evolution of our Universe, were in remarkable consistency with the predictions of ΛCDM regarding the expansion rate of the Universe, the morphology of large-scale structures (e.g. galaxies) and the abundance of various particles.

However, they required the existence of an exotic "dark sector", responsible for 95% of the total energy density in the Universe. This "dark sector" is composed of: a "dark energy", i.e. some form of dark energy component with negative pressure driving the expansion of the Universe which, in its simplest form, can be accommodated for as a cosmological constant Λ in the LHS of the Einstein field equations

[FTH08; Wei+13]; a Cold Dark Matter (CDM) given by some weakly interacting (apart gravitationally) cold, matter component sourcing the observed growth of cosmic structures [Hou+23] and rotation curves of galaxies [RTF80]. The necessity to include exotic "dark" components within ΛCDM – which cannot be accounted for in the SM – provides a first sign that (i) our current understanding and modelling of the Universe is incomplete, and that (ii) it requires extensions and/or modifications. Although the additional "dark" components are more easily understood as newly defined, exotic particles beyond the SM, the modifications do not necessarily call for extensions of the SM as, in the spirit of the Einstein field equations, new matter contents can be traded for modifications of the gravitational dynamics. Another sign of the incompleteness of ΛCDM might be provided by the tensions that recently appeared between the early-time and late-time measurements of two parameters: the Hubble expansion rate and the matter density fluctuations at a certain scale [Abd+22].

It is, therefore, clear that the current cosmological paradigm relying on GR and the SM cannot explain our Universe without the addition of new physics.

Theoretical inconsistencies appearing in the strong-gravity regime also show that, although GR is a remarkable effective field theory of gravity, it cannot be the end of the story.

The GR vacuum BH solutions, such as the Kerr black hole, harbour curvature singularities in their centre, signalling the presence of divergent tidal forces. Moreover, those curvature singularities often come together with another issue: as these BHs form, causal geodesics on which observers may move are not extendible beyond the BH's centre, leading to the so-called *geodesic incompleteness* problem [Pen65]. Furthermore, some GR BHs have both an event horizon (which endows BHs with an outer boundary beyond which no return is possible) and an inner horizon (or Cauchy horizon) which is exponentially unstable under generic, small energy perturbations [PI89; PI90]. Due to the exponential growth of energy on that surface, the laws of determinism break well ahead the central curvature singularity: the future evolution of some initial data on spacelike hypersurfaces beyond the Cauchy horizon is unknown.

The success of the SM in the 20$^{\text{th}}$ century, which provides a unified Quantum Field Theoretic (QFT) description of all other fundamental forces but gravity, namely the EM, weak and strong interactions between particles [Gla61; Wei67; Sal68], yielded a quest to marry gravity with the SM. However, it turned out that the usual QFT quantisation methods were not applicable to GR, as the resulting theory was proven to be perturbatively non-renormalisable [GS86; Sho07] and thus requiring an infinite set of measurements to fix its infinite set of free parameters.

Altogether, the aforementioned issues triggered a search for beyond-GR theories capable of fully resolving them or, at least, partially. The vast set of proposed new-physics theories that have been put forward divides into:

- classical modifications of the gravitational dynamics within *modified gravity theories*, initially put forward to solve the "dark sector" problem on large scales;
- *Quantum Gravity (QG) theories*, in which gravity is postulated to be intrinsically quantum to resolve singularities on small scales and entirely new mathematical principles may be assumed.

While UV-completion mainly drove the development of QG theories, not all QG theories were shown to be predictive and *a priori* testable, though those are key properties to make connections with observables. Among all QG theories that have been developed, such as String Theory (ST), Loop Quantum Gravity (LQG), Causal

set theory, Asymptotically Safe Quantum Gravity (ASQG) and Group Field Theory (GFT), we will focus on ASQG for the following reasons. First, it admits a QFT formulation and does not require entirely new physical principles apart from the existence of quantum scale symmetry at very high energies. The latter requirement translates into the presence of a fixed-point regime at transplanckian energy scales. Second, it is non-perturbatively renormalisable and a simple one-loop-type equation suffices to compute the behaviour of the couplings of the theory from transplanckian to low-energy scales. Finally, it predicts that only finitely many couplings are free parameters that require to be fixed by experiments, hence rendering it predictive. In particular, it is particularly compelling that BHs inspired by ASQG results can be made free of curvature singularities.

Concurrently, phenomenological models were developed as a way to overcome the arduous challenges beyond-GR theories raised [CR+18]: the lack of possible measurements at very small scales (e.g. the Planck scale) in some QG theories or the difficulty in obtaining analytical solutions in modified gravity theories. While being largely theory-agnostic, phenomenological models proposed in the context of BHs were shown to accommodate numerous of these beyond-GR theories [KR20a].

Hence, theoretical progress on BH spacetime's characterisation beyond GR can be made faster following complementary top-down and bottom-up approaches, and will be the core of Chapters 5 and 6 of this thesis.

The last decade has led to a tremendous *progress in testing GR* on small and large scales and, first and foremost, in the strong-gravity regime.

On the cosmological side, the Planck collaboration released the most recent and accurate early-Universe measurements of the cosmological parameters [Agh+20] which, assuming ΛCDM, are in agreement with BAO, SNe, and some galaxy lensing observations, but in tension with the Dark Energy Survey results including galaxy clustering [Abb+22] and late-Universe measurements of the Hubble constant. This was later complemented by the results of DESI [Ada+24], which could indicate that DE is not constant but evolving over time. Further understanding of the formation, evolution and structure of our Universe will be provided by the James Webb Space Telescope (JWST) and the Euclid mission. JWST, launched in 2021, is sensitive to EM waves in the IR-regime, thus allowing us to see deeper and further in the early-Universe, while capturing the light emitted by fainter objects. While early results show the presence of well-formed galaxies and supermassive BHs soon after the Big Bang which challenge the timeline predicted by ΛCDM, observations in Cepheids reinforce the early- versus late-Universe tension on the Hubble expansion rate [Rie+24]. Concurrently, the Euclid mission started in 2023 will probe cosmological observables to an unprecedented level of accuracy to primarily refine constraints on the current cosmological parameters and test ΛCDM [Mel+24].

On the astrophysical side, the first detections of GWs by LIGO-Virgo in 2015-2017 indirectly confirmed the existence of (stellar-mass) BHs (in 2015) and NSs (in 2017) in binaries as well as their gravitational dynamics as prescribed by GR [Abb+16a; Abb+17a]. The Gamma-Ray Bursts (GRBs) which accompanied the detection of the first NS binary in 2017 and were detected by the Fermi GRB Monitor [Gol+17] and the International Gamma-Ray Astrophysics Laboratory (INTEGRAL) inaugurated the era of multimessenger astrophysics [Abb+17b], reviewed in [BMB22]. The field of GW astronomy developed along the three observing runs of Advanced LIGO-Virgo [Pog24], supplemented by the forthcoming detection of GWs with KAGRA. Thanks to the Earth-based GW interferometers LIGO, Virgo and KAGRA, we can test GR and examine potential deviations from it by constraining the post-Newtonian parameters

that enter the gravitational waveforms fitting the GW inspiral of compact binaries. Subsequently, the strong evidence for the detection of a Stochastic Gravitational Wave Backround (SGWB) gathered by the NANOGrav through Pulsar Timing Arrays (PTAs) in 2023 [Aga+23] shed new light on the superposition of GW signals that may originate from mergers of Supermassive Black Hole Binaries (SMBHBs) or from cosmological sources in the early-Universe. The characterisation of SMBHs via GWs will be largely enhanced by the upcoming Laser Interferometer Space Antenna (LISA) [Col+24b].

Recent observations in the EM spectrum have complemented the GW tests of GR in the strong-gravity regime. Evidence for a SMBH sitting at the centre of the Milky Way was collected by both GRAVITY and the Keck Observatory through decades of astrometric measurements of the orbital motion of stars in the Galactic centre [Gen+97; Ghe+98]. More recently, the EHT collaboration revealed shadow images of two SMBHs: SgrA* in the Galactic centre [Aki+22a], and M87* in the galaxy M87 [Aki+19a]. The images resulted from the acquisition of EM signals in the radio frequency spectrum emitted in the accretion disk surrounding the SMBHs. While the resolution and sensitivity of radio telescopes forming the EHT array limited the accuracy of testing GR, constraints on the spacetime metric could be put [Aki+22f]. Ever-increasing constraints on spacetime metrics of SMBHs and their alternatives, namely ECOs, are expected to be derived through imaging with next-generation EHT (ngEHT) arrays [Joh+23; Doe+23; Aki+24c] and space-based radio antennas [Joh+24].

It is thus of particular relevance to derive reliable signatures of spacetimes beyond GR in shadow images and gauge their detectability with future radio-telescope arrays. This will be the scope of Chapter 4 of this thesis.

The present thesis is structured as follows. As a starting point, we provide in Chapter 2 with a brief overview of GR and its main vacuum and non-vacuum BH solutions. After reviewing all types of tests of GR that have been performed so far, we build on the theoretical inconsistencies and incompleteness of GR, particularly manifest in the strong gravitational fields of BHs, to motivate the need for QG theories in Chapter 3. We then state the three ways of approaching BHs beyond GR that will all be tackled in the subsequent chapters. In Chapter 4, we first explain the theoretical and technical principles beyond BH imaging, before we exposit characteristic imprints of beyond-GR spacetimes in shadow images. We then assert their detectability with current and future radio-telescope arrays in a simplified geometric setting. In a more theoretical part, we explore how to describe more general BH spacetimes sourced by some new physics. In Chapter 5, we first report on a simple but singular model for BH gravitational collapse within GR, before we investigate the collapse of two upgraded spacetimes, each within a different approach to BHs beyond GR. Next, we give the status of existing parameterisations of BHs beyond GR and their symmetries in Chapter 6 and construct a more general parameterisation containing fewer symmetries but which accounts for the more symmetric ones. Finally, we conclude this thesis with some final remarks and promising research directions. We gather some detailed calculations and auxiliary material in a set of three appendices.

Chapter 2

Black hole spacetimes in General Relativity

In this chapter, we give a short overview of the classical theory of General Relativity (GR) which successfully describes all observed gravitational phenomena to date. We then describe the properties of its vacuum, stationary black hole (BH) spacetime solution, namely the Kerr black hole, which admits as special case the static, spherically symmetric Schwarzschild black hole. Finally, we move on to non-vacuum black-hole solutions of the Einstein-Maxwell field equations and briefly consider the addition of a non-zero cosmological constant.

2.1 Short overview of General Relativity

Alongside Quantum Mechanics (QM), the classical theory of GR has been a cornerstone of physics since its construction by A. Einstein in 1915 [Lor+52]. It generalises Newton's theory of gravitation by encompassing the principles of Special Relativity (SR) and describing the interplay between the geometry of 4-dimensional (4D) spacetime and the matter content within it [HE23; Wal84]. Its defining equations of motion, dubbed Einstein field equations, are

$$G_{\mu\nu} + \Lambda g_{\mu\nu} = R_{\mu\nu} - \frac{1}{2} R g_{\mu\nu} + \Lambda g_{\mu\nu} = \frac{8\pi G_0}{c^4} T_{\mu\nu} \tag{2.1}$$

in terms of the spacetime metric $g_{\mu\nu}$, the Ricci tensor $R_{\mu\nu}$ and the Ricci scalar R – combined in the Einstein tensor $G_{\mu\nu}$ – the cosmological constant Λ and the energy-momentum tensor $T_{\mu\nu}$ of matter. The left-hand side (LHS) characterises the spacetime's geometry and curvature, while the right-hand side (RHS) specifies the type of matter or radiation and its distribution. The cosmological constant allows for an expanding or a contracting universe and is thus absent in vacuum spacetimes for which $T_{\mu\nu} = 0$.

Newton's law of gravitation is recovered by taking the Newtonian limit of GR, namely by requiring (i) non-relativistic particles with speed $v \ll c$, (ii) a stationary spacetime metric and (iii) a weak gravitational field such that the spacetime metric is almost-flat. Nonetheless, GR's predictions extend beyond the Newtonian regime. Using the geodesic equation, which arises from a principle of least action applied to a curved line-element (i.e. a solution of the Einstein field equations), Einstein already predicted that the strength of light's deflection by massive astronomical objects would be twice the Newtonian one. This was later confirmed in solar eclipses in 1920s [DED20; CT23]. Additionally, GR could solve one open astronomical problem of the beginning of the 20th century: the anomalous precession rate of Mercury's orbit. The

confirmation of those two predictions of GR established GR as a scientifically viable and solid.

Besides accurately describing the deflection of light by massive objects and the perihelion precession of Mercury (and other planets), GR was also praised for its elegant generally covariant, geometrical formulation. However, the non-linearity of its field equations Eq. (2.1) made it very challenging to find solutions, unless stringent assumptions on spacetime symmetries and matter content were formulated. Solutions to the Einstein field equations could firstly be found in vacuum, i.e. for $T_{\mu\nu} = 0$ and among those, the simplest is the flat Minkowski metric

$$\eta_{\mu\nu} = \mathrm{diag}(-1, +1, +1, +1) \tag{2.2}$$

with line element

$$ds^2 = -dt^2 + dx^2 + dy^2 + dz^2 \tag{2.3}$$

in Cartesian coordinates (t, x, y, z).

2.2 Main vacuum black-hole solutions

Other exact vacuum solutions to the Einstein field equations are known to date. They are found by releasing the flat assumption and describe the most compact (dense) objects in the Universe, namely black-hole spacetimes.

Historically, the first and simplest solution was found by K. Schwarzschild in 1915 [Sch16]. According to Birkhoff's theorem [Jeb21; BL23; Jeb05], the Schwarzschild solution is the unique spherically symmetric and asymptotically flat solution of the Einstein field equations in vacuum. It describes spherically symmetric, static and asymptotically flat black holes as well as the (approximate) exterior spacetime of any (approximately) spherically symmetric star or planet. Its corresponding Lorentzian metric[1] is expressed in Schwarzschild coordinates as

$$ds^2 = -f(r)dt^2 + \frac{1}{f(r)}dr^2 + r^2 d\Omega^2, \quad f(r) = 1 - \frac{2G_0 M}{r}, \tag{2.4}$$

where

$$d\Omega^2 = d\theta^2 + \sin\theta^2 \tag{2.5}$$

is the metric on the 2-sphere, and M is the black-hole mass (as seen by an asymptotic observer). The salient features of such a metric are:

- the presence of an event horizon at $r_{\mathrm{EH}} = 2G_0 M$ (dubbed "Schwarzschild gravitational radius" r_g), i.e. when $g^{rr} = f(r) = 0$;
- for $r < r_{\mathrm{EH}}$, r becomes timelike and t spacelike;
- a photon sphere at $r_{\mathrm{p}} = 3G_0 M = \frac{3}{2} r_g$;
- 4 Killing vector fields and their corresponding symmetries: a timelike Killing vector field $\xi_t = \frac{\partial}{\partial t}$ (staticity) and three spacelike Killing vector fields $\xi_\phi = \frac{\partial}{\partial \phi}$, $\xi_1 = \cos\phi \frac{\partial}{\partial \theta} - \cot\theta \sin\phi \frac{\partial}{\partial \phi}$ and $\xi_2 = \sin\phi \frac{\partial}{\partial \theta} - \cot\theta \cos\phi \frac{\partial}{\partial \phi}$ (spherical symmetry);

[1] We will use the words "metric" and "line-element" interchangeably.

- a curvature singularity at the centre $r = 0$.

The *apparent* curvature singularity, a.k.a. *coordinate* singularity, at the event horizon can be removed by a coordinate transformation, contrary to the curvature singularity at $r = 0$. The latter central singularity expresses itself in the divergence of the Kretschmann curvature invariant

$$\mathcal{K} = R_{\mu\nu\alpha\beta}R^{\mu\nu\alpha\beta} = \frac{48G_0^2M^2}{r^6} \tag{2.6}$$

at the centre $r = 0$. Note that all other curvature invariants either reduce to the Kretschmann scalar (e.g. those solely involving the Weyl tensor or its dual) or are zero (because both the Ricci tensor $R_{\mu\nu}$ and the Ricci scalar R are zero).

It is proven that spherically symmetric, static black holes, defined by their event horizon, must be veiled by a photon sphere [CRE24] (see also earlier proofs in [CVE01; HP02; Per04; Hod13; CH20]). The photon sphere at $r_{\rm p} = \frac{3}{2}r_g$ corresponds to a set of circular, unstably bound null geodesics on which freely falling photons (not subject to any other forces than gravity) orbit. Those orbits are unstable in the sense that, if one slightly perturbs photons on those orbits, the latter photons either plunge into the event horizon and get absorbed by the black hole or escape away from the black hole. Only the photons that escape towards infinity might be detected by an asymptotic observer.

About 50 years later, a more general exact vacuum solution of the Einstein equations was found by R. Kerr [Ker63]. The Kerr solution relaxes the spherical symmetry to describe an axisymmetric (thus rotating), stationary, asymptotically flat black-hole spacetime with metric

$$\begin{aligned} ds^2 &= -\left(1-\frac{2G_0Mr}{\Sigma}\right)dt^2 + \frac{\Sigma}{\Delta}dr^2 + \Sigma d\theta^2 + \left(r^2+a^2+\frac{2G_0Mra^2}{\Sigma}\sin\theta^2\right)\sin\theta^2 d\phi^2 \\ &\quad -\frac{4G_0Mra\sin\theta^2}{\Sigma}dtd\phi \end{aligned} \tag{2.7}$$

in Boyer-Lindquist (BL) coordinates (t, r, θ, ϕ) and

$$\begin{aligned} a &= \frac{J}{M}\,(\text{reduced spin}) \\ \Sigma &= r^2 + a^2\cos\theta^2 \\ \Delta &= r^2 - 2G_0Mr + a^2. \end{aligned} \tag{2.8}$$

The Kerr BH is proven to be the unique axisymmetric, stationary, asymptotically flat solution of the Einstein equations in vacuum [Car71; Car73; Rob75; Maz82]. The Kerr black hole is solely characterised by two quantities: its mass M and its angular momentum J (or reduced spin a), although its metric is more involved than the Schwarzschild one, cf. Eq. (2.4). In the static limit $a \to 0$, it reduces to the Schwarzschild metric, while in the limit $M \to 0$, we recover flat Minkowski spacetime.
Its principal features are:

- the presence of an event horizon at $r_{\rm EH} = G_0M + \sqrt{G_0^2M^2 - a^2}$ (which only exists for $a \leq G_0M$) when $g^{rr} = 0$;

- the presence of an inner Cauchy horizon at $r_{\rm C} = G_0M - \sqrt{G_0^2M^2 - a^2}$;

- the presence of an ergoregion (see below for more detail) whose boundaries are

$$r_{\mathrm{erg},\pm} = G_0 M \pm \sqrt{G_0^2 M^2 - a^2 \cos\theta^2},$$

  solutions of $g_{tt} = 0$;

- a 3D photon shell;

- 2 Killing vectors and their corresponding symmetries: $\xi_t = \frac{\partial}{\partial t}$ (stationarity) and $\xi_\phi = \frac{\partial}{\partial \phi}$ (axisymmetry);

- a curvature singularity at $\left(r = 0,\, \theta = \frac{\pi}{2}\right)$ whose topology is a ring.

Similarly to Schwarzschild, the central curvature singularity expresses itself in the divergence of curvature invariants, such as the Kretschmann scalar

$$\mathcal{K} = \frac{48 G_0^2 M^2 \left(r^6 - 15 a^2 r^4 \cos\theta^2 + 15 a^4 r^2 \cos\theta^2 - a^6 \cos\theta^6\right)}{\left(r^2 + a^2 \cos\theta^2\right)^6}. \tag{2.9}$$

The latter is indeed divergent for $r^2 + a^2 \cos\theta^2 = 0$, that is at $\left(r = 0, \theta = \frac{\pi}{2}\right)$.[2]

The 3D photon shell, whose existence was proven in [CH20; CRE24], is the axisymmetric generalisation of the 2D photon sphere surrounding a Schwarzschild BH. Photons contained within the photon shell travel on unstable bound null geodesics or "bound orbits" which, in BL coordinates, span a finite range in r, oscillate in θ, and wind in ϕ as they complete a full orbit in the polar angle θ. Hence, the photon shell for a typical stationary, axisymmetric BH, such as the Kerr BH, is the spacetime region defined by [Joh+20]

$$r_-^\gamma \leq r \leq r_+^\gamma, \quad \theta_- \leq \theta \leq \theta_+, \quad 0 \leq \phi \leq 2\pi, \tag{2.10}$$

where

$$r_\pm^\gamma = 2 G_0 M \left(1 + \cos\left(\frac{2}{3} \arccos\left(\pm \frac{a}{G_0 M}\right)\right)\right), \quad \theta_\pm = \arccos\left(\mp \sqrt{u_+}\right) \tag{2.11}$$

with

$$\begin{aligned} u_\pm = & \frac{r}{a^2 (r - G_0 M^2)} \Big(-r^3 + 3 G_0^2 M^2 r - 2 a^2 G_0 M \\ & \pm 2 \sqrt{G_0 M \Delta (2 r^3 - 3 G_0 M r^2 + a^2 G_0 M)} \Big). \end{aligned} \tag{2.12}$$

On the boundaries of the photon shell, photons travel on circular equatorial bound orbits: the latter is prograde at the inner boundary r_-^γ and retrograde at the outer boundary r_+^γ. Thus, in principle, photons in the photon shell do not escape towards infinity nor fall into the event horizon. However, those bound orbits are unstable, meaning that, when slightly perturbed, photons on those trajectories either fall into the event horizon or escape towards an asymptotic observer. "Nearly bound" photons on those trajectories that fall into the event horizon can never be seen by an asymptotic observer. Being relatively close to the BH on nearly-bound orbits, the

[2] The fact that the central curvature has the topology of a ring can be seen by writing the Kerr metric in Kerr-Schild "Cartesian" coordinates (t, x, y, z). Those coordinates are expressed in terms of BL coordinates as $t = t$, $x + iy = (r - ia) e^{i\phi} \sin\theta$, $z = r\cos\theta$. In the new coordinates, the central singularity reads $(r = 0, \theta = \frac{\pi}{2})$, $r^2 + a^2 \cos\theta^2 = 0 \Leftrightarrow x^2 + y^2 = a^2$, i.e. it is a ring of radius a.

escaping photons are strongly lensed: they wind around the BH a certain number of times (up to infinitely many times when the photons approach fully bound orbits) before escaping away and potentially reaching an asymptotic observer.

In addition to the symmetries generated by the aforementioned Killing vectors and their corresponding constants of motion, namely the energy E and the z-component of the angular momentum L_z, the Kerr spacetime possesses another (hidden) constant of motion dubbed *Carter constant* C. It is built out of a rank-2 Killing tensor $K^{\mu\nu}$ and the test particle's velocity u^μ as

$$C = K^{\mu\nu}u_\mu u_\nu = p_\theta^2 + \cos\theta^2\left(a^2\left(m^2 - E^2\right) + \left(\frac{L_z}{\sin\theta}\right)^2\right) \tag{2.13}$$

in BL coordinates. Together with the conserved mass m of test particles, those three constants of motion render the geodesic equations

$$\frac{d^2x^\mu}{d\lambda^2} + \Gamma^\mu_{\alpha\beta}\frac{dx^\alpha}{d\lambda}\frac{dx^\beta}{d\lambda} = 0, \tag{2.14}$$

for a test particle with position $x^\mu(\lambda)$ and affine parameter λ, fully separable, a.k.a. integrable.

The presence of an ergoregion is specific to rotating black holes. In the ergoregion, the timelike wordlines become spacelike, i.e. g_{tt} (or the Killing vector ξ^t) transitions from positive (timelike) to negative (spacelike). For rotating black holes like Kerr, this implies that observers within the ergoregion cannot stay stationary, whatever the force is exerted on them: they must instead co-rotate spinward with the BH, i.e. on prograde orbits, at an angular velocity

$$\Omega = -\frac{g_{t\phi}}{g_{\phi\phi}} = \frac{2G_0Mra}{\Sigma(r^2+a^2) + 2G_0Mra^2\sin\theta^2}. \tag{2.15}$$

This effect is an extreme version of the so-called *frame-dragging* effect [LT18]. Note that the ergoregion closes up at the poles $\theta = 0$ and $\theta = \pi$, as shown in Fig. 2.1. Moreover, the Kerr event horizon coincides with its (null) Killing horizon, as prescribed by the Hawking rigidity theorem [HE23]. The null Killing horizon is a null hypersurface to which the following Killing vector field

$$\xi^\mu = \left(\frac{\partial}{\partial t}\right)^\mu + \Omega\left(\frac{\partial}{\partial\phi}\right)^\mu \tag{2.16}$$

is orthogonal, i.e.

$$g_{\mu\nu}\xi^\mu\xi^\nu = 0. \tag{2.17}$$

Note that the different surfaces in Kerr satisfy $r_{\mathrm{erg},-} \leq r_{\mathrm{C}} < r_{\mathrm{EH}} \leq r_{\mathrm{erg},+}$, with the first and last inequalities being saturated at the poles $\theta = 0,\ \pi$. A graphical representation of those surfaces is visible in Fig. 2.1.

In addition to that, the existence of a Cauchy horizon r_{C} is a new feature of the Kerr spacetime. It delineates the boundary of the spacetime region in which the future evolution of initial data on a spacelike hypersurface is not well-defined. Within the Cauchy region, closed timelike curves can exist and signal a breakdown of predictivity.

Finally, note that something special happens when $a = G_0M$: the inner Cauchy horizon and the event horizon coincide, i.e. $r_{\mathrm{C}} = r_{\mathrm{EH}} \equiv r_{\mathrm{H}}$, leading to a single

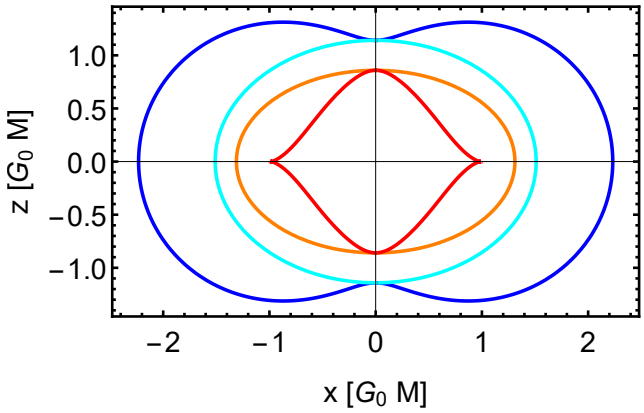

FIGURE 2.1: We show a slice at $y = 0$ of the main surfaces of Kerr spacetime with $a = 0.99\,G_0M$ in Cartesian Kerr-Schild coordinates (see Footnote 2): outer boundary of the ergoregion (dark blue), event horizon (cyan), inner Cauchy horizon (orange), inner boundary of the ergoregion (red). The central singularity lies at the kink in the inner boundary of the ergoregion. Inspired by Fig. 3 of [Vis07].

degenerate horizon at $r_{\rm H}$. The resulting spacetime is *extremal* as the spin saturates, and the whole spacetime is time-independent. Mathematically, this means that there is no point in spacetime where all Killing vectors are spacelike: one or more must be timelike or null. For larger spins $a > G_0M$, the degenerate horizon disappears and the spacetime is left horizonless. However, it harbours a naked singularity, thus violating the cosmic censorship conjecture [Wal97].

2.3 Non-vacuum black-hole solutions

Apart from vacuum black-hole exact solutions, other solutions of the Einstein field equations were found in the presence of certain matter contents, such as non-zero Electromagnetic (EM) fields or a non-vanishing cosmological constant. A non-zero and positive value of the cosmological constant is motivated by the accelerated expansion of the Universe confirmed in 1998 through Supernovae's (SNe) observations [Rie+98; Per+99b].

Shortly after A. Einstein formulated GR, a static solution to the Einstein-Maxwell equations

$$G^{\mu\nu} = \frac{8\pi G_0}{\mu_0}\left(F^{\mu\alpha}F^{\nu}_{\alpha} + \frac{1}{4}g^{\mu\nu}F_{\alpha\beta}F^{\alpha\beta}\right), \tag{2.18}$$

where the EM field strength tensor is expressed in terms of the vector potential A_μ as

$$F_{\mu\nu} = \partial_\mu A_\nu - \partial_\nu A_\mu, \tag{2.19}$$

was discovered: the Reisser-Nordström solution [Rei16; Wey17b; Nor18; Jef21]. The right-hand side of the field equations being the energy-momentum tensor for EM fields in free space, a solution to Eq. (2.1) describes a static, spherically symmetric, charged black-hole spacetime of mass M and charge Q with metric

$$ds^2 = -\left(1 - \frac{2G_0M}{r} + \frac{Q^2G_0}{4\pi\epsilon_0 r^2}\right)dt^2 + \left(1 - \frac{2G_0M}{r} + \frac{Q^2G_0}{4\pi\epsilon_0 r^2}\right)dr^2 + r^2d\Omega^2. \tag{2.20}$$

In the limit $Q \to 0$, we recover the uncharged Schwarzschild metric, while the Newtonian limit is reached for $r \to \infty$. Although the Reisser-Nordström metric resembles the Schwarzschild one when $\frac{Q^2}{4\pi\epsilon_0} \ll 2M$, it has two horizons which are solutions of $g^{rr} = 0$, namely

$$r_\pm = G_0 M \pm \sqrt{G_0^2 M^2 - \frac{Q^2 G_0}{4\pi\epsilon_0}}. \tag{2.21}$$

Those horizons only exist for $\frac{Q^2 G_0}{4\pi\epsilon_0} \leq G_0^2 M^2$ and are degenerate when the inequality is saturated, i.e. when the black hole is extremal. Similarly to Schwarzschild, the Reisser-Nordström spacetime has a point-like singularity at the centre $r = 0$.

The Kerr-Newman black-hole spacetime, found in 1965 by E. T. Newman [NJ65; New+65], is a generalisation of the Reisser-Nordström black hole to a rotating, axisymmetric solution to the Einstein-Maxwell field equations. In BL coordinates, its metric reads

$$\begin{aligned} ds^2 &= -\left(\frac{\Delta - a^2 \sin\theta^2}{\Sigma}\right) dt^2 + \frac{\Sigma}{\Delta} dr^2 - 2a \left(\frac{r^2 + a^2 - \Delta}{\Sigma}\right) \sin\theta^2 dt d\phi \\ &\quad + \Sigma d\theta^2 + \left(\frac{(r^2 + a^2)^2 - \Delta a^2 \sin\theta^2}{\Sigma}\right) \sin\theta^2 d\phi^2, \end{aligned} \tag{2.22}$$

with

$$\begin{aligned} \Delta &= r^2 + a^2 + \frac{Q^2 G_0}{4\pi\epsilon_0} - 2G_0 M r \\ \Sigma &= r^2 + a^2 \cos\theta^2, \end{aligned} \tag{2.23}$$

supplemented with the EM vector potential

$$A_\mu = \left(\frac{r Q^2 G_0}{4\pi\epsilon_0 \Sigma}, 0, 0, -\frac{a r Q^2 G_0 \sin\theta^2}{4\pi\epsilon_0 \Sigma}\right). \tag{2.24}$$

As prescribed by the no-hair theorem [MTW73] and uniqueness theorem, the Kerr-Newman metric is entirely characterised by its mass M, its charge Q and its angular momentum J. Nonetheless, it can be extended to include an additional magnetic charge Q_B.
In analogy with the Kerr black hole, the Kerr-Newman spacetime possesses:

- an event horizon at $r_{EH} = G_0 M + \sqrt{G_0^2 M^2 - a^2 - \frac{Q^2 G_0}{4\pi\epsilon_0}}$ and an inner Cauchy horizon at $r_C = G_0 M - \sqrt{G_0^2 M^2 - a^2 - \frac{Q^2 G_0}{4\pi\epsilon_0}}$, both solutions of $g^{rr} = 0$;
- an ergoregion whose boundaries are located at

$$r_{erg,\pm} = G_0 M \pm \sqrt{G_0^2 M^2 - a^2 \cos\theta^2 - \frac{Q^2 G_0}{4\pi\epsilon_0}};$$

- a central curvature singularity at $\left(r = 0, \theta = \frac{\pi}{2}\right)$ with the topology of a ring;
- 4 conserved quantities for test particles, namely their energy E, the z-component of their angular momentum L_z, the Carter constant C and their mass.

In addition to EM fields in free space, we can consider non-asymptotically flat solutions, i.e. solutions with a non-zero cosmological constant Λ that is either positive (de Sitter-like) or negative (anti-de Sitter-like). As an example, the anti-de Sitter Schwarzschild metric is given by

$$ds^2 = -\left(1 - \frac{2G_0M}{r} - \frac{\Lambda}{3}r^2\right)dt^2 + \frac{1}{1 - \frac{2G_0M}{r} - \frac{\Lambda}{3}r^2}dr^2 + r^2d\Omega^2 \tag{2.25}$$

with $\Lambda < 0$. This black-hole solution has only one horizon located at

$$r_{\mathrm{EH}} = \left(-\frac{3G_0M}{\Lambda}\right)^{\frac{1}{3}}\left[\left(1 + \sqrt{\frac{-1}{9\Lambda G_0^2M^2}}\right)^{\frac{1}{3}} + \left(1 - \sqrt{\frac{-1}{9\Lambda G_0^2M^2}}\right)^{\frac{1}{3}}\right]. \tag{2.26}$$

In the limit where the cosmological horizon $l^2 = -\frac{3}{\Lambda}$ approaches infinity, the spacetime becomes asymptotically flat and the horizon of the anti-de Sitter Schwarzschild black hole asymptotes the Schwarzschild horizon $r_{\mathrm{EH}} = 2G_0M$. Additionally, a curvature singularity forms at the centre $r = 0$.

Chapter 3

Theories and black hole spacetimes beyond General Relativity

In this chapter, we introduce the successes and failures of GR in various regimes and motivate the need to derive theories that go beyond GR and bridge the gap with quantum matter, in particular in the strong-energy regime of BHs. While classical modified theories of gravity can capture the leading-order corrections to GR, they can only be considered as Effective Field Theories (EFTs) which break down at high enough energy scales. Semiclassical gravity partially bridges the gap between classical gravity and quantum matter by accounting for backreaction onto the classical spacetime. In chapter Chapter 5, we will discuss the results of paper [DE24] that explains how to motivate non-singular black-hole spacetimes from Asymptotically Safe Quantum Gravity (ASQG). To provide background for that chapter, we give an overview and motivation for Quantum Gravity (QG), focusing in particular on a non-perturbative, UV-complete and predictive QG framework, namely ASQG.

3.1 The need to go beyond General Relativity

The advent of GR in the early 20^{th} century opened a new era in gravitational physics, in which the spacetime geometry and the matter content are interconnected. The construction of GR led to a series of predictions that were later successfully confirmed observationally. Besides GR, Quantum Mechanics (QM), subsequently developed as Quantum Field Theory (QFT), marked the dawn of a new era in the description of the other fundamental forces and the interactions of the fundamental matter constituents. Since then, GR and QFT have been the two main pillars of theoretical physics.

However, those two theoretical paradigms suffer both from theoretical and observational cracks and reconciling them turns out to be especially challenging. Hence, there is a need to go *beyond GR*, both in the weak- and strong-gravity regimes. This can be done classically, through modified theories of gravity, or by extending gravity to Quantum Gravity (QG).

3.1.1 General Relativity: successes and failures in the weak-field regime

GR has been extremely well tested in the weak-field regime, i.e. the regime in which the strength of the gravitational field is weak. This occurs in laboratories and in the solar system ($1\,\mu\text{m} \leq l \leq 1\,\text{AU} \sim 10^{11}\,\text{m}$), and up to cosmological scales. In the following, we distinguish tests in the low-energy regime according to their length scale: laboratory and solar-system tests on one side, and cosmological tests on the other side. Some of the weak-field astrophysical and cosmological probes

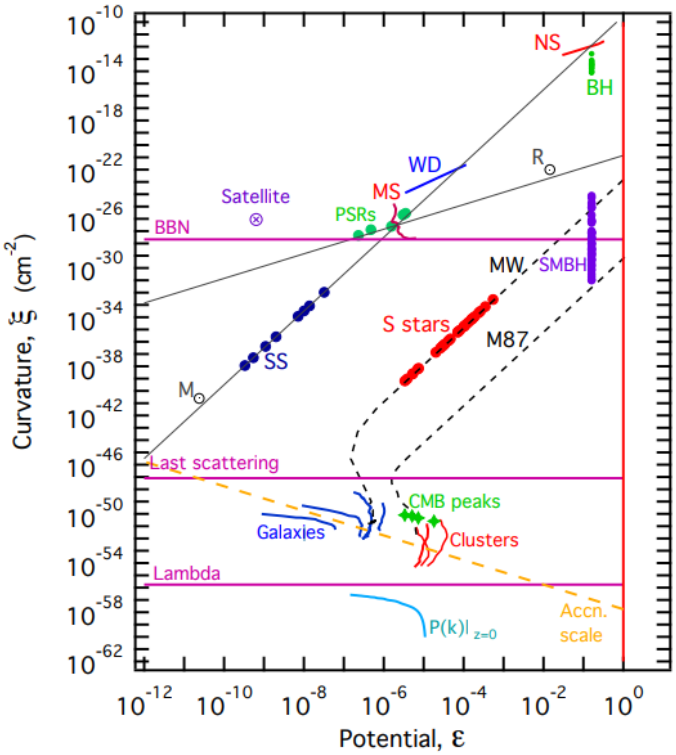

FIGURE 3.1: We show the parameter space of astrophysical and cosmological systems in terms of the gravitational potential and curvature strength they probe. Label abbreviations are: Cosmic Microwave Background (CMB), planets of the Solar System (SS), Main Sequence stars (MS), White Dwarfs (WD), binary pulsars (PSRs), individual Neutron Stars (NS), stellar-mass Black Holes (BH), the Milky Way (MW), Supermassive Black Holes (SMBH), Big Bang Nucleosynthesis (BBN). The magenta curve labelled "Lambda" gives the curvature of a Friedmann-Robertson-Walker universe completely dominated by the cosmological constant, while the magenta line labelled "last scattering" represents the curvature at redshift $z \approx 1100$. The dotted yellow line is the phenomenological acceleration scale. The cyan curve represents the perturbative part of the Kretschmann curvature at redshift $z = 0$.
Taken from [BPS15] and reproduced with permission ©AAS.

are represented in Fig. 3.1 in terms of their potential ε and their curvature ξ. For astrophysical probes, the latter quantities are defined as fractions of the Newtonian potential $\varepsilon = \frac{G_0 M}{r}$ and the Schwarzschild Kretschmann scalar $\xi = K_S = \sqrt{\frac{48 G_0^2 M^2}{r^6}}$ respectively. For cosmological probes, analogous expressions are obtained for the potential $\varepsilon(k, a)$ and the curvature $\xi(a)$ (see Eqs. 11 and 14 of [BPS15]).

As GR relies on Special Relativity (SR) and thus Lorentz invariance, successful tests of SR are a prerequisite for the viability of GR. Among all tests of SR, those challenging the Weak Equivalence Principle (WEP)[1], birefringence and anomalous dispersion of photons are of particular relevance to gravitational theories. The corresponding tests and their successful results are reviewed in [Tin+20; Wil14] and continue to be updated.

[1]The WEP is conjectured to imply the Einstein Equivalence Principle (EEP) in any complete and consistent theory of gravity [Sch60].

A. Einstein originally proposed three *classical* solar-system tests of GR in 1916[2]: the perihelion precession of Mercury, the deflection of light by the Sun and the gravitational redshift of light. All three *classical* tests were successfully passed in the first half of the 20th century [DED20; CT23; Pop54].

Another class of solar-system and laboratory tests consists of testing predictions of GR, namely: gravitational lensing (first confirmed in [DED20]), light travel time delay (measured by the Cassini probe [BIT03]), frame-dragging effects (see the recently improved measurement in [Ciu+19]), the shape of the gravitational potential (well constrained to the Newtonian potential, see recent results in [Lee+20]). They put constraints on the slow-motion, weak-field limit of GR given by the *Parameterised Post Newtonian (PPN)* formalism (described in detail in [WN72; Wil16]) governed by ten post-Newtonian parameters encoded in the metric. The latter PPN parameters have well-defined values in GR, c.f. Table 3 in [Wil16]. So far, the experimental values of the PPN parameters from solar-system experiments match those of GR with very good accuracy. Thus, GR is compatible with all laboratory and solar system tests.

On cosmological scales, another prediction of GR was confirmed in clusters of galaxies in 1990 [TWV90], namely weak gravitational lensing, i.e. the distortion of images of background astronomical objects by other massive objects (or "lenses") in their foreground.

The ΛCDM model, which assumes GR, provides us with the standard description of the formation and evolution of the Universe on cosmological scales. Assuming the cosmological principles of homogeneity and isotropy for comoving observers, the Einstein equations admit the Friedmann-Robertson-Lemaître-Walker spacetime as an exact solution. The latter solution can describe the observable Universe as a spatially flat, homogeneous and isotropic universe which undergoes an accelerated expansion (driven by some form of matter with negative pressure, usually assumed to be a Dark Energy (DE)) and contains baryonic matter, radiation and (cold) Dark Matter (DM) in the proportions spelt out in [Agh+20].

ΛCDM passes most of the cosmological tests performed so far. The first confirmation of the expansion of the Universe came out in 1929 by E. Hubble, who established the redshift-distance law dubbed *Hubble law* [Hub29]. The homogeneity and isotropy of the Universe on large scales were demonstrated with the detection of the largely homogeneous and istrope polarisation of the Cosmic Microwave Background (CMB) [Kov+02]. Baryon Acoustic Oscillations (BAO) have been predicted by GR and confirmed in 2005 [Eis+05; Col+05].
However, within the standard ΛCDM model, extra assumptions are required to fully account for all cosmological observations:

- a DE component should be included to explain the late-time accelerated expansion of the Universe, whose energy density amounts to $\sim 68\%$ of the total energy density in the Universe. This DE component is usually introduced in the Einstein field equations as a cosmological constant Λ (hence Λ in ΛCDM) whose energy density – the zero-point energy density – follows an equation of state $\rho_\Lambda = -p$ with negative state parameter [Agh+20]. In QFT, the zero-point energy corresponds to a renormalised coupling Λ which decomposes into its

[2]The word *classical* should be understood here as *standard* or *foundational*, in the sense that these tests challenge the foundations of GR.

bare value and quantum fluctuations. The component induced by quantum fluctuations is computed to be of order $\mathcal{O}\left(M_{\rm P}^2\right)$, with $M_{\rm P}$ the Planck mass. To match the experimentally observed value of Λ, i.e. $\Lambda \sim 10^{-122}\, l_{\rm P}^{-2}$, the bare coupling also has to be chosen as $\mathcal{O}\left(M_{\rm P}^2\right)$, leading to a fine-tuned difference of the order of the measured Λ. This fine-tuning leads to unusually small dimensionless couplings, if one agrees that dimensionless couplings should be of order $\mathcal{O}(1)$, and constitutes the so-called *cosmological constant problem*. Together with the coincidence problem [Wei00], it motivates a modified cosmological model with a dynamical description of DE. While the latest Dark Energy Spectroscopic Instrument (DESI) results show a weak preference for a simple time-varying DE equation of state [Ada+24], modified models that encapsulate such dynamical DE (see e.g. [CK24]) usually predict a "fifth force" which needs to be screened in the solar system in order not to be ruled out by solar-system tests of gravity;

- a DM component should be included to account for the large-scale structures in the Universe, the shape of galaxies' rotation curves and the (tiny) CMB anomalies [Gre22; MEM24]. Indeed, the largest fraction of the matter energy density in the Universe stems from DM with $\sim 27\%$, compared to $\sim 5\%$ for visible baryonic matter. Although the standard ΛCDM describes DM as being *cold* (hence the name *Cold Dark Matter*; CDM), the exact nature of DM remains unknown: it may be sourced by some exotic matter beyond the SM, such as axions [O'H24; Nav+24], or encapsulated in alternative theories which replace DM by some *Modified Newtonian Dynamics (MOND)* (see [FM12; Mil22] for a review on simple MOND and covariant extensions such as Bimetric MOND (BIMOND) models). According to current observations, MOND scenarios seem to be disfavoured [Ban+24] but not BIMOND models [Bas+23];

- an early phase of accelerated exponential expansion of the Universe should be included, to elucidate why the Universe today is so homogeneous, isotropic and spatially flat. The standard candidate for this early-universe accelerated expansion is cosmic inflation [Gut81], which dynamically solves the *horizon problem*. While CMB observations are in agreement with cosmic inflation with nearly-scale invariant power spectrum [Agh+20], it is yet unclear which scenario of cosmic inflation is realised, see [Odi+23] for a discussion;

- if current tensions on the cosmological parameters H_0 and σ_8, dubbed H_0- and σ_8-*tensions*, are to be confirmed, some new physics beyond ΛCDM should be included as to explain the discrepancies between the early-Universe (e.g. CMB [Agh+20]) and late-Universe (e.g. SNe [Gal+23]) measurements of H_0 and σ_8. While systematic and experimental uncertainties are claimed to be under control on both sides, the disagreement is as large as $\sim 5\,\sigma$ for some combinations of data sets, thus calling for new physics;

- a new theoretical description of the cosmic dipole should be provided, to alleviate the *cosmic dipole tension* in which the amplitudes of the dipole in the temperature anisotropies of the CMB and the angular distribution of sources mismatch, see [PS22].

Therefore, ΛCDM – the standard fit to cosmological data relying on GR – cannot fully explain the observed Universe on cosmological scales without including some new physics: either in the form of new matter fields (within some extensions of the SM and modifying the RHS of the Einstein equations) or as modified gravity dynamics (modifications in the LHS of the Einstein equations).

3.1.2 General Relativity: successes and failures in the strong-field regime

GR has evolved from *the general theory of relativity* at the beginning of the 20th century to *a more realistic EFT of gravity* valid up to a cutoff scale usually taken to be the Planck mass $M_P = 2.176\,434(24) \times 10^{-8}\,\mathrm{kg}^{-1}$.[3] Beyond the cutoff scale, the standard description of gravity provided by GR breaks down, as well as the SM.

Before elaborating on the failures of GR in the high-energy regime, where the gravitational field is strong, let us highlight its successes.

As already described in Sections 2.2 and 2.3, various black-hole solutions to the Einstein equations were derived in the 20th century and therefore predicted to exist. Black holes are the most compact astronomical objects with the strongest gravitational fields. They can either exist as isolated objects (e.g. at the centre of galaxies) or in binaries (within galaxies). They are represented in Fig. 3.1 in terms of the strength of their gravitational potential and their curvature.
The detection of the first Gravitational Wave (GW) signal from a binary black hole merger in 2015 by the Laser Interferometer Gravitational Wave Observatory (LIGO) and Virgo collaborations [Abb+16a] indirectly confirmed the existence of stellar mass black holes. Subsequent observation runs with LIGO and Virgo corroborated the existence of black holes with masses in the range $2M_\odot \lesssim M \lesssim 100M_\odot$, with two predicted mass gaps[4]: $2M_\odot \lesssim M \lesssim 5M_\odot$ and $50M_\odot \lesssim M \lesssim 150M_\odot$.
Independently, a high-resolution Near Infrared (NIR) analysis of stellar dynamics near the very centre of our Milky Way revealed in 2000 that the central compact object was a supermassive black hole named SgrA* [Ghe+98; Gen+00] (see [Ale17; Gen22] for a review). This discovery was awarded a Nobel prize in 2020. The analysis determined and tracked during 16 years 28 orbits of stars, called S-stars, closely orbiting the Galactic centre. The observation time was long enough for one of these stars, namely S_2, to complete a full orbit, thus providing enough data points to compare with GR's predictions [Gil+09]. The S-stars have been shown to revolve in the gravitational potential of a supermassive black hole whose latest inferred mass $M = 4.297 \times 10^6\,M_\odot$ at a distance $R = 8.277\,\mathrm{kpc}$ from the Earth are found by the GRAVITY collaboration [Abu+23].
The existence of supermassive black holes was strengthened by the Event Horizon Telescope (EHT) which provided the first *direct* detection of two isolated supermassive black holes: M87* [Aki+19a] at the centre of the galaxy Messier 87 and SgrA* [Aki+22a] at the centre of our Milky Way. This detection was based on the EM emission in the radio frequency spectrum occurring in the vicinity of the two black holes, out of which *shadow images* could be computed in 2019 for M87* [Aki+19a] and in 2022 for SgrA* [Aki+22a].[5] However, the resolution and sensitivity of the radio telescopes forming the EHT during the observation campaign in 2017 were – and are still – not high enough to confidently assert that the central object was indeed a Kerr BH (see [Aki+19e; Aki+22f]). The ring-like bright emission encircling the shadow in

[3] Although the cutoff scale of GR as seen as an EFT is usually taken to be the Planck mass, especially in QG approaches, there is no consensus on the Planck mass being the cutoff scale, see [Wea23]. Throughout this paper, we will adopt a more agnostic approach in which the (length) scale where new-physics effects become important is set free.

[4] The two mass gaps are predicted by some models of stellar evolution and state that black holes in these mass ranges cannot directly form by the gravitational collapse of a star. However, LIGO and Virgo collaborations found several candidate events whose first-generation black-hole masses lied in one of the two mass gaps, see e.g. [Aba+24; Abb+20].

[5] We will discuss *shadow images* in Chapter 4.

the images is thought to result from the deflection of light in the presence of strong gravitational fields, as predicted to occur near BHs in GR, while the shadow itself can be explained by the presence of a BH's event horizon absorbing light.Compared to the stellar-mass BHs detected by LIGO-Virgo, M87* and SgrA* are supermassive BHs, meaning that their masses lie in the higher mass range $10^5 M_\odot \lesssim M \lesssim 10^{10} M_\odot$, and are isolated. Therefore, they cannot be detected indirectly by LIGO-Virgo.

Note that no intermediate-mass BH with mass $10^2 M_\odot \lesssim M \lesssim 10^5 M_\odot$ has been *reliably* identified so far, although the set of potential candidates is growing [GSH20; Häb+24].

Apart from black holes, Neutron Stars (NSs) are the second most compact astronomical objects in the Universe, as shown in Fig. 3.1. They form after the gravitational collapse of the core of massive Supernovae (SNe) (stars with mass $M \geq 8 M_\odot$) and are left fast rotating, very dense (denser than the atomic density in nuclei) and with a complex internal structure modelled by an equation of state. The existence of NSs has been reinforced by their detection in NS-BH or NS-NS binary systems by the LIGO-Virgo collaboration [KKPM21].
The level of complexity of the equation of state of NSs remains unclear, because the "correct" theoretical equation of state for cold, dense, neutron-rich matter in chemical equilibrium is troublesome. Indeed, deriving a theoretical equation of state for NSs requires dealing with complex, many-body, strongly interacting quantum systems in the core of NSs, a regime that cannot be tested experimentally and in which standard perturbative methods fail. Nonetheless, new theoretical and observational avenues have come at help that are detailed in [Lat12; OF16; Lat21] and summarised in the following: measurements of mass and radii of the most massive pulsars found up to now, mass and radii estimates from X-ray observations of quiescent and isolated NSs accompanied by developments of the cooling tail model, experimental measurements of nuclear properties and nuclear collisions, advancements in many-body theory, novel parameterisations of the equation of state of high-density matter revealing semi-universal relations among global NS properties, gravitational wave observations from the binary NS merger GW170817 and its γ-ray burst and optical follow-ups, and X-ray pulse-profile measurements of rapidly rotating pulsars [Kum+24a].

The discovery of radio pulsars, which are highly magnetised rotating NSs emitting periodic pulses of EM radiation, in binary systems in 1974 [Hul94] initiated a new class of precision tests of gravity summarised in [Wex14; Kra+21]. The latter tests include the analysis of: GW emissions and quadrupole formula (best constrained by the Double Pulsar [Bur+03; Lyn+04]), the emission of dipolar radiation (with relativistic systems made of a pulsar and a white dwarf, e.g. PSR J1738+0333), the Strong Equivalence Principle (SEP) (tested with wide pulsar-white dwarf systems [DS91]), the local Lorentz invariance (tested with isolated and binary pulsars [SW12; Sha+13; Liu+20]), and the Stochastic Gravitational Wave Background (SGWB) – see the recent results by the NANOGrav and International Pulsar Timing Array (IPTA) collaborations [Aga+23; Afz+23; Ant+24]. Tests of GR with pulsars are much more stringent than solar-system tests since they are also sensitive to the relatively strong gravitational fields of neutron stars, as visible in Fig. 3.1.

As it turns out, GR has passed all these tests successfully. Nonetheless, uncertainties remain (i) in *accurately* modelling the interior of neutron stars, in particular their equation of state and phase transitions, see [Wex16] for a review, and (ii) in the existence of GR signature of the SGWB, namely the Hellings-Downs correlation

[HD83; Aga+23].

Although no clear *observations* have come in disagreement with GR and its predictions so far, GR *theoretically* predicts its own breakdown in the strong-field regime.

On the cosmological side, a consistent theoretical description of the Big Bang should be provided, in order to cure the *Big Bang singularity*. The latter singularity can refer both to curvature singularities and past-incomplete non-spacelike curves, see [Tri24] for a more in-depth discussion.

Regarding compact objects: firstly, all vacuum BH solutions within GR are plagued by curvature singularities at their centre, signalled by the divergence of one or more of their non-derivative curvature invariants, hence the presence of diverging tidal forces. Secondly, GR vacuum BHs obey the Penrose-Hawking singularity theorems [Pen65; Pen69; HE23]. Those theorems state that BH spacetimes unavoidably contain (future-) incomplete inextendible causal geodesics[6], provided that: (i) they satisfy some pointlike energy conditions, (ii) they are globally hyperbolic (equivalent to a non-compact Cauchy surface) and (iii) they contain a closed future-trapped surface. The existence of a closed future-trapped surface is key: it entails that both ingoing and outgoing geodesics contained within that surface shrink under the strength of the gravitational pull. Mathematically, the expansions of a pair of future-directed affine-parameterised geodesic null vector fields $k^{\mu}_{\pm}$ ($+$ for outgoing, $-$ for ingoing geodesics) are given by

$$\Theta_{\pm} = \nabla_{\mu} k^{\mu}_{\pm}, \tag{3.1}$$

with ∇_{μ} the spacetime covariant derivative. A closed future-trapped surface thus has strictly negative expansions

$$\Theta_{+} < 0, \quad \Theta_{-} < 0, \tag{3.2}$$

confining both ingoing and outgoing geodesics within a surface whose boundary is a marginally future-trapped surface defined as

$$\Theta_{-} < 0, \quad \Theta_{+} = 0. \tag{3.3}$$

As GR BH solutions satisfy the requirements of the singularity theorems, they are said to be *geodesically incomplete*. Note that, while a curvature singularity does not imply geodesic incompleteness (and vice-versa), they are sometimes traded one for another [Ger68] and often go hand in hand (as in the Kerr spacetime).

Additionally, the Kerr and Reisser-Nordström spacetimes possess a Cauchy horizon located inwards with respect to their event horizon. It corresponds to a null trapping surface which delineates the boundary of the spacetime region in which the future evolution of the initial data is not well-defined. As an example of ill-defined initial data, a set of closed timelike curves can form within a region of spacetime bounded by a Cauchy horizon. Hence, determinism is broken past the Cauchy horizon. Moreover, the Cauchy horizon is unstable to perturbations [SP73; BC95] – triggering so-called *mass inflation instabilities* – which render numerical simulations of BH formation challenging.

While all observations so far, whether in the strong-field or weak-field regime, are in good agreement with GR, the existence of theoretical failures within it calls

[6] The term *causal* in "causal geodesics" is used as a synonym for *non-spacelike* geodesics.

for a *beyond-GR* theories. In order to be consistent and viable, those theories should resolve GR singularities and inconsistencies or, at least, weaken them [SJ22].

3.1.3 The need to account for time-dependent black hole spacetimes

Although they probe BHs in different mass ranges, both transient GW signals and BH shadow images are presently consistent with BHs being described by the Kerr solution. However, the Kerr black-hole hypothesis or *Kerr paradigm* – which postulates that observed BHs are well described by the Kerr spacetime – theoretically fails for the reasons mentioned in Subsec. 3.1.2. Moreover, as it starts to be challenged observationally [Bam11; Psa19; Ber19], alternative spacetimes need to be developed.

In addition to presenting a central curvature singularity, an unstable Cauchy horizon and incomplete inextendible causal geodesics, the Kerr spacetime is an *eternal*, *vacuum* black hole solution.

Eternal black holes are stationary, which means they rotate with a constant angular velocity Ω over time. While this assumption is valid for isolated black holes on timescales of observations, it no longer holds for coalescing BHs in binaries or for BHs on cosmological timescales. Astrophysical BHs must form dynamically, either as end-states of gravitational collapse of massive stars or as remnants of NS-NS, NS-BH or BH-BH binary mergers. Hence, it motivates time-dependent spacetimes describing the gravitational collapse of astrophysically-motivated matter and the coalescence of compact binaries.

Numerous classical analytical scenarios of gravitational collapse have been developed, assuming spherical symmetry: the Oppenheimer-Snyder-Datt model of homogeneous dust cloud collapse [Dat38b; OS39], the Lemaître-Tolman-Bondi model for inhomogeneous dust collapse [Lem33; Tol34; Bon47], the Vaidya model for null dust collapse [Vai51; Vai66] and a model for adiabatic fluid collapse [JD92; JD93; DJ94; JD99; Lak92]. Only a few models of gravitational collapse have been put forward beyond spherical symmetry, namely Kerr-Vaidya-like spacetimes [MT70; Her80; BH17; DT20a] and the Einstein-Vlasov model [Ren02] (studied numerically in [AAR21]).

In GR, the Penrose-Hawking singularity theorems [Pen65; Pen69; HE23] imply that gravitational collapse results in geodesic incompleteness. Simultaneously, scenarios of gravitational collapse usually form black-hole horizons which, by the weak cosmic censorship conjecture [Pen69], shield geodesic singularities from asymptotic observers. However, simple spherically symmetric models for gravitational collapse such as the Vaidya-Kuroda-Papapetrou (VKP) model [Vai66; Kur84b; Pap85a] violate both the weak and the strong cosmic censorship conjectures, as a naked singularity can form in association with a Cauchy horizon. The unphysical nature of such a simplistic model, discussed in [Wal97], exemplifies the need to study dynamical spacetimes of gravitational collapse with fewer symmetries (than spherical symmetry) and with more realistic matter contents (than null dust).

3.1.4 The need to account for accreting black hole spacetimes and backreaction

Vacuum BH solutions in GR describe the exterior curved spacetimes outside a spherically symmetric or axisymmetric mass with no matter source, i.e. with a zero RHS in the Einstein equations. However, BHs are gravitationally attractive due to their strong gravitational fields, hence they accrete any matter present around them.

Accretion onto supermassive black holes has been indirectly observed in Active Galactic Nuclei (AGN) [MS16; HA24], whose quasars emit very bright EM radiation across the whole spectrum as a result of inwardly spiralling gas accretion flows, and directly observed in the shadow images computed from the radio emission in the neighbourhood of the supermassive BHs SgrA* and M87* [Aki+19a; Aki+22a]. Relativistic astrophysics well establishes that BHs are surrounded by an accretion disk composed of charged gas particles in a plasma, which heats up through radial angular momentum transport, and strong poloidal magnetic fields [Aki+21b; Col+24a]. Angular momentum is transported radially from the centre of the accretion disk to its exterior through turbulences called *Magneto-Rotational Instabilities* (MRIs). The latter instabilities turn on as the relativistic charged fluid forming the accretion disk is in differential rotation: it rotates faster near the centre of the disk than at larger radii. In addition to pressure and gravity, the differentially rotating fluid is subject to the Lorentz force. Hence, it undergoes shears which are prone to turn it into a turbulent (unstable) flow with MRIs and drive the inward spiralling accretion flow.

At the same time, charged particles in the relativistic fluid heat up and emit EM radiation across a broad range of frequencies. In the vicinity of supermassive black holes, the strong magnetic field lines can collimate fast outflows of relativistic particles in polar jets yielding powerful and variable EM radiation. The dynamics of the accretion-ejection flows near SMBHs is thus governed by the strong poloidal magnetic fields and MRIs.

The composition of the relativistic charged fluid and the influence of the strong magnetic fields on it suggest to treat the accreting plasma with the formalism of relativistic Magnetohydrodynamics (MHD) [Alf42]. The effect of the matter distribution on the background curved geometry of a supermassive BH, known as *backreaction*, is typically small because the mass of the BH largely dominates over the mass of its accretion disk. Therefore, we can assume within GR that the background spacetime geometry is and remains a Kerr BH during accretion. Once combined with such a GR background geometry, the dynamics of astrophysical BHs is best described by state-of-the-art 3D GRMHD simulations, reviewed in [DT20b] for AGNs and in [Gol19; CG24] for Massive and Supermassive Binary BHs ((S)MBBHs).

Extending the GRMHD formalism beyond GR, that is beyond Kerr geometries, to test the Kerr paradigm is particularly challenging. Nonetheless, recent progress has been made for generic metrics encoding parameterised deviations from Kerr [NYK22; Koc+23].[7]

3.2 Classical modified theories of gravity

Classical modified theories of gravity are rooted in Lovelock's theorem [Lov71; Lov72], a uniqueness theorem for the Einstein field equations in 4D. The latter theorem states that, in four dimensions (4D), the only possible second-order differential equations of motion stemming from a local action are the Einstein field equations Eq. (2.1). Hence, any consistent gravity theory that goes *beyond GR* needs to violate at least one of Lovelock's assumptions, i.e. it should feature either:

- extra spacetime dimensions, i.e. $D > 4$;

[7] An overview of generic metrics parameterising deviations from Kerr is given in Subsec. 3.6.2, while an in-depth discussion of them is the matter of Chapter 6.

- additional gravitational fields than the metric tensor $g_{\mu\nu}$. Those fields can be scalars ϕ, vectors A_μ or tensors $f_{\mu\nu}$;
- higher-order equations of motion, i.e. e.o.m. for the metric field that contain three or more derivatives;
- non-localities, e.g. manifest in the presence of inverse powers of the d'Alembertian operator;
- non-general covariance (e.g. by breaking local Lorentz symmetry) and/or non-invariance under diffeomorphisms.

Any modified theory of gravity which exhibits one or more of these features generally introduces additional d.o.f. to those present in GR, except if non-localities are introduced. In the latter case, a non-local gravity theory does not lead to extra poles in the propagator, and thus no new d.o.f. [BCR22].

The Einstein field equations follow from an action principle applied to the Einstein-Hilbert (EH) action

$$S_{\rm EH} = \frac{1}{16\pi G_0}\int d^4x\sqrt{-g}\,(R-2\Lambda) + S_m = \frac{M_{\rm P}^2}{2}\int d^4x\sqrt{-g}\,(R-2\Lambda) + S_m, \quad (3.4)$$

where $\sqrt{-g} \equiv \sqrt{-\det(g)}$ and S_m denotes the matter action. Taking the variation of the gravitational action with respect to the Lorentzian metric $g_{\mu\nu}$, we obtain the LHS of the Einstein equations, while the RHS is given by stress-energy tensor

$$T_{\mu\nu} = -\frac{2}{\sqrt{-g}}\frac{\delta S_m}{\delta g^{\mu\nu}}, \quad (3.5)$$

which stems from the variation of the matter action. Classically, the EH term, a.k.a. GR term, is expected to be the leading-order term in an infinite series of higher-order curvature terms which become relevant at sufficiently high energies. GR should therefore be viewed as a consistent low-energy EFT of some yet unknown UV-complete theory of gravity [Don23]. The perturbative non-renormalisability of GR is believed to derive from its EFT nature.

In the following, we will focus on modified gravity theories with higher-order curvature terms which are especially relevant for two reasons: (i) they possess desirable properties such as (perturbative) renormalisability or the absence of ghosts, and (ii) they lead to a rich BH phenomenology which can differ from the GR one.

One way of modifying GR can be, for example, to consider higher spacetime's dimensions D than the usual four, i.e. $D > 4$. One relevant example in $D = 5$ dimensions is the Einstein-Gauss-Bonnet theory whose gravitational action

$$S_{\rm EGB} = \frac{1}{16\pi G_0}\int d^5x\sqrt{-g}\,(R-2\Lambda+\alpha\mathcal{G}) \quad (3.6)$$

contains the *Gauss-Bonnet term*

$$\mathcal{G} \equiv R^2 - 4R_{\mu\nu}R^{\mu\nu} + R_{\mu\nu\rho\sigma}R^{\mu\nu\rho\sigma}, \quad (3.7)$$

FIGURE 3.2: Mindmap of the various possible modified theories of gravity according to their feature(s). Theories encircled in black are Lorentz-violating. Inspired by Fig. 3 of [Bul+16].

which is topologically invariant in $D = 4$ dimensions [Fer+22].[8] Einstein Gauss-Bonnet gravity is particularly interesting as its action appears in the context of low-energy limits of String Theory [FKM96; Ant+97; Zwi85; GS87]. The appearance of the Gauss-Bonnet term in string-related theories of gravity has motivated more general theories in 4D, dubbed *Einstein-scalar-Gauss-Bonnet (ESGB)*, of the form

$$S_{\rm ESGB} = \frac{M_{\rm P}^2}{2}\int d^4x\sqrt{-g}\left(R - (\nabla\phi)^2 + \frac{\alpha}{8}f(\phi)\mathcal{G}\right), \tag{3.8}$$

with non-minimal coupling between a scalar field ϕ and the Gauss-Bonnet term $\mathcal{G}$ set by a dimensionless coupling α. Due to the non-minimal coupling, the Gauss-Bonnet term contributes to the 4D e.o.m. and leads to theories with a rich BH phenomenology [Bak20; Fer+22; KBP22] (among others). Remarkably, GR BH uniqueness theorems can be broken in these theories for a finite high-mass range of BHs [Eic+23]. Hence, stellar-mass BHs on the one hand, and supermassive BHs falling in this specific mass range on the other hand, are expected to be different in nature, which provides the ideal framework to compare the LIGO-Virgo observations with the EHT results.

Among modified theories of gravity in 4D that include additional higher-order derivative terms, Stelle's quadratic gravity

$$S_{\rm quad} = \int d^4x\sqrt{-g}\left(\frac{M_{\rm P}^2}{2}R + c_1R^2 + c_2R_{\mu\nu}R^{\mu\nu} + c_3R_{\mu\nu\rho\sigma}R^{\mu\nu\rho\sigma}\right), \tag{3.9}$$

rewritten in terms of the Gauss-Bonnet invariant $\mathcal{G}$ and the Weyl tensor $C_{\mu\nu\rho\sigma}$ as

$$S_{\rm Stelle} = \int d^4x\sqrt{-g}\left(\frac{M_{\rm P}^2}{2}R + \frac{\tilde{c}_2}{3\tilde{c}_1}R^2 - \frac{1}{2\tilde{c}_1}C_{\mu\nu\rho\sigma}C^{\mu\nu\rho\sigma} - \tilde{c}_3\mathcal{G}\right), \tag{3.10}$$

is particularly interesting as it contains higher-order (quadratic) curvature terms while being perturbatively renormalisable for suitable values of the dimensionless couplings $\tilde{c}_1$, $\tilde{c}_2$, $\tilde{c}_3$ [Ste77].[9] However, due to higher-order derivatives (i.e. more than second derivatives) appearing in the e.o.m., the theory is non-unitary. This translates into the presence of a scalar ghost d.o.f. and leads to instabilities [HZ23].

Changing the expansion in curvature terms can render a class of theories healthy. An example is provided by the action of *Starobinsky inflation* [Sta80]

$$S_* = \frac{M_{\rm P}^2}{2}\int d^4x\sqrt{-g}\left(R + \frac{1}{6G_0^2M^2}R^2\right), \tag{3.11}$$

which is a particular instance in the more general class of $f(R)$-theories whose actions are expressed in terms of functions of the Ricci scalar R. The additional R^2 term in the action Eq. 3.11 introduces a new scalar d.o.f. compared to GR, which corresponds to the conformal metric mode [BC88] and can account for cosmic inflation in the early Universe. In other words, the additional curvature term $\propto R^2$ only kicks in in the strong-gravity regime at the beginning of the Universe. The Starobinsky model with a mass scale $\frac{M}{M_{\rm P}} \sim \mathcal{O}(10^{-5})$ is currently in agreement with CMB data [Akr+20]. More

[8] The Gauss-Bonnet term can therefore be added to the EH action without contributing to the e.o.m. in 4D.

[9] Einstein Gauss-Bonnet theory is recovered by choosing $c_1 = 1$, $c_2 = -4$, $c_3 = 1$. Stelle's gravity is thus a generalisation of Einstein Gauss-Bonnet theory.

interestingly, stable spherically symmetric BH solutions that do not belong to the GR class exist within $f(R)$-theories, see e.g. [NC19]. While they are still singular, the central singularity is generically weakened.

Finally, the ESGB theory, $f(R)$-theories and many more all belong to an even broader class of scalar-tensor theories entitled *(modern) Horndeski theories* [Kob19; HS24]. The Horndeski class defines the most general, four-dimensional scalar-tensor theories with second-order equations of motion. The action depends on four arbitrary functions of the scalar field ϕ and its kinetic term $\chi \equiv -\frac{1}{2}\nabla_\mu\phi\nabla^\mu\phi$. Fixing those functions leads to different branches of the Horndeski class. In the case of the purely geometrical action of ESGB gravity, the scalar field is only allowed to couple to the Ricci scalar and the Gauss-Bonnet term. Horndeski theories encompass various theories which attempt to provide viable DM and DE candidates, inflation scenarios and spontaneously scalarised compact objects. They are not expected to alter predictions in the weak-field regime where GR is well tested (see Subsec. 3.1.1), thanks to screening mechanisms [Qui19; Kob19] and spontaneous scalarisation (which only occurs in the strong-gravity regime near BHs and NSs) [Don+24].

The extensive web of modified theories is depicted in Fig. 3.2 according to the assumption they break in Lovelock's theorem.

3.3 Quantum matter on classical spacetimes: QFT on curved background and semiclassical gravity

Remarkable discoveries and progress were made in particle physics in the 20$^{\text{th}}$ century, which led to the Standard Model (SM) of particle physics [Sch14; Wor+22]. The latter model remains the standard QFT description of strong, weak and EM interactions between fundamental particles today, and thus governs the dynamics of quantum matter.

In the SM, particles are quantum fields whose interactions obey the local $SU(3) \times SU(2) \times U(1)$ internal gauge symmetry: the strong force, or *Quantum Chromodynamics (QCD)* with non-Abelian $SU(3)$ symmetry, and the combined Electroweak forces, c.f. the pioneering works [Gla61; SW64; Wei67; Sal68], with a spontaneously broken $SU(2)_{\text{L}} \times U(1)$ symmetry. From the unification of the weak and EM forces above the electroweak scale ($\sim 10^2$ GeV), and their combination with QCD into a single description, namely the SM, we can infer that the three interactions may all be unified under a single, more complex gauge group at very high energies. Such scenarios are outlined in QFT-based *Grand Unified Theories (GUT)* and universally predict the unification scale to be $\sim 10^{16}$ GeV close to the Planck mass $M_{\text{P}} \sim 10^{19}$ GeV [Wor+22]. Since accessing the GUT scale is out of reach for any hadron collider experiment, one may look at the indirect detection of some phenomena allowed in GUT, such as proton decay or electric dipole moments of elementary particles.[10]

Although numerous experimental tests have supported the validity of the SM and its predictions, the latter model fails to account for several phenomena, e.g. the elusive nature of DM and DE. These anomalies underline that the SM is merely the

[10] Note however that proton decay may be suppressed rather than enhanced if one considers quantum gravitational fluctuations near the GUT scale on top of the strong, weak and EM forces, as shown in [ER24] within Asymptotically Safe Quantum Gravity (ASQG). Furthermore, stringent bounds exist on the electric dipole moments of quarks [LZG18], which limit the strength of CP-violating terms implemented in GUT theories.

leading-order term of a more general EFT [IWW24] and call for more comprehensive extensions dubbed *Beyond Standard Model (BSM) scenarios*, as reviewed in [CM24; Sai24].

Ordinary QFTs describe the interactions of quantum matter on a flat Minkowski background, an approximation that applies to microscopic particles in weak gravitational fields. However, there are regions of spacetime in which the weak-field approximation ceases to be valid, in particular in the neighbourhood of very compact objects such as black holes. QFT on curved backgrounds came as a first attempt in reconciling quantum matter fields with fixed, curved, classical background spacetimes [Kay23] on sufficiently large scales l, i.e. $\frac{l_P}{l} \ll \alpha = \frac{e^2}{4\pi\epsilon_0}$. In this hybrid approximate theory, quantum fields propagate on a fixed, classical, curved background and the strong gravitational fields near a stationary BH are predicted to polarise the (quantum) vacuum state, leading to particle-pair creation.[11] However, the backreaction of quantised fields on the spacetime geometry is ignored within QFT on curved spacetimes. While QFT on curved background seems rather straightforward to implement, some obstacles emerge:

- For a general non-stationary spacetime, the absence of a timelike Killing vector is such that there is no unique quantum vacuum state but a set of compatible quantum vacua;
- The notion of quantum vacuum is observer-dependent;
- The notion of asymptotic particles breaks down on non-asymptotically flat spacetimes.

Those obstacles disappear when restricted to the asymptotically flat, stationary Kerr and Schwarzschild spacetimes. In 1974, Hawking postulated a black-hole Unruh effect [Ful73; Dav75; Unr76], dubbed *Hawking radiation* or *black-hole evaporation* [Haw74]. The production of thermal radiation in the vicinity of a black hole can be understood in the following (simple) way: the strong gravitational fields inside the event horizon of a stationary black hole, where observers are forced to accelerate to stay at constant radius, can induce the creation of pairs of particles with positive and negative energies from a regular quantum vacuum state.[12] The particle with negative energy tunnels through the event horizon and gets absorbed by the black hole, while the one with positive energy escapes to infinity and corresponds to a black-body radiation with finite Hawking temperature $T = \frac{1}{8\pi G_0 M}$ proportional to the BH mass. That is, an asymptotic observer could detect outgoing thermal radiation with a (redshifted) temperature inversely proportional to the black-hole Arnowitt-Deser-Misner (ADM) mass.[13] As such, QFT on a curved classical background is not self-consistent and fails to account for the backreaction of quantum matter (e.g. Hawking radiation) on the classical background spacetime.

[11] The production of pairs of particles is prevented when at least one Killing vector is timelike everywhere in the spacetime. As the timelike Killing vector becomes spacelike within the event horizon of a stationary BH, particle-pair creation can take place.

[12] The quantum vacuum state needs to be regular in the Hadamard sense at the event horizon, see [Car19].

[13] Because of the inverse mass factor in the Hawking temperature (c.f. $T = 6.0 \times 10^{-8} \left(\frac{M_\odot}{M}\right)$ K for a Schwarzschild black hole [Car19]), the temperature of the Hawking radiation drops below the CMB for astrophysical black holes and is therefore too faint to be detected.

Semiclassical gravity arises as an upgrade of QFT on curved background in two ways: the classical background spacetime is dynamical and quantum matter fields backreact on it. The dynamics of semiclassical gravity is encoded in the modified Einstein field equations

$$G_{\mu\nu} = 8\pi G_0 \langle \hat{T}_{\mu\nu} \rangle_\psi \tag{3.12}$$

in which the LHS is the Einstein tensor of a dynamical classical metric $g_{\mu\nu}$ and the RHS is the expectation value of the quantum stress-energy tensor operator $\hat{T}_{\mu\nu}$ evaluated on a quantum matter state ψ. The backreaction of quantum matter on the classical background spacetime is usually treated in a perturbative approach. To that end, the metric tensor $g_{\mu\nu}$ is decomposed into its classical background $\bar{g}_{\mu\nu}$ and a small perturbation $\epsilon h_{\mu\nu}$ assumed to result from quantum fluctuations. We find the leading-order term in backreaction by solving

$$H_{\mu\nu} = 8\pi G_0 \, \langle \hat{T}_{\mu\nu} \rangle|_{\bar{g}_{\mu\nu}} \tag{3.13}$$

for the first-order perturbation $h_{\mu\nu}$. $H_{\mu\nu}$ is the perturbed Einstein tensor and $\langle \hat{T}_{\mu\nu} \rangle|_{\bar{g}_{\mu\nu}}$ is the expectation value of the quantum stress-energy tensor evaluated on a classical background $\bar{g}_{\mu\nu}$. The validity of the perturbative treatment used in semiclassical gravity is limited to the cases where the quantum states are quasi-coherent states and the backreaction fo quantum matter on the geometry is small.

The Hawking radiation has severe consequences within semiclassical gravity since it impacts the geometry of classical spacetimes. If the black hole is not accreting matter while radiating away, the energy carried away by the outgoing Hawking radiation decreases its mass. As a result, the black hole slowly evaporates and shrinks to the Planck mass. Whether it eventually disappears on a finite (but extremely long) timescale or not is subject to research.[14]

The Hawking effect, and the conjecture that black holes have an entropy proportional to the area of their event horizon A [Bek72; Bek73; Haw75]

$$S_{\mathrm{BH}} = \frac{A}{4l_{\mathrm{P}}^2}, \tag{3.14}$$

have launched an entirely new field that marries classical mechanics with quantum thermodynamics and evolved into the formulation of the four laws of *black-hole thermodynamics* [Car14]. Simultaneously, it sourced a paradox: the *information loss paradox* [Haw76]. Let us consider some initial data to be some matter in a pure quantum state (in the statistical sense) that collapses down to a black hole which later evaporates via Hawking radiation. Upon full evaporation (i.e. the black hole entirely disappears through radiation) and thermality of Hawking radiation, the quantum state evolves from an initial pure state to a mixed thermal state, which violates the quantum mechanical postulate of unitary evolution.

No evident solution exists within semiclassical gravity, as the full description of a potential BH remnant would require a working theory of quantum gravity. Nonetheless, possible scenarios of the end-state of the evaporation process should belong to the following three categories. In the case of full evaporation, the quantum state ends up being mixed and this violates the unitarity principle rooted in QM. Unitarity can be restored, but at the price of violating locality [ATV08; Mar17]. Hence, a final mixed state either violates unitarity or locality. Another possible outcome is that

[14] Evaporation occurs on too long timescales (estimated as $t \sim 10^{67} \left(\frac{M}{M_\odot}\right)^3$ [Lop03; Pag05; Tot16]) for the end-state to be ever observed, even for stellar-mass black holes.

the evaporation process halts after a finite time, leaving a remnant BH of finite mass $M \equiv M_{\rm r} \gtrsim M_{\rm P}$ and finite size. This remnant would be in a largely degenerate state, an atypical feature for a quantum state, that would couple to standard matter and modify the standard scattering processes in particle physics. Finally, the information associated with the quantum state could be prevented by some mechanism from crossing the event horizon or even from forming it in the first place. The nature of such mechanism is elusive and the absence of matter absorption contrasts with the essence of a BH event horizon.

In short, semiclassical gravity cannot be the final answer in reconciling quantum matter fields with spacetime geometry at all scales. A more complex structure is required, which would embed both the gravitational force and the three other forces into a common quantum framework.
Naive attempts to apply the usual quantisation procedure from QFT to GR fail. GR is non-linear in nature as it contains self-interactions governed by the Newton coupling constant G_0. It is because this coupling constant has a negative mass dimension for $D = 4$ that GR is perturbatively non-renormalisable, as shown in two different ways in [GS86; Sho07]. Concretely, this means that the loop expansion of the EH action in the perturbation $\epsilon h_{\mu\nu}$ around a flat background $\eta_{\mu\nu}$ introduces new types of UV-divergent terms at every order. These terms must be renormalised by counterterms to absorb their UV-divergences. The lack of perturbative renormalisability of GR translates into an infinite number of these counterterms, each one coming with new free couplings. These infinitely many free parameters must be fixed by experiments, which is clearly out of reach experimentally: GR's predictive power is lost. An *EFT of GR* developed by J. Donoghue [Don95] gives a perturbative QFT of GR which is predictive below the Planck scale, but remains UV-incomplete. Once we abandon perturbative treatments or usual quantisation schemes, promising ways out appear under the realm of *Quantum Gravity (QG) approaches* or, alternatively, *postquantum theories of stochastic classical gravity*.

3.4 Postquantum theory of stochastic classical gravity

Alternative theories dubbed *postquantum theories of classical gravity* have been proposed that assume gravity to be classical but modify the quantum field theory and/or the classical dynamics. The *postquantum theory of classical gravity* put forward by J. Oppenheim belongs to this class [Opp23].

Instead of changing the state space of quantum field theory, it postulates that the classical gravitational dynamics is stochastic in nature and relaxes the measurement postulate of quantum theory. Due to the stochastic nature of both the metric d.o.f. and the quantum matter fields, this theory evades various *no-go theorems* which usually speak in favour of quantising gravity, e.g. [MV17; GGS22]. Moreover, the measurement postulate is superfluous as the classical-quantum interactions naturally decohere the quantum d.o.f, providing an apparent mechanism for the collapse of the wave function [Sch19].

In this theory, combined classical-quantum states described by a positive density matrix evolve according to a master equation whose dynamics preserves linearity, positivity and the trace of the density matrix. The theory satisfies the consistency check that, in the classical limit, the Einstein equations supplemented by a backreaction term are recovered. Despite this success, Oppenheim's postquantum theory does not yet provide a clear answer to the following issues:

- renormalisation. Although it was shown in [Gru+24] that the theory was renormalisable in the classical gravitational d.o.f., covariance may be lost and renormalisation of the quantum matter d.o.f. remains to be addressed;
- the fate of singularities in black holes;
- the accelerated expansion of our Universe. While [OR24] finds both DE-like and DM-like contributions from stochastic fluctuations of spacetime, it is unclear whether the postquantum theory would pass independent tests ΛCDM does well in.

3.5 Quantum Gravity

The general belief is that to remedy all singularities, paradoxes and open questions raised in Sec. 3.1, gravity should be quantum in nature.[15] This is the path followed by QG approaches such as String Theory [Muk11; May20; Har+22; Cve+22], Loop Quantum Gravity (LQG) [Rov08; AP17; Cas18; AB21] and its phenomenology titled Loop Quantum Cosmology [AS17; AP17; AB21], Asymptotic Safety (AS) [Per07; Bon+20; PR23], Causal Sets [Sur19], Causal Dynamical Triangulations [Lol20; Amb24], Euclidean Dynamical Triangulations [Lai+17; Amb24], EFTs [Don23], Group Field Theory (GFT) [Ori09], Spin foams [ES23], Quadratic Gravity [DM22] etc. Links among distinct QG approaches are reviewed in [Boe+22]. Connections between QG approaches on one side and phenomenology and observations on the other side are accounted for in the Swampland program [Pal19; Agm+22; Eic+24] and in the broader field of QG phenomenology [Add+22; AB+23].

3.5.1 Asymptotically Safe Quantum Gravity

In this thesis, we focus on QG approaches where gravity d.o.f. are quantised and, among them, on *Asymptotically Safe Quantum Gravity (ASQG)*.

ASQG is a quantum field theoretic approach to QG which assumes that non-perturbative QFT methods are valid, in particular at transplanckian scales (i.e. at the Planck scale and above). Its main features are:

1. UV-completion. It is postulated to be achieved at transplanckian scales thanks to asymptotic safety: quantum scale symmetry is realised at an interacting UV fixed point [Wei80; Reu98];[16]
2. Predictivity, i.e. non-perturbative renormalisability. In the UV-regime, all dimensionless couplings are driven towards their non-zero UV fixed-point values. In the IR-regime, only a finite number of couplings are free and need to be determined by performing a finite number of experiments. The other couplings are driven towards their IR fixed-point values and are thus predictions of the theory.

The presence of quantum scale symmetry at the UV fixed point implies that the theory is scale-invariant or *self-similar*, in other words, that the properties of the theory

[15] What is meant by "gravity" here is intentionally ambiguous and varies from one QG approach to another, as it sometimes refers to the gravitational field or, adopting the geometrical point of view, to the spacetime itself [WR24].

[16] *Asymptotic safety* distinguishes itself from *asymptotic freedom* by the non-zero but constant values of its couplings at the UV fixed point. An asymptotically safe UV fixed point is thus called *interacting*, while an asymptotically free UV fixed point is *trivial*.

do not change with scale.[17] This is exemplified by the fact that the dimensionless couplings of the theory stay constant once the UV fixed point of the Renormalisation Group (RG) has been reached. Therefore, the finiteness of the dimensionless couplings and their associated operators in the UV regime pertains to the existence of quantum scale symmetry.

In addition to being UV-complete, ASQG is predictive, making it a viable QG approach. Indeed, only QG approaches with finitely many free parameters in the IR-regime can be tested, since we can only perform finitely many experiments to fix the values of the free parameters. The free parameters in the low-energy regime turn out to be associated with relevant directions and real positive critical exponents, as detailed below.

There is by now compelling evidence for an interacting UV fixed point in gravity, as well as in gravity plus suitable matter, in 4D in Euclidean signature[18], see [Per17a; Eic19; RS19b; Bon+20; ES22; Sau23; PR23].

Although ASQG is rooted in Weinberg's idea of an interacting RG fixed point in the UV-regime [Wei80], evidence for such a fixed point only started growing with the development of Functional Renormalisation Group (FRG) techniques [Reu98]. These techniques are based on an RG equation for an effective average action, which defines a flow on the theory space of all diffeomorphism-invariant functionals of the (Euclidean) metric $g_{\mu\nu}$.
Adopting the background field method to gauge-fix the fluctuations, the quantum expectation value of the metric, i.e. $g_{\mu\nu} = \bar{g}_{\mu\nu} + h_{\mu\nu}$, is split into arbitrary large fluctuations $h_{\mu\nu}$ on an auxiliary fixed background $\bar{g}_{\mu\nu}$. The effective average action for gravity $\Gamma_k[g_{\mu\nu}]$ then reads

$$\begin{aligned}\Gamma_k[\bar{g}_{\mu\nu}, h_{\mu\nu}, \xi_\mu, \bar{\xi}^\mu] \;=\; & \int d^4x\sqrt{\bar{g}}\left(J^{\mu\nu}h_{\mu\nu} + \bar{\sigma}_\mu\xi^\mu + \sigma^\mu\bar{\xi}_\mu\right) - \log \mathcal{Z}_k[J_{\mu\nu}, \bar{\sigma}_\mu, \sigma^\mu] \\ & -\Delta S_k[\bar{g}_{\mu\nu}, h_{\mu\nu}] \end{aligned} \tag{3.15}$$

in terms of sources $J_{\mu\nu}$, $\bar{\sigma}_\mu$, σ^μ and conjugated Faddeev-Popov ghost fields $\bar{\xi}_\mu$, ξ^μ [FP67]. The (regularised) generating functional $\mathcal{Z}_k[J_{\mu\nu}]$ associated to $\Gamma_k[g_{\mu\nu}]$ is written as

$$\mathcal{Z}_k[J_{\mu\nu}] = \int_{\Lambda_{\mathrm{UV}}} \mathcal{D}h_{\mu\nu}\, e^{-S[\bar{g}_{\mu\nu}+h_{\mu\nu}] - S_{\mathrm{gf}}[\bar{g}_{\mu\nu};h_{\mu\nu};\bar{\xi}_\mu;\xi^\mu] - S_{\mathrm{r}}[\bar{g}_{\mu\nu};h_{\mu\nu};\bar{\xi}_\mu;\xi^\mu] + S_{\mathrm{s}}[\bar{g}_{\mu\nu};h_{\mu\nu};\bar{\xi}_\mu;\xi^\mu]}. \tag{3.16}$$

In the exponent, the gauge-fixing term S_{gf} includes the Faddeev-Popov ghosts and the source term S_{s} is

$$S_{\mathrm{s}}[\bar{g}_{\mu\nu}; h_{\mu\nu}; \bar{\xi}_\mu; \xi^\mu] = \int d^4x\sqrt{\bar{g}}\left(J_{\mu\nu}h^{\mu\nu} + \bar{\sigma}_\mu\xi^\mu + \sigma^\mu\bar{\xi}_\mu\right). \tag{3.17}$$

[17] The scale in Asymptotic Safety can be thought of as an energy that interpolates between the UV- and the IR-regimes. However, we should rather consider it as an abstract mathematical quantity for reasons that will be detailed thereafter [Bon+20].

[18] Within gravity, we usually work with Lorentzian metrics. However, non-perturbative methods in ASQG require almost necessarily to start with Euclidean metrics, see [Feh+23; BN22; D'A+24; Bra+23; D'A24] for the first gravity results in Lorentzian signature. Therefore, unless otherwise stated, we work in Euclidean signature in the discussion of ASQG.

Moreover, the expression

$$S_{\rm r}[\bar{g}_{\mu\nu};h_{\mu\nu};\bar{\xi}_\mu;\xi^\mu] = -\frac{1}{2}\int d^4x\sqrt{\bar{g}}\left(h_{\mu\nu}\mathcal{R}_h^{\mu\nu\kappa\lambda}[-\bar{D}^2/k^2]h_{\kappa\lambda} + \bar{\xi}_\mu\mathcal{R}_{\xi}^{\mu\nu}[-\bar{D}^2/k^2]\xi_\nu\right) \tag{3.18}$$

corresponds to the IR-regulator term which implements the Wilsonian idea [WK74] of integrating quantum fluctuations shell by shell according to the values of their generalised momentum, i.e. the eigenvalues of the background-covariant Laplacian $-\bar{D}^2$. It means in practice that, when decomposing the fluctuation field $h_{\mu\nu}$ in terms of the eigenmodes of $-\bar{D}^2$, those with eigenvalues $p^2 > k^2$ are integrated out first. Then, by successively lowering the RG scale k, all fluctuations are integrated out. Hence, the IR-regulator term ensures that: (i) at the UV-cutoff $k \sim \Lambda_{\rm UV}$, $\Gamma_{k\sim\Lambda_{\rm UV}} \approx S_{\Lambda_{\rm UV}}$, i.e. the microscopic bare action (which neglects all quantum fluctuations) is recovered; (ii) in the deep IR-regime $k = 0$, $\Gamma_{k=0} = \Gamma$, i.e. the full effective action including all quantum fluctuations is obtained.

The scale dependence of Γ_k is encoded in the RG flow equation [Wet93; Mor94; Ell94]

$$\begin{aligned}\partial_t\Gamma_k &= \frac{1}{2}{\rm Tr}\left[(\Gamma_k^{(2)}+\hat{\mathcal{R}}_k)^{-1}_{hh}\,(\partial_t\hat{\mathcal{R}}_k)_{hh}\right]\\ &\quad -\frac{1}{2}{\rm Tr}\left[\left\{(\Gamma_k^{(2)}+\hat{\mathcal{R}}_k)^{-1}_{\bar{\xi}\xi} - (\Gamma_k^{(2)}+\hat{\mathcal{R}}_k)^{-1}_{\xi\bar{\xi}}\right\}(\partial_t\hat{\mathcal{R}}_k)_{\bar{\xi}\xi}\right],\end{aligned} \tag{3.19}$$

derived for gravity by M. Reuter in his seminal work [Reu98]. In Eq. (3.19), the "RG time" t is related to the RG scale k through $\partial_t \equiv k\partial_k$. $\Gamma_k^{(2)}$ denotes the second functional derivative of Γ_k with respect to all dynamical fields $h_{\mu\nu}$, $\bar{\xi}^\mu$, ξ_μ at fixed background $\bar{g}_{\mu\nu}$, and the gravitational and ghost regulator matrices have entries

$$\begin{aligned}(\hat{\mathcal{R}}_k)^{\mu\nu\kappa\lambda}_{hh} &= \frac{1}{32\pi G_0}Z_k^{\rm grav}k^2\mathcal{R}_h^{\mu\nu\kappa\lambda}\left[-\frac{\bar{D}^2}{k^2}\right],\\ (\hat{\mathcal{R}}_k)^{\mu\nu}_{\bar{\xi}\xi} &= \sqrt{2}\,Z_k^{\rm gh}k^2\mathcal{R}_{\xi}^{\mu\nu}\left[-\frac{\bar{D}^2}{k^2}\right],\end{aligned} \tag{3.20}$$

respectively. The RG flow equation is an exact and non-perturbative one-loop equation. Hence, we caution the reader that the one-loop structure of the RG flow equation should not be understood as only encoding the perturbative one-loop effects, as $\Gamma_k^{(2)}$ is the inverse propagator fully dressed by quantum fluctuations.

The gravitational effective average action $\Gamma_k\left[\bar{g}_{\mu\nu},h_{\mu\nu}\right]$ in the path integral formalism linearly decomposes into all operators of the metric fields $\mathcal{O}_i[\bar{g}_{\mu\nu},\,h_{\mu\nu}]$ compatible with the symmetries of the theory and their associated scale-dependent dimensionful couplings $\bar{g}_i(k)$ as

$$\Gamma_k[g_{\mu\nu}] = \int d^4x\sum_{i=1}^{\infty}\Big(\bar{g}_i(k)\mathcal{O}_i[\bar{g}_{\mu\nu},h_{\mu\nu}]\Big). \tag{3.21}$$

This sum is in principle infinite and the associated couplings span an infinite-dimensional theory space, on which the RG flow equation cannot be solved by current techniques (unless a closed form for the flow of a certain effective average action exists). Therefore, the sum in the effective average action Eq. (3.21) is usually truncated

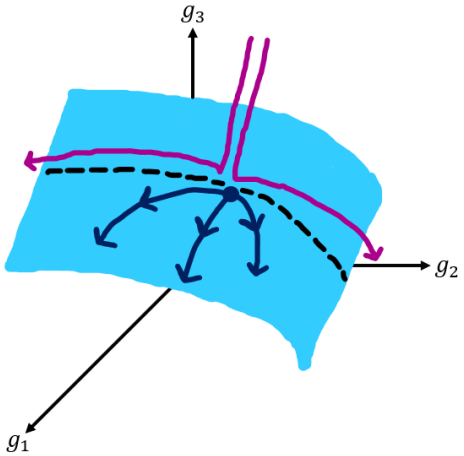

FIGURE 3.3: We show in light blue a two-dimensional UV critical surface in a three-dimensional coupling space spanned by (g_1, g_2, g_3). RG trajectories (dark blue) on this surface emanate from the UV fixed point (dark blue point). Trajectories (magenta) not connected to the fixed point never cross nor belong to the critical surface. The surface and the flow are solely characterised by the relevant directions given by g_1 and g_2, while the irrelevant direction g_3 is a prediction of the theory. Inspired by Fig. 2 of [Eic19].

at a finite order $i = N < \infty$[19] and inserted in the flow equation to solve for a finite set of couplings.
In practice, the RG flow equation is best written in terms of the dimensionless couplings g_i defined in terms of the dimensionful ones as $\bar{g}_i = k^{d_g} g_i$ with canonical mass dimension d_g of the bare coupling. This is because the finiteness of observables is ensured by the finiteness of dimensionless couplings in the UV-regime, as argued in [Wei80]. The RG flow equation leads to a non-trivial system of coupled equations

$$\beta_{g_i}(g_1, g_2, \ldots, g_N) = \partial_t g_i = k\frac{\partial g_i}{\partial k} \tag{3.22}$$

which involve all the dimensionless couplings g_i, $i = 1, \ldots, N$ and their β-functions determining how couplings "run" as a function of the RG scale k. Consequently, quantum scale symmetry is realised if there exists an interacting fixed point $g_* \neq 0$ in the UV-regime, i.e. if there is a set of constant couplings $g_* = (g_{1,*}, g_{2,*}, \ldots, g_{N,*}) \neq 0$ such that

$$\beta|_{g_*} = 0. \tag{3.23}$$

RG trajectories that belong to the UV critical surface start at such a fixed point in the UV-regime, flow from the UV- to the IR-regime and determine how the couplings of the theory change. For the theory to be predictive, the UV critical surface is spanned by finitely many couplings which correspond to the *relevant directions*. The critical exponents of relevant couplings are finite and have a positive real part near the fixed point; hence, relevant couplings tend to depart from the UV fixed point as the scale is lowered. See Fig. 3.3 for a visual representation of a finite-dimensional critical surface. Couplings that are finite but have a negative real part near the fixed point are said to be *irrelevant*; they tend to approach the fixed point when the scale is lowered. They

[19] In addition to performing computations in Euclidean signature, truncated Ansätze for the effective average actions have constituted the major criticisms against Asymptotic Safety, see [Don20; Bon+20].

are thus predictions of the theory and their low-energy values are given theoretically. Finally, *marginal* couplings – whose critical exponents have a null real part – may or may not contribute to the flow.

As an illustrative example of the FRG machinery in ASQG, let us briefly discuss the Einstein-Hilbert truncation worked out in [Reu98].

In gravitational theories, the effective average action $\Gamma_k = \Gamma_k^{\text{grav}} + \Gamma_{\text{gf}} + \Gamma_{\text{gh}}$ depends on the gravitational dynamics Γ_k^{grav}, the gauge-fixing term Γ_{gf} and the Faddeev-Popov ghost term Γ_{gh}. In the Einstein-Hilbert truncation, Γ_k^{grav} is given by

$$\Gamma_k^{\text{grav}} = \frac{1}{16\pi G k^{-2}} \int d^4x \sqrt{g} \left(2\Lambda k^2 - R\right), \tag{3.24}$$

with $G \equiv G_0 k^2$ and $\Lambda = \bar{\Lambda} k^{-2}$ the dimensionless Newton and cosmological constants and $g_{\mu\nu}$ an Euclidean metric. After a split of the metric $g_{\mu\nu}$ into a fixed background $\bar{g}_{\mu\nu}$ and quantum fluctuations $h_{\mu\nu}$, we can compute the remaining terms Γ_{gf} and Γ_{gh} and derive the flow equation for $\Gamma_k \left[\bar{g}_{\mu\nu}, h_{\mu\nu}, \bar{\xi}^\mu, \xi_\mu\right]$. The resulting β-functions can be found in [RS02] for different choices of the regulator and the gauge-fixing parameter. Whatever the gauge-fixing parameter and the type of regulator, two fixed points are found for the couplings G and Λ: a trivial one at $(G_*, \Lambda_*) = (0, 0)$ and an interacting fixed point at $(G_*, \Lambda_*) = (0.403, 0.330)$, assuming a sharp (exponential) IR-regulator (see [Lit01]). While the exact values of the critical exponents of the two couplings change with gauge-fixing parameters and IR-regulators, the positivity of their real parts does not. Hence, both couplings define relevant directions in the RG flow, and the IR-values of G_0 and $\bar{\Lambda}$ are to be set experimentally. This was considered a decisive result favouring the existence of an interacting UV fixed point in the full theory (the latter extending beyond the Einstein-Hilbert truncation).

Tremendous work has been done to extend the EH truncation to higher-order derivative and curvature terms, as reviewed in [Per17a; Eic19; RS19b; Bon+20; ES22; Sau23; PR23]. Those include the extension of the EH action up to all curvature-squared terms in [FOP20], the inclusion of Ricci and Riemann terms in [CP06; CPR09; BMS09; BMS10; OP14; Gie+16; Fal+18; FOP20], the study of $f(R)$-actions in [MS08; CPR08; CPR09; BC12; DM13; Fal+16; DSZ15; OPV15; FLS19] and R^n terms in [LR02; MS08; CPR09; Fal+13; Fal+16; Nag+18; FLS19].

3.6 Black holes: 3 approaches beyond General Relativity

As reviewed in Sections 2.2 and 2.3 and Subsec. 3.1.2, eternal GR black holes are plagued by singularities and instabilities on scales smaller than their event horizon. However, those singularities are conjectured to be hidden from any asymptotic observer by the weak cosmic censorship [Pen69]. Dynamical spacetimes describing black-hole formation through gravitational collapse are not left unscathed. Simple classical models can exhibit a naked singularity associated with a Cauchy horizon and, according to Penrose-Hawking singularity theorems, are geodesically incomplete, thus breaking the strong cosmic censorship. Sections 3.3 and 3.5 motivated the necessity to go *beyond GR* and find a consistent, UV-complete QG theory that would cure all the singularities classical BH spacetimes suffer from.

Hence, a natural approach to finding BH spacetime solutions is the *fundamental approach*, in which we pick each QG or classical modified gravity theory at hand, and either derive their corresponding BH solutions through an action principle or motivate their metrics. Although appealing, this "top-down" approach turns out to be tremendously difficult, even restricted to spherical symmetry, and lacks comprehensiveness. Therefore, an alternative and complementary "bottom-up" approach, dubbed *parameterised approach*, has been developed alongside. This theory-agnostic approach parameterises generic deviations from GR black holes at the level of the spacetime metric. Finally, an in-between approach is provided with the *principled-parameterised approach* set forth in [EH21b; EH21a; EHJ23], which combines features of the two other approaches.

3.6.1 The fundamental approach

In the fundamental approach, black-hole metrics are derived (through an action principle) or motivated from a specific form of new physics. The latter can either come from a "fundamental" QG theory and be quantum, or from a classical modified theory of gravity, hence being classical.

This approach has been followed only in a handful of QG theories to find quantum-(-inspired) black holes, namely LQG [Per17b; Boj20] and ASQG [EH22; Pla23]. In both LQG and ASQG, the black-hole spacetimes are universally better-behaved as in GR in the sense that either (i) the central gravitational singularity is weaker, or (ii) the spacetime is free of curvature singularities, i.e. non-singular. In ST the picture is more subtle, as the BH information loss paradox is usually resolved by *fuzzballs* [Mal96; Mat05], i.e. quantum-sized compact objects without horizon whose surface radiates. Those compact objects possessing no horizon but an outer surface belong to the class of *Exotic Compact Objects (ECOs)* and will be discussed in Sec. 3.7.

Modified black-hole metrics have also been proposed within various classical modified theories of gravity discussed in Sec. 3.2: in quadratic gravity [Pod+20], in Einstein-dilaton-Gauss-Bonnet gravity [BS+16], in $f(R)$-theories [DFT10; CDL15], in massive gravity [Rha14], more generally in Horndeski theories [BCL16] and in other theories with modified dynamics [Cli+12].

BH shadow images can be derived in all three approaches beyond GR, thus allowing to test GR and alternatives with EM radiation. However, it is only possible to test GR and alternatives with GWs in the fundamental approach, since obtaining a GW signal from a coalescing binary requires to solve the equations of motion for the binary (exactly or numerically). In a nutshell, the main advantage of the fundamental approach is to allow for tests of GR and alternatives with both EM and GW signals.

Nonetheless, several caveats remain when applying the fundamental approach. First, it must be applied to each currently available QG proposal or modified theory of gravity, which can assume vastly different forms of new physics. This is both tedious and fails to be comprehensive. Second, most BH metrics proposed within LQG and ASQG do not arise as solutions to an action but have been proposed *inspired* by some characteristic results and/or equations. For example, most bounce-based BH metrics proposed in LQG fail to preserve general covariance or determinism [Boj20]. General covariance can be restored by modifying the algebraic relations between the modified Hamiltonian constraints, but this leads to signature changes in the BH interior. As for ASQG, BH metrics are derived via an RG improvement procedure, which promotes classical coupling constants to their running counterparts as given by ASQG and can only capture leading-order deviations to GR. Additionally, vacuum

BH metrics in modified theories of gravity might not satisfy Birkhoff's (uniqueness) theorem (see e.g. [DP19]) as well as the original no-hair theorem (when a non-trivial scalar- or vector-field profile is present, see e.g. [XMS20]). Lastly, finding BH metrics generally requires to rely on highly symmetric settings, such as spherical symmetry, or extra assumptions. Finding BH spacetimes with slightly fewer symmetries, such as stationary and axisymmetric BHs, remains tremendously difficult, although some analytical and numerical examples have recently been derived [KKR11; Kle+16; Cha+19; Bab+20; DHR20; BA+20; Gra24]. On the numerical side, new types of codes have helped computing stationary and axisymmetric black hole solutions and their properties. As an example, the code developed in [FM23] has been successfully applied to ESGB gravity and EH coupled to an EM field and an axion field [Bur+23]. On the analytical side, approximate solutions have been derived by perturbatively solving the e.o.m. up to a certain order in small spin and/or small coupling [YP09; Pan+11; NC23]. For example, only the first eight terms in the spin-expansion in quadratic gravity theories are necessary to compute observables with a better accuracy than the statistical uncertainties of current and future experiments [CDY24],.

3.6.2 The parameterised approach

As opposed to the fundamental approach, the parameterised approach is "bottom-up". Being theory-agnostic, it does not specify the form of new physics and parametrises the deviations of metric elements from the Kerr ones by finitely many free parameters. These parameters enter the metric in finitely many, new free functions of the coordinates, such that the Kerr metric is recovered when they are set to zero. By doing so, it aims at capturing leading-order deviations from the Kerr spacetime introduced by new physics effects beyond GR, in the spirit of the PPN formalism. In particular, observables can be analysed in terms of a few of the new free parameters, allowing to put constraints on the new-physics parameters.

The main axisymmetric proposals that have been derived following this approach are the bumpy-Kerr black holes [VH10; VYS11], the Johannsen-Psaltis parameterisation [JP11; Joh13a] and its generalisation [CPR14], a parameterisation suited for X-ray tests [Lin+15], the Konoplya-Rezzolla-Zhidenko (KRZ) parameterisation [KRZ16], parameterisations that preserve the symmetries of Kerr [PK18] such as the Carson-Yagi parameterisation [CY20], and non-circular parameterisations [Min20; BA+20; Ans+21; DEH22].[20]

Each parameterisation has its advantages and drawbacks. A common pitfall is that they are "ad-hoc" metrics in the sense that they are not *a priori* solutions of some dynamics beyond GR. Moreover, by construction, there is no one-to-one connection between the deviation parameters and the corresponding new-physics phenomena, and parameters are often degenerate with each other. This renders tests of those parameterisations difficult to interpret.
Despite the aforementioned issues, many of the parameterised metrics match those of solutions to beyond-GR theories. In particular, there are parameterised metrics which correspond to non-singular spacetimes – spacetimes free of the central curvature singularity – found within the fundamental approach. This is the case, for example, for the Hayward [Hay06], Bardeen [Bar68a] and Simpson-Visser spherically symmetric black holes [SV19b]. The main idea behind those non-singular parameterisations is that of the QG proposals and modified gravity theories: some (possibly

[20]The notion of circularity as well as non-circular parameterisations will be discussed in detail in Chapter 6.

quantum) new physics beyond GR counteracts the standard gravitational pull in the deep strong-field regime and suppresses the central curvature singularity.

3.6.3 The principled-parameterised approach

The principled-parameterised approach derived in [EH21b; EH21a; EHJ23] is an intermediate and largely theory-agnostic approach that complementarily combines the advantages of the parameterised and the fundamental approaches. It brings together the direct connection between theoretical new-physics principles and the spacetime properties of the fundamental approach, and the generality and comprehensiveness of the principled approach.

The principled-parameterised approach relies on a set of four guiding principles, common to theories beyond GR, that motivate specific properties of a family of spacetime metrics. Starting from a singular classical spacetime, it aims at finding the minimal modification of that spacetime which implements four principles: locality, a Newtonian limit, regularity and simplicity. For stationary spacetimes, the minimal modification amounts to upgrading the constant ADM mass parameter M to a spacetime-dependent function enforcing the above four principles.

The locality principle is implemented by upgrading the ADM mass parameter M not to a general function of spacetime coordinates, but to a function of a coordinate-invariant local quantity, namely a suitable combination of local classical curvature invariants. Because the argument of such a function must be dimensionless, the upgrade necessarily introduces a new scale, namely a new-physics scale $r_{\rm NP}$. The latter sets the length scale at which new-physics effects become important. Simplicity is then fulfilled when no other scale is introduced in the spacetime. The last two principles prescribe the asymptotic dependencies of the upgraded mass function: the Newtonian limit at low curvatures and regularity (defined here as the absence of curvature singularities) at high curvatures. Simplicity then ensures that the upgraded mass function monotonically increases with r. Altogether, the four guiding principles give rise to a family of regular metrics defined by a free function – the upgraded mass $M_{\rm NP}(x^\mu)$ – with well-defined asymptotic behaviours and a free length scale $r_{\rm NP}$ delineating the transition between the two asymptotic behaviours. The application of the principled-parameterised approach to a particular model of gravitational collapse will be discussed in Chapter 5.

The principled-parameterised approach is motivated by an EFT point-of view in which modifications of gravity set in at large curvature scales, as they do in both classical (see e.g. [DFT10; Car+18; Xie+21; CD24]) and quantum (see e.g. [BR89; Ven92; EH22]) modifications of GR. While the approach seems general enough to encompass many black-hole metrics beyond GR, the metric put forward in [EH21a; EH21b] fails to be brought to a Boyer-Lindquist form (except in the weak-field regime) in which most black-hole parameterisations are expressed. Another limitation of the approach is that it upgrades the ADM mass to a mass function depending on the curvature invariants of the classical spacetime we use as starting point. Obviously, the upgraded spacetime will have curvature invariants which differ from the classical ones, which can then be used to perform a new upgrade of the mass function etc., calling for an iterative sequence of mass upgrades. This turns out to be particularly involved, c.f. [DE24], therefore limiting the approach to the first mass upgrade in practice. Finally, the principled-parameterised approach suffers from the same ad hocness as the parameterised approach: the spacetime metrics are postulated rather

than arising from an action principle. [BP23] provides a first attempt to bridge the gap with the fundamental approach.

3.7 Exotic compact objects and black-hole mimickers

To remedy the singularities GR BH spacetimes suffer from, modified BH metrics have been postulated or derived within various modified theories of gravity and QG proposals. Those metrics share a universal feature: their gravitational singularities are weaker than in their classical counterparts, and some spacetimes are even partially or fully non-singular.[21]

Although no observations have so far disproved the standard paradigm that the dark compact objects emitting GWs and whose images have been captured by the EHT are black holes, we can question their existence in the first place. On the one hand, BH spacetimes are surprisingly simple in GR, and even in theories beyond GR: they are only characterised by a few parameters and fields. On the other hand, GR BHs harbour singularities behind their event horizon, c.f. Subsec. 3.1.2, and no fully non-singular, spinning BH spacetime can be derived from an action principle in a UV-complete and consistent beyond-GR theory yet. Therefore, BHs might not be the only candidates for the most compact objects we observe in the Universe. On the observational side, we have not yet reached the accuracy required to assert the presence or the absence of an event horizon, but the situation will greatly improve with the advent of the ngEHT and the 3$^{\text{rd}}$ generation GW observatories. Thereby, nurturing horizonless alternatives (other than NSs) to BH spacetimes, dubbed *Exotic Compact Objects (ECOs)*, can provide the strongest tests of GR and its BH solutions [CP19].

ECOs gather (super)massive horizonless objects enclosed within a surface of radius r_0 and for which their coordinate-invariant *compactness* – in spherical symmetry – is given in terms of the "closeness" parameter $0 < \epsilon \leq 1$ as

$$r_0 = 2G_0M(1+\epsilon). \tag{3.25}$$

This guarantees that a Schwarzschild BH is recovered in the limit of maximal compactness $\epsilon \to 0$. ECOs that are sufficiently compact possess a photon sphere. Thus, they can be alternatively characterised by the time τ taken by a radially-directed light signal to travel between the photon sphere and the surface of the object, i.e.

$$\tau = G_0M\left(1-2\epsilon-\ln\left(4\epsilon^2\right)\right) \overset{\epsilon\to 0}{\longrightarrow} -2G_0M\ln\epsilon, \tag{3.26}$$

which is measurable by detectors. As a result, massive compact objects in the zoo of ECOs split according to the allowed range of values for ϵ or τ.
Besides compactness, ECOs largely differ in curvature scales. For BHs, the largest curvature we can probe observationally is the curvature of the event horizon.[22] For a Schwarzschild BH, it corresponds to the square root of the Kretschmann scalar $\mathcal{K}$

[21] The notion of *full singularity-resolution* here means that both curvature singularities and geodesic incompleteness are absent of the considered spacetimes. If one of these issues remains, we talk about *partial singularity-resolution*. For simplicity, we will call *non-singular* spacetimes those that are free of curvature singularities (but can be geodesically incomplete) and comment about the past- and future-extensibility of geodesics.

[22] Actually, the gravitational radius of the event horizon is at best *inferred* from the EHT data products and not measured directly.

evaluated at the event horizon, i.e.

$$\mathcal{K}^{\frac{1}{2}}\Big|_{r=2G_0M} = \sqrt{\frac{48G_0^2M^2}{r^6}}\Bigg|_{r=2G_0M} = \sqrt{\frac{3}{4G_0^4M^4}} \sim 4.6\times10^{-13}\left(\frac{10M_\odot}{M}\right)^2 \text{cm}^{-2}, \tag{3.27}$$

while for an ordinary NS it is $\mathcal{K}^{\frac{1}{2}} \sim 10^{-14}\,\text{cm}^{-2}$ at its centre. Comparatively, ECOs can be:

- *soft*, if their curvature is similar to the curvature of a Scharzschild BH at its event horizon;
- *hard* if their curvature is significantly larger.

Soft and *hard* ECOs distinguish themselves in the following way: while the near-surface geometry of *soft* ECOs smoothly approaches that of an event horizon in the BH limit $\epsilon \to 0$, *hard* ECOs can exhibit large geometrical modifications at their surface compared to BHs. Adding to their more complex structure, ECOs can have soft interiors but hard surfaces (and vice-versa) resulting from curvature gradients that stretch from their interior to their surface.

Finally, and more importantly for the derivation of observable signatures in images, particularly compact classes of ECOs possess a photon sphere. As such, their phenomenology closely resembles that of a BH, in particular in images derived from EM signals. Hence, ECOs can also be classified according to the presence (or the absence) of a photon sphere and its characteristics as [CP19]:

- *compact objects* if they display an Innermost Stable Circular Orbit (ISCO), i.e. if $r_0 < 6G_0M$ or $\epsilon < 2$;
- *Ultracompact Objects (UCOs)* if, in addition to an ISCO, they possess a photon sphere; in other words, if $r_0 < 3G_0M$ or $\epsilon < \frac{1}{2}$;[23]
- *Clean Photon Sphere Objects (ClePhOs)* if, in addition to having an ISCO and a photon sphere, the photon sphere is "clean", that is $r_0 < 2.038G_0M$ or $\epsilon \lesssim 0.019$.

In this thesis, we are mostly interested in horizonless objects that can mimick BHs and, thus, we focus on UCOs and ClePhOs.

Without relying on any particular theory or model, spinning ECOs on near-horizon scales are well approximated by rotating surfaces that absorb and/or reflect radiation [Kle+23]. This simple description has been first developed in the context of searches for gravitational wave echoes [ADA17; Wes+18], before it was transposed to imaging [Aki+22f]. The description of ECOs in terms of rotating surfaces is convenient since these surfaces are described by only a few parameters: their mass M, their spin a, their radius R or their compactness ϵ, their albedo A, and their intrinsic brightness $\mathfrak{B}$ (if the emission of radiation is included). The albedo A gives a measure of the relative amount of incoming EM radiation that is reflected. That is, all incoming radiation is transmitted or absorbed when $A = 0$, while perfect reflection corresponds to $A = 1$. The reflection of light off the surface is usually restricted to be specular or elastic. The intrinsic brightness $\mathfrak{B}$ corresponds to a locally isotropic surface emission due to a non-zero temperature. Image prospects of spherically symmetric and static ECOs as well as stationary and axisymmetric ECOs described by reflecting surfaces

[23] Note that, as $\epsilon < \frac{1}{2}$ in UCOs, the parameter τ in Eq. 3.26 is positive and makes sense as a physical time.

have been studied in [CRCY22; Kle+23]. Significant deviations w.r.t. GR BHs appear inside the "shadow region" in the limit $A \to 1$, hence such reflecting surface models can already be excluded by the EHT.

Beyond their simple description in terms of reflecting surfaces, ECOs can arise in specific theories beyond GR, sourced by new fields and particles beyond the SM or by the violation of some assumptions of the Buchdahl's theorem [Buc59]. Within GR, the compactness of self-gravitating objects is bounded from above, i.e. $\frac{G_0 M}{r_0} \leq \frac{4}{9}$ or $\epsilon \leq \frac{1}{8}$, assuming spherical symmetry and a mildly anisotropic perfect fluid [Buc59]. However, if one (or more) assumption entering the theorem break down, self-gravitating horizonless objects of lower compactness (larger ϵ) can exist. So Buchdahl's theorem is to ECOs what Lovelock's theorem is to beyond-GR theories as it provides a mean to classify ECOs according to which assumption is violated among the following:

- GR is the correct theory of gravity;
- the solution is spherically symmetric and static;
- the matter content consists of a single perfect fluid;
- the fluid is (quasi-)isotropic or mildly anisotropic or, equivalently, its tangential pressure is bounded from above by its radial pressure;
- the radial pressure and the energy density of the fluid are both positive;
- the fluid's energy density decreases radially with r.

Giving up one or several of those assumptions enables us to bypass Buchdahl's theorem, hence allowing the existence of the zoo of ECOs depicted in Fig. 3.4.

Among the simplest examples of ECOs are the boson (Proca) stars (see [Vis21] for a review on boson stars), where a massive real or complex scalar (vector) field ϕ (A_μ) minimally couples to Einstein's gravity as

$$S_{\rm boson} = \frac{1}{16\pi G_0} \int d^4x \sqrt{-g} \left(R - g^{\mu\nu} \partial_\mu \bar{\phi} \partial_\nu \phi - \frac{\mu_s \bar{\phi} \phi}{2} \right) . \tag{3.28}$$

The configuration of the boson star is controlled by the parameter μ_s related to the mass of the scalar $m_s = \mu_s$: the larger μ_s is, the more compact and massive the boson star is. Static boson stars are not compact enough to host a photon sphere. Boson stars are of particular interest because of their simple structure, their stability across a large portion of the parameter space and the fact that ultralight scalar fields provide us with a good model of DM [Ant+22]. However, static boson stars are limited in compactness, i.e. $\epsilon \geq 0.44$.

This limit in compactness if lifted, potentially leading to light rings and ergoregions, when: (i) spin is included, (ii) the scalar field self-interact non-linearly, or (iii) considering both a massive real scalar field ϕ and a massive complex fermionic field ψ that minimally couple to Einstein's gravity – yielding soliton stars [DG+23]. Fermion soliton solutions exist for a wide range of parameters. Depending on which degenerate fermion species dominates (neutron or electrons), a fermion soliton star can be of subsolar mass or supermassive. Hence, soliton stars can exist in the all mass ranges of known BHs, allowing for tests of the uniqueness theorem (in spherical symmetry) [Isr67].

FIGURE 3.4: Mindmap of the various possible exotic compact objects according to their feature(s). Inspired by Fig. 4 of [CP19] and [CR+18].

Other classes of ECOs contain even more compact objects than soliton stars. This is the case of anisotropic stars (reviewed in [KB21]), formed when the object is subject to large anisotropic stresses. Anisotropy can arise in many different contexts (including in GR) and produce compact objects that are very close to the compactness of BHs, i.e. ClePhOs (possessing a photon sphere). Additionally, anisotropic stars exist across a wide range of masses (from solar mass to supermassive objects), thus being ideal contenders for both GW and EM tests. ECOs that are so compact that they closely resemble a BH for an asymptotic observer are dubbed *BH mimickers*. While the near-horizon region of BH mimickers can be quite different from that of a BH, they (almost) look like BHs for an asymptotic observer, thus being effectively (nearly) indistinguishable.

All ECOs described so far are relatively simple: they come from (relatively) simple theories with well-defined equations of motion governing their dynamics. However, more peculiar compact objects are present in the taxonomy of ECOs which are theoretically well-motivated but for which the understanding of their formation scenarios remains patchy.

Novel horizonless configurations have appeared in modified gravity theories and semiclassical gravity.

Horizonless solutions of (potentially infinite) higher-derivative theories, dubbed *2-2 holes*, were derived in [HR17; Hol22]. The latter objects are extremely compact (ClePhOs) ($\epsilon \in \left[10^{-78}, 10^{-92}\right]$), thus mimicking BHsand their associated photon sphere (or shell if spinning), but are not well understood yet. Wormholes (introduced in [ER35] and reviewed in [BS23; BS21]) also belong to the ClePhOs' class. They connect different patches of spacetimes via a throat of radius $r_0 > 2G_0M$ and can be stabilised by and built from reasonable matter content. Within semiclassical gravity, dark stars [Arr+22] are thought to emerge either as the result of semiclassical effects stopping the gravitational collapse of BHs or horizonless objects, or as dark massive remnants left behind BHs' partial evaporation. However, they seem unlikely according to the counter-argument given in [Che+18], which states that apparent horizons are unavoidable in a gravitational collapse, even in the presence of a "pre-Hawking radiation". Gravastars are compact objects that could arise as a hydrodynamical description of one-loop QFT effects in classical curved spacetime [RSN20]. They are made of one or several layers of anisotropic fluid(s) that are supported by a negative pressure, thus violating some of the pointlike energy conditions. Hence, they can be made stable and non-singular, see e.g. [Sha+24] for an example.

Within QG theories, String Theory has been one of the most prolific theories in suggesting new types of ECOs. *Fuzzballs* give a regular, horizonless, geometrical description of classical BHs [Mat05]. The interior of a static fuzzball, whose outer radius matches the Schwarschild BH radius, contains a large number of (fuzzy) string excitations or *individual microstates*. Averaging over a large number of coherent superpositions of microstates, the BH geometry is thought to emerge as a result of "coarse-graining". However, matching coherent superposition of microstates with a few BH-like global charges has only been performed in idealised spacetimes, such as non-asymptotically flat spacetimes. Moreover, the fuzzball program as a viable alternative to BHs has recently been criticised [RS19a]. Hence, another alternative to fuzzballs, called "collapse polymers", has come up in String Theory [BM23].[24] Additionally, horizonless spacetimes can generically be formed by overspinning Kerr black holes. These *superspinars* can be realised when the classical angular momentum receives sizeable quantum corrections as, for example, in ST or in ASQG [EH23]. As opposed to classical superspinars, which are plagued by singularities, QG superspinars may be regular and lead to an additional set of internal photon rings which may be detected by future extensions of the EHT [Tor24]. They suffer, however, from instabilities [Pan+10].

Finally, we provide a brief overview of the large variety of observable consequences of ECOs which distinguish them from GR BH spacetimes, both dynamically (in terms of GW signals) and stationarily (in terms of EM radiation). GW signals from ECOs (particularly ClePhOs) may exhibit [CP19; Mag23]:

- a broken isospectrality of their Quasi-Normal Modes (QNMs) between the axial and polar gravitational sectors;
- QNMs with lower frequencies and much longer lived (as they cannot leak into an event horizon);

[24] The term "collapsed polymer" refers to the description of BH's interior, and should not be mistaken with *polymer quantum black holes* that are particular regular, spherically symmetric BH spacetimes in LQG [M+23].

- echoes, i.e. transient series of damped GW signals bouncing off ECO's surface or its centre;
- arbitrary multipole moments (for spinning Kerr-like ECOs);
- a broken equatorial symmetry (for spinning ECOs);
- small but non-zero tidal Love numbers.

The EM emission in stationary ECOs may give rise to:

- a second set of (inner) nested photon rings [EH23; EHJ23; EGH23] if they possess a photon sphere (limited to UCOs and ClePhOs);
- a bright EM emission when tidally disrupted, if they have a hard surface;
- a bright spot within their "shadow".

Altogether, these dynamical and stationary features dispense theoretical ways of testing the Kerr hypothesis and, more generally, the very existence of BHs. However, ECOs can only become astrophysical contenders to BHs if they are (numerically) proven to form through a viable dynamical scenario, be stable against small perturbations and long-lived [BSG24].

Chapter 4

Current and future imaging tests of spacetimes beyond General Relativity

In this chapter, we show how future imaging capabilities of compact objects will help us to test GR and alternative theories. This field of research has gained interest with the recent observations and image reconstructions of two supermassive black holes, namely M87* and SgrA*, by the Event Horizon Telescope (EHT) collaboration. Even though M87* and SgrA* are, within 10% uncertainty on the observed image size of the shadow boundary and within current resolution, consistent with GR Kerr BHs, they are equally well explained by alternatives, see [Aki+19a; Aki+19b; Aki+19c; Aki+19d; Aki+19e; Aki+19f; Aki+21a; Aki+21b; Aki+23; Aki+24d] for M87* and [Aki+22a; Aki+22b; Aki+22c; Aki+22d; Aki+22e; Aki+22f; Aki+24a; Aki+24b] for SgrA*.

Below, we introduce the principle of gravitational lensing by compact objects, the main supermassive black-hole targets of the EHT and the principle of Very Long Baseline Interferometry (VLBI) with current EHT and future ngEHT arrays. We then present photon rings as an ideal probe of spacetime geometry and describe their characteristic features in alternative spacetimes beyond GR, as presented in [DEH22; CR+24]. Finally, we assess whether we can tell apart two "clean" spacetime probes, namely two (high-order) photon rings, with current and future VLBI observations of compact objects using simple geometric modelling. This falls within the scope of our work [CR+24].

4.1 Black hole shadow imaging

BH shadow imaging is based on the physical principle of deflection of light, a.k.a. gravitational lensing, by a supermassive BH. Deflection of light is a fundamental consequence of GR encoded in the null geodesic equations for a solution to the Einstein field equations: compact (super)massive objects curve spacetime around them and light gets lensed, thus deflected or bent, to follow the shortest paths on this curved spacetime called *geodesics*. A geodesic generalises the notion of a "straight line" in flat spacetime to the shortest arc in curved spacetime. A shadow image of a BH is reconstructed by collecting the lensed light rays emitted (in the radio frequency band) near a BH, then making them interfere and obtaining resulting interference fringe patterns. This is enabled by VLBI, a powerful image reconstruction technique which couples many radio telescopes spread across the Earth together to form a single, effective radio telescope roughly the size of the Earth.

4.1.1 The principle of black hole gravitational lensing

The idea that light could be bent by gravity was put forward by I. Newton in 1704 and the Newtonian deflection angle of photons grazing the surface of the Sun was computed a century later by J. G. von Soldner to be $\alpha = 0.9\,\text{as}$.[1] The computation assumed Newton's laws of gravity and the existence of (lightly) massive photons and proved that very light particles are affected by gravity in the same way as ordinary massive matter.

With the advent of General Relativity in 1915, freely moving particles (massive or massless), i.e. not subject to any other forces than gravity, were shown to travel on *geodesics*. Geodesics are solutions of the geodesic equation written in Eq. (2.14) and define the shortest paths $x^\mu(\lambda)$ parameterised by an affine parameter λ in 4D curved spacetime. The spacetime curvature is understood to be sourced by the energy-momentum tensor of some matter, as described by the Einstein field equations in Eq. (2.1), or by the presence of a massive compact object. Assuming GR, the deflection angle α of photons in a Schwarzschild BH spacetime is

$$\alpha = 2\frac{r_{\text{EH,S}}}{b}, \tag{4.1}$$

with $r_{\text{EH,S}}$ the Schwarzschild radius of the event horizon and $b = \frac{L}{E}$ the impact parameter (only defined asymptotically). For photons grazing the surface of the Sun (assumed to be spherically symmetric as Schwarzschild), α turned out to be twice as big as the Newtonian value, i.e. $\alpha \simeq 1.8\,\text{as}$. The deflection of light by a massive spherical body is depicted in Fig. 4.1.

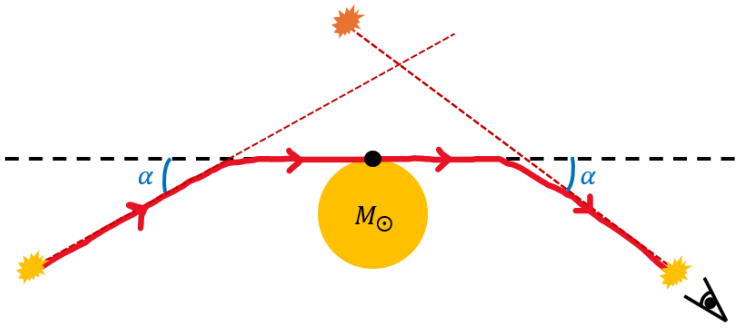

FIGURE 4.1: Schematical illustration of the deflection of light (yellow flash) by an angle α (in blue) passing by a massive body (the Sun; yellow disk). The initial and final asymptotic lines of light form an angle α w.r.t. the plane tangential to the black point at the surface of the Sun, as light follows its geodesic (continuous red line) before reaching the observer (dark eye). The apparent location of the incoming light is given by the orange flash.

The deflection of light is significant when the gravitational field strength is large, so particularly near NSs and BHs. The latter astrophysical objects are the most compact in the Universe and, as such, exert the strongest gravitational pull on massive particles and massless particles such as photons. This is best understood in terms of the escape velocity at the event horizon of a BH: a photon can only escape the

[1] In astrophysics, angles are usually computed in arcseconds or as, with $1\,\text{as} = \frac{1}{3600}\cdot 1^\circ = \frac{\pi}{648000}\,\text{rad}$.

"gravitational pull" of the BH at the event horizon if its velocity exceeds the speed of light, which is not allowed in SR. As GR includes SR, this also cannot occur in GR.

Photons composing the synchrotron radiation emitted in the vicinity of BHs by ultra-relativistic charged particles all get gravitationally deflected by the BH they pass by. Since the deflection angle in Eq. (4.1) is inversely proportional to the impact parameter b, light passing closer to the BH gets more deflected than light passing further away from it. Hence, whether a photon is deflected away or absorbed the event horizon of the central BH is determined by the critical impact parameter $b_c = 3\sqrt{3}G_0M$ (for a Schwarzschild black hole). Photons with $b > b_c$ are deflected away from the BH and can reach an asymptotic observer, while photons with $b < b_c$ fall into the event horizon. The absorbed photons are invisible to any external observer by definition of an event horizon, thus creating a dark central region in the image called *central brightness depression* or *shadow*. Photons that are deflected away by the BH can reach an asymptotic observer and form a bright ring surrounding the shadow in the image, as visible in the BH shadow images computed by the EHT collaboration, see Fig. 4.4.

4.1.2 Main EHT targets: M87* and SgrA*

The primary targets of the EHT collaboration are supermassive BHs with bright synchrotron emission in the radio frequency range. Indeed, early simulations [Lum79] predicted that the combination of:

- an event horizon;
- light bending in accreting black holes embedded in a geometrically thick, optically thin accretion disk

leads to the appearance of a shadow surrounded by a bright emission ring in images that should be detectable through VLBI experiments [FMA00]. This was later confirmed by the shadow images of M87* and SgrA*, the two supermassive black holes with the largest apparent angular sizes, produced by the EHT collaboration and visible in Fig. 4.4. Those two shadow images indeed exhibit a dark central brightness depression, the shadow, and a bright ring with modest, azimuthal, north-south brightness asymmetry, a signature of clockwise rotation as seen by the observer. Altogether, the observed images of M87* and SgrA* are consistent with the expected appearance of Kerr BHs as predicted by GR.

The first BH to be imaged in 2019 was M87* [Aki+19a; Aki+19b; Aki+19c; Aki+19d; Aki+19e; Aki+19f; Aki+21a; Aki+21b; Alg+21; Koc+21; Sat+22; Aki+23], the central BH of the supergiant elliptic galaxy M87, one of the largest and most massive galaxies in the local Universe. This supermassive BH has a mass $M \sim 6 \times 10^9\, M_\odot$ located at a distance $D = 16.8 \pm 0.8$ Mpc from the Earth. Assuming for simplicity that M87* can be described by a Schwarzschild spacetime with photon capture radius $r_{cap} = \sqrt{27} r_{S,EH}$, these mass and distance subtend a photon ring with angular size $\theta \sim 36.5\,\mu$as. Imaging M87* thus requires interferometric capabilities with a resolution down to a few tens of μas; in other words, it requires VLBI. M87* was found by several observations [Per+99a; BSM99; OEK00; Mar+02; Kov+07; LWJ07; Abr+12; Bei12; Asa+13; Had+13; Alg+24] to emit a collimated jet of relativistic particles with an inclination angle $\iota \sim 17^\circ$ with respect to the direction of the source, and emitting across a wide EM frequency band, from radio to X-ray wavelengths. Due to the emission of a powerful jet, its rather small inclination angle ι and the shape of the

photon ring's brightness asymmetry, M87* is found to be spinning clockwise. The observed astrophysics of its accretion and ejection flows are consistent with a model of magnetically arrested accretion flows [Aki+19a; Aki+19e; Aki+23].

The second BH to be imaged was SgrA* in 2022 [Aki+22a; Aki+22b; Aki+22c; Aki+22d; Aki+22e; Aki+22f; Wie+22; Tor+23; Aki+24a; Aki+24b]. SgrA* is the supermassive BH with mass $M \sim 4 \times 10^6\, M_\odot$ that sits at the centre of our Milky Way galaxy, i.e. at a distance $D \sim 8000\,\mathrm{pc}$ from the Earth. The existence of SgrA* was first firmly established by two experiments: the GRAVITY collaboration [Gen+97] and the Keck Observatory [Ghe+98] which performed Near-IR (NIR) interferometry with adaptive optics in the galactic centre with a resolution down to $\sim 2-4\,\mathrm{mas}$. The GRAVITY collaboration could reconstruct the partial or full orbits of approximately 45 faints stars or *S-stars* around the central compact object. The latter was found so massive that, assuming GR, it could only be a supermassive Kerr BH [GEG10; FM13; Vin+16]. Similarly to M87*, assuming that SgrA* can be described by a Schwarzschild spacetime, its mass and distance subtend a photon ring with angular size $\theta \sim 51.1\,\mu\mathrm{as}$. This very small angular size explains why the GRAVITY interferometric experiment could not directly resolve SgrA*. While no jet has been directly observed, SgrA* might power a relatively weak one with an inclination angle $< 50°$ [Aki+24b], which might be visible with future VLBI capacities [Cha+24b]. SgrA*'s emission is characterised by a low luminosity, a low radiative efficiency and a weak Faraday rotation, and is thus consistent with a weakly bound, magnetised accretion flow [Aki+22a].

Although M87* and SgrA* share some similarities, they differ in many ways. First, M87* is roughly 1500 times more massive than SgrA*. Second, M87* has much larger bolometric luminosity L and accretion rate $\dot{M}$ than SgrA*: $L = 10^{42}\,\mathrm{erg}\cdot s^{-1}$ (compared to $L \leq 10^{36}\,\mathrm{erg}\cdot s^{-1}$ for SgrA*) and $\dot{M} \sim 10^{-3} M_\odot \cdot \mathrm{yr}^{-1}$ (compared to $\dot{M} \sim 10^{-7} - 10^{-9} M_\odot \cdot \mathrm{yr}^{-1}$ for SgrA*).[2] These differences in luminosity and accretion rates are likely connected to the presence (respectively, the absence) of a powerful jet emitting at multiple wavelengths in the EM spectrum and across a wide range of length scales for M87* (respectively, SgrA*) [Alg+21; Aki+22a]. The jet launched by M87* constrains the inclination angle to $\iota \sim 17°$, while no such constraints can be derived for SgrA*. Finally, another stringent difference between M87* and SgrA*, resulting from their mass difference, is their variability timescales gauged by the period of the ISCO. While the latter period varies between 5 days and a month for M87*, thus being nearly stationary during VLBI observational campaigns of a few days, it only amounts to $4-30$ minutes for SgrA*. This small period implies that SgrA*'s structure changes within a single night of observation, thus providing the strongest limitation on the imaging process.

Both M87* and SgrA* are supermassive BHs surrounded by an accretion disk and magnetic fields, which define their astrophysical environment. The physics of the accretion/ejection flows in the accretion disk depends on the content, characteristics and dynamics of the latter environment, reviewed in [AF13]. Together with the background spacetime geometry, the properties of the accretion disk are the two pillars of GR Magnetohydrodynamical (GRMHD) simulations of black holes.

The accretion disk is delineated by its outer boundary, roughly set by the radial fall-off of its density and whose location varies with the mass of the enclosed black

[2] The bolometric luminosity of an astrophysical object is defined as the total luminosity (or output rate of energy) integrated over all wavelengths.

hole, and its inner boundary is usually assumed to match with the ISCO.[3] The ISCO is defined as the smallest radius at which freely moving particles (not subject to any other forces than gravity) can stably and circularly orbit the central black hole, thus only unstable orbits exist for $r < r_{\rm ISCO}$.

The accretion disk is made of a plasma of relativistic, charged particles, mainly ions and electrons, that settle into a disk in the equatorial plane and orbit the central BH. The accretion disk is surrounded and pierced by poloidal magnetic field lines which, together with the centripetal force, make relativistic, charged particles emit synchrotron radiation.
Particles forming the accretion disk are governed by four forces: (i) gravity (determined by the background black-hole spacetime), (ii) pressure, (iii) rotation and (iv) electromagnetic Lorentz forces. Depending on the relative importance of each of these forces, the accretion disk belongs to one of the four main types: thin (concentrated near the equatorial plane, optically thick, low accretion rate), slim (moderately extended along the normal to the equatorial plane, optically thick, large accretion rate), thick (extended along the normal to the equatorial plane, optically thick, very large accretion rate) and advection-dominated accretion flows (concentrated near the equatorial plane, very low accretion rate, optically thin). Each of these types of accretion disks possesses analytic models, which put restrictions on the various contributions to the disk's energy-momentum tensor, namely the fluid part (which distinguishes between electrons and ions), the viscous/resistive or stress part (sourced by the turbulences induced by the MRIs [BH91; BH98; Win19]), the Maxwell part (modelling the magnetic fields, usually as ideal MHD, i.e. with infinite conductivity that freezes the magnetic field lines into the fluid) and the radiation part (which carries energy away from the disk).

MRIs sourcing MHD turbulences in the disk is the driving mechanism for (outwards) angular momentum transport. It occurs in weakly magnetised (i.e. low magnetisation) disks in differential rotation, that is with an outwardly decreasing angular velocity. The outwards angular momentum transport is then responsible for the accretion flow onto the central BH.
Finally, the radiation part can be highly efficient, e.g. in a geometrically thin but optically thick disk – where the disk remains relatively cold – or inefficient, for example in advection-dominated accretion flows whose corresponding accretion disks tend to remain geometrically thick and optically thin. The possibility of the co-existence of two (or more) phases in accretion flows, namely a corona (hot) and a disk (cold), has been confirmed in GRMHD simulations [Jia+19], see [LQ22] for a review.

In ideal GRMHD simulations [PM21] where the conductivity is infinite, the plasma is initialised to a prograde or retrograde, pressure-supported torus (or geometrically thick disk) with seeds of weak poloidal magnetic fields, and two main types of accretion/ejection flows are used: Magnetically-Arrested Disks (MAD, [NIA03]) and Standard And Normal Evolution (SANE, [Nar+12]). In MAD models, the ordered magnetic field lines significantly affect the dynamics of the flow and can episodically stop the accretion on the BH, while SANE models have weaker and more turbulent magnetic fields. It seems that M87* and SgrA* observations favour the MAD model in simulations [Aki+21b; Aki+22a; Aki+22e; Aki+24b]. Both those accretion/ejection flows give rise to synchrotron emission in radio and IR frequencies produced by thermal and non-thermal electrons.

[3] The inner boundary of an accretion disk actually depends on its type, ranging from the event horizon to the radius of the marginally bound orbit. More details are provided in [AF13].

The jet launched by M87* strongly depends on the magnetic fields around it. It might be powered either by magnetic fields threading the event horizon and extracting the rotational energy from the BH – a process called *Blandford-Znajek mechanism* [BZ77] – or directly from the accretion flow, i.e. *à la Blandford-Payne* [BP82]. Those mechanisms, relevant for GRMHD simulations of jets, are reviewed in [Miz22].

Due to the high computational cost of 3D GRMHD simulations with detailed disk models, magnetic fields and accretion/ejection flows, other routes have been developed to derive black-hole shadow images accounting for the astrophysical environment, namely semi-analytic models. These semi-analytic models assume a background stationary and axisymmetric spacetime geometry and specify on top of that a simple, non-dynamic emission model. The emission model aims to reproduce the time-averaged emission from an accretion disk characterised by its emissivity and absorptivity [Gol+20]. When using semi-analytical models to derive shadow images for an optically thin, geometrically thick accretion disk around a supermassive BH, the latter assumptions are made: (i) a finite, frequency-independent emissivity and (ii) a vanishing absorptivity. Then, the radiative transfer equation is integrated along null geodesics in the background spacetime, c.f. [Gol+20]. The latter null geodesics on which photons travel are obtained by numerical ray tracing. We do not expect such a simple model to accurately describe realistic astrophysical environments near BHs, but to provide us with a phenomenological model which approximates well the interplay between the spacetime geometry and the photon emission near the BH.

4.1.3 Very Long Baseline Interferometry with EHT and ngEHT arrays

Very Long Baseline Interferometry

The construction of the BH shadow images of M87* and SgrA* by the EHT collaboration [Aki+19a; Aki+22a] relies on VLBI. The latter refers to an advanced technique in radio astronomy that couples several radio telescopes spread across the Earth to form a "radio telescope array", i.e. a virtual effective radio telescope whose dish's diameter roughly corresponds to the diameter of the Earth. This enables us to substantially increase the angular resolution in observing supermassive BHs. Indeed, the imaging angular resolution θ of a radio telescope is inversely proportional to the diameter of the dish d at a given wavelength λ of observation, as given by the Rayleigh criterion

$$\theta \approx 1.22 \frac{\lambda}{d} \text{ as.} \tag{4.2}$$

A single radio telescope typically has a diameter of the order of $d \sim 10$ meters, and thus an angular resolution limited to $\theta \sim 33\,\text{as}$ at the radio wavelength $\lambda = 1.3\,\text{mm}$. However, a VLBI array with a virtual effective telescope of diameter matching the diameter of the Earth $d \sim d_\oplus \approx 13000\,\text{kms}$ has an angular resolution of $\theta \sim 25\,\mu\text{as}$ at the same wavelength, hence resulting in an improvement by six orders of magnitude in angular resolution. The latter resolution is needed to resolve the primary EHT targets, namely M87* and SgrA*, as shown in Subsec. 4.1.2.

A schematic diagram of the VLBI technique used by the EHT collaboration is shown in Fig. 4.2. The mechanism of Earth-based VLBI is as follows: first, each radio telescope receives a radio signal from the observed compact object whose arrival time

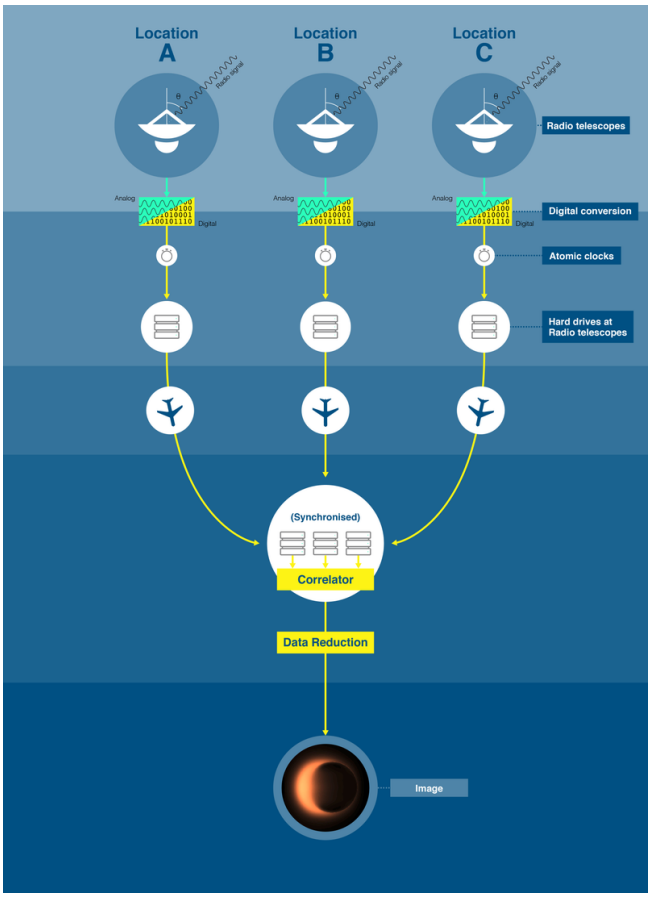

FIGURE 4.2: Schematic diagram of the VLBI mechanism, from the acquisition of data to the reconstruction of a black hole shadow image. Taken from [Vlb]. Credit: ALMA (ESO/NAOJ/NRAO), J.Pinto and N.Lira.

is precisely measured thanks to a local atomic clock.[4] Then, the analogue signal is converted to a digital signal and stored locally on hard drives. The hard drives of each radio telescope are later shipped to a single location where their data is synchronised and processed by a supercomputer. After that, all processed data is combined, i.e. the signals are correlated to produce interference fringe patterns. The last step involves performing (inverse) Fourier transforms on the interference fringe patterns and, together with data reduction techniques (i.e. image reconstructing algorithms), it allows us to reconstruct an image of the observed compact object.

Seen from the compact radio source, a VLBI array of radio telescopes has an effective dimension and orientation set by its projection onto the plane perpendicular to the direction of the source. A curve on the surface of the Earth connecting two radio telescopes at two different locations is called a projected *baseline* $\mathcal{B}$ once projected onto a plane perpendicular to the direction of the source. Each such baseline is sensitive to a particular length scale of structures in the source at a particular angular orientation, i.e. each such baseline is sensitive to a particular spatial frequency in a particular angular orientation in the space of Fourier transform of the intensity distribution

[4] As the radio telescopes are spread across the (curved) surface of the Earth, a radio signal emitted by the observed compact object does not reach each of them at the same time. It is thus essential for interferometry to synchronise the signals obtained at different locations, and thus to accurately measure the arrival time of each radio signal at each radio antenna.

coming from the source. Hence, in principle, correlating the data collected from N stations at different locations on the Earth enables us to measure $\frac{N(N-1)}{2}$ independent spatial frequencies in particular orientations in Fourier space.

Composition of the current EHT array

The current EHT array of radio telescopes consists of $8+3$ radio telescopes shown in black on the world map in Fig. 4.3. The first 8 telescopes are the Submillimeter Telescope (SMT) in Arizona, USA, the Atacama Pathfinder Experiment (APEX) in the Atacama desert in Chile, the IRAM telescope in Spain, the James Clerk Maxwell Telescope (JCMT) in Hawaï, the Large Millimeter Telescope (LMT) in Mexico; the Submillimeter Array (SMA) in Hawaï, the Atacama Large Millimeter/Submillimeter Array (ALMA) in the Atacama desert in Chile and the South Pole Telescope (SPT) in the South Pole. The 3 telescopes which joined the EHT array in 2018-2020 are the Greenland Telescope (GLT) in Greenland, the IRAM Noema telescope in the French Alps and the Kitt Peak Telescope (KP) in Arizona, USA. While some of those radio telescopes are composed of a single radio antenna, e.g. the SMT, some are themselves arrays of radio telescopes, e.g. ALMA which combines 66 radio antennas located up to 16 kilometres apart from each other.

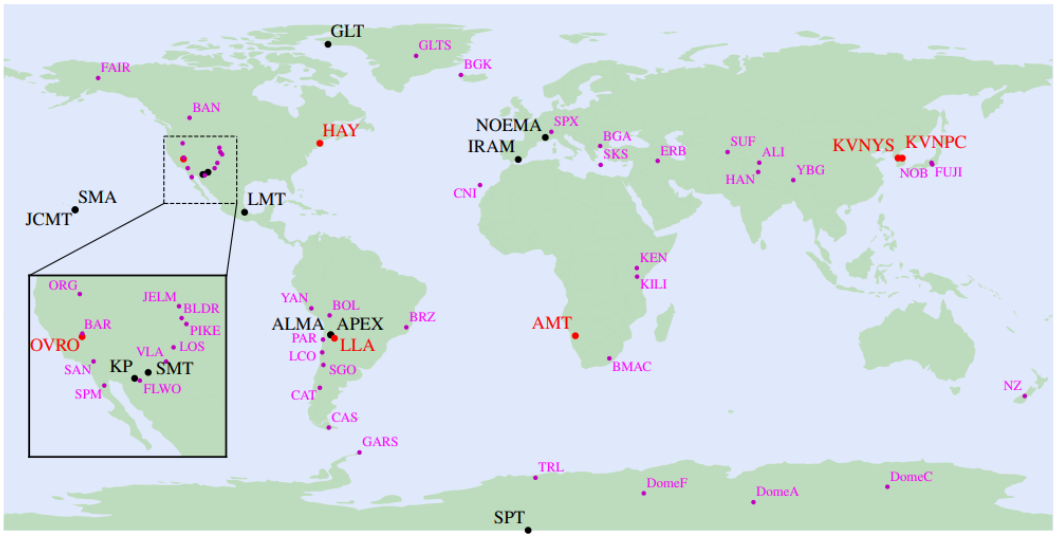

FIGURE 4.3: We show the locations of current and prospective radio telescopes for VLBI on a world map. The current EHT sites are in black, existing or near-future sites joining the EHT array are in red and prospective sites for the next generation EHT array (ngEHT) are in magenta. Taken from [Doe+23].

Both M87* and SgrA* BHs have a peak in their Spectral Energy Distribution (SED) in the radio frequency range around 10^4 GHz (c.f. Fig. 13 in [Aki+22b]), corresponding to a quiescent emission with millimetre wavelengths. This is the reason why the EHT currently operates at (around) 230 GHz or, equivalently, at (around) a wavelength of $\lambda = 1.3\,\text{mm}$. For this wavelength, the longest EHT baselines such as LMT-PV or JCMT/SMA-PV, give a theoretical value for the maximum angular resolution of $\theta \sim 25\,\mu\text{as}$, represented by the outermost dashed grey circle in both panels of

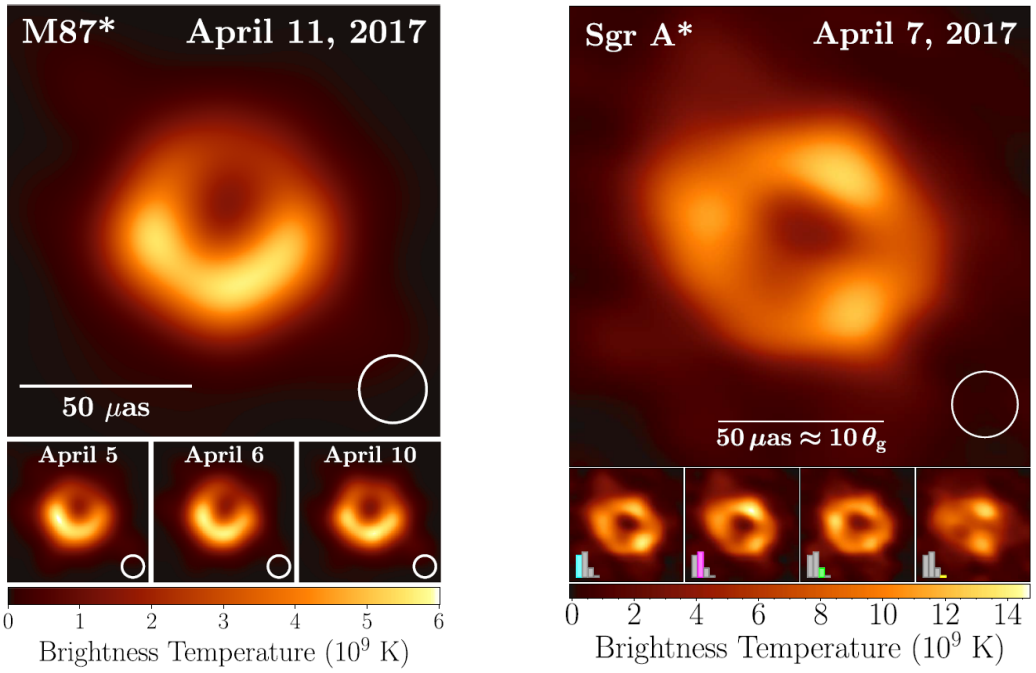

FIGURE 4.4: We show the EHT images of M87* (left panel) and SgrA* (right panel) on different days in April in the 2017 observational campaign. Each image is the average of three different image reconstruction methods after convolving each method with a circular Gaussian kernel to match current resolutions. The largest Gaussian kernel with Full Width at Half Maximum (FWHM) FWHM $= 20\,\mu$as is shown in the lower right. The colour gives the specific intensity of each image, shown in units of brightness temperature.The brightness temperature T_b is defined as $T_b = \frac{S\lambda^2}{2k_B\Omega}$, with S the flux density, λ the observing wavelength, k_B the Boltzmann constant and Ω the solid angle of the resolution element. The inset bars in the right panel give the prevalence of each type of image in the whole set of images of SgrA*. All but one reconstructed image show a prominent bright ring morphology of angular size $42 \pm 3\,\mu$as for M87* and $51.8 \pm 2.3\,\mu$as for SgrA*. Taken from [Aki+19a; Aki+22a].

Fig. 4.5.[5] The latter VLBI angular resolution is sufficient to resolve the shadows of M87* and SgrA* whose angular sizes are inferred to be $42 \pm 3\,\mu$as and $51.8 \pm 2.3\,\mu$as, respectively.

uv-coverage in Fourier space

Due to the small number of radio telescopes forming the current EHT array, i.e. 11, the uv-coverage in Fourier space is sparse.[6] Each pair of telescopes gives two (u, v)-points in Fourier space, related by a point reflection of π. Considering 11 telescopes, this leads to $\frac{11\times10}{2} = 55$ independent (u, v)-points or spatial frequencies, c.f. Fig. 4.5.

[5]Note that the angular size is given in Fourier space, where large spatial frequencies correspond to small source's structures. Therefore, accessing larger and larger spatial frequencies in Fourier space corresponds to resolving smaller and smaller structures in the source.

[6]The uv-coverage of the 2017 EHT array was even sparser because only 8 radio telescopes were operating. Additionally, not all telescopes can "see" a given source due to their location on Earth, which reduces even more the uv-coverage. As an example, SPT can receive signals from SgrA* but not from M87*.

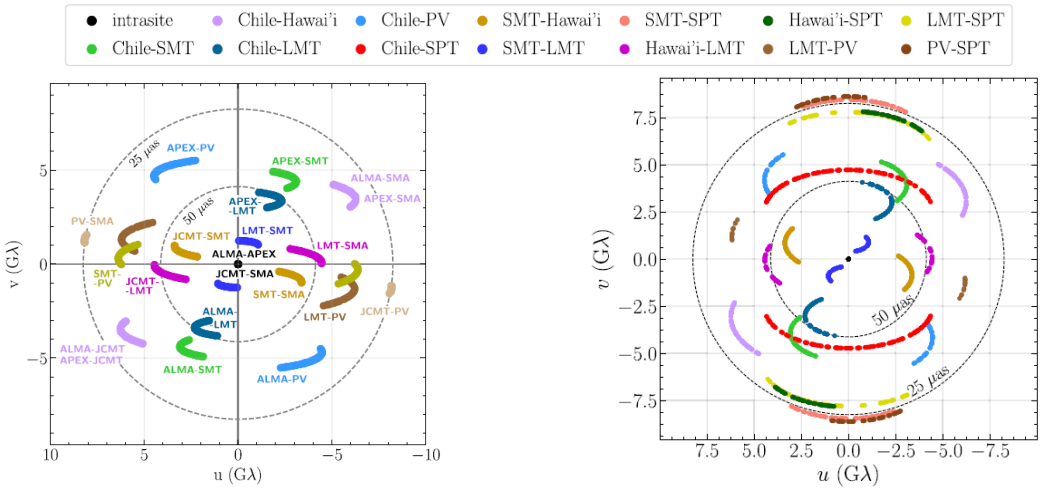

FIGURE 4.5: We show the spatial frequencies u, v in units of Gλ $= 10^9\lambda$ probed by the EHT array in 2017, i.e. the interferometric *uv-coverage* of the current EHT array at 230 GHz, for M87* (left panel) and SgrA* (right panel). The outer and inner dashed grey circles mark baselines accessing features with an angular scale of 25 μas and 50 μas respectively. Colours indicate the spatial frequencies probed by each pair of radio telescopes in the EHT array. Taken from [Aki+19a; Aki+22a].

Notwithstanding, the sparsity of the EHT uv-coverage is naturally but partially counteracted by the rotation of the Earth. Indeed, as the Earth rotates throughout a VLBI observation, the projection of a given curve connecting two telescopes onto the plane perpendicular to the direction of the source changes both in magnitude and in direction, thus sweeping arcs in the (u, v)-plane. This enables us to access structures with different scales and orientations in the source and leads to a finer and more faithful reconstruction of BH shadow images. The outcome of the interferometric fringe patterns is the complex visibility amplitudes $V(u, v)$, i.e. the Fourier components of the brightness distribution on the sky at spatial frequencies (u, v) determined by the projected baselines $\mathcal{B} = \sqrt{u^2 + v^2}$ in units of Gλ.[7] They are displayed in Fig. 4.6 for M87* (left panel) and SgrA* (right panel).

The *uv*-coverage of a given source in Fourier space, and hence the image fidelity, is increased by including new radio telescopes at different locations, creating new baselines. While the *uv*-coverage with Earth-based only telescopes will remain sparse, it will be enhanced if new Earth-based stations are added to the current EHT array and if at least one space-based antenna is included (see the paragraph below). The inclusion of a space-based station constitutes one lever arm to tell apart two thin photon rings in shadow images, as discussed in [CR+24] and in Sec. 4.3.

[7]Due to the sparse uv-coverage, the obtained visibility amplitudes are discrete. A pair of radio telescopes (i, j) in the array with baseline $\mathcal{B}_{ij} = \sqrt{u_{ij}^2 + v_{ij}^2}$ gives a visibility amplitude of $V_{ij} = V(u_{ij}, v_{ij})$. Note that a given pair of radio telescopes define several baselines thanks to Earth's rotation, thus giving a small set of points in the visibility amplitude.

[7]We may use different wordings to denote the visibility amplitude throughout this thesis, e.g. brightness distribution or flux density. Those are all equivalent and given in units of Jansky (Jy) corresponding to $1\,\text{Jy} = 10^{-23}\,\text{erg}\cdot\text{s}^{-1}\cdot\text{cm}^{-2}\cdot\text{Hz}^{-1}$ with $1\,\text{erg} = 10^{-7}\,\text{J}$.

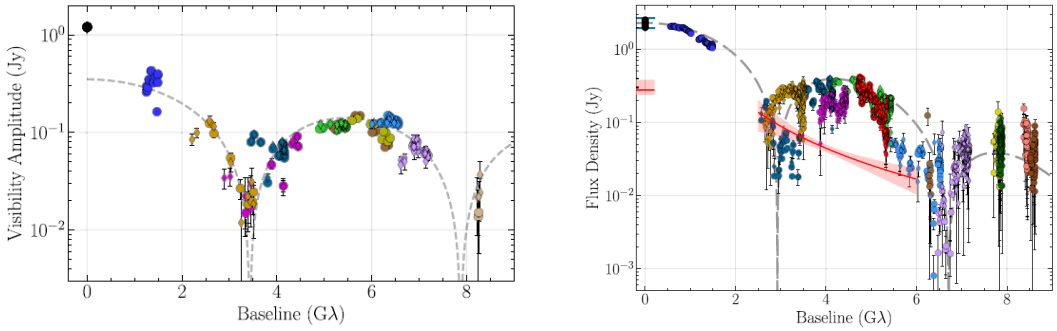

FIGURE 4.6: We show the calibrated discrete visibility amplitudes in units of Jansky (Jy) as a function of the projected baseline for both M87* (left panel) and SgrA* (right panel). The colour code is given in Fig. 4.5 in the bottom left panel for M87* and in the top panel for SgrA*. The error bars give the $\pm 1\sigma$ thermal/statistical uncertainties. The grey dashed lines correspond to the Fourier transform of an azimuthally symmetric thin ring model with diameter 45 μas (54 μas) for comparison with M87* (SgrA*) data. Right panel: the red and shaded region shows the Root Mean Square (RMS) variability of the flux density and its corresponding 68% credible interval over a selected range of baselines. The blue horizontal lines at zero baseline delineate the range of variations in the total flux density. Taken from [Aki+19a; Aki+22a].

Towards combining multiple frequencies

Note in Fig. 4.7 that the angular resolution of a source increases with the frequency, as prescribed by the Rayleigh criterion in Eq. 4.2. Hence, observing at $\sim$ 345 GHz improves the angular resolution of the virtual effective telescope by up to 50%. There are therefore two ways of increasing the angular resolution that can be combined to improve the capabilities of the EHT array: (i) increasing the size of the virtual effective telescope, and (ii) increasing the frequency of observation. Those improvements define the scope of the future ngEHT array(s) [Ayz+23; Joh+23; Doe+23; Ray+24; SP24; Aki+24c].

If one restricts to Earth-based telescopes only, the size of the virtual effective telescope is limited by precisely the size of the Earth, and is almost reached by the current EHT array. Increasing the frequency of observation is promising, in particular, once combined with data acquired at lower frequencies, e.g. 86 GHz and 230 GHz, c.f. [Cha+23; Iss+23], and is already available on a subset of radio telescopes in the current EHT array [Doe+23]. However, atmospheric opacity strongly prevents the observation at 345 GHz on most locations on Earth, thus restricting prospective sites to lie on the highest and driest places that are often remote and drive high operating costs.

An innovative way out consists of sending one or several radio telescopes into space to operate in addition to the Earth-based array: this is dubbed "space-based VLBI" and is reviewed in [TMS17; Gur20; Gur23]. Radio telescopes in space get rid of all limitations associated with the atmosphere and the finite size of the Earth, but are costly and trigger several technical challenges. Due to the enormous amounts of data that will be recorded in space, it is especially challenging to transfer them at a fast enough rate and reliably to the ground. The necessary high bandwidth of space-based VLBI requires a downlink infrastructure with optical laser communications, which may seem achievable with current technologies [Wan+24]. Several proposals for space-based VLBI have been made in the past years, namely the Space VLBI [Roe+19; Shl+24], the THEZA mission [Gur+21], the Black Hole Explorer (BHEX) programme

[Joh+24] and others [FSA20; Haw+19; Pes+19; Pal+19] which, among other scientific targets, aim to probe closer and closer to the event-horizon scale of BHs.

Simulations of distinct array configurations at different observation frequencies, and with or without a space-based antenna are performed in [CR+24] (see also Sec. 4.3) within the scope of disentangling two thin photon rings in shadow image products.

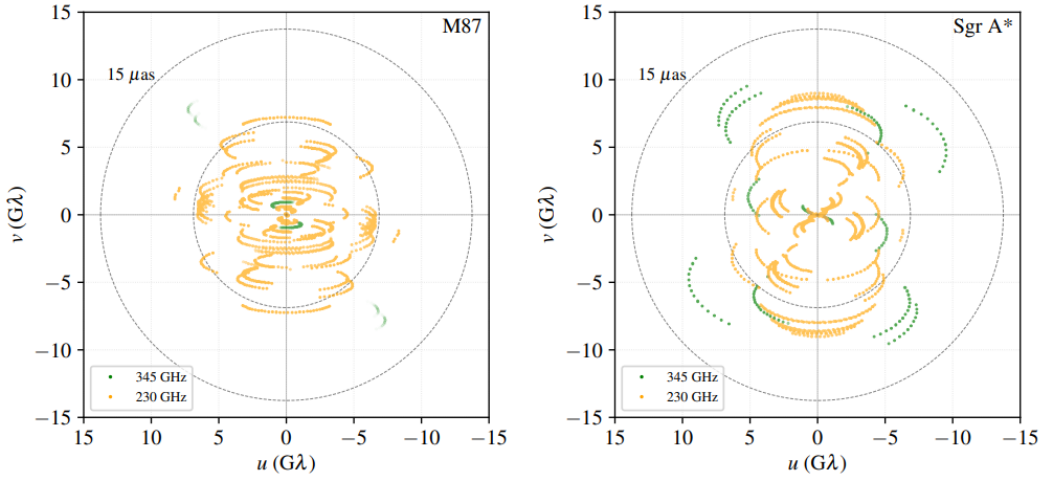

FIGURE 4.7: We show the interferometric *uv-coverage* of the current EHT array with spatial frequencies u, v in units of G$\lambda = 10^9\lambda$ at two different radio frequencies – 230 GHz in light orange and 345 GHz in green – and for two supermassive BHs – M87* (left panel) and SgrA* (right panel). The outer and inner dashed grey circles mark baselines accessing features with an angular scale of 15 μas and 30 μas respectively. Taken from [Doe+23].

Towards an increased sensitivity of arrays

In addition to strongly increasing the angular resolution, the proposals for future VLBI arrays target a higher image dynamical range (from ~ 10 with the current EHT to $\geq 10^3$)[8] and time-resolved images of the dynamical activity in M87* and SgrA* over hundreds-to-thousands of gravitational timescales. This will be allowed by increasing the sensitivity of some of the radio telescopes forming the VLBI array, and thus the Signal to Noise Ratio (SNR). Indeed, current VLBI observational data is affected by thermal noise and systematic errors that result from the finite sensitivity of radio telescopes. The thermal noise is dominated by the System Equivalent Flux Density (SEFD) [Aki+19b] of the respective telescopes, given by

$$\mathrm{SEFD} = \frac{T^*_{\mathrm{sys}}}{\mathrm{DPFU} \times \eta_{\mathrm{el}}}, \tag{4.3}$$

where T^*_{sys} is the effective system noise temperature, DPFU the Degree Per Flux density Unit and η_{el} the gain curve. More details on SEFD are provided in [Aki+19c]. A high SEFD value indicates a high thermal noise in the data and decreases the SNR

[8] The image dynamical range is defined as the ratio between the brightest and the dimmest pixels in the image, the dimmest pixel lying within the central brightness depression or dark shadow.

of a given pair (i, j) of radio telescopes as

$$\mathrm{SNR}_{ij} = \frac{\eta_Q \sqrt{2\Delta\nu T_{\mathrm{int}}} S_{\mathrm{cor}}}{\sqrt{\mathrm{SEFD}_i \mathrm{SEFD}_j}}. \tag{4.4}$$

$\eta_Q \sim 0.88$ is the digital loss due to sampling the received signal at each antenna with finite precision, $\Delta\nu$ is the bandwidth around the observing frequency ν, S_{cor} is the expected correlated flux on the baseline between stations i and j and T_{int} is the integration interval of the VLBI signal. The SNR is thus limited by the SEFD on the one side, and by both the bandwidth $\Delta\nu$ around the frequency of observation ν and the integration time T_{int} on the other side. As the integration time is itself constrained by the coherence time set by atmospheric fluctuations, it is easier to improve the sensitivity of radio telescopes by either decreasing the SEFD or increasing the bandwidth, ideally reaching a ratio of 1 between the observing frequency and its associated bandwidth. The importance of arrays with low-SEFD radio telescopes to distinguish the presence of a second thin photon ring in shadow images is discussed in [CR+24] and Sec. 4.3.

4.1.4 An ideal probe of spacetime geometry: photon (sub)rings

As presented in Sections 4.1.1 to 4.1.3, the BH shadow images result from bright radio emission in the accretion disk surrounding the central BH – forming the astrophysical environment – which propagates and is subject to gravitational deflection in the vicinity of the BH – as prescribed by the spacetime geometry. If we assume that the central compact object is well described by a Kerr BH as predicted in GR, the spacetime geometry is well understood and the astrophysical environment can be investigated through multiple GRMHD simulations (although with high computational costs [DZ+24]).

Within the scope of testing the Kerr paradigm, we need to understand the interplay between the spacetime geometry and the astrophysical environment and be able to disentangle one from the other [LVB21; OPY22; YPO23; KR22]. This turns out to be much more complex beyond GR than in GR, because:

- no fully consistent and UV complete theory beyond GR is known to date, let alone their analytical stationary and axisymmetric BH solutions;
- uncertainties remain on the modelling of the astrophysics of the accretion disk and the magnetic fields;
- no clean beyond-GR MHD setups exist. Tentative procedures rely on approximations (e.g. spherical symmetry or the validity of the GR geodesic equation), neglect backreaction, only allow to vary a few new-physics parameters and are even more computationally costly than GRMHD simulations [Miz+18; WOR20; NYK22];
- degeneracies exist between putative deviations from GR and both the modelling of the accretion flow and the uncertainties on the BH mass and spin.

However, photon rings are increasingly coming into focus as the cleanest probe of BH spacetimes in the context of shadow images [Vin+22; Pau+22; Bro+22b; Tie+22; Koc+24; BSG23; Pal+23; Joh+23; SBG24; CAnL23; Lup+24; Gal+24; Jia+24; SP24]. The VLBI images of M87* and SgrA* in Fig. 4.4 mainly capture the direct emission, i.e. the

light rays emitted in the disk which are not winding around the BH but directly reach the observer. The direct emission highly depends on the emission profile of the disk, and thus the astrophysical environment of the BH. In contrast to that are the (higher-order) photon subrings contained within the bright ring structure circling the shadow, see Fig. 4.8 for a graphical representation.[9]

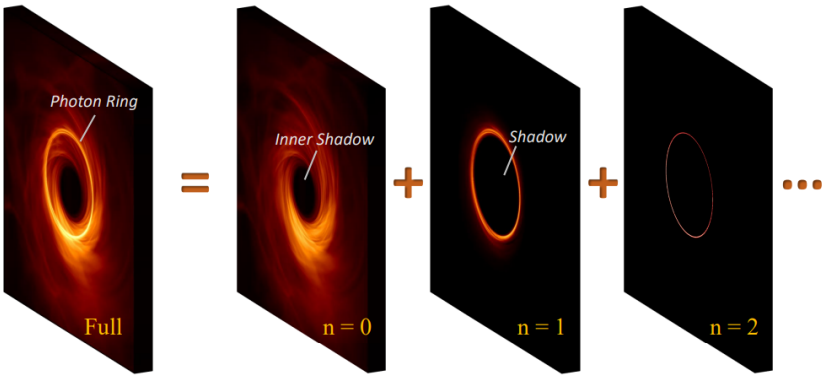

FIGURE 4.8: We show the decomposition of a full BH shadow image with a bright ring circling a shadow into its direct emission's component ($n = 0$) surrounding the inner shadow and its stacked set of photon subrings. The leading $n = 1$ subring and its next-to-leading $n = 2$ subring are represented, while the ellipsis indicates the presence of higher-order photon subrings $n > 2$. Taken from [Joh+23].

Photon rings are intimately connected to the presence of a 2D photon sphere (in spherically symmetric and static BHs) or a 3D photon shell, its generalisation for an axisymmetric and stationary spacetime. As an example in GR, the axisymmetric, stationary and asymptotically flat Kerr BH possesses both an event horizon and a photon shell defined analytically in Eqs. 2.10 to 2.12 and discussed in Sec. 2.2. The proof of the existence of photon shells extends beyond GR to any stationary, axisymmetric, asymptotically flat BH spacetime in 4D in [CH20; CRE24].[10] Additionally, photon shells can exist around particularly compact ECOs, namely UCOs and ClePhOs, as reviewed in Sec. 3.7.

Free-falling photons contained within a photon shell travel on unstable, bound null geodesics or "bound orbits" which, once perturbed, can either fall into the central compact object or escape towards infinity and potentially reach an asymptotic observer. "Nearly bound" photons on those trajectories that fall into the event horizon give rise to the shadow. Escaping photons on nearly-bound trajectories get strongly lensed: they first wind around the BH a certain number of times (up to infinitely many times when the photons approach fully bound orbits) before escaping from the gravitational pull of the compact object and potentially reaching radio telescopes on Earth. For geometrically thick, optically thin disks, those strongly lensed, escaping photons lead to a nested set of lensed images of the compact objects' surroundings labelled by a set of integers $n \in [1, \infty[$. The integer label n can be defined as the number of times a given photon emitted in the accretion disk and following a nearly-bound, strongly lensed trajectory crosses the equatorial plane before escaping. For

[9] In the sequel, we will omit the prefix "sub" in "photon subrings" and use "photon rings" instead. These should, however, not be mistaken for the bright photon ring circling the shadow, as the latter is composed of both the photon rings and the direct lensed emission.

[10] The proof has only been given assuming circularity (see Chapter 6 for a discussion of that spacetime isometry). It is yet unknown whether it extends to non-circular spacetimes.

stationary and axisymmetric spacetimes, it amounts to counting the number of times the polar angle θ takes the value $\theta = \frac{\pi}{2}$ defining the equatorial plane.

The $n = 0$ contribution is usually referred to as the weakly lensed direct emission and dominates the brightness of the ring feature in the shadow image. The direct emission is thus highly sensitive to the physics of the accretion disk or, more broadly, the astrophysical environment of the compact object. In contrast, the high-order photon rings, i.e. $n \geq 1$, are asymptotically insensitive to the astrophysics of the emission region. The $n \to \infty$ photon rings asymptote to the critical curve bounding the shadow in the image. The critical curve is the theoretical curve in the image plane delineating the boundary between photons captured by the source and lensed photons winding around the source before escaping away. The critical curve thus relates to the critical impact parameter b_c, see Fig. 4.9 in spherical symmetry. It is solely defined by the background spacetime geometry on which free-falling, nearly-bound photons travel. Therefore, the fact that higher-order photon rings are quite insensitive to the astrophysical environment, thus encoding direct information about the background geometry, makes them suitable signatures of the spacetime metric.

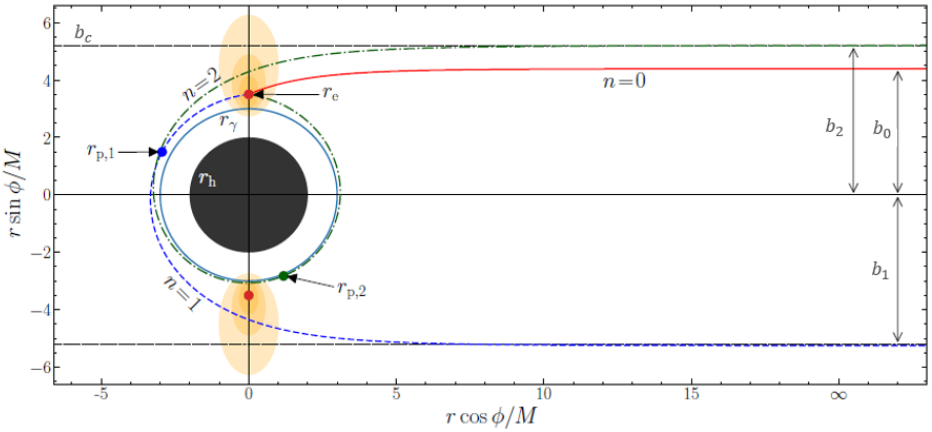

FIGURE 4.9: We provide a schematic view of the formation of photon rings on the image plane of an asymptotic, face-on observer located at $r \to \infty$ (on the far right) for a spherically symmetric and static BH with a simple accretion disk (in orange). The shadow is represented by a black disk with radius r_h and the photon sphere (blue circle) lies at r_γ. The emission from the accretion disk is dominated by the direct flux (red curve labelled by $n = 0$) emitted at an effective radius r_e. Strongly lensed photons emitted at r_e reach the observer after one half-orbit (dashed blue curve labelled by $n = 1$) or two half-orbits (dashed green curve labelled by $n = 2$), leading to the $n = 1$ and $n = 2$ subrings. The $n \to \infty$ subring defines the critical curve on the image with impact parameter b_c, which the $n = 2$ subring already tracks closely. Taken and adapted from [Wie21].

While higher-order photon rings are clean probes to test the Kerr paradigm with alternatives, the way to reliably detect them is fraught with difficulties.

One of them arises as we do not yet have access to sufficiently large baselines to narrow down the location and shape of the $n \geq 1$ photon rings. Another difficulty lies in the dimming and the reduced thickness of each subsequent photon ring as it gets exponentially closer to the critical curve when n increases, as illustrated in Fig. 4.10. While the intensity of each subsequent photon ring increases, the photon

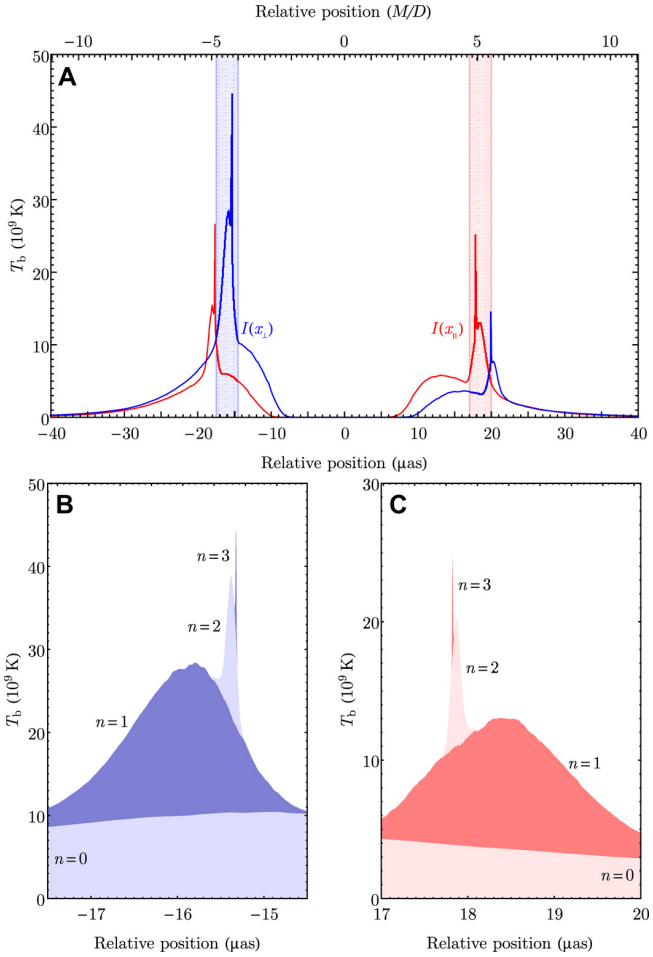

FIGURE 4.10: We show the image cross-sections of a bright ring for a time-averaged GRMHD simulation of M87* consistent with the 2017 EHT data. Top panel (A): brightness cross-sections whose blue (red) curves correspond to cross-sections perpendicular (parallel) to the projected spin axis. Bottom panels (B and C): decomposition of the left perpendicular peak (in blue) and the right parallel peak (in red) into the brightness associated with direct emission and the first three photon rings labelled by $n = 1, 2, 3$. Similar results are also seen in image cross-sections of simple geometrical models of rings. Taken from [Joh+20].

ring becomes narrower, thus leading to an exponential dimming in flux [Joh+20]

$$\frac{F_{n+1}}{F_n} \approx e^{-\gamma} \tag{4.5}$$

controlled by the Lyapunov exponent γ. Higher-order photon rings being fainter and fainter in GR, they require higher and higher sensitivity of radio telescopes and image dynamical range. Alternative spacetimes might have photon rings with comparable fluxes, c.f. Sec. 4.2.

4.2 Characteristic image features of spacetimes beyond General Relativity

The BH shadow images of M87* and SgrA* in Fig. 4.4 are both consistent with a Kerr black hole predicted by GR. However, as discussed in Sec. 4.1, we do not yet have access to the resolution and sensitivity needed to gauge the existence of an event horizon[11] and the failures of GR in the interior of BHs motivate possible alternatives such as regular BHs [Lam+18; Vin+21; KG21; EH21b; EH21a; EHJ23; KWGM22; KW23; LW22; Isl+23; Guo+23; Olm+23; DMDMRG23; QWF24; Zar+24], horizonless (ultra) compact objects [EH23; EHJ23; Cun+17; EGH23; Gue+22b; CRCY22], wormholes [ORGG22; Gue+22a; NPP23; Olm+23] and BHs in theories beyond GR [Gyu+21; Sen+23; Daa+23; HKM24], broadly reviewed in [Ayz+23].

Because images of compact objects result from the combination of a spacetime geometry and an astrophysical environment, distinguishing a Kerr BH from an alternative compact object remains difficult [LVB21; YPO23; KR22; CAnKL24]. As discussed in Subsec. 4.1.4, this is where photon rings enter the scene as smoking guns of new physics: they can shine a light on the underlying spacetime geometry of the central compact object.

Photon rings of GR BH spacetimes are known analytically and their separation and flux density decrease exponentially as their winding number n increases. This makes them hard to detect by VLBI arrays with current capabilities. However, many alternative compact objects produce photon rings' structures which differ from the ones predicted by GR. They can be distinct in at least four ways, which we focus on:

- there can be an additional (inner) set of photon rings arising from trajectories that approach the photon sphere from the inside or bounce off the object's surface in horizonless spacetimes [Sha+19; Gyu+20; EH23; EHJ23; EGH23; CRCY22; Gue+22a; Gue+22b; MS24];
- subsequent photon rings may have similar flux densities when absorptivity is set to zero and the peak intensity increases with n, thus being more easily detectable [CRCY22];
- photon rings may be more widely separated than in GR [Bro+22a; Pau+22; Tie+22; LG22; CR+24; ATP24; MS24], thus being more easily resolvable;
- photon rings may simultaneously harbour cusps, dents and lack of (image) reflection symmetry in spacetimes with fewer symmetries than GR ones, e.g. non-circular spacetimes [VH10; Vig10; HGE19; Min20; Ans+21; BA+20; EH21b; EH21a; DEH22].

To produce simulated images[12] of spinning spacetimes with those "smoking gun" photon rings with a reasonable computational costs, we rely on one of the semi-analytic emission models mentioned in Subsec. 4.1.2. In this model, e.g. used in

[11] Actually, event horizons are not observables that can be detected in a finite amount of time, contrary to apparent horizons [Vis14]. However, the apparent and event horizons coincide for stationary black holes whose event horizon is a Killing horizon, and one can thus loosely use one for another in that case.

[12] Images of compact objects can be split into two main categories: *real* images that are reconstructed from observational data and *simulated* images reconstructed from simulated data. The latter category further divides into two subcategories: *ideal* simulated images at very high resolution and simulated images reconstructed from simulated data through a simulated observation, i.e. taking into account the limited capabilities of the VLBI arrays. In this thesis, we solely focus on simulated images, ideal or not.

[DEH22; CR+24], the emission in the disk is accounted for in a disk profile defined by a number density function (c.f. [Bro+22a; EH21a; EGH23])

$$n(r,\theta) = n_0 r^{-\alpha} e^{-\frac{\cos\theta^2}{2h^2}} \cdot \begin{cases} 0, & r < 0 \\ e^{-\frac{(r-r_{\rm cut})^2}{\omega^2}}, & 0 \leq r \leq r_{\rm cut} \\ 1, & r > r_{\rm cut}, \end{cases} \tag{4.6}$$

parameterised by the disk height h, the radial location $r_{\rm cut}$ and the sharpness ω of the exponential inner cutoff, the power-law exponent α of the large distance radial falloff and a global normalisation factor n_0. The rotation of the disk is set by the fluid velocity (in BL coordinates)

$$u_\mu = u_0 \left(-1, 0, 0, \tilde{u}_\phi\right), \tag{4.7}$$

whose azimuthal part, a.k.a polar angular momentum, corresponds to $\tilde{u}_\phi = \frac{R^{\frac{3}{2}}}{1+R}$ with $R = r\sqrt{1-\cos\theta^2}$ and whose normalisation factor u_0 is chosen such that $u_\mu u^\mu = -1$. The number density function enters the radiative transfer equation which, assuming finite, frequency-independent emissivity and vanishing absorptivity (i.e. optically thin disk), reads

$$\frac{d}{d\lambda}\left(\frac{I_\nu}{\nu^3}\right) = C n(x^\mu(\lambda)). \tag{4.8}$$

It is expressed in terms of a dimensionful global constant C and the emission frequency ν. This equation describes how the frequency-dependent intensity I_ν changes along null geodesics $x^\mu(\lambda)$ (affinely parameterised by λ) followed by light rays in the relativistic fluid of the accretion disk. The global constant $C \cdot n_0$ drops out when normalising the intensity profile on the image to the brightest point.

Geodesics on which photons travel are computed via analytical or numerical (when the geodesic equations are not integrable) ray tracing whose principle is the following: an observer located at $(r_{\rm obs}, \theta_{\rm obs}, \phi_{\rm obs})$ (in BL coordinates) far away from the central compact object (i.e. $r_{\rm obs} \gg M$) places their observational 2D screen with coordinates (x, y) whose origin matches $(r_{\rm obs}, \theta_{\rm obs}, \phi_{\rm obs})$. The image plane is set perpendicularly to the vector starting at $(r_{\rm obs}, \theta_{\rm obs}, \phi_{\rm obs})$ and pointing towards the central compact object. Geodesics are sent perpendicularly to the screen of the observer and integrated backwards in time, i.e. from the observer towards the central compact object.[13]

Assuming that the central compact object is a spinning BH, all geodesics that fall into the photon shell and end up crossing the event horizon without intersecting the accretion disk will correspond to a point lying within the central brightness depression in the image for small inclination angles.[14] All geodesics falling into the photon shell on unstable orbits and intersecting the accretion disk a certain number of times before escaping to infinity will pick up emission from the disk and give a bright point located outside of the central brightness depression in the image. As a result, sending and ray-tracing sufficiently many geodesics with different initial conditions will produce an image of the compact object with a generic central brightness depression surrounded by a bright ring feature. If the compact object is horizonless, additional features can occur in the image. Photons approaching the

[13] As a side note, a forward ray tracing method was proposed in [Zho+24] to better trace and track hotspots in a Kerr BH.

[14] The shape and "darkness" of the central brightness depression of a rotating BH varies with the inclination angle as the latter departs from 0°, see e.g. [Psa19].

object's surface before escaping are highly gravitationally redshifted, such that they can also appear "dark" in the image and produce a central brightness depression. However, the "darkness" of the latter is (much) less pronounced than for a BH, see e.g [EH23], as additional (inner) photon rings can form within the central brightness depression and illuminate it. Those additional inner photon rings result from photons approaching the photon shell from the inside, i.e. from smaller radii.

4.2.1 Non-circular spacetimes

Specific image features can be connected (though not necessarily in a one-to-one way) to fundamental principles of spacetimes such as their symmetries. Hence, establishing a connection between reduced symmetries of some spacetimes beyond GR and specific photon ring features would tentatively give (though not necessarily conclusively) insight as to whether or not M87* and SgrA* are described by the stationary, axisymmetric and asymptotically flat – thus highly symmetric – Kerr spacetime.

As a first example, a distinguishing feature of stationary and axisymmetric spacetimes is that their shadow boundary is flattened on the prograde side compared to shadows of static and spherically symmetric spacetimes.

As another example, images of BH spacetimes based on the regularity and the locality principle in [EH21b; EH21a] exhibit, c.f. left panel in Fig. 4.11:

- cusps in the shadow boundary and photon rings;
- a dent in (the photon rings surrounding) the shadow boundary, i.e. in the $y = 0$ image axis;
- a broken reflection symmetry about the $y = 0$ image axis at non-edge-on and non-face-on inclinations.

Simulatenously, those axisymmetric and stationary spacetimes break circularity, a symmetry defined as

$$\begin{aligned} \xi_1^{[\mu}\xi_2^{\nu}\nabla^{\kappa}\xi_1^{\lambda]} &= 0 \text{ at at least one point,} \\ \xi_2^{[\mu}\xi_1^{\nu}\nabla^{\kappa}\xi_2^{\lambda]} &= 0 \text{ at at least one point,} \end{aligned} \tag{4.9}$$

$$\begin{aligned} \xi_1^{\mu}R_{\mu}^{[\nu}\xi_2^{\kappa}\xi_1^{\lambda]} &= 0 \text{ everywhere,} \\ \xi_2^{\mu}R_{\mu}^{[\nu}\xi_1^{\kappa}\xi_2^{\lambda]} &= 0 \text{ everywhere,} \end{aligned} \tag{4.10}$$

in terms of the two commuting, spacetime Killing vectors $\xi_{1,2}$ [Car70], the Ricci tensor $R_{\mu\nu}$, the covariant derivative ∇_μ and the antisymmetrisation of indices enclosed in square brackets. For asymptotically flat spacetimes, which we consider, axisymmetry implies the existence of an axis of rotation on which the Killing vector, e.g. ξ_2, associated with azimuthal rotations must vanish. Hence, for the considered spacetimes, the two first conditions Eq. 4.9 always hold. Together with the latter two conditions Eq. 4.10, they imply the existence of a spacetime isometry which, in BL coordinates, corresponds to the invariance under the simultaneous transformations $t \to -t$ and $\phi \to -\phi$ [ABCG06]. Owing to its Ricci-flatness $R_{\mu\nu} = 0$, the Kerr spacetime naturally fulfils the circularity conditions Eqs. 4.9 and 4.10 and is thus circular.

Although no one-to-one correspondence has been established between these specific three photon rings' features and the breaking of circularity, we are only aware of circular spacetimes that show none or one of the three image features, but not all

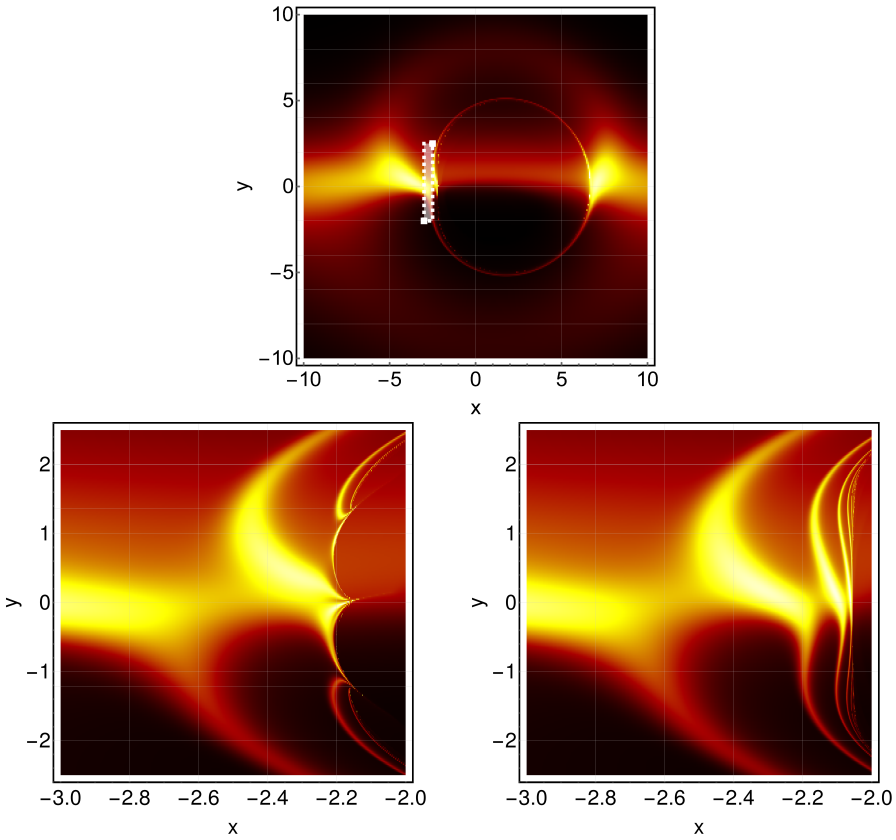

FIGURE 4.11: We show a full image of a non-circular regular BH (top panel) and a detailed view of the prograde image side (spacetime spinning towards the observer) for a non-circular (left panel) and a circular (right panel) regular BH. The white dashed rectangle indicates the (prograde) region in the full image where we focus on in the detailed views. Successive photon rings stack exponentially towards the shadow boundary from left to right in each image. The images are obtained by a numerical ray tracing code developed by A. Held and radiative transfer of a semi-analytical emission model, c.f. [EH21a, Eq. (3.4)]. The image intensity is normalised to the brightest image point. The non-circular and circular spacetimes are given in [DEH22, Eq. 6], with mass functions $M_{\text{non-circular}}(K_{\text{GR}}) = M\, e^{-(\ell_{\text{NP}}^4 K_{\text{GR}}(r,\chi))^{1/6}}$ and $M_{\text{circular}}(K_{\text{GR}}) = M\, e^{-(\ell_{\text{NP}}^4 K_{\text{GR}}(r,0))^{1/6}}$, respectively. We choose a large spin $a = 0.9 G_0 M$ and a near-extremal new-physics scale $\ell_{\text{NP}} = 0.1188\, G_0 M$. All quantities are given in units of $G_0 M$ with M the classical asymptotic BH mass.

three in combination [DEH22]. Thus, the detection of all three photon rings' features in a BH shadow image by future VLBI observation campaigns may indicate that BHs are non-circular or, in other words, that circularity is a principle that characterises BH spacetimes in nature. Moreover, as circularity appears in particular modified gravity theories which deviate perturbatively from GR [Xie+21], observing signatures of non-circularity in photon rings can help ruling out these theories and narrow down the set of theories compatible with observations.

4.2.2 Photon rings' features

Apart from modifying their shape, new physics beyond GR can also impact the structure of photon rings and lead to substantial deviations. The latter may be detectable by future VLBI arrays, provided that several of the following improvements are made [CR+24]:

- the addition of a space-based radio telescope;
- the extension of the current VLBI array with many new sites;
- the increase in sensitivity of all radio telescopes in an extended array;
- the combination of observations at lower and higher frequencies than 230 GHz;
- the use of high-performance super-resolution techniques.

Photon rings in regular BHs are more widely separated than in GR, under the conditions spelt out in [EHJ23], as shown by comparing the first two rows in Fig. 4.12. Regular BHs, reviewed in [Tor22; Bam23; Lan+23], have been proposed as phenomenological models for BH spacetimes beyond GR [Hay06; SV19a; CR+20; MFL21; SV22; CR+23b]. In regular spinning BHs, the classical, central curvature singularity is tamed by upgrading the ADM mass to a mass function which (i) asymptotes to the Kerr ADM mass at infinity and (ii) goes to zero in the BH core. This phenomenological model captures the expected physics of singularity resolution beyond GR, namely a weakening of gravity through quantum fluctuations or appropriate (exotic) matter fields. As gravity is weakened, both the event horizon and the photon shell are shifted inwards with respect to their classical locations. Thus, photons on null geodesics circling a regular BH in its photon shell are pulled further inwards more strongly if they orbit closer to the BH, leading to an increased relative separation between photon rings [EHJ23].[15]

Photon rings can also be more widely separated in parameterised spacetimes beyond Kerr, even if they have the same ADM mass and are embedded in the same accretion disk as Kerr. In those parameterised spacetimes beyond GR, deviations from the Kerr geometry are encoded in general deviation functions whose (new) parameters relate to new-physics effects and spacetime symmetries. Within the parameter space of the circular Konoplya-Rezzolla-Zhidenko (KRZ) parameterisation [KRZ16], there are instances whose photon-ring separation is significantly larger than that of a Kerr BH with the same mass and accretion disk, as shown in the third row of Fig. 4.12. The fact that it is now the absolute separation between photon rings that increases and not the relative one, as for regular BHs discussed above, originates from differences in the construction of both underlying spacetimes. Whereas regular BHs discussed above are constructed and regularised through a mass function encoding a weakening of gravity, a physical phenomenon, the KRZ parameterisation contains generic deviation parameters which can be tuned to produce desirable results, e.g. enlarging the photon shell.

Finally, horizonless spacetimes can feature a more complex photon ring structure than the two previous BH spacetime types. Indeed, the absence of an event horizon

[15] We distinguish *absolute separation* from *relative separation* of photon rings. At a fixed ADM mass, the shadow boundary of such regular BHs has a smaller diameter than of a Kerr BH, and so the *absolute separation* of photon rings is not necessarily larger than in Kerr. However, if one picks a different (larger) ADM mass so that the shadow boundary has the same diameter, then also the *absolute separation* of photon rings increases. Hence, it is the *relative separation*, i.e. the separation normalised to the shadow boundary diameter, that always increases.

allows for a secondary (inner) set of photon rings labelled by another integer $m > 0$. There is an infinite number of secondary photon rings in the presence of a photon shell, arising from strongly lensed photons on trajectories approaching the photon shell from the inside. This can happen in regular black-hole spacetimes at supercritical spin parameter or supercritical new-physics scale or naked singularities [Sha+19; Gyu+20; ORGG22; EH23; EHJ23; EGH23; Gue+22a; Gue+22b] or in horizonless spacetimes with a fully reflective surface [CRCY22]. In the absence of a photon shell, only a finite number of secondary rings are formed [EHJ23]. Additionally, the $n = 1$ and $m = 1$ can be well separated and have comparable flux densities, c.f. the bottom row of Fig. 4.12 or a perfectly reflective surface in [CRCY22].

4.3 Disentangling photon rings with future radio telescope arrays

We have shown in Subsec. 4.1.4 that high-order photon rings are a clean probe of the spacetime geometry photons travel on, and in Subsec. 4.2.2 that they could be smoking guns of new physics beyond GR. Indeed, we highlighted in Subsec. 4.2.2 that, beyond GR, images containing two or more photon rings that are widely separated and with comparable flux densities can occur. These features motivate a study on the ability of current and future VLBI arrays to detect two such rings, irrespective of the theory beyond GR. We move one step forward in this direction in [CR+24] by considering a simple geometric model of the flux density in two thin rings. In this section, we thus assess whether we can disentangle two photon rings with current and future radio telescope arrays in synthetic images using simple geometric models. This is the scope of our work [CR+24].

4.3.1 Synthetic data and geometric ring models

Images of BHs are reconstructed from complex visibility data, which is directly related to the Fourier transform of the flux density collected by VLBI radio telescopes. Each pair of radio telescopes defines (a series of) baselines, to which discrete, complex visibilities are associated. We define our geometric model of two thin rings in the image plane and map it to the Fourier plane, denoting it by *synthetic data*.

Our synthetic data depends on 6 parameters: 4 are left free and 2 are held fixed at values inspired by the VLBI observations of M87* released by the EHT collaboration [Aki+19a].
The first parameter entering our model is the total flux density $F_{\rm tot}$ in the image, which is kept fixed to $F_{\rm tot} = 0.7\,$Jy inspired by the VLBI observation of M87* [Aki+19d].
The second parameter ΔF is the (dimensionless) relative flux density between the two thin rings, i.e.

$$\Delta F = \frac{F_2}{F_1}, \tag{4.11}$$

where F_i is the flux density in the ith-ring such that $F_{\rm tot} = F_1 + F_2$. The respective flux densities are thus

$$F_1 = \frac{F_{\rm tot}}{1+\Delta F}, \quad F_2 = \frac{F_{\rm tot}}{1+1/\Delta F}. \tag{4.12}$$

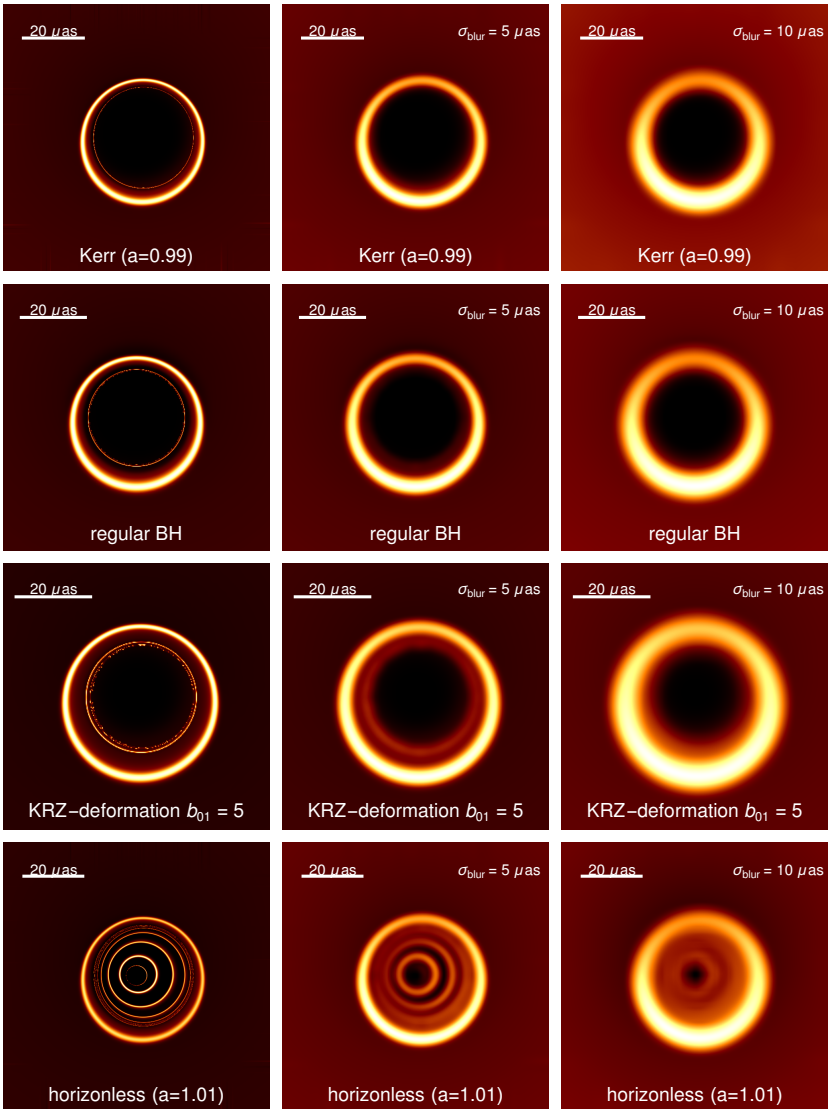

FIGURE 4.12: For each type of spacetimes discussed in the main text, we show three shadow images generated in [DE24], from the ideal image (left column) to the ideal image along with a Gaussian blurring of variance $\sigma_{\rm blur} = 5\,\mu$as (middle column) and finally with a Gaussian blurring of variance $\sigma_{\rm blur} = 10\,\mu$as (right column). As FWHM $= 2\sqrt{2\ln 2}\,\sigma_{\rm blur}$, the variances of the Gaussian blurrings correspond to FWHMs of $\sim 12\,\mu$as and $\sim 24\,\mu$as (within the current nominal EHT resolution), respectively. Top row: Kerr BH with spin $a = 0.99\,G_0M$. The image is generated with a disk model as in [EH23, slow falloff model in Tab. 1]. Second row: regular BH with exponential falloff function, see e.g. [EH21b, Eq. (3)]. Third row: circular [Pap66] deformation in the KRZ parameterization [KRZ16] of a Kerr BH with spin $a = 0.9\,G_0M$ and a single deformation parameter $b_{01} = 5$. Bottom row: marginally overspun (with $a = 1.01\,G_0M$) and thus horizonless regular spacetime, cf. [EGH23].

The four other parameters characterise the geometry of the rings in the image. The

outer ring is kept at a fixed diameter $d_1 = 42\,\mu$as[16] which matches the inferred diameter of the bright ring feature in the image of M87* [Aki+19a].[17] We do not vary the widths $\omega_{1,2}$ of the two rings but keep them small, to match the expectation of thin (higher-order) photon rings, which both holds in GR (c.f. first row in Fig. 4.12) and beyond GR (c.f. all other rows in Fig. 4.12). Finally, we implicitly vary the diameter of the second/inner ring d_2 through the variation of the separation

$$s = \frac{d_1 - d_2}{2} \tag{4.13}$$

between the two rings. The resulting synthetic data is thus radially symmetric which, although producing a good approximation of spherically symmetric spacetimes (apart from the brightness asymmetry in the ring, which we do not account for in the present study), does not accurately describe highly spinning spacetimes in which the shadow boundary and the photon rings flatten on the prograde side.

From the four motivation examples shown in Fig. 4.12, it appears that the relative flux density ΔF and the separation s are the most relevant parameters to assess the detectability of two rings, at least in the thin-ring limit that we adopt. We thus mark the location of all four motivating examples of spacetimes on a $(s, \Delta F)$ plane in Fig. 4.13.

To generate synthetic data, the above 6 parameters enter a flat flux density profile for each of the two radially symmetric rings. The flat flux density profiles are defined in terms of an auxiliary function

$$\mu(r; d, \omega) = \frac{1}{\pi d \omega} \Theta\left(\frac{d+\omega}{2} - r\right) \Theta\left(r - \frac{d-\omega}{2}\right), \tag{4.14}$$

normalised such that

$$\int_0^\infty dr\, 2\pi r \int_0^{2\pi} d\theta\, \mu(r; d, \omega) = 1. \tag{4.15}$$

The resulting total flux density profile combines two flat rings given by a function of the radius in the image plane as

$$F_{\text{Cresc}}(r) = \frac{F_{\text{tot}}}{1+\Delta F} \mu(r; d_1, \omega_1) + \frac{F_{\text{tot}}}{1+1/\Delta F} \mu(r; d_1 - 2s, \omega_2). \tag{4.16}$$

The subscript refers to the crescent profile introduced in [KD13] on which the flat flux density profile is based. Note that we parameterise the flux density profile in terms of the total flux density in the image and the total flux density in each ring, instead of peak flux densities. While our parameterisation is less simple than one using peak flux densities, it is closer to the EHT observations which are sensitive to the total flux density in the image. The prefactors correspond to the total flux density in each ring, i.e. $F_{1,2}$ defined in Eq. 4.12, such that

$$\int_0^\infty dr\, 2\pi r \int_0^{2\pi} d\theta F_{\text{Cresc}}(r) = F_{\text{tot}}. \tag{4.17}$$

[16] Although lengths, such as diameters, are usually given in the SI unit of metres, here we adopt astronomical conventions and explicitly write them in angular units of μas. This owes to the fact that astrophysical objects, e.g. supermassive black holes, are located far away from us at a distance D such that their characteristic lengths d subtend small angles $\theta \approx \tan\theta = \frac{d}{D}$ expressed in μas.

[17] We use outer/1 and inner/2 interchangeably.

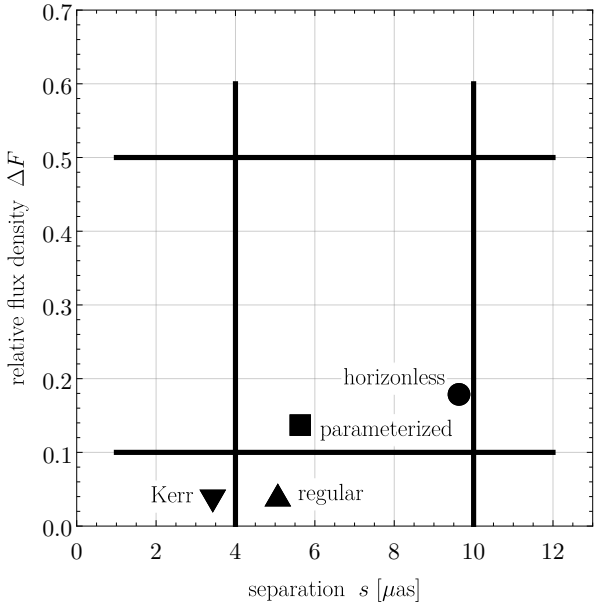

FIGURE 4.13: We visualise the locations of our four motivating examples in the $(s, \Delta F)$ projection of the 2-ring model's parameter space: the different markers correspond to the expected parameter values of the four spacetimes in Fig. 4.12, i.e. Kerr, regular black holes, parametric deformations and horizonless objects, respectively. The data points are obtained by minimising the divergence between a Gaussian two-ring model, see App. A.1, and the obtained synthetic image. The black lines indicate lines along which we perform our analysis in Subsec. 4.3.4.

With the total flat or crescent profile at hand, we produce a synthetic image by discretising it on a grid. We define the image plane with Cartesian coordinates (x, y), where x refers to the relative right ascension (rRA, in μas) and y to the relative declination (rDEC, in μas), in which the origin $(x_0, y_0) = (0, 0)$ matches the centre of our two thin rings. We then construct synthetic image data by discretising the flat flux density profile into an effective 2D square array of pixels $(x_k, y_k, F(x_k, y_k))$, where the index k runs from 1 to the square of the number of pixels N_{pix}^2. Hence, each pixel in our effective square array carries a flux density $F(x_k, y_k)$.
The Field of View (FOV, in μas) of our image is determined by the spans of the x-axis (y-axis) which are symmetric, equal and centred on $x_0 = 0$ ($y_0 = 0$ respectively). It corresponds to

$$\text{FOV} = (N_{\text{pix}} - 1) \cdot \delta\theta, \tag{4.18}$$

where $\delta\theta$ is the pixel "length" (in μas). As a result, our synthetic data are entirely determined by the crescent profile in Eq. 4.16, which has an analytically known form in the Fourier plane [KD13]. This naturally provides us with an analytical fitting function in the Fourier plane, once the synthetic data are passed on to simulations with chosen VLBI arrays.

We do not consider other total flux density profiles in our analysis because we focus on the thin ring limit in which the widths of the two rings are small compared to their diameters $\omega_i \ll d_i$, and hence the type of radially symmetric profile does not matter, c.f. Fig. A.1. Finally, we emphasise that we do not account for the broad, diffuse direct emission from the accretion disk and discuss this limitation in the conclusions in Subsec. 4.4.1.

4.3.2 Visibilities in the Fourier plane

The complex visibility is defined as the Fourier transform of any continuous intensity profile in the image plane

$$V(u,v) = \int\int dx\, dy\, I(x,y)\, e^{-\frac{2\pi i(ux+vy)}{\lambda}}, \tag{4.19}$$

where λ is the wavelength of observation, (x,y) are angular coordinates on the sky, (u,v) are projected (on the plane orthogonal to the direction of the source) baseline coordinates in the Fourier plane. $I(x,y)$, in units of $10^{26}\,\mathrm{Jy}\cdot\mathrm{sr}^{-1}$, is the continuous intensity profile related to the flux density profile by a dimensionless factor of solid angle in steradian (sr), see below. It is standard to express the projected baselines (u,v) in units of $10^9\cdot\lambda$ (i.e. Gλ).

In practice, a VLBI array does not sample $V(u,v)$ continuously due to its sparse uv-coverage. Thus we define the discrete visibility counterpart as

$$V_{ij} = V(u_{ij}, v_{ij}), \tag{4.20}$$

where (u_{ij}, v_{ij}) is the 2D vector of projected baselines associated with stations i and j in the array.

Calculating the discrete visibility V_{ij} analytically is only possible for particularly simple choices of synthetic data such as the crescent model [KD13] on which our fitting flux density profile F_{Cresc} is based. The discrete visibility $V_{ij,\,\mathrm{Cresc}}$ of a single disk of radius R is based on the Fourier transform of a constant intensity I_0 in the disk, namely

$$V_d(k, F_0, R) = \pi R^2 I_0\, \frac{2J_1(k\,R)}{k\,R}, \tag{4.21}$$

where J_1 is the Bessel function of the first kind of order 1. Because a disk produces a radially symmetric flux density in the image plane, the resulting Fourier transform does not depend on u and v separately, but only through the combination

$$k = \frac{2\pi}{\lambda}\sqrt{u^2+v^2}. \tag{4.22}$$

Based on Eq. 4.21, [KD13] explicitly derives the visibility amplitude for a 1-ring, flat flux density profile, by subtracting the visibility amplitude of two disks with outer radius R_{outer} and inner radius R_{inner} as

$$\begin{aligned} V(k) &= \frac{2\pi I_0}{k}\Big[R_{\mathrm{outer}}J_1(kR_{\mathrm{outer}}) - R_{\mathrm{inner}}J_1(kR_{\mathrm{inner}})\Big] \\ &= \frac{2F_0}{k\left(R_{\mathrm{outer}}^2 - R_{\mathrm{inner}}^2\right)}\Big[R_{\mathrm{outer}}J_1(kR_{\mathrm{outer}}) - R_{\mathrm{inner}}J_1(kR_{\mathrm{inner}})\Big]\,. \end{aligned} \tag{4.23}$$

The complex visibilities for the 2-ring model are obtained by adding two visibilities of the type Eq. 4.23, resulting in

$$\begin{aligned} V(k) &= V_1(k) + V_2(k) \\ &= \frac{2\pi I_1}{k}\Big[R_{\mathrm{outer},1}J_1(kR_{\mathrm{outer},1}) - R_{\mathrm{inner},1}J_1(kR_{\mathrm{inner},1})\Big] \\ &\quad + \frac{2\pi I_2}{k}\Big[R_{\mathrm{outer},2}J_1(kR_{\mathrm{outer},2}) - R_{\mathrm{inner},2}J_1(kR_{\mathrm{inner},2})\Big]. \end{aligned} \tag{4.24}$$

where the intensities are related to the flux densities used in the previous section as $I_j = F_j/\pi(R^2_{\text{outer},j} - R^2_{\text{inner},j})$ and the radii are expressed in μas (c.f. Footnote 16) in terms of the physical parameters as

$$\begin{aligned} R_{\text{outer},1} &= \frac{d_1 + \omega_1}{2}, & R_{\text{inner},1} &= \frac{d_1 - \omega_1}{2}, \\ R_{\text{outer},2} &= \frac{d_1 - 2s + \omega_2}{2}, & R_{\text{inner},2} &= \frac{d_1 - 2s - \omega_2}{2}. \end{aligned} \tag{4.25}$$

Since we restrict our analysis to the thin-ring regime, we can first gain some intuition from the strict limit of infinitely thin rings in which the complex visibility is [Joh+20]

$$V_{\text{thin rings}}(k) = F_1\, J_0\left(\frac{k\, d_1}{2}\right) + F_2\, J_0\left(\frac{k\, d_2}{2}\right). \tag{4.26}$$

For large real argument, $x \equiv k\, d_{1,2} \gg 3/4$, the 0^{th}-order Bessel function of the first kind J_0 can be expanded as

$$J_0(x) \simeq \sqrt{\frac{2}{\pi x}}\left[\cos\left(x - \frac{\pi}{4}\right) + \mathcal{O}(|x|^{-1})\right]. \tag{4.27}$$

For one infinitely thin ring, the visibility amplitude corresponds to a damped oscillation whose period is set by the inverse diameter $1/d_{1,2}$. For two infinitely thin rings, where the separation s is not much smaller than the diameter (cf. Fig. 4.13), two damped oscillations are superposed.

When the two infinitely thin rings have comparable flux densities, the zeros of the total visibility amplitude can lie at rather distinct locations from those of the two individual rings, see the top panel in Fig. 4.14. In such a case, it is easier to tell the two rings apart. However, for some more challenging cases, e.g. the $n = 1$ and $n = 2$ photon rings with $\Delta F = 0.1$ in Fig. 4.13, the outer (e.g. $n = 1$) ring carries the largest part of the flux density and thus dominates the visibility amplitude, as shown in the middle panel in Fig. 4.14. In that case, the second ring only leads to a slight modulation of the overall visibility amplitude and shifts the locations of the zeros somewhat, but cannot fully remove them (at least in the range of k that we consider and for ring diameters which are of the same order of magnitude as we consider here), see the bottom panel in Fig. 4.14.

So far, we only discussed idealised situations in which the visibility amplitude data was either continuous or discrete but dense, and where the baselines were not particularly constrained. However, data from an actual observation with a VLBI array such as the EHT differs from the above idealised cases in several ways. Firstly, the combination of limited baselines (e.g. by the Earth) and observing frequency (by the atmosphere and source) sets an effective cutoff on the sampling of the complex visibilities, i.e. it limits the maximal resolvable uv-baseline. For any Earth-based VLBI campaign, the baseline is necessarily limited by Earth's diameter and the frequency by atmospheric scattering, see e.g. [Aki+19b]. This constrains us to consider $k \lesssim 8.5\,\text{G}\lambda$ at $\lambda = 1.3\,\text{mm}$. Secondly, the finite number of telescopes forming the array leads to a sparse sampling of the complex discrete visibility. Nonetheless, the projected baselines change during an observation campaign thanks to the rotation of the Earth. As a result, several data points in the uv-plane can be obtained from a single pair of telescopes, improving the uv-coverage. Finally, the finite sensitivity of each telescope causes additional *thermal noise* and *systematic errors* in each observational data point

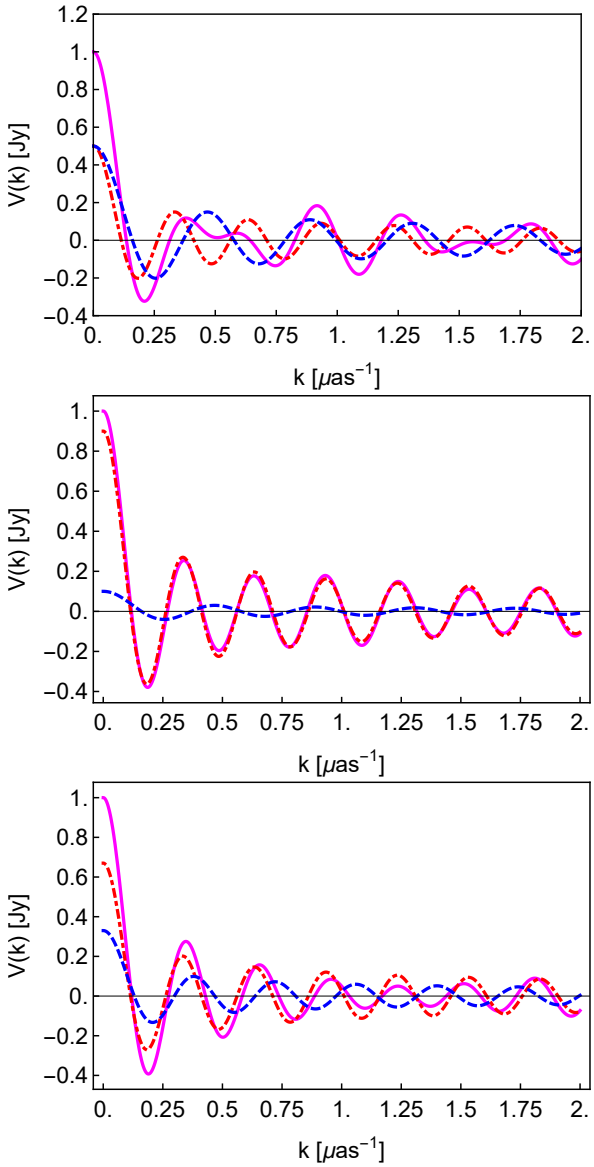

FIGURE 4.14: We show the analytic expressions of the visibility amplitude for infinitely thin rings with $F_{\rm tot} = 1\,$Jy, see Eq. 4.26, for three relative flux densities $\Delta F = 1$ (top panel), $\Delta F = \frac{1}{9} \approx 0.1$ (middle panel) and $\Delta F = \frac{3}{7} \approx 0.4$ (lower panel). An outer infinitely thin ring is represented by a red dashdotted line, an inner infinitely thin ring by a blue dashed line and the combination of both by a magenta line.

which are encoded in the SEFD (see Eq. 4.3). As a result, the lower the SEFD, the smaller the respective thermal noise. VLBI arrays also yield systematic errors that can be factorised as frequency- and time-dependent multiplicative station-based "gains". Under some assumptions, we can get rid of those systematic gains using closure amplitudes, see Subsec. 4.3.5.

To capture the effects departing from the ideal scenario and thereby gain first quantitative insight into the detectability of multi-ring features, we: (i) take the theoretical model defined above (i.e. the total flat flux density profile Eq. 4.16 and its corresponding visibility Eq. 4.24), and (ii) generate synthetic visibility data that would be obtained by a given telescope array. To do so, we use the `ehtimaging` toolkit

[Cha22], cf. also [Cha+18] for further details of the capabilities of `ehtimaging`. We summarise the set of radio telescope arrays used in our exploratory study in Tab. 4.1. The detailed tables of telescope sites and SEFD values required to reproduce our results are provided in App. A.3.

Arrays	Total number of sites	Frequencies $\nu_{\rm obs}$ (GHz)	SEFD values (Jy) of the new sites[a]
EHT 2022	11	230	See values in Tab. A.1
EHT 2022	11	230 & 345	See values in Tab. A.1
ngEHT-230-low-SEFD	19	230	74 (low; ALMA value)[b]
ngEHT-230-high-SEFD	19	230	19300 (high; SPT value)[c]
ngEHT-dualfreq-low-SEFD	19	230 & 345	250 (low; ALMA value)[b]
ngEHT-dualfreq-high-SEFD	19	230 & 345	44970 (high; KPNO value)[c]
ngEHT-230-space	$19+1$[d]	230	74 (low; ALMA value) & 36600 (space)[e]
ngEHT-dualfreq-space	$19+1$[d]	230 & 345	250 (low; ALMA value) & 56000 (space)[e]

[a] The new sites are defined as all the Earth-based sites added to the EHT 2022 array.
[b] See the detail of all SEFD values in Tab. A.2.
[c] See the detail of all SEFD values in Tab. A.3.
[d] The "+1" refers to the space-based site.
[e] SEFD values for the space-based site at 230 and 345 GHz are estimated from Tab. 1 in [Roe+19].

TABLE 4.1: We tabulate the specifications of different VLBI arrays used in the complex-visibility analysis. The number of sites determines how sparse the sampling of the Fourier plane is. The frequency influences the maximum uv-distance that is effectively resolved. The SEFD is a measure of the sensitivity of each telescope, hence the quality of single data points in the Fourier plane: high SEFD values thus correspond to worse data quality. The labels "low" and "high" in the arrays refer to the SEFD value of the new sites. More details on the array specifications are given in App. A.3.

The first radio telescope array we consider is the one used in the 2022 observation campaign of the EHT, hence the name EHT 2022. It includes 11 radio telescopes operating at 230 GHz. However, as the SPT cannot "see" M87* due to the sky-location of the latter, only 10 radio telescopes effectively contribute to acquire data. Next, we consider upgrades of this array by adding 8 new telescope sites that are discussed as part of the ngEHT proposal [Joh+23; Doe+23]. Finally, we also include a single space-based telescope (ngEHT-space) to quantify the potential gain in detectability as compared to purely Earth-based observation campaigns. In addition to alter the number of sites and their locations, we also vary:

- the observation frequency from the current 230 GHz to 345 GHz, as proposed by the ngEHT initiative [Joh+23], the BHEX mission [Joh+24] and planned for any upgrade of the EHT;
- the SEFD values for the additional ngEHT sites (those of the EHT 2022 array are known, c.f. [Aki+19b; Bro] and App. A.3). To investigate the effect of varying SEFD values in the additional ngEHT sites, we distinguish between one set of lower and one set of higher SEFD values, dubed low-SEFD and high-SEFD, respectively. For the low-SEFD case, we assume that all future ngEHT sites can reach the SEFD value of ALMA, the most sensitive site in the EHT 2022 array. For the high-SEFD case, we assume that the future ngEHT sites are limited to the SEFD value of SPT/KP, the least sensitive sites in the EHT 2022 array.

With this selection of reference arrays at hand, we use `ehtimaging` to generate synthetic data for each set of model parameters corresponding to the 2-ring model specified in Subsec. 4.3.1. In particular, we perform scans along each of the four rays indicated in the $(s, \Delta F)$ plane in Fig. 4.13.

4.3.3 Disentanglement's method

To decide about the detectability of the second ring, we fit the synthetic dataset (i.e. the visibility amplitude in Fourier space) with both a 1-ring and a 2-ring model. To perform the fits of the visibility amplitude, we use the `lmfit` python package [New+16] which minimises the least-square residuals between data points and fitting function while taking into account the error budget at each data point. With the 1-ring and 2-ring fits at hand, we perform a statistical test to quantify whether the 2-ring fit is favoured over the 1-ring fit.

The non-linear nature of the problem, in the sense that a fit to visibility amplitude data cannot be written as in [ASHM10, Eq. 4], makes using a reduced chi-squared test questionable [ASHM10]. Alternatively, we choose to determine the respective minimised residuals and perform a 2-sample Kolmogorov-Smirnov (KS) test. The latter returns a p-value which, when compared to the set significance level α, quantifies how confidently one can exclude the hypothesis that both sets of residuals are drawn from the same probability distribution. In other words, the comparison of the p-value with α quantifies with how much confidence given by $100 \cdot (1-\alpha)\%$ the '1-ring hypothesis' can be rejected. For instance, a $p \leq \alpha = 0.01 = 1\%$ rejects the '1-ring hypothesis' with 99% confidence. Two examples are shown in Fig. 4.15 displaying the synthetic data (denoted by black crosses), together with the best 1-ring (in red) and 2-ring (in blue) fits. In the left panel, the p-value test states that the two models cannot be distinguished. In the right panel, the data at the largest accessible uv-distances sufficiently differ for the two fits to be able to distinguish them. In particular, the second zeros of the 1-ring and 2-ring (visibility) fits are distinct, while the first zeros match.

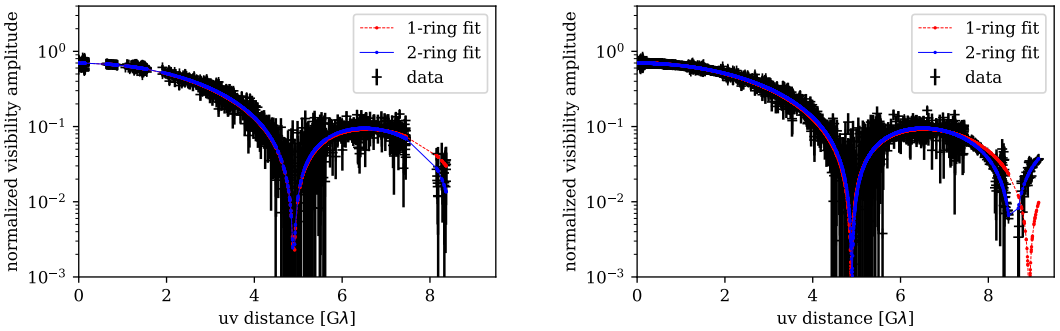

FIGURE 4.15: We show two examples of fits corresponding to the $s = 12\,\mu$as ray in the right-hand upper panel in Fig. 4.16. The left-hand panel shows simulated data taken with the EHT 2022-230 array and finds no detection of the presence of a second ring. The right-hand panel shows simulated data taken with the ngEHT-230-low-SEFD array and finds a detection of the presence of a second ring.

4.3.4 Detecting new physics at sub-resolution scale in visibilities

Motivated by theoretical studies beyond GR, where photon rings are typically thin just as in GR, see e.g. [Ayz+23; EHJ23; Sta+23], we focus on synthetic data in the limit of relatively thin rings. Specifically, we now set $\omega_1 = 2\,\mu$as and $\omega_2 = 1\,\mu$as in all simulated observations but expect that our results do not depend much on this exact

choice and would remain similar for other values of $\omega_{1,2}$, as long as $\omega_{1,2} \ll d$.

One might worry that using the same fitting profile that is also used to generate the synthetic data could compromise the results. However, in the thin-ring limit, changes in the flux density profile within a ring do not affect the (non-)detectability of the second ring, because widths of $1 - 2\,\mu$as are sufficiently far below the resolution limit of the VLBI arrays we investigate (except when a space-based station is included). Thus, the simplest fitting profile, i.e. a flat flux density within the rings, described by the crescent model in Eq. 4.16, suffices. To further strengthen this point, we have explicitly checked in App. A.1 that using e.g. a Gaussian profile to generate synthetic data does not alter our conclusions regarding the (non-)detectability, as shown in Fig. A.1.
Thus, the two remaining parameters which determine whether or not a 2-ring model can be distinguished from a 1-ring model indeed are the relative flux density ΔF and the separation s between the rings; these two span our 2D parameter space. We perform four scans through this parameter space, as indicated in Fig. 4.13, which are motivated by the new-physics cases discussed in Sec. 4.3 and whose shadow images were plotted in Fig. 4.12. For each scan, we consider the 8 different array configurations specified in Tab. 4.1. The results of the p-value test are presented in Fig. 4.16.

First, we observe that the 2022 EHT configuration is only sensitive to the presence of a second ring if the separation between the two rings is larger than $\sim 12\,\mu$as, which roughly corresponds to the expected resolution for this array configuration.[18]

Second, we find that a ring separation of $\sim 5\,\mu$as could be detectable with an Earth-based array; this, however, requires high sensitivities and is therefore only reachable with an optimistic ngEHT array design (c.f. ngEHT-low, in which the SEFD is very low, thus the sensitivity is very high in all telescopes added beyond the 2022 array). This is an important result because some of the motivating new-physics cases have separations which are of the order of $\sim 5\,\mu$as. It suggests that – if the results from our idealised study extended to simulated observations of beyond-GR spacetimes – a ground-based array design with very low SEFD values could potentially probe spacetimes beyond GR. As an alternative, we achieve similar results when a space-based telescope (again with low SEFD) is added.

Third, we find an interplay between separation and relative flux: at higher values of the relative flux density, the threshold in detecting a second ring is lower, at least for the less advanced array configurations (cf. left and right upper panels in Fig. 4.16). This is as expected: for less sensitive arrays, even structures separated further than the nominal resolution cannot be resolved if the total flux density in one of them is too low.

Fourth, we find that parameter scans at fixed separation and increasing relative flux density show a somewhat surprising result: at some low value of relative flux density, there is a detection threshold at which the p-value drops significantly below 10^{-3} or even 10^{-5}. At higher values of the relative flux density, the p-value increases again, i.e. it becomes more difficult to distinguish the 1- and 2-ring models. The reason lies in the fact that at relative flux densities $\Delta F \approx 1$, the visibility amplitude for low baselines k is nearly degenerate with that of a 1-ring model with a diameter that is roughly the average of the diameters of the two rings. This degeneracy can be lifted once higher baselines k are reached, which is achievable with a space-based

[18] The nominal resolution is well approximated by the Rayleigh criterion in Eq. 4.2. This works out to 25 μas at 230 GHz and 16 μas at 345 GHz. These angular resolutions can be reduced by a factor of roughly 2 by using regularised maximum likelihood imaging methods, see section 2.1 in [Aki+19b].

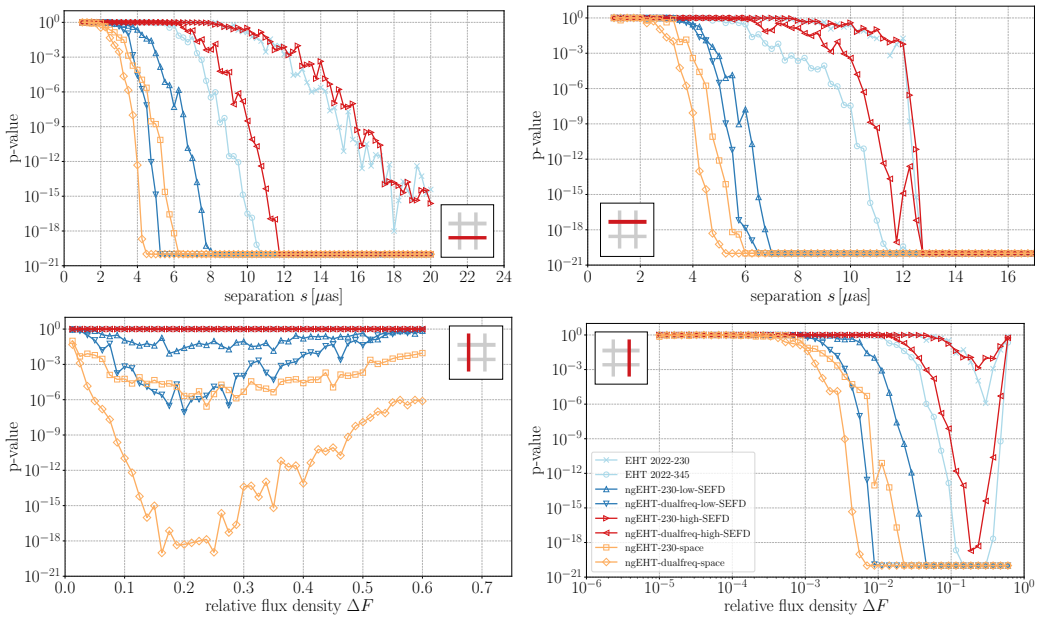

FIGURE 4.16: We show the 2-ring detectability (according to the p-value test, cf. Subsec. 4.3.3) projected onto the four rays in the $(s, \Delta F)$ plane, cf. Fig. 4.13. A transition of the p-value from (close to) one to (close to) zero indicates the transition from non-detectable to detectable cases, see main text. For visual purposes, we have added a p-value floor of 10^{-20} to all data points. The different lines therefore indicate the varying detectability thresholds that we find for various arrays as in Tab. 4.1. In all cases, we focus on the thin-ring limit, i.e., the remaining 2-ring parameters are chosen as $\omega_1 = 2\,\mu$as and $\omega_2 = 1\,\mu$as. Moreover, we generate and fit the data with a crescent profile, i.e., the conducted p-value test implicitly assumes perfect knowledge about the ring profile. No constraints, especially on the widths, have been added. The inset hash shows the ray along which we perform the scan, as in Fig. 4.13.

array. The lower left panel in Fig. 4.16 highlights that only the space-based array confidently detects the presence of a second ring at the highest values of relative flux density that we consider.

This result motivates the use of super-resolution techniques, which have been pioneered for M87* in [Bro+22b] and which we here implement as a constraint on the width of the rings.

Photon rings are typically thin compared to the shadow diameter, both in and beyond GR. To fully demonstrate the power of super-resolution techniques in our simplified setting, we now include a constraint on the width of the rings $\omega_{1,2} \leq 2\,\mu$as in the fits as a prior in our reconstruction and call it "super-resolution technique". We then investigate how strong such a prior has to be to significantly improve the detectability of a second ring feature, especially for high-SEFD arrays. The width's prior brings the detection threshold for the separation between the two rings to below $2\,\mu$as for the better-performing arrays and $3-4\,\mu$as for the worse-performing arrays, cf. Fig. 4.17. This highlights the presence of a nontrivial interplay between i) the scale imposed by the super-resolution constraint, ii) the nominal resolution, and iii) the sensitivity.

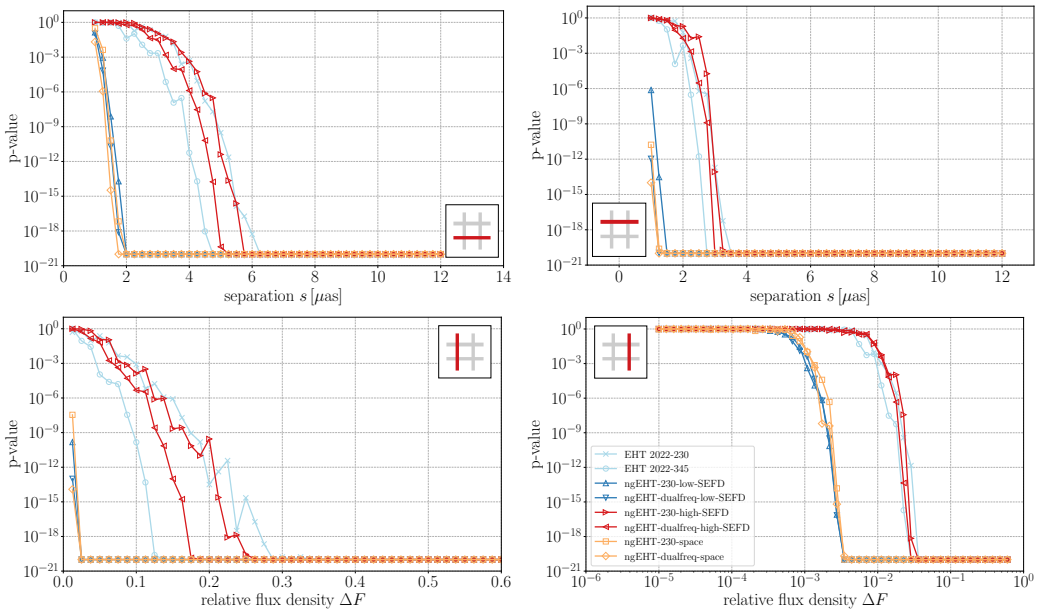

FIGURE 4.17: We show the 2-ring detectability (according to the p-value test, cf. Subsec. 4.3.3) projected onto the four rays in the $(s, \Delta F)$ plane, cf. Fig. 4.13. A strong constraint on the widths $\omega_{1,2} \leq 2\,\mu$as has been added in the fits.

Overall, these results suggest that even current Earth-based arrays can distinguish a 2-ring fit from a 1-ring fit at values of s and ΔF that are relevant to existing new-physics cases, provided that super-resolution techniques (such as a wdith's prior) are used. Within the class of theories that produce thin photon rings, super-resolution techniques can distinguish between one and two rings or, in other words, show that the presence of a second ring is a better fit to the data than just a single ring at sufficiently large separation. We caution that this result is not sufficient to rule out new-physics cases with these parameters, because we only compare the performances of a simple 1-ring and a simple 2-ring model fit and do not perform a more general fit to our simulated data. It is, however, a result that motivates an in-depth future study that systematically simulates images of such new-physics spacetimes and analyses the simulated data with: (i) a larger class of fits and/or (ii) more general image-reconstruction and data-analysis models. We also caution that restricting to photon rings, we neglected any (direct) emission coming from the accretion disk, which dominates the flux density in EHT observation campaigns.

4.3.5 Closure quantities

Thermal noise and systematic uncertainties impact visibility amplitudes, but can be (partially) removed by using closure quantities. These are therefore important EHT data products [Aki+19d; Aki+22c; Cha+18; TMS17; LG21]. We review closure quantities and explore how the 1-ring and 2-ring flux density profiles discussed above look like in terms of these variables.

For each pair of telescopes, labelled by indices i, j, there is actually not a single notion of visibility, but two: an idealised visibility amplitude $V_{i,j}$ and its measured counterpart $\hat{V}_{i,j}$. The measurement is affected by complex gains g_i and thermal noise

ϵ_{ij} as

$$\hat{V}_{ij} = g_i g_j^* V_{ij} + \epsilon_{ij}. \tag{4.28}$$

Here, ϵ_{ij} is a circularly symmetric (invariant under rotations in the complex plane [Lap17]), complex, Gaussian random variable with zero mean and variance σ_{ij} (determined by the radiometer equation [TMS17; Cha+18]) describing thermal noise. g_i are station-based effects including limitations imposed by constituent interferometer elements and atmospheric turbulence. The complex gains g_i enter the observed visibility amplitude data as multiplicative factors and constitute the dominant source of systematic errors.

In contrast to thermal noise, systematic errors are difficult to calibrate: complex gains may be determined from observations of calibration sources for which the visibilities are known, but it is often not practicable in VLBI arrays. Complex closure quantities are constructed to remove station gains from the data as much as possible, and split into closure amplitudes – first defined in [TCL60] – and closure phases – first defined in [Jen58]. They were first applied to the analysis of radio emission from quasars in [Rog+74; Rea+80], later in VLBI in [Doe+01; Fis+16; Cha+18], and have been generalised in [Lan91; BP20; SNT22; TNS22; ARMV23; Mü24].

We split the complex measured visibility $\hat{V}_{ij}$ into its amplitude $|\hat{V}_{ij}|$ and phase. Closure phases vanish identically for symmetric sources (e.g., [PMM03]), and are therefore not useful for the analysis of the idealised synthetic flux density profiles we consider, thus we solely focus on closure amplitudes.

The variable $|\hat{V}_{ij}|$ is statistically distributed according to a Rice distribution[19]

$$\text{Rice}\left(|g_i||g_j||V_{ij}|, \sigma_{ij}\right) \tag{4.29}$$

as a direct consequence of Eq. 4.28. Its expectation value is given by

$$\langle|\hat{V}_{ij}|\rangle = |g_i| \cdot |g_j| \cdot |V_{ij}| \cdot \left[1 + \mathcal{O}(\sigma_{ij}^2)\right]. \tag{4.30}$$

Due to the $\mathcal{O}(\sigma_{ij}^2)$ term, $\langle|\hat{V}_{ij}|\rangle$ is a biased estimator of the parameter $|g_i| \cdot |g_j| \cdot |V_{ij}|$ in the Rice distribution. Thus, one introduces an unbiased estimator

$$A_{ij} = \sqrt{|\hat{V}_{ij}|^2 - \sigma_{ij}^2}. \tag{4.31}$$

Because the expectation values of both $|\hat{V}_{ij}|$ and A_{ij} are proportional to quadratic combinations of gain factors, they are undesirably sensitive to uncertainties in these factors. This sensitivity is removed by defining closure amplitudes. Closure amplitudes Z_{ijkl} can be defined for subsets of 4 stations $\{i, j, k, l\}$ in a VLBI array. The quantities

$$Z_{ijkl}^{(1)} = \frac{A_{ij}A_{kl}}{A_{ik}A_{jl}}, \qquad Z_{ijkl}^{(2)} = \frac{A_{ik}A_{jl}}{A_{il}A_{jk}} \tag{4.32}$$

are independent of gain factors g_i in the absence of thermal noise [MTC91].[20] Their

[19] A Rice distribution is a probability distribution of the magnitude of a circularly-symmetric, bivariate, normal random variable x with a potential non-zero mean μ. Its probability density function is expressed as $f(x|\mu, \sigma) = \frac{x}{\sigma^2} e^{-\frac{x^2+\mu^2}{2\sigma^2}} I_0\left(\frac{x\mu}{\sigma^2}\right)$ in terms of the standard deviation σ and the modified Bessel function of the first kind with order zero I_0.

[20] We can also define $Z_{ijkl}^{(3)} = A_{il}A_{jk}/(A_{ij}A_{kl})$, which does not add new information due to the constraint $Z_{ijkl}^{(1)} Z_{ijkl}^{(2)} Z_{ijkl}^{(3)} = 1$ [TMS17].

corresponding expectation values $\langle Z^{(1)}_{ijkl}\rangle$ and $\langle Z^{(2)}_{ijkl}\rangle$ are only affected by gain factors at subleading order. This is a marked improvement over the visibility amplitude and the main reason behind the use of these variables. As a final step, we take the logarithm of closure amplitudes, which simplifies the propagation of thermal errors [Bla+20; Bro+20].

The disadvantage of closure amplitudes is that, due to their dependence on four stations, they are naturally represented in a five-dimensional space, making their interpretation more involved than, e.g., the visibility amplitude. This is addressed in Subsec. 4.3.6.

To prepare for the interpretation of synthetic data from an (ng)EHT array, we first analyse an idealised setting with a very large, densely populated, even square array. This idealised square array has $N_{\rm st} = M_{\rm st} \times M_{\rm st}$ stations, so that there are two adjustable parameters: the length of the baseline between adjacent corners $L_{\rm max}$ (setting the maximum baseline to $k_{\rm max} = \sqrt{2L_{\rm max}}$), and the number of stations M_{st} on each side of the square array, which determines the density of stations. For any array with $N_{\rm st}$ stations, there are

$$\frac{N_{\rm st}(N_{\rm st}-3)}{2} \tag{4.33}$$

independent quadrangles [TMS17], see for [Bla+20] a derivation, on which we evaluate the closure amplitude. Using the total visibility amplitude $V(k)$ of a total flat flux density profile, defined in Eq. 4.24, and $k_{ij} = \frac{2\pi\sqrt{u_{ij}^2+v_{ij}^2}}{\lambda}$, we have

$$\ln\left(Z^{(1)}_{ijkl}\right) \equiv \ln\left(\frac{A_{ij}A_{kl}}{A_{ik}A_{jl}}\right) \simeq \ln\left(\frac{V(k_{ij})V(k_{kl})}{V(k_{ik})V(k_{jl})}\right). \tag{4.34}$$

This expression is thus indeed independent of the gains and can be evaluated numerically once $L_{\rm max}$ and $M_{\rm st}$ are fixed.

To display the 5D information on logarithmic closure amplitudes, we first represent it as a function of the quadrangle perimeter in the uv-plane, discarding all other information on the distribution of stations in the array, see Fig. 4.18. This type of representation of closure quantities has been used before, e.g. in [Aki+19f; Isb+22]. The only distinguishable pattern in Fig. 4.18 is the existence of periodic peak structures which are, however, somewhat obscured by the representation in terms of quadrangle perimeters. The analytical expressions in Eqs. 4.24 and 4.34 indicate that an oscillatory pattern of divergences is expected due to the presence of Bessel functions inside a logarithm: the zeros of the Bessel functions will induce positive and negative divergences in the logarithmic closure amplitudes. The location of these divergences thus matches the zeros of the Bessel functions and is controlled by the parameters of the crescent model. By isolating the diverging features, we can therefore infer the parameters of the 2-ring model. The complete set of logarithmic closure amplitudes evaluated on the $\frac{N_{st}(N_{st}-3)}{2}$ independent quadrangles contains information about the whole image. However, it is possible to identify and isolate subsets of quadrangles containing information about the oscillatory pattern of divergences in logarithmic closure amplitudes.

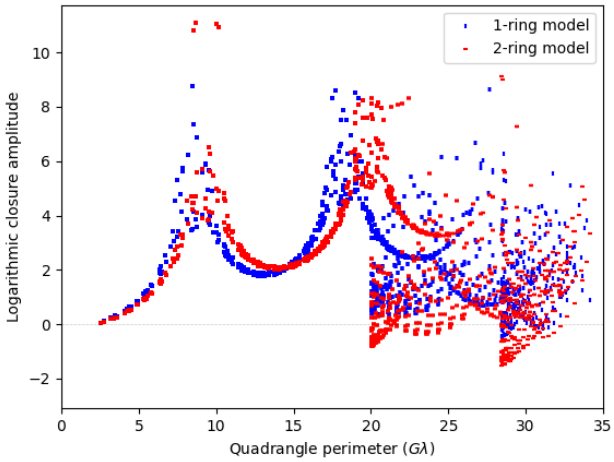

FIGURE 4.18: We show the logarithmic closure amplitudes as a function of the perimeter of the independent quadrangles of a square array with $M_{\rm st} = 20$ stations on each side ($N_{\rm st} = 400$) and a size $L_{\rm max} = 10\,{\rm G}\lambda$. Independent quadrangles are selected following the algorithm in [Bla+20], and perimeters up to 35 Gλ are represented. Closure amplitudes are evaluated with the analytical expressions valid for the 1-ring crescent model with $d_1 = 42\ \mu$as, $\omega_1 = 2\ \mu$as, and a 2-ring model with an additional ring characterised by $s = 5\ \mu$as, $\omega_2 = 0.5\ \mu$as and $\Delta F = 0.5$.

4.3.6 Isolating features in closure quantities with idealised arrays

We present a possible algorithm to identify subsets of quadrangles providing an alternative representation that isolates ring-like features in logarithmic closure amplitudes. This representation is based on slicing the space of closure amplitudes by fixing 3 stations out of 4 and forming quadrangles by varying the remaining $4^{\rm th}$ station. We first introduce this "peak slicing" procedure on purely theoretical grounds, based on the structure of logarithmic closure quantities, before discussing practical implementations of this slicing procedure in Subsec. 4.3.7.

For a clear graphical representation, we introduce 3 "auxiliary stations" which we place outside the previous ideal square array as illustrated in Fig. 4.19. This slicing contains less information than the full set of closure amplitudes, but provides a cleaner representation of the peak periodic structures for comparable data densities, as illustrated in Fig. 4.20. Fig. 4.20 shows a clear interference pattern, with logarithmic closure amplitudes becoming large (formally, divergent) at specific values of the quadrangle perimeter.

The introduction of auxiliary stations outside of the square array also allows us to represent logarithmic closure amplitudes as a function of projected baselines in the uv-plane instead of the quadrangle perimeter, as the remaining stations span a square subset of the uv-plane. In this representation, we associate the value obtained by forming one quadrangle with the 3 auxiliary fixed stations and 1 movable station of the main array to one point in the uv-plane. The result is presented in Fig. 4.21.

Both panels in Fig. 4.21 show the same interference pattern, and also illustrate the existence of both positive and negative divergences of the logarithmic quantities. Going back to the analytical expressions in Eqs. 4.24 and 4.34 allows for a clear

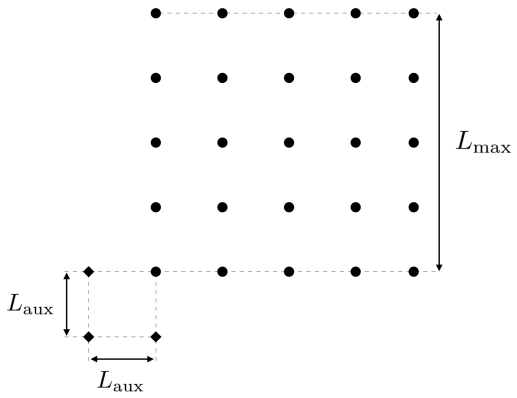

FIGURE 4.19: Schematic representation of the array used in the slicing procedure: a square array with $M_{\rm st} = 5$ stations on each side (circles) and maximum baseline between adjacent corners $L_{\rm max}$, and 3 auxiliary stations (diamonds) with relative separation $L_{\rm aux}$, which we take as $L_{\rm aux} = L_{\rm max}/M_{\rm st}$.

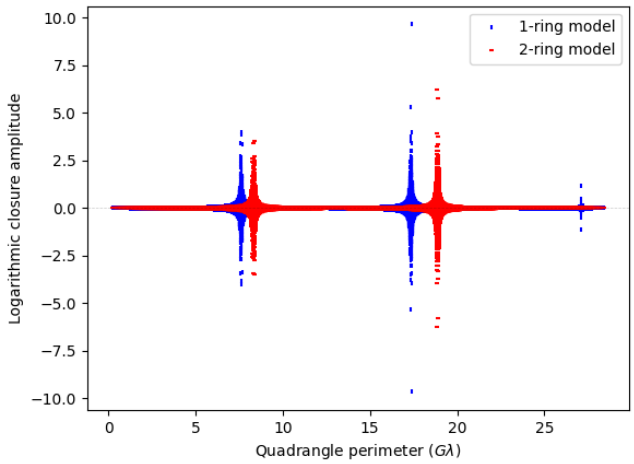

FIGURE 4.20: We show the logarithmic closure amplitudes as a function of the quadrangle perimeter for a square array with $M_{\rm st} = 200$ stations on each side ($N_{\rm st} = 40000$) and a size $L_{\rm max} = 10$ Gλ, and with 3 auxiliary stations with relative baseline $L_{\rm aux} = L_{\rm max}/M_{\rm st}$. Quadrangles are formed holding the 3 auxiliary stations fixed and choosing the $4^{\rm th}$ to be each of the stations in the main array. Closure amplitudes are evaluated with the analytical expressions for the 1-ring crescent model with $d_1 = 42$ μas, $\omega_1 = 2$ μas, and a 2-ring model with an additional ring characterised by $s = 5$ μas, $\omega_2 = 0.5$ μas and $\Delta F = 0.5$. The 1- and 2-ring models become more distinguishable for larger quadrangle perimeters (baselines), as expected from the fact that larger baselines allow for the detection of smaller features.

interpretation of these features. As 3 of the stations forming quadrangles stay fixed, e.g. $\{i, j, k\}$, there are only 2 baselines, namely k_{kl} and k_{jl}, that change as different stations in the main array are chosen for the $4^{\rm th}$ station l. Depending on the position of the $4^{\rm th}$ station, the Fourier transform along these baselines, namely the visibility amplitude in Eq. 4.24, can be (close to) zero. In the argument of the logarithmic closure amplitude in Eq. 4.34, one of these baselines, i.e. k_{kl}, enters the Fourier transform in

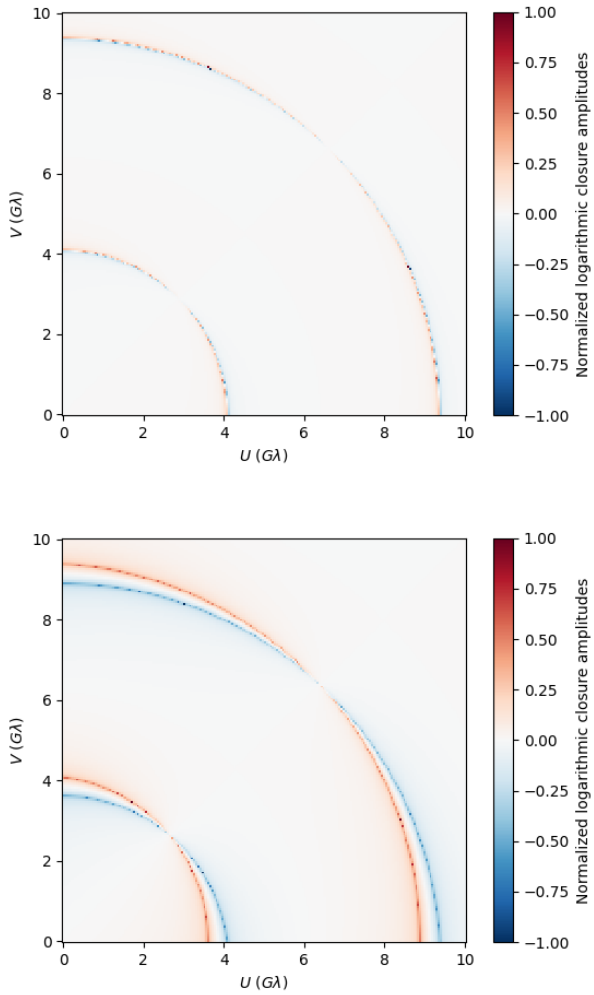

FIGURE 4.21: We show the normalised logarithmic closure amplitudes in the uv-plane for a square array with $M_{\rm st} = 200$ stations on each side ($N_{\rm st} = 40000$) and a size $L_{\rm max} = 10$ Gλ, with 3 auxiliary stations with relative baselines $L_{\rm aux} = L_{\rm max}/M_{\rm st}$ (top panel) and $L_{\rm aux} = 10 \times L_{\rm max}/M_{\rm st}$ (bottom panel). Closure amplitudes are evaluated for the 2-ring crescent model with $d_1 = 42$ μas, $\omega_1 = 2$ μas, $s = 5$ μas, $\omega_2 = 0.5$ μas and $\Delta F = 0.5$. Logarithmic closure amplitudes are positive and formally divergent within the regions marked as dark red, and negative and formally divergent within the regions marked as dark blue. Information about the model parameters is encoded in the location of these divergences, and not the maximum values reached which depend on the parameters of the array, thus we are normalising the logarithmic closure amplitudes. The larger relative distance between auxiliary stations in the bottom panel allows for better differentiation of the two types of divergent behaviour.

the numerator and the other, i.e. k_{jl}, in the denominator. As a result, the zero of $V(k_{kl})$ leads to a negative divergence, while $V(k_{jl})$ vanishing leads to a positive divergence. Although the specific location of these divergences depend on the underlying ring model being used, the existence of these divergences is model-independent and is based on robust interferometric features. We can then understand Fig. 4.18 as a convolution of the aforementioned interference patterns and a choice of independent

quadrangles that partially obscures these features.

To summarise, the full set of closure quantities in Fig. 4.18 contains information about the whole image and is therefore the best possible choice for image reconstruction using fitting procedures. However, some features are easier to see and understand in the sparse representation in Fig. 4.20.

Moving on to the practical application of the slicing procedure, we can determine the baseline distances needed to distinguish between 0-, 1- and 2-ring flat ring models, using the form of the Bessel function of the first kind $J_1(x)$. The zeros of the Fourier transform of the 0-ring model (i.e. a disk model with radius R_{outer}) are controlled by a single parameter R_{outer}. Therefore, we would need to be able to resolve at least 2 zeros to falsify this model. The second zero of $J_1(x)$ is located at $x \approx 7$ [AS68], which yields a lower bound on the maximal baseline k_{max}

$$k_{\text{max}} \gtrsim \frac{7}{2\pi} \cdot \frac{\lambda}{R_{\text{outer}}}. \tag{4.35}$$

required to differentiate a 0-ring from a 1-ring model. To discriminate among a 1-ring or 2-ring crescent models and potentially falsify the 1-ring model (characterised by an inner R_{inner} and an outer R_{outer} radius), we would need to determine the location of at least 3 divergences. We can visually check in Fig. 4.21 that this requirement is not satisfied by the idealised square array with $L_{\text{max}} = 10\,\text{G}\lambda$, since only two divergences are visible.

The location of these divergences can be calculated more precisely from numerical values of $J_1(x)$ for the 1-ring model, or by visually inspecting the behaviour of logarithmic closure amplitudes. This can be performed in detail by focusing on a set of quadrangles formed with three fixed auxiliary stations and one movable remaining station, represented in Fig. 4.22, around a specific baseline b_0. This procedure yields

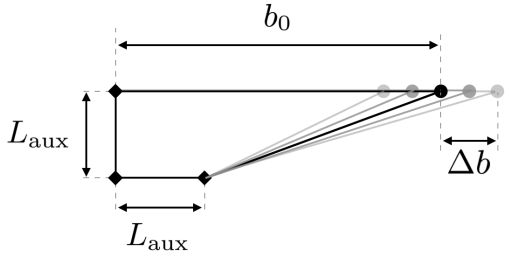

FIGURE 4.22: Schematic representation of a specific set of quadrangles formed by 3 fixed stations (diamonds) and one movable station (circles) around the baseline b_0. Values for the movable horizontal baseline are given by the set $\{b_0 + j\Delta b\}_{j=-J}^{J}$, which in realistic settings would be naturally provided by Earth's rotation.

Fig. 4.23 which shows that to probe the first three peaks for 1-ring and 2 ring-models characterised by $d_1 = 42\,\mu$as, $\omega_1 = 2\,\mu$as, $s = 5\,\mu$as, $\omega_2 = 0.5\,\mu$as and $\Delta F = 0.5$, it is necessary to have quadrangles with 3 auxiliary stations close to each other and one remaining movable station inducing baselines of about $b_0 = 3.9\,\text{G}\lambda$, $b_0 = 9.0\,\text{G}\lambda$ and $b_0 = 14\,\text{G}\lambda$.

The maximum baseline k_{max} is not the only relevant parameter when assessing the detectability of these features. While a minimum value of the latter is a necessary condition to distinguish 0-, 1- and 2-ring models, it is also necessary to have enough

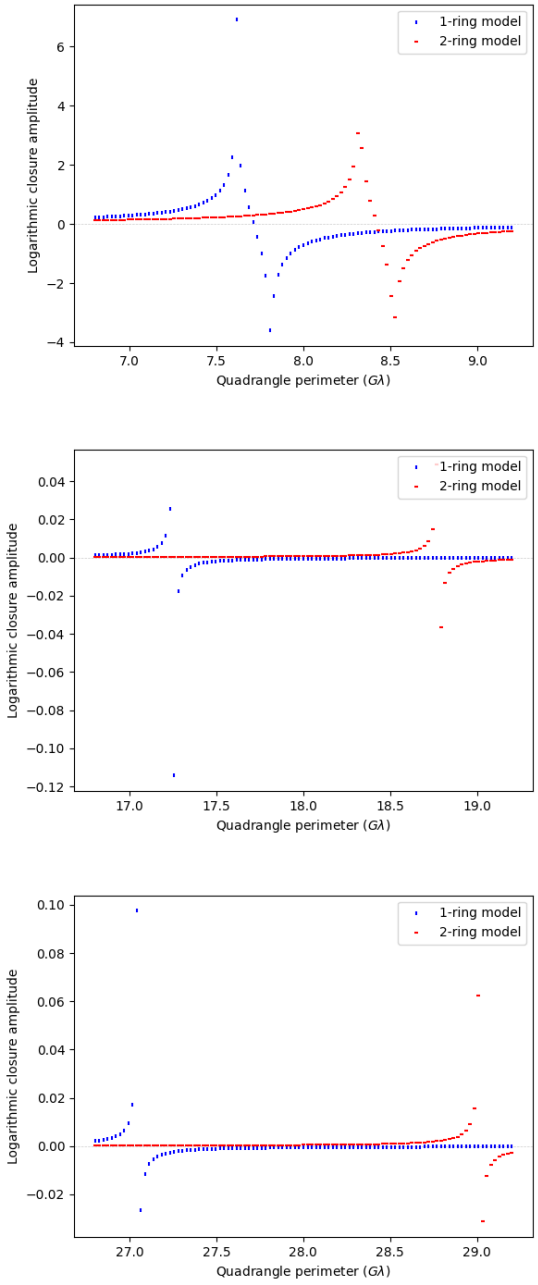

FIGURE 4.23: We show the logarithmic closure amplitudes as a function of the perimeter of the quadrangles depicted in Fig. 4.22, for the 1-ring crescent model with $d_1 = 42\ \mu$as, $\omega_1 = 2\ \mu$as, and a 2-ring model with an additional ring characterized by $s = 5\ \mu$as, $\omega_2 = 0.5\ \mu$as and $\Delta F = 0.5$. In all cases, $\Delta b = 0.6\ \mathrm{G}\lambda$ and $J = 50$, while $b_0 = 3.85\ \mathrm{G}\lambda$ for the top panel, $b_0 = 9.0\ \mathrm{G}\lambda$ for the middle panel, and $b_0 = 14.0\ \mathrm{G}\lambda$ for the bottom panel.

density of data points in the space of logarithmic closure amplitudes to be able to determine the location of the divergences with enough confidence. In short, the higher the density, the better constrained the location of these divergences will be. This is exemplified in Fig. 4.24, which contains hundred times less stations than the array used in Fig. 4.21. In the idealised situation we are describing, with a fixed,

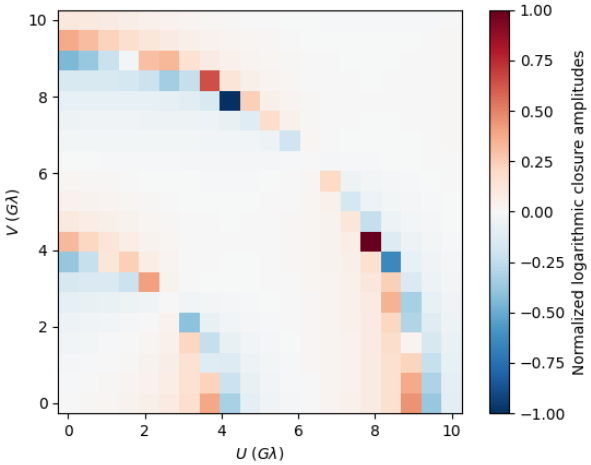

FIGURE 4.24: Equivalent of the top panel of Fig. 4.21 but for $M_{\rm st} = 20$ (one order of magnitude lower) stations on each side (i.e. $N_{\rm st} = 400$). The lower density of stations leads to a less precise localisation of the divergences of logarithmic closure amplitudes in the uv-plane.

evenly spaced, square array with respect to the source, the density of data points in logarithmic closure amplitudes is only related to the density of stations with distinct locations in the array. However, each (ng)EHT observation campaign lasts for an extended period (i.e. a few hours per observation night) in which the position of the array relative to the source changes due to Earth's rotation, so that the density of data points is a combination of the density of stations in the array and the resolution in time. Both factors thus contribute to a better differentiation between 1-ring and 2-ring models.

In summary, using the information about the location of the peaks to distinguish between 1-ring and 2-ring models requires to know the location of the first three peaks: the first two peaks allow us to falsify a 0-ring model and determine whether a 1-ring model provides a better fit, while the third peak enables us find out whether a 2-ring model provides a better fit than the 1-ring model.

4.3.7 Isolating features in closure quantities with a space-based telescope

The slicing procedure described in Subsec. 4.3.6 provides a clear way to isolate and locate the three first divergent features in logarithmic closure amplitudes, and infer which model among the 0-ring, 1-ring and 2-ring models gives the best fit to synthetic data generated with an idealised array. We now explore a practical implementation of the slicing procedure for a more realistic sparse array including a space-based station.

The latter array is formed by a single space-based antenna together with 3 stations on Earth (ALMA, APEX and the planned site LLA(MA), see Fig. 4.3). BHEX mission [Joh+24] is a concrete proposal of such an array, though it will include additional Earth-based stations. As previously, synthetic data for both the 1-ring and 2-ring model is generated for that array through the `ehtimaging` toolkit [Cha+18].

Probing the first peak structure in Fig. 4.23 requires a baseline of around $8\,\mathrm{G}\lambda$ that is attainable solely with Earth-based stations. For the second and third peaks in Fig. 4.23, we require longer baselines. Here, we are not concerned with a realistic

placement of the space-based antenna, e.g. on a certain low-Earth orbit. We assume that a placement can be found such that the projected baseline subtended between the space-based antenna and the 3 Earth-based stations can vary by a large amount throughout an observation night. We mimic those displacements by running a set of simulated observations in which the space-based station is moved "by hand" further away from the Earth. We place the space-based telescope above Odense (Denmark) at distances ranging from 500 kms (first simulation) to 8000 kms (last simulation) over Earth's surface.

The set of possible altitudes considered for the space-based antenna spans a large range of quadrangle perimeters with ALMA, APEX and LLA(MA), but only a few of those are necessary to target the second and third peaks in logarithmic closure amplitudes with the slicing method. As Earth rotates during an observation period, the projection of baselines between the Earth-based stations and the space-based antenna onto the direction of the source (taken to be located as M87*) changes – as implemented in the `ehtimaging` toolkit. Provided that the location and altitude of the space-based station are chosen appropriately, i.e. such that they form near-to-peak quadrangle perimeters, Earth's rotation effectively sweeps out a limited but sufficient range of quadrangle perimeters around the peaks. This effectively enables us to probe the second or third peak, as shown in Fig. 4.25.

4.4 Conclusion and outlook

4.4.1 Conclusion

The EHT cannot detect photon rings with the features expected in GR without using super-resolution techniques [Bro+22b; Him+20]. However, we showed that, beyond GR, photon rings can be more abundant, more widely separated from each other and also of comparative brightness. Among the four classes of beyond-GR spacetimes discussed, one example is given by horizonless spacetimes with a photon sphere. In that spacetime, both an inner and an outer set of photon rings exist, and the $n = 1$ photon ring can be at several μas distance[21] from the first inner photon ring.

These observations motivated our study, in which we worked in a simplified geometric setting to investigate detection capabilities of the EHT and potential future upgrades [Joh+23; Ayz+23; Doe+23] for photon rings. We first generated synthetic data that contained either one or two thin rings, geometrically parameterised by a ring separation s, a relative flux density ΔF and the widths $\omega_{1,2}$ of the two rings. We then used the `ehtimaging` toolkit [Cha+18; Cha22] to simulate an observation and reconstruct the Fourier data of such a simulated observation for given array configurations. With the simulated data at hand, we fitted the visibility amplitude of both 1-ring and 2-ring crescent flux density profiles and statistically compared their fit quality. We thereby obtained the detection threshold of a 2-ring model as a boundary in the parameter space of interest, namely $(s, \Delta F)$. We also explored the impact of super-resolution techniques for thin (compared to the diameter) rings by imposing priors on the reconstructed widths $\omega_{1,2}$ of the rings.

First, we found that for our three new-physics spacetimes which motivated our study, simulated data from the EHT 2022 configuration does not allow to infer the presence of a second ring, see the uppermost panel in Fig. 4.26. Thus, current VLBI arrays need to be improved. Two properties of VLBI arrays are critical to lower the

[21] This assumes a mass of and distance to the source roughly similar to M87*.

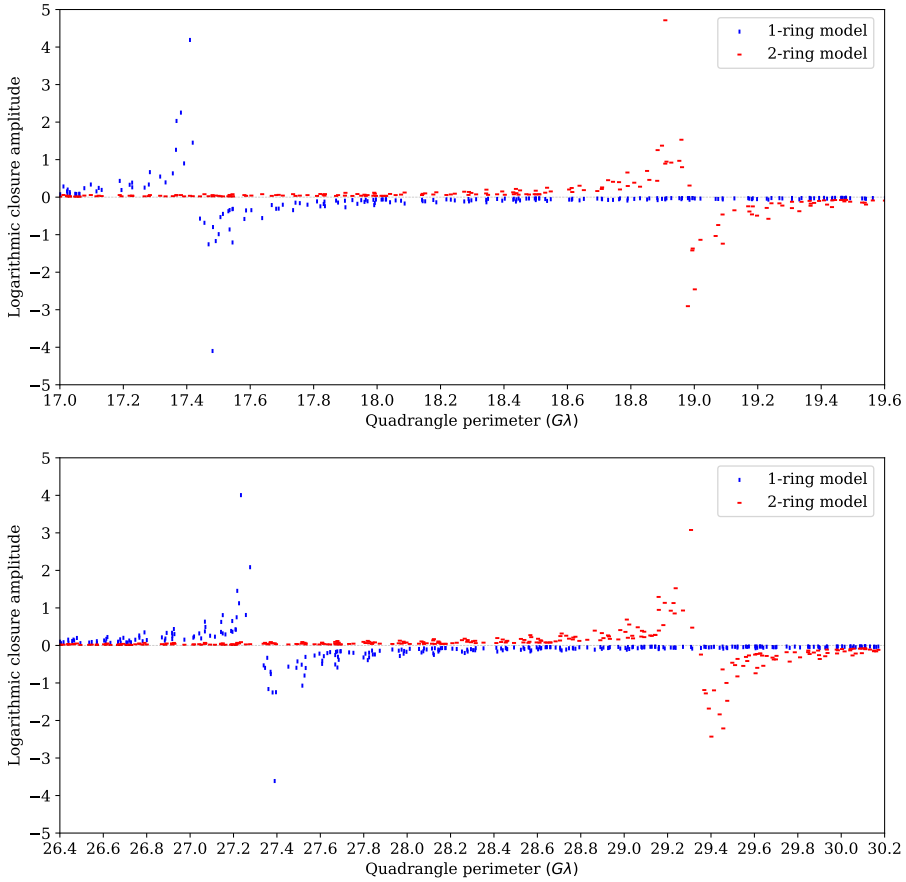

FIGURE 4.25: We show the logarithmic closure amplitudes as a function of the perimeter of the quadrangles formed by 3 Earth-based stations (ALMA, APEX, LLAMA) and a space-based station (see Tab. A.4), for the 1-ring crescent model with $d_1 = 42$ μas, $\omega_1 = 2$ μas, and a 2-ring model with the second ring characterised by $s = 5$ μas and $\omega_2 = 0.5$ μas. In all cases, the altitude of the space-based station varies between 500 kms (i.e. 0.38 Gλ at 230 GHz) and 8000 kms (i.e. 6.15 Gλ) above Odense (Denmark), by steps of 200 kms (i.e. 0.15 Gλ).

detection threshold towards rings with lower separation from each other and also a second ring with low relative flux density: first, a high sensitivity (thus a low SEFD) and second, a high resolution (thus a higher frequency than 230 GHz and/or much larger baselines).

We found that the following setups bring the detection threshold to what is needed to rule out some of the new-physics cases that motivated our study, see Fig. 4.26. First, an ngEHT array in which 8 stations are added to the EHT 2022 array and all these stations have low SEFD values corresponding to those of the ALMA station; and where 230 and 345 GHz frequencies are simultaneously used in observations. This provides both the sensitivity and resolution needed. Second, a space-based array in which an additional space-based station is added to the previous ngEHT configuration, which results in larger baselines and thus a lower detection threshold in terms of separation of the rings. Third, the EHT 2022 array combined with super-resolution techniques. These provide a substitute for the resolution that is needed.

The first two options are clearly more expensive and more technically challenging, and may therefore be more difficult to realise. However, even the existing EHT array,

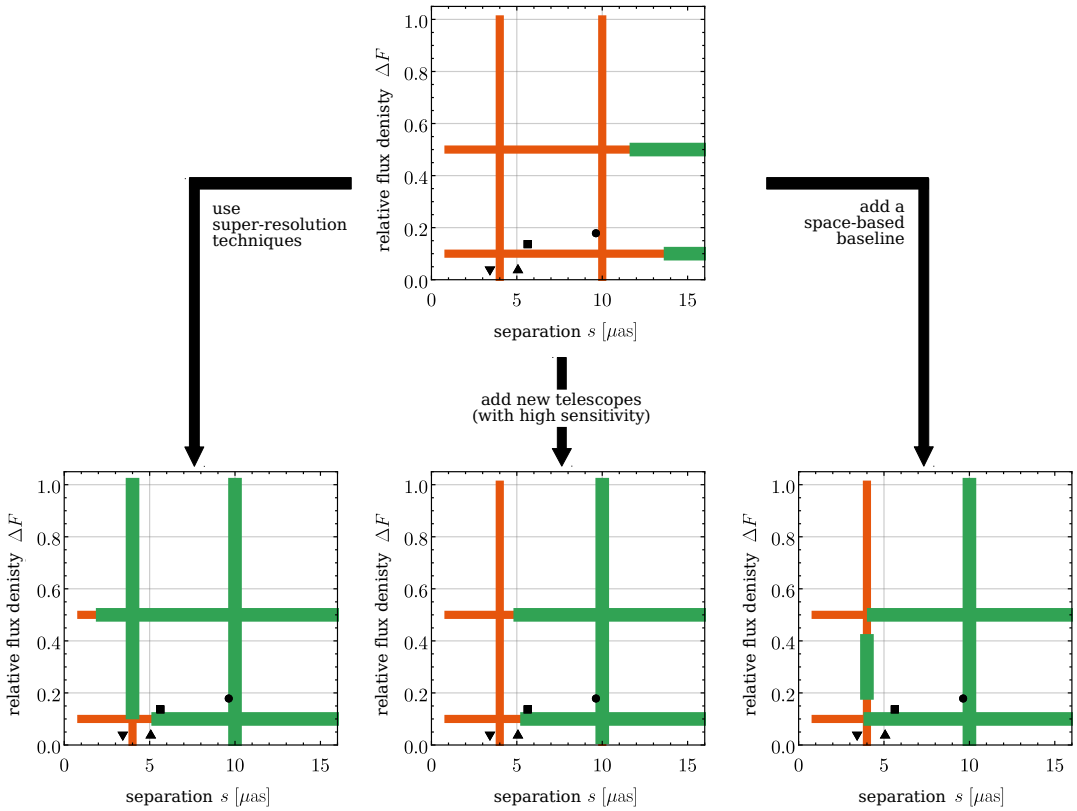

FIGURE 4.26: Summary of three tentative pathways to improve the detectability of a 2-ring model, as suggested by the statistical analysis in Fig. 4.16 and 4.17. In all panels, the detectable (not detectable) parameter ranges are marked as thicker green (thinner red/orange) lines. Here, detectability refers to a p-value of 10^{-5}. Top panel: results for the EHT 2022 array without super-resolution constraints. Three bottom panels: different ways of improving the detectability of a 2-ring model. Left bottom panel: results for the EHT 2022 array but with a super-resolution constraint. Middle bottom panel: results for the ngEHT array, assuming optimistic, i.e., low SEFD values. Right bottom panel: results for the same ngEHT array with a single additional space-based telescope. All arrays shown here observe at 230 GHz. For details, cf. notation and figures in Subsec. 4.3.1.

if combined with super-resolution techniques, can approach the region in parameter space where our new-physics examples are located. Using super-resolution techniques implies that any statement about ruling out/detecting signatures of new physics can only be valid within the class of spacetimes that generates photon rings that are thin compared to their diameter. To the best of our knowledge, this is the generic case and no counter-examples are known.
We caution that all our conclusions are to be understood within our simplified setting in which the image consists of two geometric thin rings and the broad image feature corresponding to foreground emission is not accounted for. It contrasts with realistic observations, in which the foreground emission dominates the measured flux density in the ring feature.

The visibility amplitude of a (simulated) observation is subject to systematic uncertainties, some of which can be removed by considering closure quantities based on ratios of four visibility amplitudes. Rings generically generate zeros in visibility

amplitudes and, accordingly, divergences in closure quantities such as the logarithmic closure amplitudes, obtained for each independent set of four stations in the array.

We first investigated an idealised, dense, evenly spaced, square array to which three auxiliary stations are added and held fixed, while a fourth one is displaced in a controlled way. In that setting, dubbed "peak slicing procedure", divergences of the logarithmic closure amplitudes of the 1-ring and 2-ring models can be separated from each other. In a realistic setting, the (projected) baselines between all four stations change throughout an observation, because of Earth's rotation. Earth's rotation thus paves the way for practical implementation of this idealised setting, which can be obtained when choosing three auxiliary stations as close as possible and the fourth station placed so that it can target higher-order zeros for specific compact sources. Using the `ehtimaging` toolkit, we have shown that such a setting enables one to probe the first divergence of the logarithmic closure quantity by an Earth-based array, and the second and third divergences by choosing a space-based station as the fourth station. We argued that knowing the locations of the first three divergences is sufficient to distinguish the 1-ring from the 2-ring model. This provides further motivation for arrays featuring space-based stations such as, e.g., the BHEX mission [Joh+24; Lup+24; Gal+24].

In summary, our study showed that in an idealised setting, simulated observations with VLBI arrays can distinguish between one and two rings at parameter values motivated by new physics beyond GR, if the array is sensitive enough and dual -frequency capabilities are assumed. Existing arrays can distinguish between one and two rings, if super-resolution techniques are used. This motivates future upgrades of our investigation along the following lines:

- First, our simulated data does not come from ray-tracing photons in a given spacetime geometry but consists of an ad-hoc geometric model which we used to perform a first parameter study. Given the largely positive outcome of this study, a more extensive study starting from given spacetime geometries is warranted. In such a study, also the following additional points should be addressed, that correspond to simplifying assumptions of our analysis;

- Second, our simulated data consists of images with either one or two rings, but no diffuse ($n = 0$) emission is included. Investigating the detection capabilities in the presence of a (broad) feature generated by a diffuse emission is one important future direction. We expect that the detection threshold is shifted towards higher separations and higher relative flux densities, once foreground emission is accounted for. The extent of the shift depends on the properties of the foreground emission: for a sufficiently broad image feature with approximately constant flux density,[22], from which two thin rings stand out in peak flux density, our conclusions will likely not be altered much;

- Third, in such a study, accounting for uncertainties from the imperfectly understood astrophysics of the accretion disk is important; that is, such a study must fit not only the parameters of the spacetime, but also the parameters of a consistent accretion disk model to determine whether two rings can be distinguished from one ring.

[22]We highlight that both shadow images of M87* and SgrA* possess a brightness asymmetry in the broad feature, c.f. Fig. 4.4 which might obscure the thin rings.

4.4.2 Outlook

To complement our study, we could investigate whether (optical) intensity interferometry – pioneered in [HBT54] and revived in past years – can help lower the detection threshold of a second ring feature in shadow images. Indeed, thanks to the tremendous improvement in fast photodetectors, SNRs reached in intensity interferometry now allow us to probe accreting supermassive black holes such as M87* and SgrA* [Dal+24].

While radio interferometry, i.e. VLBI, relies on the analysis of correlations in visibilities (proportional to the data of electric fields collected at two different locations), intensity interferometry involves the analysis of correlations in the data of photon counts collected at different locations. The latter photon count data is proportional to the square of the visibility amplitude integrated in frequency, dubbed *normalised fringe visibility*. Hence, both the amplitude and phase information can be extracted in radio interferometry, whereas intensity interferometry is insensitive to phases.[23] However, for radially symmetric intensity profiles such as the ones analysed in our study [CR+24], only the closure amplitudes matter. Therefore, the lack of information on phases does not seem to limit the scope of the analysis. Since it is possible to write analytical expressions for the normalised fringe visibility for disk-like models, which have similar features (in terms of oscillations and zeros) as the visibility amplitude, we could analyse the feasibility of resolving two rings depending on array properties with optimistic intensity interferometry.[24]

4.4.3 Synergy of shadow imaging with gravitational waves

The reason we focused on VLBI observations to probe BH beyond GR in this chapter and, to a mild extent, also in Chapters 5 and 6, is twofold, as detailed below. Nonetheless, we stress that GW astronomy provides complementary results on testing the Kerr paradigm, hence developing synergies between EM and GW observations is essential.

The theoretical reason is that we do not expect black-hole uniqueness theorems generically to hold beyond GR, and thus that stellar-mass BHs probed by the LVK collaboration and supermassive BHs probed by the EHT correspond to the same branch of solutions of a theory beyond GR. There exists indeed simple BH examples supporting this expectation: in quadratic gravity [Lu+15; Lü15; Ste17], in semiclassical gravity [Fer23] and in ESTGB theory with scalarised black-hole solutions and the Kerr solution being simultaneously present [DY18; Her+21; Dim+20; Don+24; Eic+23]. It is therefore crucial to make use of the complementarity of EM and GW probes to test the Kerr paradigm in the strong-field regime. Once those probes are combined, they allow to scrutinise BHs that differ by 6 or even 9 orders of magnitude in mass. Second, their synergy will be enhanced with the advent of the Laser Interferometer Space Antenna (LISA) as the latter will probe the coalescence of MBHBs in the mass range $[10^4, 10^7]\,M_\odot$ to which SgrA* belongs.

[23] The 2-point correlations (i.e. at 2 different stations) are blind to phase data, but 3-point correlations allow the measurement of closure phases [TMS17; Law00].

[24] Applying the Rayleigh criterion Eq. 4.2 at the optical wavelength $\lambda \approx 500\,\text{nm}$ and with baselines $D \approx 10^4$ kms achievable on Earth leads to an angular resolution of $\theta \approx 0.01\,\mu$as, resulting in an improvement by four orders of magnitude w.r.t. the current nominal resolution of the EHT. However, in practice, unambiguously detecting two rings would require very high SNRs.

The pragmatic reason is that deriving images of compact objects beyond GR via VLBI observations only requires to know the underlying spacetime metric (on top of the astrophysical environment) and the geodesic equations.

By contrast, GW observations necessarily call for the knowledge of the full dynamics beyond GR and computationally costly, numerical simulations of binary black-hole mergers. Not only this subtends to know the action of a theory beyond GR, but it also requires to find a well-posed initial-value formulation of the equations of motion – pertaining to the action – that is amenable to numerical simulations.

Finding such a formulation remains a significant challenge in many theories beyond GR that has only partially been met in a limited number of theories: in simple scalar-tensor theories with a single, non-minimally coupled scalar field in the Jordan frame [Sal06], in Einstein-aether theory [SBPL19], in a 4-derivative scalar-tensor theory [ASCF22], in polynomial higher-derivative EFTs of vacuum gravity [FHK24] and in Lovelock and Horndeski theories at weak coupling [Kov19; KR20b]. Among the latter class of Horndeski theories at weak coupling, specific proofs were derived for k-essence theories [Ren06] and ESGB in weak-coupling and spherically symmetric regime [RRY23]. Finally, [HB24] derived a proof of the well-posedness of the initial value problem for Unimodular Gravity (UG).[25]

The challenge arises because well-posedness of an initial value problem may be spoiled if the equations of motion are not at most second order (due to the potential apparition of Ostrogradsky instabilities [Ost50; PU50], reviewed in [Woo07; Woo15]) or if elliptic regions develop in the spacetime (see e.g. simulations of BHBs and NSBs in ESGB gravity [ER21b; ER21a; EP22]). Those requirements are particularly constraining for theories beyond GR, as many possess higher-derivative and higher-curvature terms in their action, thus potentially leading to e.o.m. of third order or more.

Although solving the full dynamical, nonlinear regime of modified theories of gravity remains difficult, approximate numerical methods are often used.

The first type of approximate numerical methods exploits the fact that corrections to GR ought to be subleading, such that we can incorporate their effects on the dynamics order by order in a perturbative expansion and evaluate the corrections w.r.t. the solution obtained at lower order. It was employed for example in [AY09; Oko+17; Oko+19; Oko+20; Oko20].

The second type adopts an EFT point of view that a modified theory is only valid up to some short length scale, and "fix" the evolution equations below this scale, hence the name "fixing approach" used in [COL17; AL19; Bez+21; Ger+22]. This is performed by substituting high derivative terms in the original evolution equations by new dynamical fields, while including the effect of corrections via suitable coupling among relevant fields. These new fields are dynamically driven to the values they would have in the original theory on some short length scale. Only recently was an EFT put forward that introduces higher order modifications to GR without adding new fields [End+17], applied in [CL20; Bez+22; LBB22; Fra+22].

When those methods are evaluated on a benchmark theory, their predictions might differ and their solutions might not be fully consistent with the "true" solution [Cor+24], thus requiring a more careful analysis of approximate methods and a comparison to the full solution.

[25] Vacuum UG is classically equivalent to GR with a cosmological constant at the level of the equations of motion, and GR is known to admit a well-posed initial value problem [CBG69]. Despite this equivalence, demonstrating the well-posedness of UG is non-trivial, as its symmetries and constraint structure are different from that of GR.

Hence, it sounds more promising to first identify and constrain potential deviations from the Kerr spacetime in VLBI data, before trying to elaborate the underlying theory, find a tractable dynamical formulation amenable to numerical simulations [Pre06; BR16; BSG24] and compare to GW data.

Finally, the synergy between EM and GW probes manifests, for example, in the Lyapunov exponents, which govern the decay rate of the amplitude of a GW ringdown signal, the damping time and frequencies of the Quasi Normal Modes (QNMs) as well as the ratio of fluxes measured between successive photon rings, see [Car+09; Yan21] and Subsec. 4.1.4. They thus constitute a good starting point to bridge the gap between EM and GW observations.

Chapter 5

The principled-parameterised approach to gravitational collapse

In this chapter, we review a simple GR model of spherically symmetric gravitational collapse, which exhibits a naked singularity for low enough accretion rates. This motivates us to perform two regular upgrades of such a simple, classical dynamical spacetime: one constructed through the RG improvement method from ASQG, and one following the principled-parameterised approach put forward in [EH21b; EH21a; EHJ23] for stationary spacetimes. These two upgrades are equivalent upon specific choices within the principled-parameterised approach. We explore the consequences of the upgrade on the spacetime's structure and null geodesic motion.

We begin by reviewing a simple, classical model of spherically symmetric gravitational collapse of null dust dubbed Vaidya spacetime. To understand whether singularities arise and, if yes, of which type, we compute the null energy condition, determine the location of the various horizons and study the null geodesic motion as a function of the ratio of the accretion rate to its critical value. Due to the appearance of a naked singularity in this model, we generalise the Vaidya model and consider two upgrades within the class of generalised Vaidya spacetimes. Both models implement regular modifications which weaken gravity, and thus change the spacetime's structure and geodesic motion. Similarly to the classical case, we check whether or not the null energy condition is satisfied, determine the distinct horizons that form within the upgraded spacetime and investigate the consequences of the modifications on radial null geodesics near the centre. Finally, we conclude and sketch an outlook on how to apply the principled-parameterised approach beyond the Vaidya spacetime.

5.1 A review: the classical Vaidya-Kuroda-Papapetrou model for gravitational collapse

We start by reviewing a simple classical model for gravitational collapse to a black hole, namely the Vaidya-Kuroda-Papapetrou (VKP) model [Vai66; Kur84a; Pap85b], which gives rise to a naked singularity and thus violates Penrose's cosmic censorship conjecture [Pen69].

The classical advanced Vaidya spacetime is a generalisation of the static, spherically symmetric Schwarzschild solution to a non-vacuum, dynamical, spherically symmetric solution of GR. Its line element in advanced Eddington-Finkelstein (EF)

coordinates (v, r, θ, ϕ) is[1]

$$ds^2_{\text{EF}} = -f(v)dv^2 + 2dv\,dr + r^2 d\Omega^2, \quad f(v) = 1 - \frac{2G_0 M(v)}{r}. \tag{5.1}$$

To encode the accretion of spherically symmetric shells of null dust, the time-varying Misner-Sharp mass function satisfies $M(v) \geq 0$. In the limiting case $M(v) = \text{const.}$, the line element reduces to the Schwarzschild spacetime.

The VKP model encompasses all Vaidya metrics in which shells of null dust are linearly accreted during a finite time, namely from $v = 0$ to $v = \bar{v}$. Thus, the dynamical mass function is a piecewise function with a phase of linear growth, that is

$$M(v) = \begin{cases} 0, & v \leq 0 \\ \mu\, v & 0 < v < \bar{v} \\ M = \mu\, \bar{v} & v \geq \bar{v}. \end{cases} \tag{5.2}$$

At advanced times $v \leq 0$, the spacetime is locally isometric to Minkowski spacetime. At $v = 0$, ingoing shells of null dust start to collapse under their own gravity. The amount of matter falling towards the centre at $r = 0$ is encoded in the accretion rate μ.[2] Theoretically, a critical value of μ lies at $\mu_c = \frac{1}{16G_0}$, because a singularity forms in the spacetime before a horizon forms. Thus, the VKP model is one of the first counterexamples [Kur84a] to Penrose's cosmic censorship conjecture [Pen69]. In our analysis, we will thus consider both $\mu > \mu_c$ and $\mu < \mu_c$.
In all cases, the dynamical spacetime finally settles down to a static, spherically symmetric black-hole spacetime, i.e. for $v > \bar{v}$ the spacetime is locally isometric to a Schwarzschild spacetime with ADM mass $M = \mu\, \bar{v}$.

5.1.1 Energy conditions for the VKP model

The Vaidya spacetime described by the metric Eq. 5.1 contains a curvature singularity at $r = 0$ (for $v > 0$) and is geodesically incomplete, as we review below. Geodesic incompleteness follows from singularity theorems that hold in GR, reviewed in [Ong20; Lan22], which assume that the energy-momentum tensor describing the infalling radiation satisfies certain energy conditions. We review these conditions for the Vaidya spacetime because we later examine whether and how they fail in a singularity-free, upgraded spacetime, c.f. Subsec. 5.6.2.

To describe the gravitational collapse of ingoing null dust, the energy-momentum tensor constructed from the four-velocity $n_\mu \equiv \delta^0_\mu$ of the null dust must be pressure-less.[3] In terms of the energy density of the null dust

$$\rho \equiv T_{00} = \frac{\dot{M}(v)}{4\pi r^2}, \quad \text{where } \dot{M}(v) \equiv \frac{\partial M(v)}{\partial v}, \tag{5.3}$$

we can write

$$T_{\mu\nu} = \rho\, n_\mu n_\nu. \tag{5.4}$$

[1] The advanced null "time" coordinate v is defined in terms of the Schwarzschild time coordinate t as $v = t + r + 2G_0 M \ln\left(\frac{r}{2G_0 M} - 1\right)$.

[2] While astrophysically realistic accretion rates are estimated as $G_0\mu \leq 10^{-8}$, see [SP22], to simplify our numerical studies we will consider larger values of $G_0\mu$ throughout the rest of this chapter.

[3] It holds that $n_\mu n^\mu = 0$, because for the line-element Eq. 5.1, $g^{00} = 0$.

If the energy-momentum tensor Eq. 5.4 satisfies the appropriate pointlike energy condition, the formation of a spacetime singularity, which renders the spacetime geodesically incomplete, is inevitable [Pen65]. In particular, the weakest pointlike energy condition is the Null Energy Condition (NEC) which requires

$$\varepsilon = T_{\mu\nu}k^\mu k^\nu \geq 0 \tag{5.5}$$

for every future-pointing null vector field k_μ. It restricts the mass function of the classical Vaidya spacetime to be

$$T_{00} \equiv \rho \geq 0 \overset{\text{Eq. 5.3}}{\Longleftrightarrow} \dot{M}(v) \geq 0. \tag{5.6}$$

This ensures that "well-behaved" null dust has to undergo gravitational collapse (as opposed to the opposite process, namely evaporation, for which $\dot{M}(v) < 0$). This condition is satisfied (for all v) by the linearly growing mass function in Eq. 5.2 of the VKP model, for which the NEC simply leads to positive accretion rates $\mu \geq 0$.

5.1.2 Behaviour of null geodesics near the centre

The classical Vaidya spacetime is geodesically incomplete, because it (i) describes gravitational collapse, (ii) solves the non-vacuum Einstein field equations Eq. 2.1 and (iii) satisfies the pointlike NEC. In many spacetimes, geodesic incompleteness goes hand in hand with curvature singularities at the centre. However, they are not equivalent, nor one implies the other. For example, some analytical extensions of non-singular black holes have been shown to be geodesically incomplete [ZM23], while there are spacetimes, e.g. in some $f(R)$-theories, which are geodesically complete but harbour curvature singularities [BORG17]. For those reasons, we review the behaviour of null geodesics as well as curvature invariants near $r = 0$. To provide a comprehensive overview of the starting point of our analysis, we also discuss its horizons, photon sphere and photon surfaces.

It is sufficient to follow radial null geodesics to show the geodesic incompleteness of the spacetime, as the latter only requires *some* geodesics to be incomplete. Null geodesics in Vaidya spacetime solve the equation [MGM14]

$$\frac{dr}{dv} - \frac{1}{2}\left(1 - \frac{2G_0 M(v)}{r}\right) = 0. \tag{5.7}$$

This equation can be obtained from the general expression for null geodesic equation

$$\frac{d^2x^\mu}{d\lambda^2} + \Gamma^\mu_{\alpha\beta}\frac{dx^\alpha}{d\lambda}\frac{dx^\beta}{d\lambda} = 0, \tag{5.8}$$

with λ an affine parameter and $x^\mu(\lambda) = (v(\lambda), r(\lambda), \theta(\lambda), \phi(\lambda))$ the photon's position in EF coordinates. Indeed, by specialising to radially infalling geodesics, i.e.

$$\frac{d\theta(\lambda)}{d\lambda} = 0 = \frac{d\phi(\lambda)}{d\lambda}, \tag{5.9}$$

we obtain two equations which describe $r(\lambda)$ and $v(\lambda)$

$$r\frac{d^2v}{d\lambda^2}+\frac{G_0M(v)}{r}\left(\frac{dv}{d\lambda}\right)^2=0,\quad \frac{dr}{d\lambda}-\frac{1}{2}\left(\frac{dv}{d\lambda}\right)\left(1-\frac{2G_0M(v)}{r}\right)=0. \tag{5.10}$$

The separate dependence of r and v on the affine parameter λ can be traded for a dependence of r on v, hence the two equations in Eq. 5.10 can be combined into Eq. 5.7.

For any value of μ, it has been shown that Eq. 5.7 admits an analytical, implicit general solution [BKP17] of the form

$$-\frac{2\arctan\left(\frac{v-4r(v)}{v\sqrt{-1+16G_0\mu}}\right)}{\sqrt{-1+16G_0\mu}}+2\log(v)+\log\left(2\mu G_0-\frac{r(v)}{v}+\frac{2r^2(v)}{v^2}\right)=C, \tag{5.11}$$

with C being an arbitrary integration constant that is potentially complex. A set of outgoing null geodesics is obtained by varying the constant C. Whereas this solution Eq. 5.11 holds for all values of μ, a simpler representation of the solutions exists for $\mu\leq\mu_c=\frac{1}{16G_0}$, found in [Isr85; Isr86],

$$\frac{|r(v)-\lambda_-v|^{\lambda_-}}{|r(v)-\lambda_+v|^{\lambda_+}}=\tilde{C}, \tag{5.12}$$

with $\tilde{C}$ being an arbitrary real positive (due to the absolute values) constant and

$$\lambda_\pm=\frac{1\pm\sqrt{1-16\mu G_0}}{4}. \tag{5.13}$$

From Fig. 5.1, the behaviour of null geodesics near $r=0$ indicates that the spacetime is indeed geodesically future incomplete.[4] Outgoing null geodesics are deflected towards $r=0$, which they reach in a finite amount of advanced and affine time, as confirmed in Fig. 5.2. The gravitational lensing that applies to null geodesics gets stronger when either G_0 or μ increases, i.e. when gravity becomes stronger or the energy density is increased. This already provides us with a first hint on the two alternatives of how to avoid geodesic incompleteness in a spacetime describing gravitational collapse, namely (i) altering the effective mass function (or accretion rate) or (ii) altering the strength of the Newton coupling. Both alternatives will be explored, see Sec. 5.5.
We also see that the behaviour of null geodesics changes around $\mu_c=\frac{1}{16G_0}$, where null geodesics starting at $(r,v)=(0,0)$ can actually escape to infinity. This results in a naked singularity, which manifests itself in the divergence of curvature invariants.

5.1.3 Singular curvature invariants at the centre

Even though geodesic incompleteness and singular curvature invariants are two independent concepts, they go hand in hand in many black-hole spacetimes in the

[4] While future null geodesic incompleteness can be *inferred* from outgoing null geodesics reaching the central singularity at finite advanced time v, it can only be confirmed by checking that $r(\lambda)$ reaches zero and $v(\lambda)$ becomes constant at finite value of the affine parameter λ. The behaviour of null geodesics in a Vaidya spacetime has been extensively studied, e.g. in [GP09; JM11]. Those studies confirm that, in such a spacetime, outgoing null geodesics that reach the centre in a finite affine parameter λ, i.e. future-incomplete null geodesics, do so in a finite advanced time v. See Fig. 5.2 for an illustration.

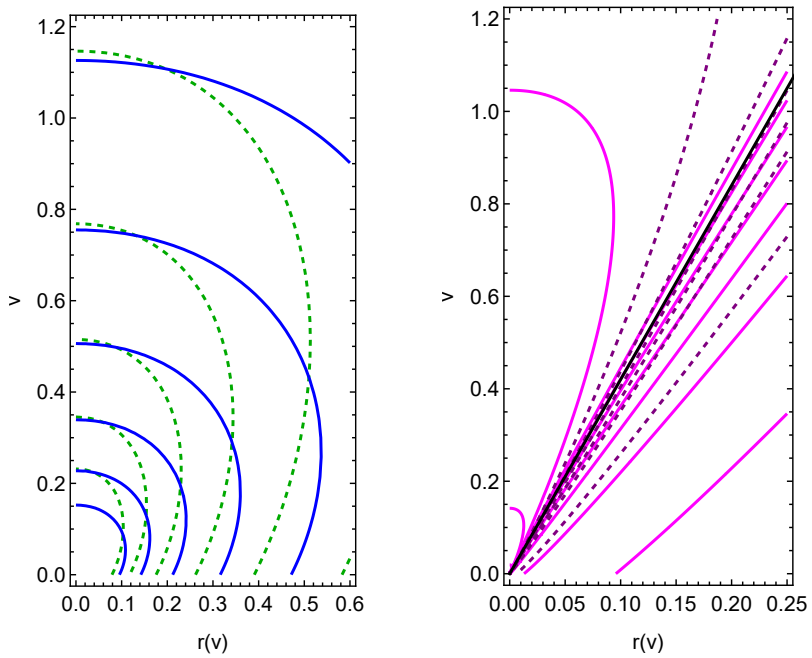

FIGURE 5.1: We show outgoing null geodesics near $r = 0$ in a Vaidya spacetime Eq. 5.1 with linearly growing VKP mass Eq. 5.2 for $G_0\mu > \mu_c$ (left panel) and $G_0\mu < \mu_c$ (right panel). Left panel: $G_0\mu = 1/2$ (green dashed lines) and $G_0\mu = 1$ (blue continuous lines). Right panel: $G_0\mu = 1/16.5$ (magenta continuous lines) and $G_0\mu = 1/15.5$ (purple dashed lines) and a tangent to a geodesic near the origin $(r = 0, v = 0)$ (black continuous line). The critical value is $G_0\mu_c = 1/16$, as a subcritical geodesic crosses its tangent at the origin, while a supercritical geodesic does not. Note that all plots in this chapter are in Planck units in which, in addition to $\hbar = c = 1$, $G_0 = 1$.

sense that an infalling observer will experience both a finite future and diverging tidal forces. Here, we confirm the singular behaviour of curvature invariants near $r = 0$.

Under rather generic assumptions (spelt out in [CHP09]), a spacetime metric can be characterised by an algebraically complete basis of seventeen non-derivative curvature invariants, referred to as Zakhary-McIntosh (ZM) invariants [CM91; ZM97; CZ02], built out of the Weyl tensor $C_{\mu\nu\rho\sigma}$, the (left-)dual Weyl tensor $\overline{C}_{\mu\nu\rho\sigma} = \frac{1}{2}\epsilon_{\mu\nu\kappa\lambda}C^{\kappa\lambda}{}_{\rho\sigma}$ (with $\epsilon_{\mu\nu\kappa\lambda}$ the totally anti-symmetric Levi-Civita tensor) and the Ricci tensor $R_{\mu\nu}$. The set of invariants decomposes into four real Weyl-invariants I_{1-4}, four real Ricci-invariants I_{5-8} and nine real mixed invariants I_{9-17} as listed in App. B.1.

For spacetimes which admit Killing vectors, one typically finds that not all of the non-zero invariants are independent. For the classical Vaidya spacetime with VKP mass function, the only non-zero, non-derivative curvature invariants are

$$\begin{aligned} I_1 &= C_{\mu\nu\rho\sigma}C^{\mu\nu\rho\sigma} = \frac{48G_0^2\mu^2v^2}{r^6}, \\ I_3 &= C_{\mu\nu}{}^{\rho\sigma}C_{\rho\sigma}{}^{\alpha\beta}C_{\alpha\beta}{}^{\mu\nu} = \frac{96G_0^3\mu^3v^3}{r^9} = \frac{1}{2\sqrt{3}}I_1^{3/2} \end{aligned} \tag{5.14}$$

for $v < \bar{v}$. Because the invariant I_3 can be expressed in terms of I_1, I_1 is the only independent, non-zero, non-derivative curvature invariant. As I_1 is clearly singular at the centre $r = 0$ for all times v, the resulting spacetime indeed contains a curvature

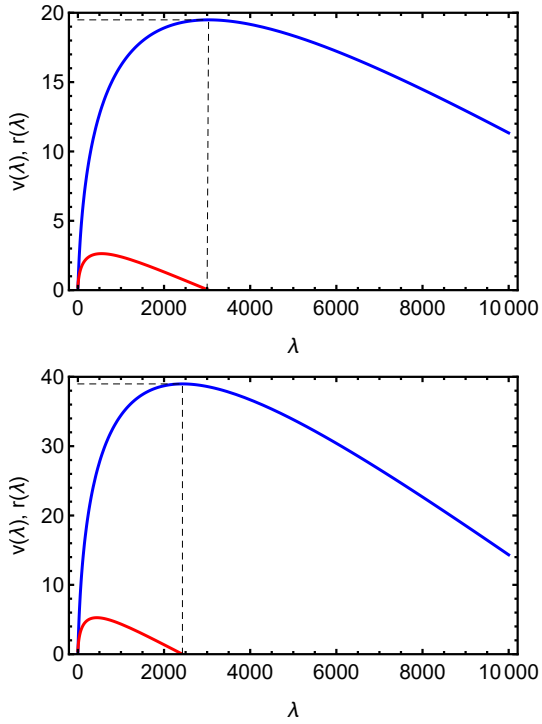

FIGURE 5.2: We show outgoing null radial geodesics near $r = 0$ in a Vaidya spacetime Eq. 5.1 with linearly growing VKP mass Eq. 5.2 with $G_0\mu = \frac{1}{10}$ as a function of the affine parameter λ. The blue curve corresponds to $v(\lambda)$ and the red curve is $r(\lambda)$. Top panel: $r(0) = \frac{1}{4}$, $v(0) = 10^{-5}$, $v'(0) = \frac{1}{10}$. Bottom panel: $r(0) = \frac{1}{2}$, $v(0) = 10^{-5}$, $v'(0) = \frac{1}{4}$. The dashed lines indicate the values $\lambda, v(\lambda)$ when $r(\lambda)$ falls back to the centre.

singularity at $r = 0$.

5.1.4 Apparent, event, and Cauchy horizons

Stationary black-hole spacetimes are usually characterised by their event horizon. To locate the event horizon, global knowledge of the entire spacetime is required, because the event horizon is the boundary of the causal past of future null infinity. In a time-dependent spacetime, another notion of horizon is often more useful, namely that of an apparent horizon, reviewed in [AK04; Boo05; GJ08]. At an apparent horizon, the expansion of both in- and out-going null geodesics is negative semi-definite, i.e. gravitational lensing is so strong that locally, all geodesics are prevented from reaching larger distances from the centre. For the VKP model, this condition translates into [NV06; Far13]

$$g^{rr}_{\mathrm{EF}} = g_{\mathrm{vv,EF}} = 0, \tag{5.15}$$

see the derivation in App. B.4 in a form that can be generalised when we modify the spacetime. For the VKP line element Eq. 5.1, this condition can be solved to obtain

$$g_{\mathrm{vv,EF}} = 0 \Leftrightarrow 1 - \frac{2G_0\mu v}{r_{\mathrm{AH}}} = 0 \Leftrightarrow r_{\mathrm{AH}} = 2G_0\mu v. \tag{5.16}$$

To find the event horizon for the VKP model, we use the initial condition

$$r_{\mathrm{EH}}[v = \bar{v}] = r_{\mathrm{EH,Schw}} = 2G_0\,\mu\,\bar{v} \tag{5.17}$$

for the null geodesic equation Eq. 5.7 and numerically solve the equation backwards in time to find the event horizon at $v < \bar{v}$.

For $\mu < \mu_c = \frac{1}{16G_0}$, a third notion of horizon is realised, namely that of a Cauchy horizon. A Cauchy horizon exists when the initial-value problem is no longer well-defined, i.e., when initial data defined on a spatial hypersurface is not sufficient to determine the entire future evolution. The Cauchy horizon delineates the boundary of the spacetime region in which the future evolution of the initial data is not well-defined. Thus, Cauchy horizons appear in particular when there are naked singularities. Fig. 5.1 already contains a hint that there is a (globally) naked, null singularity for $\mu < \mu_c$ because the right panel shows null geodesics emanating from $(r, v) = (0, 0)$ which are not focused back towards small r. This singularity is actually only partially naked. It contains both a spacelike and a lightlike part, but only a section of the lightlike part is naked while the rest of the singularity is shielded behind the horizon [GP09, Fig. 9.19].

The Cauchy horizon can be found from Eq. 5.12, because it is itself a null surface. Eq. 5.12 admits two linear solutions, $r_\pm(v) = \lambda_\pm \cdot v$, which both emanate from the point $(r, v) = (0, 0)$ and extend to infinity. Those solutions derive from the existence of a conformal Killing vector field ξ^μ defined by

$$\nabla_\mu \xi_\nu + \nabla_\nu \xi_\mu = \frac{1}{2} g_{\mu\nu} \left(\nabla_\rho \xi^\rho\right) \propto g_{\mu\nu} \tag{5.18}$$

and correspond to conformal Killing horizons. We check that the vector field $\xi^\mu = (v, r, 0, 0)$ in EF coordinates is a conformal Killing vector field of the Vaidya spacetime with VKP mass function by computing the left-hand side in Eq. 5.18, i.e.

$$\nabla_\mu \xi_\nu + \nabla_\nu \xi_\mu = 2g_{\mu\nu} + \frac{2G_0}{r}\left(M(v) - \dot{M}(v)v\right)\delta^v_\mu \delta^v_\nu \overset{M(v)=\mu v}{=} 2g_{\mu\nu}, \tag{5.19}$$

which is indeed proportional to $g_{\mu\nu}$. The two conformal Killing horizons delineate a wedge in the (r, v)-spacetime diagram, see Fig. 5.4c. This wedge is bounded on the left by r_-, the degenerate conformal Killing horizon occurring at $\mu = \mu_c$ which is tangent to the event horizon at the centre $(r, v) = (0, 0)$. Accordingly, the wedge is bounded on the right by r_+, which constitutes the Cauchy horizon of the Vaidya spacetime. Therefore, all null geodesics that emanate from the point $(r, v) = (0, 0)$ and are not focused back towards $r = 0$ in the future lie within the wedge in between r_- and r_+ and this wedge is non-empty.

5.1.5 Photon sphere and photon surfaces

To complete our discussion of the VKP model and null geodesic motion within it, we review what is known about the photon sphere and photon surfaces – using the nomenclature of [CVE01].[5]

[5] We make the distinction between a *photon sphere* and a *photon surface*. A *photon sphere* is a sphere within which photons are so strongly lensed that they can orbit the central compact object up to infinitely many times and yield unbounded deflection angles. In a *photon surface*, photons may orbit the central compact object a certain number of times but not arbitrarily many. Hence, photons are not trapped

The VKP model is time-dependent, there is no Killing vector associated with stationarity, and hence energy is not conserved for geodesic motion. However, as seen in Subsec. 5.1.4, there is a conformal Killing vector field which makes the null geodesic equations separable [NV06]. For subcritical accretion $\mu < \mu_c$, this conformal Killing vector field is timelike, that is $\xi^\mu \xi_\mu < 0$, in the wedge bounded by r_- and r_+ given in Eq. 5.13. Due to the existence of a constant of motion associated with the timelike conformal Killing vector, a photon sphere in the sense of [CVE01] exists in the wedge and has been computed in [SP22]. This photon sphere is associated with strong lensing and unbounded deflection angles.

We choose here not to restrict to a particular regime and consider all possible accretion rates μ, for which a photon sphere might not always exist (e.g. for $\mu > \mu_c$). Instead, we focus on solving the null geodesic equation explicitly to find the location of the so-called "photon surfaces" – as defined in [CVE01]. This is also motivated by the fact that when we will consider upgrades of the mass function $M(v)$ to more general mass functions of the form $M(v, r)$ in Sec. 5.5, the conformal Killing vector field will be lost and no photon sphere will exist, while the notion of photon surfaces will remain.

Due to spherical symmetry, we can restrict ourselves to the equatorial plane to solve the geodesic equation, without loss of generality. Note that in contrast to Eq. 5.7, we are not considering radial geodesics and refer the reader to [MCS19] on how to derive the appropriate geodesic equation. For the VKP model, it reads

$$\ddot{r}_{\rm p}(v) - \frac{6G_0^2 v^2 \mu^2}{r_{\rm p}^3(v)} + \frac{G_0 v \mu (5 - 9\dot{r}_{\rm p}(v))}{r_{\rm p}^2(v)} + \frac{3\dot{r}_{\rm p}(v) - 1 + G_0\mu - 2\dot{r}_{\rm p}^2(v)}{r_{\rm p}(v)} = 0. \tag{5.20}$$

Since accretion stops at $v = \bar{v}$ and yields a spacetime locally isometric to Schwarzschild, we have to impose the following initial condition at $v > \bar{v}$: photon surfaces should coincide with Schwarzschild's photon sphere

$$\begin{cases} r_{\rm p}(v) = 3G_0\mu\bar{v}, \\ \dot{r}_{\rm p}(v) = 0. \end{cases} \tag{5.21}$$

Numerically, we find that the sharp transition in $M(v)$ at $v = \bar{v}$ impacts the stability of the evolution equation for the photon surface. Hence, in practice, we derive the location of the photon surface for a smooth function that well approximates the VKP mass, i.e.

$$M_{\rm sVKP}(v) = \frac{\mu v}{1 + e^{-2k(\bar{v}-v)}} + \frac{\mu\bar{v}}{1 + e^{-2k(v-\bar{v})}}, \tag{5.22}$$

with k sufficiently large. Fig. 5.3 shows the original VKP mass function, its smooth version corresponding to Eq. 5.22 and the corresponding photon surface for $G_0\mu = \frac{1}{2}$.

One may think of a photon surface as a location where photons undergo substantial gravitational lensing, such that they may circle the central compact object finitely many times, but without being unboundedly deflected, c.f. Footnote 5. For black holes, a photon surface surrounds the apparent horizon at radii not much larger than the radius of the apparent horizon. However, in a dynamical spacetime, gravitational lensing may also occur where the local concentration of matter is high enough. In

for many orbits within a compact region surrounding the central compact object and will not lead to unbounded deflection angles.

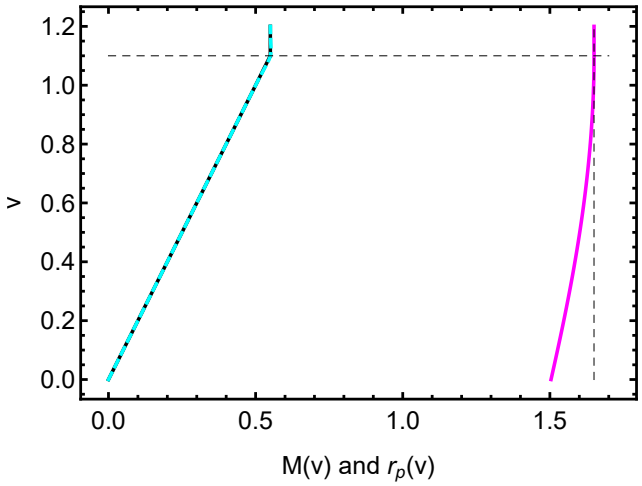

FIGURE 5.3: We show a graphical representation of the VKP mass function (black; see Eq. 5.2), its smooth approximation with $k = 30$ (dashed cyan; see Eq. 5.22) and the evolution of the photon surface for the latter mass function with $G_0\mu = \frac{1}{2}$ (magenta). The accretion stops at $\bar{v} = 1.1$ as indicated by the horizontal dashed line. The radial location of the Schwarzschild's photon sphere is indicated by the vertical dashed line.

particular, for the VKP model with a low enough accretion rate, the location of substantial gravitational lensing is initially not close to the centre at $r = 0$, but instead at very large radii, where the infalling shell of null dust is located. Thus, for very low accretion rates, the photon surface follows the infalling radiation and therefore approaches the initial condition Eq. 5.21 from large r, c.f. Fig. 5.4c, see also [CVE01]. In contrast, for very large accretion rates $1 > G_0\mu \gg G_0\mu_c$, the situation is closer to the case where the spacetime for $v < 0$ already contains a black hole which grows through accretion for $0 < v < \bar{v}$, see e.g. [Kog+22]. In that case, a photon surface grows from a finite value towards the initial condition given by Schwarzschild's photon sphere. Finally, the case $\mu \gtrsim \mu_c$ is in between these two: a photon surface starts at finite radius r_p, but then moves inwards as it follows the accreting matter. Only later does it move towards larger radii.

5.1.6 Spacetime diagrams

We can now summarise our review of the classical VKP model in the three spacetime diagrams in Fig. 5.4. The spacetime diagrams show two distinct regimes, depending on the value of the accretion rate μ compared to its critical value $\mu_c \equiv \frac{1}{16G_0}$. In both regimes, the classical VKP model is geodesically incomplete, as indicated by the finite advanced time v taken by light rays to fall back to the singularity located at the centre $r = 0$ (see Footnote 4). This is consistent with the NEC condition and the Einstein field equations, cf. Subsec. 5.1.1, as implied by the null version of the Penrose-Hawking singularity theorems [Pen65].

The spacetime always possesses an apparent horizon given in Eq. 5.16 which forms a straight line contained inside an event horizon, both forming at $v = 0$. The apparent horizon loses its dynamical nature when accretion stops and corresponds to the event horizon for $v > \bar{v}$.

The curvature singularity in the centre $r = 0$ is always entirely covered by an event horizon for $\mu > \mu_c$, i.e. for all $v \geq 0$, satisfying the strong cosmic censorship

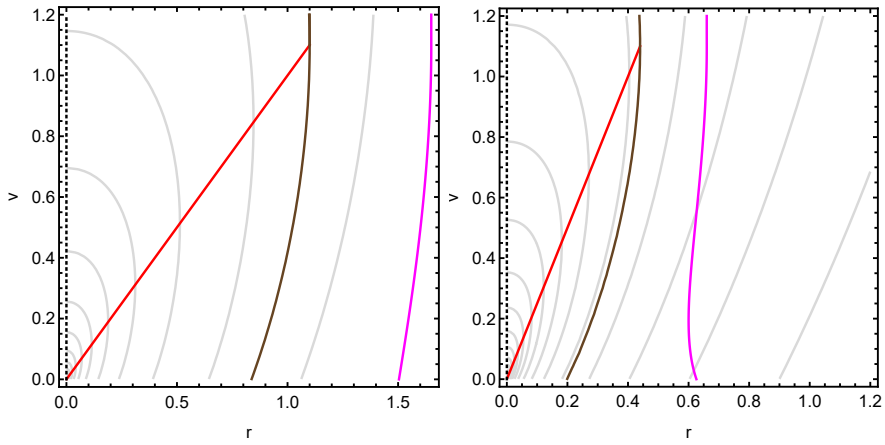

(A) $1 > G_0\mu \gg G_0\mu_c$

(B) $G_0\mu \gtrsim G_0\mu_c$

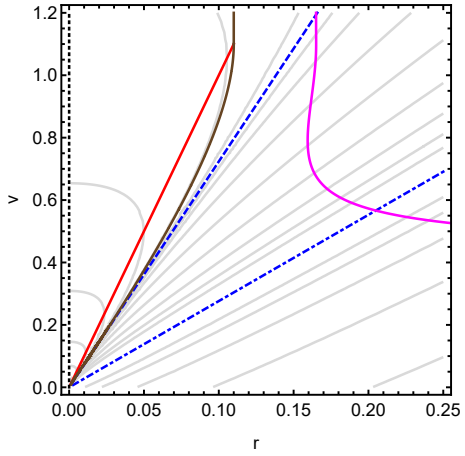

(C) $G_0\mu \leq G_0\mu_c$

FIGURE 5.4: We show the (r, v)-spacetime diagrams of null geodesics for the classical VKP model for three different values of $G_0\mu$. In all panels, the apparent horizon is represented by a straight red line, the event horizon by a brown curve and the photon surface by a magenta curve. Top left panel: for $G_0\mu = \frac{1}{2} \gg G_0\mu_c$ the curvature singularity is hidden behind an event horizon. Top right panel: $G_0\mu = \frac{1}{5} > G_0\mu_c$ (same behaviour). Bottom panel: for $G_0\mu = \frac{1}{20} < G_0\mu_c$ a globally naked singularity is present and the photon surface crosses the Cauchy horizon (blue dash-dotted line) and the other conformal Killing horizon (blue dashed line). The accretion stops at $\bar{v} = 1.1$ for all three cases.

conjecture. However, for $\mu \leq \mu_c$, shown in Fig. 5.4c, a globally naked singularity with lightlike and spacelike sections forms: all null rays comprised between the two linear solutions $r_\pm(v)$ emanate from the lightlike section of the singularity at $(r(v), v) = (0, 0)$ and can reach an observer at infinity. Thus the spacetime contains a Cauchy horizon that forms the causal boundary of the region in which the initial-value problem has a well-defined future evolution.

Hence, despite its simplicity, the VKP model for spherically symmetric gravitational collapse can violate the strong cosmic censorship conjecture in the regime $\mu \leq \mu_c$.

5.2 Beyond the simple VKP model

The Vaidya spacetime provides us with a simple example of a dynamical spacetime in GR, as it is spherically symmetric and sourced only by the accumulation of null dust over time. We focused on a particularly simple class of Vaidya spacetimes describing gravitational collapse, namely the VKP model, in which the increasing mass function $M(v)$ grows linearly with v. However, the simplicity of the VKP model precludes its astrophysical realisation: we do not expect astrophysically viable BH formation scenarios to yield a curvature and/or a naked singularity.

Other spherically symmetric, idealised models of gravitational collapse in GR share similar issues. The Oppenheimer-Snyder-Datt pressureless dust collapse [Dat38a; OS39] can exhibit a naked singularity once inhomogeneities in the initial density profile are accounted for, and similarly for the Lemaître-Tolman-Bondi isotropic but radially inhomogeneous collapse [Lem33; Tol34; Bon47]. Other dust or self-similar, spherically symmetric collapse models also show locally or globally naked singularities [Lak91; JD92; DJ92; JD93; Car00].

Hence, we expect that models of gravitational collapse with fewer symmetries will exhibit a modified gravitational dynamics, e.g. as in the Kerr-Vaidya spacetime [ST15], or more general matter content, e.g. a combination of null dust and non-null fluid, sourcing dynamically increasing mass functions of the form $M(v,r)$.
One example of such a more generalised dynamical spacetime within GR is the generalised Vaidya spacetime [Hug71] given by the line element

$$ds^2_{\rm EF} = -f(v,r)dv^2 + 2dv\,dr + r^2 d\Omega^2, \quad f(v,r) = 1 - \frac{2G_0 M(v,r)}{r}. \tag{5.23}$$

in EF coordinates. The energy-momentum tensor associated with null dust and non-null fluid reads

$$T_{\mu\nu} = \rho n_\mu n_\nu + (\varrho + p)(l_\mu n_\nu + l_\nu n_\mu) + p g_{\mu\nu}, \tag{5.24}$$

where l_μ and n_μ are null vectors satisfying the condition $l_\mu n^\mu = -1$, ρ is the energy density of the null dust, and ϱ and p are the energy density and pressure of the non-null fluid.

In Sec. 5.5, we will put forward a family of upgraded Vaidya metrics that we construct by implementing a set of principles for phenomenological models of spacetimes beyond GR, following the *principled-parameterised approach*. We use the VKP model as our starting point and upgrade spacetimes within the class of generalised Vaidya spacetimes in which $M = M(v,r)$. Incidentally, one member of this family of metrics can be constructed in a different, independent approach, namely by Renormalisation-Group (RG) improvement within asymptotically safe gravity.

5.3 RG-improved black holes

RG improvement starts from a specific theory, typically asymptotically safe gravity discussed in Subsec. 3.5.1, and is thus part of what one might call a "principled" or "fundamental" approach to spacetimes beyond GR. RG improvement is a method to incorporate loop corrections into the solutions of the equations of motion and is as such well-established in quantum field theory [CW73]. Within asymptotically safe

gravity, it has first been used in [BR99; BR00]. However, in the context of gravity, there are ambiguities in the procedure, see e.g. [Hel21], reviewed in [EH22]. Thus, the resulting black-hole spacetimes have the status of toy models inspired by asymptotically safe gravity, rather than solutions to a full theory of quantum gravity.

In its simplest incarnation, RG improvement in gravity starts from a classical spacetime and promotes the coupling constants to scale-dependent couplings that "run" as a function of scale, as described by the RG. The final step consists of identifying the RG scale with a suitable physical scale of the spacetime. This step is well-motivated in asymptotically safe gravity, in which the specific version of an RG equation that is used is the functional RG, see [Dup+21] for a review. The functional RG is based on an infrared cutoff in the path integral. This infrared cutoff is lowered successively, such that fluctuations are integrated over step by step. The decoupling mechanism (see [RW04] for its first use in gravity) causes fluctuations to decouple once their mass scale is reached, i.e. fluctuations in a given field no longer impact the effective dynamics once the infrared cutoff lies below their mass scale. Because curvature can act as an effective mass, the identification of the RG scale with a curvature scale is well-motivated, see [Pla23; BP23] for further discussion. There are, however, examples in the literature in which the RG scale is instead equated to an inverse length scale, e.g. the geodesic distance from the black hole's centre, as in [BR00; RT11; FLR12; Tor14]. This is not motivated by the decoupling mechanism, because the geodesic distance does not enter the effective mass of modes. In settings with a high degree of symmetry, e.g. in spherically symmetric black holes, the results are equivalent with those obtained by using the curvature scale as the RG scale. In settings with fewer Killing vectors, the results are no longer equivalent [EH22].

Taking as our starting point the Vaidya metric Eq. 5.1, the only coupling in that metric is the Newton coupling G_0, which will first be promoted to a running coupling G and then chosen to depend on the curvature.[6]

5.4 The principled-parameterised approach

The principled-parameterised approach (see also Subsec. 3.6.3), developed in [EH21a; EH21b; EHJ23], is largely agnostic with respect to the theory of gravity. It is a phenomenological approach, in which the guiding question is: what is the minimal modification of a given singular, classical spacetime that implements four principles, namely locality, simplicity, regularity and a Newtonian limit?

In practice, for stationary black-hole spacetimes, the minimal modification consists in an upgrade of the ADM mass parameter M to a function of the spacetime coordinates $M(x^\mu)$. Based on [EH21a; EH21b; EHJ23], this mass modification is sufficient to implement all principles; based on [DEH22], an upgrade of the spin parameter is not, see Subsec. 6.2.2.

[6] Even if the scale is chosen to be a function of curvature through non-derivative curvature invariants, which are coordinate-invariant quantities, it does not remove all ambiguities. In particular, applying such an RG improvement at the level of a given stationary, axisymmetric and asymptotically flat spacetime written in two sets of coordinates renders the two RG-improved spacetimes inequivalent, as shown in [Hel21]. This arises because the metric on which RG improvement is applied transforms as a tensor and not as a scalar (invariant) quantity. Despite this ambiguity, RG improving spacetime metrics may capture some of the salient features of the would-be BH solutions in full ASQG.

To implement locality, the ADM mass M is not upgraded to a general function of the spacetime coordinates x^μ, but instead depends on a coordinate-invariant quantity, namely a suitable choice of local curvature invariants. Because the upgraded mass function must have a dimensionless argument, the upgrade introduces a new scale into the spacetime, namely the new-physics scale $r_{\rm NP}$. Simplicity is achieved if no second scale is introduced. The last two principles, regularity (i.e., absence of curvature singularities) and the Newtonian limit dictate the asymptotic dependence of the mass function on the curvature; simplicity dictates the monotonicity of the mass function between the two asymptotic limits of low and large curvatures. Thereby, the four principles are sufficient to arrive at a family of regular metrics. This family has one free function $M_{\rm NP}(x^\mu)$, of which the asymptotic behaviours are fixed and which must satisfy monotonicity requirements, and one free scale $r_{\rm NP}$ that determines the transition between the two asymptotic behaviours.

5.5 A regular metric for gravitational collapse in two approaches

Restricting to static and spherically symmetric spacetimes, the constants G_0 and M always appear in combination with each other, e.g. in the Schwarzschild spacetime. Hence, we can either apply the RG-improvement method to G_0 and replace it with its running counterpart, or implement the principled-parameterised approach to upgrade the ADM mass M to a spacetime-dependent function $M(x^\mu)$. It is thus not surprising that RG improvement of static black-hole spacetimes results in a metric that also arises in the principled-parameterised approach, see [EH22].

We discover that the correspondence found for static and spherically symmetric spacetimes continues to hold when spacetimes become *dynamical*. That is, we find that the RG-improved Vaidya metric is equivalent to one member in the family of regular metrics constructed in the principled-parameterised approach. The reason is twofold: first, as in the static case, the Newton coupling always appears as a multiplicative factor in front of the mass function in the classical Vaidya metric. Thus, an upgrade of the Newton constant G_0 to a curvature-dependent function can be traded for an upgrade of the Misner-Sharp mass M to a curvature-dependent function. Second, the RG dependence of the Newton coupling satisfies two of the four principles of the principled-parameterised approach automatically, namely simplicity and the Newtonian limit. Simplicity holds because the only special scale in the running of the Newton coupling is the Planck scale, where the transition between the asymptotically safe scaling regime and the classical regime occurs.[7] The second principle is the Newtonian limit which is realised because, in the low-curvature regime, the Newton coupling is constant to recover classical GR from asymptotic safety, thus the metric is not modified in this regime. Non-trivially, the fixed-point scaling of the Newton coupling is also just sufficient to make (non-derivative) curvature invariants regular; thus the metric also satisfies regularity and is, therefore, one special choice in the family of regular metrics.

Going from static to stationary spacetimes, the situation already becomes more subtle, because the locality principle is not always respected when RG improvement is implemented by choosing a non-local notion of scale [RT11; LN14; PS18], see the discussion in [EH22]. This results in important differences, e.g. (non-)circularity of

[7] The presence of a single scale in ASQG, namely the Planck scale, is a non-trivial result which follows from the compelling evidence of a single fixed-point in the UV-regime. If several distinct fixed points were to be present, more than one scale would play a role in ASQG.

the spacetime [DEH22]. Similarly, in time-dependent settings describing gravitational collapse, the regularity principle is not obeyed in examples in which the locality principle is neglected [BKP17; BP23]. Here, we thus aim at exploring whether or not implementing the locality principle within a dynamical spacetime gives rise to a regular spacetime.

5.5.1 In the principled-parameterised approach

... where the Misner-Sharp mass $M(v)$ is upgraded to a generalised mass function $M(v,r)$ satisfying the locality, Newtonian limit, regularity and simplicity principles rooted in the principled-parameterised approach.

Implementing the locality principle

We start from the Vaidya metric with the line element Eq. 5.1. In contrast to previously-derived spacetimes in the principled-parameterised approach [EH21a; EH21b; EHJ23], the considered spacetime is not stationary, and the mass is not a constant parameter, but already depends on the advanced time v. We promote it to a more general function of the coordinates

$$M(v) \to M_{\rm NP}(x^\mu), \tag{5.25}$$

where the subscript NP stands for "new physics" and indicates that this upgrade should be understood as a phenomenological approach to a more complete theory of gravity beyond GR. To implement locality, $M_{\rm NP}(x^\mu)$ may only depend on the spacetime coordinates through curvature invariants.[8] This follows an EFT reasoning, in which higher-order curvature invariants are expected to be present in the action and to modify the metric at high enough values of the classical curvature [RSW20].

As discussed in Subsec. 5.1.3, the only independent, non-derivative curvature invariant of the Vaidya spacetime is I_1 and thus we choose

$$M_{\rm NP}(x^\mu) = M_{\rm NP}(I_1\, r_{\rm NP}^4) = M_{\rm NP}\left(\frac{48G_0^2M(v)^2}{r^6}r_{\rm NP}^4\right). \tag{5.26}$$

The new-physics scale $r_{\rm NP}$ appears to keep the argument of the mass function dimensionless.[9] The upgraded mass function $M_{\rm NP}$ also depends on the classical mass function $M(v)$. To avoid confusion between the original mass function $M(v)$ and the upgraded mass function, the latter always carries the subscript NP, i.e. $M_{\rm NP}(I_1 r_{\rm NP}^4)$.

Implementing the Newtonian limit

At this stage, $M_{\rm NP}$ is a completely arbitrary function. We now fix its asymptotic behaviour at low values of the curvature.

We require that for $I_1 r_{\rm NP}^4 \to 0$, $M_{\rm NP} \to M(v)$, such that the classical spacetime (which has the appropriate Newtonian limit for $v > \bar{v}$) is recovered. This is easiest implemented by writing

$$M_{\rm NP}\left(\frac{48G_0^2M(v)^2}{r^6}r_{\rm NP}^4\right) = M(v)\cdot f_{\rm NP}\left(\frac{48G_0^2M(v)^2}{r^6}r_{\rm NP}^4\right), \tag{5.27}$$

[8] Because we work at the level of the spacetime metric and not the action or the equations of motion, we do not know whether locality as we implement it here translates into a local action or not.

[9] Recall that we work in units in which $c = 1$ but $G_0 \neq 1$.

where $f_{\rm NP}$ is a function that parameterises the modifications and of which we now require

$$\lim_{I_1 r_{\rm NP}^4 \to 0} f_{\rm NP}\left(\frac{48 G_0^2 M(v)^2}{r^6} r_{\rm NP}^4\right) = 1. \tag{5.28}$$

In principle, subleading coefficients of $f_{\rm NP}$ can be adjusted in the low-curvature expansion to account for specific post-GR corrections, e.g. from the EFT approach to QG [Don23], but we do not do so here and keep the subleading coefficients general.

Implementing regularity

The other asymptotic limit at large curvature, is fixed by the regularity principle, that is the absence of curvature singularities.

To determine the correct fall-off of $f_{\rm NP}(I_1 r_{\rm NP}^4)$ at large $I_1 r_{\rm NP}^4$, we first need to evaluate the (non-derivative) curvature invariants with the upgraded mass function Eq. 5.27. Because the upgraded mass function is also a function of r, not just v, the upgraded spacetime is part of the class of generalised Vaidya spacetimes [Hug71], see Eq. 5.23.

We study the complete set of 17 non-derivative curvature ZM invariants of a generalised Vaidya spacetime. Their explicit dependence on the generalised mass function $M(v,r)$ is given in App. B.3. With the exception of I_1 and I_3, all curvature invariants are polynomial in $M'(v,r) \equiv \frac{\partial M(v,r)}{\partial r}$ and $M''(v,r) \equiv \frac{\partial^2 M(v,r)}{\partial r^2}$. This is consistent with the fact that all curvature invariants except for I_1 and I_3 vanish for the Schwarzschild spacetime, for which $M(v,r) = M = \text{const}$.

Because the curvature invariants are generically singular as $r \to 0$, see App. B.3, the mass function must acquire an r-dependence to lift the singularity. To determine the minimal power of r required, we make a power-law ansatz for the small-r-limit of the generalised mass function

$$M_{\rm NP}(v,r) \overset{r\to 0}{\simeq} h(v)\, r^\alpha. \tag{5.29}$$

The exact form of $h(v)$ does not matter for the following argument. All non-vanishing Weyl invariants (which include the Weyl tensor or its dual) of the upgraded spacetime vanish for $\alpha = 2, 3$ (unless $h(v) = \text{const.}$, in which case $\alpha = 2$ is still singular). However, all Ricci invariants of the upgraded spacetime are singular for $\alpha < 3$, singling out

$$\alpha = 3 \tag{5.30}$$

as the critical case, i.e. the minimal power of r required to lift the singularity in all polynomially independent, non-derivative curvature invariants. This agrees with the limiting case of the modified Schwarzschild, static spacetime, reached for $h(v) \to \text{const.}$, in which the curvature singularity of the Schwarzschild spacetime is lifted if the mass is upgraded to a radially dependent function with leading-order behaviour $M_{\rm NP}(r) \sim r^3$, cf. [EHJ23].

We now translate the results of this asymptotic analysis into a requirement on the modification function $f_{\rm NP}(I_1 r_{\rm NP}^4)$. To achieve $M_{\rm NP}(v,r) \sim r^3$ or higher powers of r, we must have

$$f_{\rm NP}(I_1 r_{\rm NP}^4) \sim \frac{1}{\left(I_1 r_{\rm NP}^4\right)^{\frac{n}{2}}}, \quad \text{for } I_1 r_{\rm NP}^4 \to \infty, \tag{5.31}$$

with $n \geq 1$. Hereeafter, we mostly focus on the case $n = 1$, which is the minimal case to make the spacetime regular.

Implementing simplicity

Simplicity requires that $f_{\rm NP}(I_1 r_{\rm NP}^4)$ introduces only a single new physics scale into the spacetime. This translates into two constraints on $f_{\rm NP}$: first, it must not depend explicitly on any other scale than $r_{\rm NP}$; second, it must be a monotonic function of $I_1 r_{\rm NP}^4$ because any additional extremum introduces a second scale besides $r_{\rm NP}$. Hence, $f_{\rm NP}$ must be a monotonic function of a single argument, namely $I_1 r_{\rm NP}^4$.

A simple way to achieve all four principles is to choose

$$f_{\rm NP}(I_1 r_{\rm NP}^4) = \frac{1}{1 + \left(I_1 r_{\rm NP}^4\right)^{\frac{n}{2}}}, \quad n \geq 1. \tag{5.32}$$

Other functions with the same asymptotic behaviour that fulfil the monotonicity requirement, following e.g. a Dymnikova-profile [Dym92], are part of the same family of upgraded Vaidya spacetimes. One notable example that is already contained in Eq. 5.32 is Hayward's regular gravitational collapse [Hay06], with the identification $\ell^2 \equiv \sqrt{6} r_{\rm NP}^2$ and for $n = 1$.

Due to the monotonicity requirement and the two asymptotic constraints, $f_{\rm NP}$ is smaller than or equal to one everywhere. Thus, the upgraded mass is, at any given advanced time v, smaller than or equal to the classical mass

$$M_{\rm NP}(v, I_1 \cdot r_{\rm NP}^4) = M(v) f_{\rm NP}(I_1 \cdot r_{\rm NP}^4) \leq M(v) \quad \forall v. \tag{5.33}$$

As a result, the modified collapsing body is more compact than its classical counterpart in the sense that, once a horizon is formed, the latter is more compact than the classical horizon. This is a generic feature of regular black holes satisfying the conditions spelt out in [EHJ23], for which the central curvature singularity is removed by weakening gravity. The only way to avoid the resulting increase in compactness is to introduce a second scale, such that $M_{\rm NP}$ is larger than its classical counterpart in the spacetime region around the apparent horizon, and thus to violate simplicity.

To illustrate the increase in compactness, we show $f_{\rm NP}(v, r = r_{\rm AH})$ as in Eq. 5.32 for $n = 1$ at the apparent horizon $r_{\rm AH}$ given in Eq. 5.43 in Fig. 5.5.

$f_{\rm NP}$ increases as a function of v, because the mass of the black hole grows, decreasing the relative impact of new physics at the constant scale $r_{\rm NP}$ over time. Smaller accretion rates result in a smaller $f_{\rm NP}$ at a given advanced time v because the black-hole mass is smaller than for a larger accretion rate. These effects can also be read off from the Taylor expansion of $f_{\rm NP}$ in the dimensionless quantity $\frac{G_0 \mu v}{r_{\rm NP}}$, which is

$$f_{\rm NP}(r = r_{\rm AH}) = \frac{1}{2} + \frac{(G_0 \mu v)^{\frac{2}{3}}}{2^{\frac{5}{3}} \cdot 3^{\frac{1}{6}} \cdot r_{\rm NP}^{\frac{2}{3}}} + \mathcal{O}\left(\left(\frac{G_0 \mu v}{r_{\rm NP}}\right)^{\frac{4}{3}}\right). \tag{5.34}$$

We will analyse further properties of the family of upgraded spacetimes below, but we first explain how one member of the family can be constructed inspired by asymptotically safe gravity.

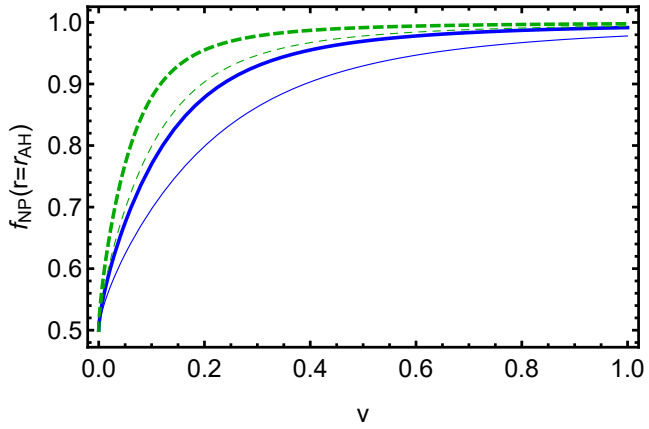

FIGURE 5.5: We show $f_{\rm NP}(v, r = r_{\rm AH})$ evaluated at the location of the apparent horizon $r_{\rm AH}$ Eq. 5.43, as a function of v for $r_{\rm NP} = 10^{-3}$ (thick lines) and $r_{\rm NP} = 6 \cdot 10^{-3}$ (thin lines). For each value of $r_{\rm NP}$ we consider two accretion rates: $G_0\mu = 10^{-2}$ (blue lines) and $G_0\mu = 2 \cdot 10^{-2}$ (green lines). The classical behaviour is recovered in the limit $f_{\rm NP} \to 1$. Conversely, the more $f_{\rm NP}$ departs from 1, the stronger are the new-physics effects.

5.5.2 Inspired by ASQG via RG improvement

. . . where the Newton constant is upgraded to its running counterpart from ASQG and chosen to depend on a specific combination of curvature invariants.

As reviewed in Subsec. 3.5.1, ASQG is a quantum field theoretic approach to quantum gravity. Gravity is asymptotically safe if there is quantum scale symmetry, encoded in an interacting fixed point of the RG, above the Planck scale. This ensures UV completion and (non-perturbative) renormalisability in the sense that only a finite number of free parameters must be fixed to make the theory predictive. There is by now compelling evidence for an interacting fixed point in gravity (as well as gravity plus suitable matter) in four dimensions in Euclidean signature, see [Eic19; Bon+20; ES22; Sau23; PR23] for reviews and [Per17a; RS19b] for textbooks. Most of these results rely on the FRG [Wet93; Ell94; Mor94], reviewed in [Dup+21] and adapted to gravity in the seminal paper [Reu98].

For our purposes, it is useful to consider the regularised generating functional on which the method relies, namely Eq. 3.16 written in short form as

$$Z_k[J] = \int_{\Lambda_{\rm UV}} \mathcal{D}h_{\mu\nu} e^{-S[\bar{g}_{\mu\nu}+h_{\mu\nu}]-S_{\rm gf}[\bar{g}_{\mu\nu};h_{\mu\nu}]-\frac{1}{2}\int d^4x\sqrt{\bar{g}}h_{\mu\nu}R^{\mu\nu\kappa\lambda}[-\bar{D}^2/k^2]h_{\kappa\lambda}+\int d^4x\sqrt{\bar{g}}J_{\mu\nu}h^{\mu\nu}}. \tag{5.35}$$

In here, the full metric $g_{\mu\nu}$ is split into an auxiliary background $\bar{g}_{\mu\nu}$ and fluctuations $h_{\mu\nu}$. The background is used to gauge-fix the fluctuations through the gauge-fixing term $S_{\rm gf}$ (understood to include the corresponding Faddeev-Popov ghost term). Because the fluctuations are not restricted to be small, $Z_k[J]$ is a fully non-perturbative path-integral. $J_{\mu\nu}$ is a source term and $\Lambda_{\rm UV}$ indicates that the path integral has been suitably regularised in the UV. Finally, $R^{\mu\nu\kappa\lambda}[-\bar{D}^2/k^2]$ is an infrared cutoff term which suppresses fluctuations according to their generalised momentum, i.e. the eigenvalues of the background-covariant Laplacian $-\bar{D}^2$: decomposing a field configuration $h_{\mu\nu}(x)$ into eigenmodes of $-\bar{D}^2$, those with eigenvalues higher than k^2 are integrated out first. Successively lowering k, one integrates out all fluctuations in the

path integral.

A functional differential equation for the Legendre transform of $Z_k[J]$ tracks the resulting scale dependence of the couplings. For instance, the resulting scale dependence of the Newton coupling is, in a simple approximation, given by [Reu00]

$$G(k) = \frac{G_0}{1 + \frac{G_0}{G_*}k^2}, \tag{5.36}$$

where G_* is a dimensionless number corresponding to the fixed-point value of the dimensionless product Gk^2 and we recall that G_0 is the classical value of the Newton constant. As a result, for $k^2 \ll \frac{G_0}{G_*}$, $G(k) = G_0 = \text{const}$, i.e. at low scales, classical gravity with a constant Newton coupling is recovered. For $k^2 \gg \frac{G_0}{G_*}$, we enter a scaling regime with $G(k) \sim k^{-2}$. This can be understood as a weakening of gravity through gravitational fluctuations. This weakening is a prerequisite for a quantum field theory of gravity to make sense. Among other things, it also suggests that classical curvature singularities could be resolved – at least, if one associates the behaviour of the coupling at high k^2 with the behaviour at high curvature scales.

This association brings us directly to the idea underlying RG improvement, in which the Newton constant G_0 is replaced by the scale dependence (5.36) in a classical metric, and the RG scale k is matched onto a physical scale of the classical spacetime. Before doing so, we clarify several points concerning both the level at which the RG improvement is made and the scale identification.

Firstly, the upgrade of the classical coupling constants to their running counterparts can be made at three different levels, cf. the discussion in the reviews [EH22; Pla23]: in the classical action, in the equations of motion or in the spacetime metric. The three improvements are in general not equivalent, resulting in potentially different upgraded spacetime metrics. It is unclear which of them actually produces results closest to the solution of the full quantum theory, however, the last one is the most straightforward to implement. We thus apply the RG improvement method at the level of the Vaidya metric. Secondly, classical gravitational systems usually possess more than one characteristic scale, resulting in some freedom of choice for the scale identification. Even in settings with a high degree of symmetry, where all scales are related to each other, different choices can produce different results. For instance, for spherically symmetric, static black holes, where the ADM mass M sets the value of all other scales, identifying k with e.g. the local curvature scale [HGE19] or the Hawking temperature [BHA23] produces different results.

There are many examples of classical gravitational-collapse spacetimes that have been RG-improved within ASQG, see [CHM11; Tor14; TF14; TF15; BKP17; BKP18; Pla19; BP23]. As highlighted, different RG-improvement procedures and scale identifications indeed lead to somewhat different conclusions regarding the singularities and the spacetime's structure. However, as a universal result, the central singularity is weakened, as first pointed out in [CHM11]. Whether the central curvature singularity is made integrable or fully cured depends both on the type of RG improvement and the choice of scale identification. For example, the central singularity is present but made weaker in [BKP17; BKP18] when identifying the RG scale with the collapsing fluid's energy density. It is also found to be weakened in [BP23], where the scale is determined via the decoupling mechanism [RW04] in an iterative sequence of RG

improvements [Pla19]. Instead, the central curvature singularity can be fully regularised by the effective repulsive forces generated by the running of the gravitational coupling, as in [Tor14]. This conclusion still holds when backreaction from Hawking radiation is included, see [TF14; TF15]. However, the absence of shell-focusing singularities does not entail that shell-crossing singularities are absent at larger radii, as interactions of dust or fluid particles, which would prevent matter shells from crossing, are usually ignored.

Due to the caveats related to the RG improvement procedure, we consider the spacetime that we construct below as a spacetime *inspired* by asymptotically safe gravity and expect that it may capture the main features that a solution to the full quantum equations of motion has, but stress that this expectation can only be checked a posteriori. We consider the scale identification with curvature invariants the most physical choice and it is reassuring to see that this choice results in an absence of curvature singularities for static black holes, stationary black holes (as reviewed in [EH22]) and, as we show here, for at least one example of gravitational collapse. Hence, we promote the classical Newton constant G_0 to its dimensionful running counterpart in Eq. 5.36 and identify $k^2 \sim \sqrt{I_1}$. Incidentally, this corresponds to a particular choice of the upgraded mass function that is included in Eq. 5.27.

5.6 Properties of the regular upgraded dynamical spacetime

We now explore the consequences of a mass upgrade (discussed in Subsec. 5.5.1) or an upgrade of the Newton coupling constant (discussed in Subsec. 5.5.2) on the structure of the resulting upgraded, regular, dynamical spacetime. Similarly to the classical case reviewed in Sec. 5.1, we first gain insight into geodesic (in)completeness by determining the behaviour of null geodesics near the centre $r = 0$ and contrasting it with the NEC. We then study the spacetime's structure and null geodesic motion within it from the centre $r = 0$ to larger radii.

5.6.1 Null geodesic motion near the centre

It is well established that regularity of (non-derivative) curvature invariants and geodesic completeness are not contingent upon one another. It is therefore not guaranteed that the upgraded spacetime we have constructed by requiring regular curvature invariants is geodesically complete. To catch a first glimpse of geodesic (in)completeness, we sketch the behaviour of null geodesics near the would-be classical singularity.

The radial null geodesic equation for the upgraded spacetime reads

$$\frac{dr}{dv} = \frac{1}{2}\left(1 - \frac{2M(v,r)}{r}\right). \tag{5.37}$$

We consider its small-r-behaviour, where we can by construction write $M(v,r) = h(v)r^\alpha$ with $\alpha \geq 3$ and $h(v)$ a positive but arbitrary function of v. We thus obtain

$$\frac{dr}{dv} = \frac{1}{2}\left(1 - 2h(v)r^{\alpha-1}\right) \approx \frac{1}{2}, \quad \text{for } r \to 0. \tag{5.38}$$

Instead of a divergent, negative right-hand side, as in the classical case, the right-hand side is positive and finite. Accordingly, null geodesics are repelled from the core at

$r = 0$ and instead move towards larger r. We confirm this behaviour numerically, cf. Fig. 5.6.

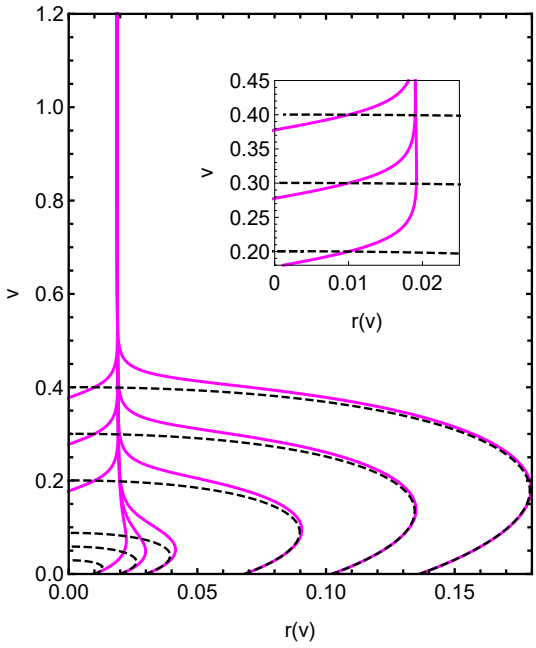

FIGURE 5.6: We show null geodesics near $r = 0$ for the upgraded case (magenta, continuous lines) and the corresponding classical case (black dashed lines) for $G_0\mu = 1/2$ and setting $G_0 = 1$ for the plot. We choose $r_{\rm NP} = 10^{-2}$. The inset zooms in on a set of trajectories at finite v, but very close to $r = 0$. The derivative $\frac{dr}{dv}$ has the opposite sign in the upgraded case to what it has in the classical case.

The change of sign of the derivative $\frac{dr}{dv}$ from negative in the classical case to positive in the upgraded case suggests that geodesics are no longer future-incomplete, but can instead be extended up to arbitrarily large v. In fact, null geodesics quickly converge towards an attractor at finite r that we will investigate in more depth in Subsec. 5.6.5.

As can be seen from the inset in Fig. 5.6, geodesics in classical and upgraded spacetime can start at small r at finite v. Thus, it is not possible to set up an initial-value problem in the spacetime, because there are always null geodesics to the future of any spatial hypersurface, which do not intersect the hypersurface when extended backwards in time. This suggests that the spacetime should be extended to $r < 0$. Numerically, null geodesics can be tracked into this region, but we do not explore this further. However, we emphasise that non-derivative curvature invariants of the upgraded spacetime might change sign at $r = 0$, hence rendering them multiple-valued, see App. B.3.

5.6.2 Energy conditions

Given the radically altered behaviour of null geodesics near $r = 0$ that we observe numerically, we expect that energy conditions, which are prerequisites to prove geodesic incompleteness, may be violated in the upgraded spacetime. In fact, all pointlike energy conditions have counter-examples; e.g. in the form of classical scalar fields with non-minimal scalar curvature coupling [Bek75; Des84; BV00; BV02] and in semiclassical gravity, see e.g. [EGJ65; ZP71; PF73; Rom86; Vis96a; Vis96b; FW96;

Vis97; BV02; KS20]. We expect them to break down in any QG-inspired spacetime, see [KC20] for an example in QG using EFT methods and [LLZ21; Hos05] in LQG. The violation of the pointwise energy conditions could then lead to geodesically complete spacetimes beyond GR. We focus on the NEC because it is the weakest of the pointlike energy conditions, i.e. if it is violated, all other pointlike energy conditions are violated as well [Vis95]. We leave aside the question of whether averaged energy conditions, reviewed in [Rom04; Cur17; KS20], hold or not.

The upgraded metric is actually a generalised Vaidya spacetime because the upgrade results in a v- and r- dependence of the mass. Therefore, the effective energy-momentum tensor associated with the upgraded metric through the Einstein field equations Eq. 2.1 is that of a generalised Vaidya spacetime. A generalised Vaidya spacetime, understood as a solution of the Einstein equations, describes the gravitational collapse of shells of non-null fluid – additionally to shells of null dust present in the classical case – flowing radially towards the centre. Outside of the shells, the vacuum exterior spacetime is spherically symmetric and asymptotically flat. Because in our case this spacetime arises as an upgrade of the Vaidya spacetime, the additional component in the effective energy-momentum tensor is not due to non-null fluid in the spacetime, but rather encodes new-physics effects at an effective level. This is particularly useful when examining energy conditions.
The energy-momentum tensor of a generalised Vaidya spacetime reads

$$T^{\text{eff}}_{\mu\nu} = \frac{\dot{M}(v,r)}{4\pi r^2}\, n_\mu n_\nu + \left(\frac{M'(v,r)}{4\pi r^2} - \frac{M''(v,r)}{8\pi r}\right)\left(n_\mu l_\nu + n_\nu l_\mu\right) - \frac{M''(v,r)}{8\pi r}\, g_{\mu\nu}, \quad (5.39)$$

with null vectors $n_\mu = \delta^0_\mu$ and $l_\mu = \frac{1}{2}\left(1 - \frac{2G_0 M(v,r)}{r}\right)\delta^0_\mu - \delta^1_\mu$ satisfying $n_\mu l^\mu = -1$ [MGM14]. Here, the dots correspond to differentiation with respect to v, while the primes refer to differentiation with respect to r.

The null energy condition requires

$$\varepsilon = T_{\mu\nu}k^\mu k^\nu = T_{00}(k^0)^2 + 2\,T_{01}k^0k^1 \geq 0 \quad (5.40)$$

for every future-pointing null vector field k^μ. The null condition on k^μ translates as

$$k_\mu k^\mu = 0 \Leftrightarrow k^1 = \frac{1}{2}\left(1 - \frac{2G_0 M(v,r)}{r}\right)k^0. \quad (5.41)$$

We insert the upgraded mass function from Eq. 5.27, focusing on the choice $n = 1$ in the following. Substituting k^1 by its expression in terms of k^0 derived in Eq. 5.41 in the mass-energy density Eq. 5.40, we obtain an expression in which k^0 appears within a positive prefactor. Since we are interested in regions of spacetime and parameter space in which the NEC is violated, i.e. $\varepsilon < 0$, we can drop this positive prefactor and obtain the following upper bound

$$\begin{aligned} 0 \leq\ & r^7 + 8\sqrt{3}\,G_0 r^4 r_{\text{NP}}^2 \mu v - 36\sqrt{3}\,G_0 r^3 r_{\text{NP}}^2 v^2 \mu + 48\,G_0^2 r r_{\text{NP}}^4 v^2 \mu^2 \\ & + 72\sqrt{3}\,G_0^2 r^2 r_{\text{NP}}^2 v^3 \mu^2 - 432\,G_0^2 r_{\text{NP}}^4 v^3 \mu^2. \end{aligned} \quad (5.42)$$

This results in an upper bound on r, namely $0 \leq r \lesssim r_{\text{NEC}}(v, \mu, r_{\text{NP}})$.

Regions of negative mass-energy density, where the NEC is violated, are shown as coloured-shaded regions in Fig. 5.7 for an accretion rate of $\mu = \frac{1}{10G_0} > \mu_c$, where

μ_c is the critical accretion rate delineating the two classical regimes discussed in Subsec. 5.1.6. We observe that the attractor for null geodesics, which we already found in Subsec. 5.6.1, coincides with the boundary of the spacetime region in which the NEC is violated. The physics of the attractor may thus be understood as follows: for values $r > r_{\rm NEC}$, gravity acts as an attractive force and thus focuses geodesics. For values $r < r_{\rm NEC}$, the modification of the mass function implements a repulsive gravitational force, expelling null geodesics from this region and resulting in a violation of the NEC. As a consequence, the boundary of the region of violations of the NEC acts as an attractor for null geodesics.

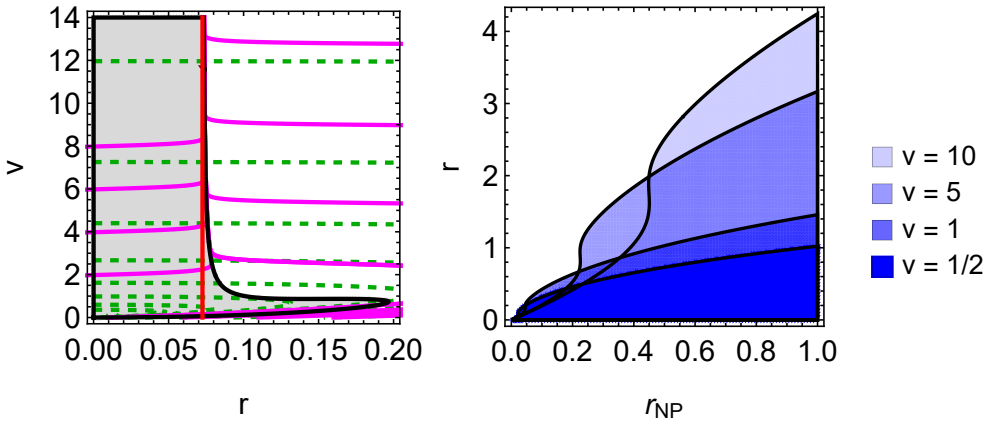

FIGURE 5.7: We show the region plots of the violation of the NEC for arbitrary k^0 and $G_0\mu = \frac{1}{10}$, i.e. coloured regions for which $\varepsilon < 0$. Left panel: region plot (r, v) of $\varepsilon < 0$ for $r_{\rm NP} = \frac{39}{1000}$ together with classical (dashed green) and upgraded (magenta) null geodesics. Right panel: region plot $(r_{\rm NP}, r)$ of $\varepsilon < 0$ from $v = \frac{1}{2}$ (dark blue) to $v = 10$ (light blue).

For this rather large value of μ, the last two terms in Eq. 5.42 dominate and lead to a constant upper bound $r_{\rm NEC} = 3^{\frac{1}{4}}\sqrt{2}r_{\rm NP}$ for r, represented by the red straight line in the left panel of Fig. 5.7. At small values of v, the other terms in Eq. 5.42 start playing a role and are responsible for the tail to larger values of r visible in the left panel of Fig. 5.7. The behaviour of the mass-energy density ε as a function of r and $r_{\rm NP}$ in the right panel of Fig. 5.7 interpolates between a linear regime at very small values of $r_{\rm NP}$ given by the contributions of the last two terms in Eq. 5.42, and a quadratic polynomial at larger values of $r_{\rm NP}$ due to the contributions of the additional terms.

We find a qualitative difference in the shape of the regions where the NEC is violated for small accretion rates, e.g. $G_0\mu = \frac{1}{1000} \ll G_0\mu_c$, in Fig. 5.8. This stems from the fact that, when μ is very small, the first three terms in Eq. 5.42 dominate. Indeed, considering only the first three terms in Eq. 5.42 and solving for $r(v)$, we obtain a very good approximation of the outer boundary of the grey shaded region in the left panel of Fig. 5.8, represented by a red curve. Similarly, we can find $r_{\rm NEC}(r_{\rm NP})$ for every chosen value of v in the right panel of Fig. 5.8, and the resulting curves delineate the outer boundary of the shaded blue regions where the NEC is violated. As displayed in the left panel of Fig. 5.8, the motion of geodesics is not correlated with the region in which the NEC is violated. This is because for $G_0\mu = \frac{1}{1000}$ and $r_{\rm NP} = \frac{39}{1000}$, the new-physics scale is larger than the critical value $r_{\rm NP} > r_{\rm NP,c}(v) \equiv \frac{2\sqrt{2}v\mu}{3^{\frac{7}{4}}}$. Hence, the upgraded spacetime is horizonless and the behaviour of null geodesics does not

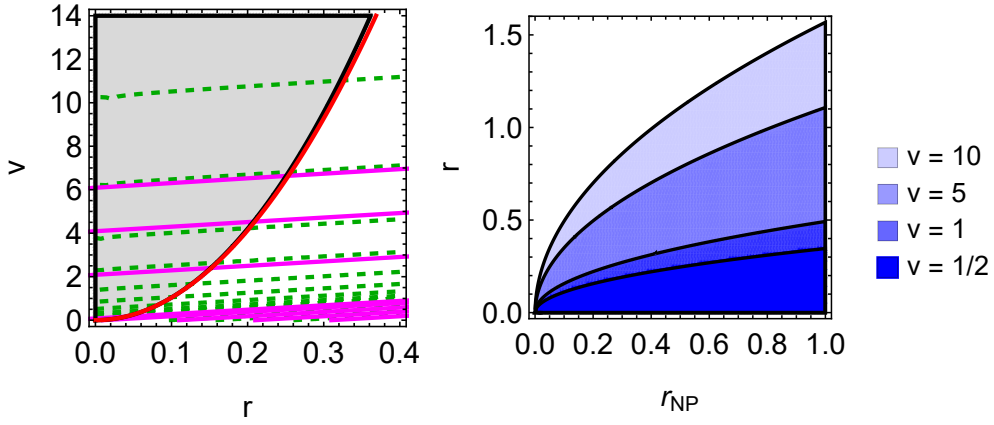

FIGURE 5.8: We show the region plots of the violation of the NEC for arbitrary k^0 and $G_0\mu = \frac{1}{1000}$, i.e. coloured regions for which $\varepsilon < 0$. Left panel: region plot (r, v) of $\varepsilon < 0$ for $r_{\rm NP} = \frac{39}{1000}$ together with classical (dashed green) and upgraded (magenta) null geodesics. Right panel: region plot $(r_{\rm NP}, r)$ of $\varepsilon < 0$ from $v = \frac{1}{2}$ (dark blue) to $v = 10$ (light blue).

change compared to the classical horizonless case; that is, null geodesics in both classical and upgraded horizonless spacetimes can escape from $r = 0$.

5.6.3 Inner, apparent, and event horizons

As explicitly demonstrated in App. B.4, the location of the apparent horizon in the upgraded spacetime is found by solving the equation $g^{rr}_{\rm EF} = 0$. This equation generically admits two real solutions. The first, given for the mass function Eq. 5.27 with $n = 1$ by

$$r_{\rm AH} = \frac{1}{3}\Bigg[2G_0\mu v + \frac{2\cdot 2^{\frac{2}{3}}\left(G_0\mu v\right)^{\frac{5}{3}}}{\left(4G_0^2\mu^2v^2 + 3\sqrt{3}\,r_{\rm NP}\left(-9\,r_{\rm NP} + \sqrt{81r_{\rm NP}^2 - 8\sqrt{3}\,G_0^2\mu^2v^2}\right)\right)^{\frac{1}{3}}} + \left(8G_0^3\mu^3v^3 + 6\sqrt{3}\,r_{\rm NP}G_0\mu v\left(-9r_{\rm NP} + \sqrt{81r_{\rm NP}^2 - 8\sqrt{3}\,G_0^2\mu^2v^2}\right)\right)^{\frac{1}{3}}\Bigg] \tag{5.43}$$

is the apparent horizon. As discussed in Subsec. 5.5.1, the upgraded collapsing object is more compact than its classical counterpart, which can be inferred from the additional new-physics terms proportional to $r_{\rm NP}$ present in the denominator of Eq. 5.43.
The second solution

$$r_{\rm IN} = \frac{1}{6}\Bigg[4G_0\mu v + \frac{4\cdot(-1+i\sqrt{3})\left(G_0\mu v\right)^{\frac{5}{3}}}{\left(8G_0^2\mu^2v^2 + 6\sqrt{3}r_{\rm NP}\left(-9r_{\rm NP} + \sqrt{81r_{\rm NP}^2 - 8\sqrt{3}G_0^2\mu^2v^2}\right)\right)^{\frac{1}{3}}} + \left(-1-i\sqrt{3}\right)\left(8G_0^3\mu^3v^3 + 6\sqrt{3}r_{\rm NP}G_0\mu v\left(-9r_{\rm NP} + \sqrt{81r_{\rm NP}^2 - 8\sqrt{3}G_0^2\mu^2v^2}\right)\right)^{\frac{1}{3}}\Bigg] \tag{5.44}$$

is a new, inner apparent horizon. This last expression is real up to the critical point $r_{\rm NP} = r_{\rm NP,c}(v) \equiv \frac{2\sqrt{2}v\mu}{3^{\frac{7}{4}}}$, after which it becomes complex. The reason the inner horizon appears is the following: the modification function $f_{\rm NP}(I_1 r_{\rm NP}^4)$ which enters the equation App. B.4 determining the location of horizons is very small at small r, such that the equation $g^{rr}_{\rm EF} = 0$ accommodates another solution. This behaviour is well-known in stationary regular black-hole spacetimes, see e.g. the conventional examples [Dym92; Hay06], and can be argued for on general grounds [CR+20; CR+23a; CR+23b].

Solutions to algebraic equations such as $g^{rr}_{\rm EF} = 0$ become complex in pairs. Thus, at $r_{\rm NP,c}$, the outer and inner apparent horizons merge and subsequently become complex, leaving behind a horizonless spacetime. These results mirror those obtained for the event horizon in the stationary limit with a constant mass [EHJ23].

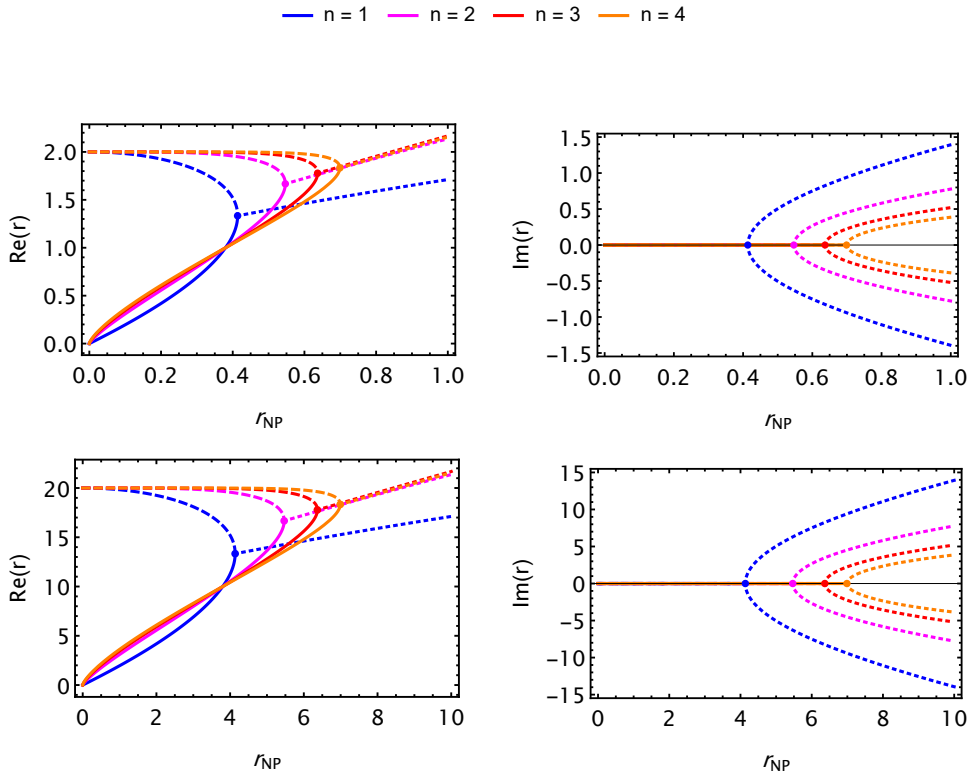

FIGURE 5.9: We show the real part (left column) and the imaginary part (right column) of the apparent $r_{\rm AH}$ (dashed line) and inner $r_{\rm IN}$ (solid line) horizons as functions of the new-physics scale $r_{\rm NP}$ and $n = 1, 2, 3, 4$. Top row: parameters are $0 \leq r_{\rm NP} \leq 1$, $G_0\mu = \frac{1}{10}$, $G_0 = 1$ and $v = 10$. Bottom row: parameters are $0 \leq r_{\rm NP} \leq 10$, $G_0\mu = \frac{1}{10}$, $G_0 = 1$ and $v = 100$. The coloured points indicate the locations of the critical points $r_{\rm NP,crit,n}$.

Fig. 5.9 shows both the real and imaginary parts of the two solutions to $g^{rr}_{\rm EF} = 0$ as a function of $r_{\rm NP}$, for the different powers $n = 1, 2, 3, 4$ in the mass function Eq. 5.27. For each power n there is, as expected, one solution which decreases with $r_{\rm NP}$ until the critical point $r_{\rm NP,c,n}$ and corresponds to the apparent horizon; and another solution which increases with $r_{\rm NP}$, corresponding to a (new) inner horizon. They merge at

the critical point where they become complex. Beyond the critical point, the two solutions acquire an imaginary part, rendering the spacetime horizonless.

As opposed to the stationary case, the critical value of the new-physics scale $r_{\mathrm{NP,crit},n}$ is not a constant but increases linearly with v, i.e.

$$r_{\mathrm{NP,c},n} \equiv r_{\mathrm{NP,c},n}(v) = c_n\,\mu v, \quad c_n = \text{const.}\,\forall n. \tag{5.45}$$

As v is taken to very small values, $r_{\mathrm{NP,c},n}$ approaches zero. Therefore, the formation of the apparent horizon is delayed by the new-physics effects: for early enough times, i.e. small enough v, r_{NP} (which is a fixed constant) is always larger than $r_{\mathrm{NP,c}}$ (which grows linearly in v). Accordingly, the apparent horizon cannot exist for these very early times and its formation can only proceed once $r_{\mathrm{NP}} < r_{\mathrm{NP,c}}(v)$.

This effect is of particular interest in situations where the classical spacetime exhibits a naked singularity. New physics effects resolve the singularity and limit the maximum value of curvature invariants. The spacetime region which is thus affected is not hidden behind an apparent horizon, given that horizon-formation is delayed by the same new-physics effects. An asymptotic observer may therefore (in principle) access this spacetime region through observations. This is an interesting distinction to the stationary case, where $r_{\mathrm{NP,c}}$ is a constant and there are thus always choices of $r_{\mathrm{NP}} < r_{\mathrm{NP,c}}$ which result in large modifications of the spacetime being hidden behind its event horizon.

The dependence of $r_{\mathrm{NP,c},n}$ on n is non-linear, cf. Fig. 5.10. The reason is that increasing n in the upgraded mass function in Eq. 5.27 leads to a faster approach of $f_{\mathrm{NP}}(I_1 r_{\mathrm{NP}}^4) \to 1$. Thus, the relative modification of the spacetime is smaller at the classical location of the apparent horizon the larger n is, and the location of the inner horizon is closer to $r = 0$ for larger n. Therefore, the merging of the two horizons is delayed to larger r_{NP} for larger n.

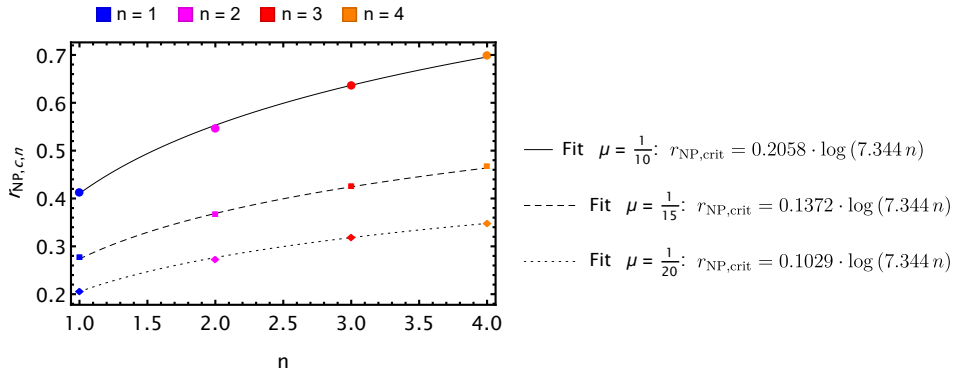

FIGURE 5.10: We show the critical points $r_{\mathrm{NP,c},n}$ as a function of n for $v = 10$ with either $G_0\mu = \frac{1}{10}$ (continuous line), $G_0\mu = \frac{1}{15}$ (dashed line) or $G_0\mu = \frac{1}{20}$ (dotted line). Logarithmic fits have been displayed to guide the eyes of the reader.

As in the classical case, in addition to the apparent horizon, there is also an event horizon. To determine its location $r_{\mathrm{EH}}(v)$, we use that for $v \geq \bar{v}$ the spacetime is locally isometric to a modified Schwarzschild black hole with constant mass

$$M \equiv \frac{\mu\bar{v}}{r_{\mathrm{EH}}(\bar{v}) + r_{\mathrm{NP}}^{2n}\left(48\,G_0^2\,\mu^2\,\bar{v}^2\,r_{\mathrm{EH}}(\bar{v})^{\left(\frac{2}{n}-6\right)}\right)^{\frac{n}{2}}}. \tag{5.46}$$

Thus, for $v > \bar{v}$, an event horizon is located at a constant radius $r_{\rm EH}(\bar{v})$ satisfying $\dot{r}_{\rm EH}(v) = 0$, providing an initial condition. In practice, we determine this initial condition by solving $1 - \frac{2G_0 M}{r_{\rm EH}(\bar{v})} = 0$ for $r_{\rm EH}(\bar{v})$ with M being the constant mass of a modified Schwarzschild BH given in Eq. 5.46. Then, starting from the initial condition $r_{\rm EH}(\bar{v})$ and $\dot{r}_{\rm EH}(v) = 0$ at $v > \bar{v}$, we numerically solve the geodesic equation backwards in advanced time, i.e. for $0 < v < \bar{v}$, for $r_{\rm EH}(v)$.

5.6.4 Photon surface

Contrary to the classical VKP model, the upgraded spacetime does not admit any photon sphere, even for $\mu < \mu_{\rm c}$. This is because the upgraded spacetime with mass function Eq. 5.27 fits within the class of generalised Vaidya spacetimes Eq. 5.23, for which the vector field $\xi^\mu = (v, r, 0, 0)$ in EF coordinates fails to satisfy the conformal Killing equation

$$\nabla_\mu \xi_\nu + \nabla_\nu \xi_\mu = 2g_{\mu\nu} + \frac{2G_0}{r}\left(M(v,r) - \dot{M}(v,r)v\right)\delta^v_\mu \delta^v_\nu \not\propto 2g_{\mu\nu}, \tag{5.47}$$

where $\dot{M}(v,r) \equiv \frac{\partial M(v,r)}{\partial v}$. Hence, we instead follow [MCS19] and write the evolution equation for the location of a photon surface $r_{\rm p}(v)$ for a general mass function $M(v,r)$ as[10]

$$\begin{aligned} 0 =& \ddot{r}_{\rm p}(v) + \frac{1}{r_{\rm p}(v)}\left(3\dot{r}_{\rm p}(v) + G_0 m'(3\dot{r}_{\rm p}(v) - 1) - 2\left(\dot{r}_{\rm p}(v)\right)^2 + G_0\dot{M} - 1\right) \\ &+ \frac{1}{r^2_{\rm p}(v)}\left(-9G_0 M\dot{r}_{\rm p}(v) + 2G_0^2 MM' + 5G_0 M\right) - \frac{6G_0^2 M^2}{r^3_{\rm p}(v)}. \end{aligned} \tag{5.48}$$

As we do not find an analytical solution to this evolution equation for $r_{\rm p}(v)$, we solve it numerically and supplement it with the appropriate initial conditions at $v > \bar{v}$. As the collapsing compact object locally settles down to a modified Schwarzschild (thus static) black hole starting from $v = \bar{v}$, with a photon sphere located at a fixed radius, the initial conditions are given by the solution to the following equation (see [EHJ23, Eq. (2.21)])

$$1 - \frac{3G_0\mu\bar{v}}{r_{\rm p}(\bar{v})} f_{\rm NP}(I_1 \cdot r^4_{\rm NP})\Big|_{r=r_{\rm p}(\bar{v})} + G_0\mu\bar{v}\frac{\partial f_{\rm NP}(I_1 \cdot r^4_{\rm NP})}{\partial r}\Big|_{r=r_{\rm p}(\bar{v})} = 0, \tag{5.49}$$

and the requirement that $\dot{r}_{\rm p}(v) = 0$ for $v \geq \bar{v}$. While finding the location of a photon surface $r_{\rm p}(v)$ for $0 < v < \bar{v}$ now seems straightforward, there is a remaining caveat: the upgraded mass function in Eq. 5.27 has the same sharp transition at $v = \bar{v}$ as the (classical) VKP mass function described in Eq. 5.2, which can cause instabilities in the numerical solution. We instead implement a smooth approximation to the full mass function by using the same approximation for $M(v)$ as in the classical case, namely Eq. 5.22.

The resulting upgraded photon surface for both $G_0\mu = \frac{1}{10}$ and $G_0\mu = \frac{1}{20}$ are displayed in magenta in Fig. 5.11 and Fig. 5.12. For both cases, the accretion rate is low enough that the photon surface initially starts at infinity together with the matter shells, and moves inwards before reaching its final radial location given by a real solution of Eq. 5.49. Comparing with Fig. 5.4, the behaviour of the upgraded

[10] As previously, we define $M \equiv M(v,r)$, $\dot{M} \equiv \frac{\partial M(v,r)}{\partial v}$ and $M' \equiv \frac{\partial M(v,r)}{\partial r}$.

photon surface differs for $G_0\mu = \frac{1}{10}$. This is likely due to the increased compactness, and thus weaker mass, of the upgraded collapsing body at equal advanced time v. Furthermore, the photon surface for the horizonless spacetime only exists for a limited range $r_{\mathrm{NP,c,-}} < r_{\mathrm{NP}} < r_{\mathrm{NP,c,+}}$ of new-physics scales, as was shown for the stationary case in [EHJ23]. If the new-physics scale r_{NP} is too large, in other words if $r_{\mathrm{NP}} > r_{\mathrm{NP,c,+}}$, then the inner and outer photon surfaces merge and the solutions to the differential equation Eq. 5.48 all become complex.

5.6.5 Spacetime diagrams

The (r, v) spacetime diagrams which summarise our analysis of the upgraded spacetime's structure are shown in Fig. 5.11 (for $G_0\mu = \frac{1}{10}$) and Fig. 5.12 (for $G_0\mu = \frac{1}{20}$).

For each value of the accretion rate μ, we study two distinct regimes that correspond to different choices of r_{NP}: the first one corresponds to a spacetime with an event horizon (left panel), while the second one is horizonless (right panel). Since the presence of an event horizon depends on the ratio $\frac{r_{\mathrm{NP}}}{r_{\mathrm{NP,c}}(v)}$, the above statement can be reformulated as follows: the upgraded spacetime has an event horizon as long as $r_{\mathrm{NP}} < \min_v (r_{\mathrm{NP,c}}(v))$ for $1 \leq v \leq 10$, and is horizonless if $r_{\mathrm{NP}} > \max_v (r_{\mathrm{NP,c}}(v))$ for $1 \leq v \leq 10$.

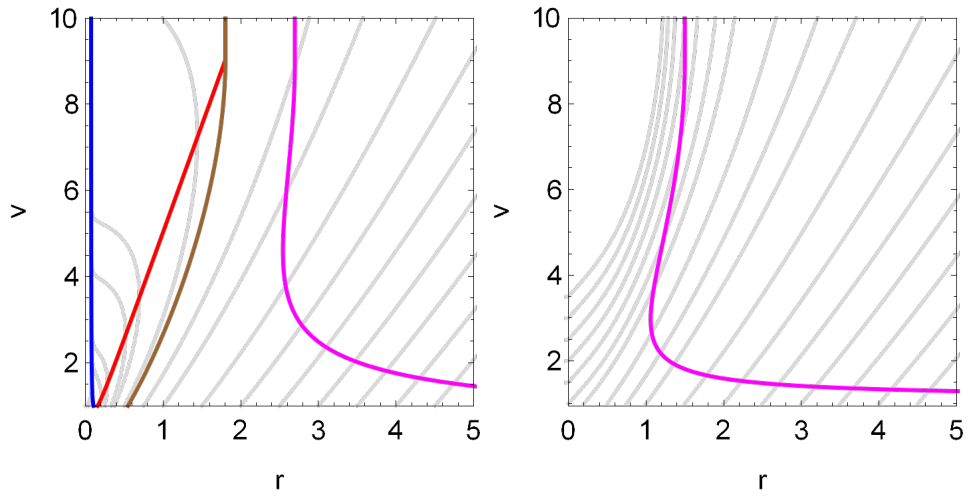

FIGURE 5.11: We show the (r, v) spacetime diagrams for null geodesics in the upgraded spacetime with $n = 1$ and $G_0\mu = \frac{1}{10}$. Photon surfaces are in magenta. Left panel: presence of an event horizon (brown), i.e. $r_{\mathrm{NP}} < \min(r_{\mathrm{NP,c}}(v))$, an apparent horizon (red) and an inner horizon (blue). Right panel: horizonless spacetime, i.e. $r_{\mathrm{NP}} > \max(r_{\mathrm{NP,c}}(v))$.

In the spacetime diagrams, it is again apparent that there is an attractor for null geodesics inside the apparent horizon which lies close to the inner horizon. However, we do not expect that an inner horizon acts as an attractor for outgoing null geodesics and confirm numerically that the attractor is close to, but not in agreement with, the inner horizon, cf. Fig. 5.13. Instead, we expect that an inner photon surface forms, as it does for the upgrade of the Schwarzschild spacetime [EHJ23]. Generically, the inner photon surface is marginally stable and thus acts as an attractor.

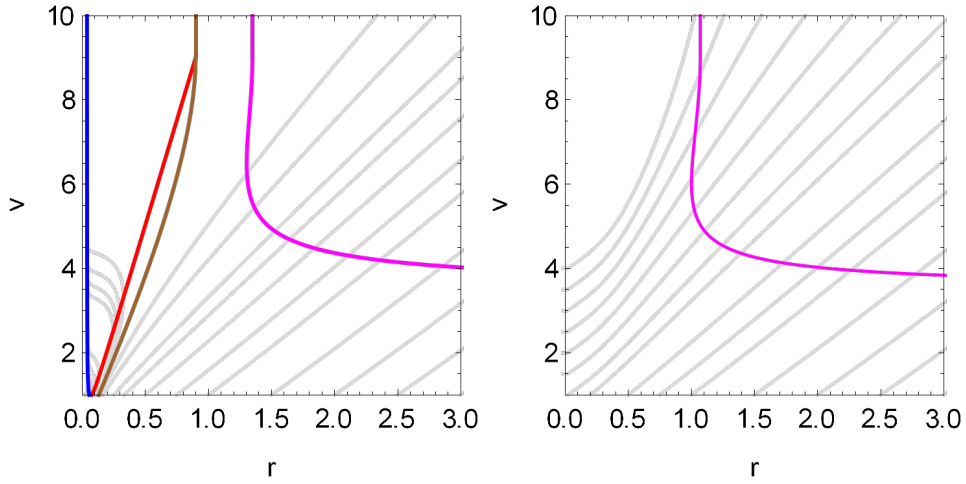

FIGURE 5.12: We show the (r, v) spacetime diagrams for null geodesics in the upgraded spacetime for $n = 1$ and $G_0\mu = \frac{1}{20}$. Photon surfaces are in magenta. Left panel: presence of a horizon (brown), i.e. $r_{\rm NP} < \min\left(r_{\rm NP,c}(v)\right)$, an apparent horizon (red) and an inner horizon (blue). Right panel: horizonless spacetime, i.e. $r_{\rm NP} > \max\left(r_{\rm NP,c}(v)\right)$.

This, in turn, likely causes a problem: the energy carried by photons trapped on an inner photon surface accumulates, leading the spacetime curvature to rise[11] and triggering a potential instability [DF+22]. Because we do not account for backreaction in our analysis, this effect is not visible in our spacetime diagrams. Future investigations of this point will be crucial to determine whether or not the upgraded Vaidya spacetime can stay regular also in the fully dynamical case. The outcome of such an analysis of course depends on the assumed dynamics; the intuition that an attractor for geodesics may result in the build-up towards a spacetime singularity may not hold in dynamics beyond GR.

However, an inner photon surface also has a desired consequence, namely that it solves the predictivity problem connected to geodesics that emanate at $(r = 0, v > 0)$. These geodesics are not past complete within the spacetime region with $r \in [0, \infty)$. Thus, they pose a problem with setting up an initial value problem. However, because those geodesics get trapped by an inner photon surface, it effectively shields the external spacetime from a breakdown of predictivity. These comments, of course, only apply to radial geodesics as we do not investigate more general null geodesics here.

A comparison of the behaviour of upgraded and classical null geodesics near the centre is shown in Fig. 5.14. As expected, the largest deviations occur for relatively small r, whereas the apparent and event horizons of the classical and the upgraded spacetime already lie nearly on top of each other.

[11] This, of course, assumes that the GR equations of motion continue to hold. However, new physics effects that limit the maximum value of curvature invariants in the upgraded spacetime and that are implemented through the regularity principle might modify that picture. We namely expect that new-physics effects can alter the response of the upgraded spacetime metric to an increase in the energy-momentum tensor, at least beyond a critical value of the energy/momentum.

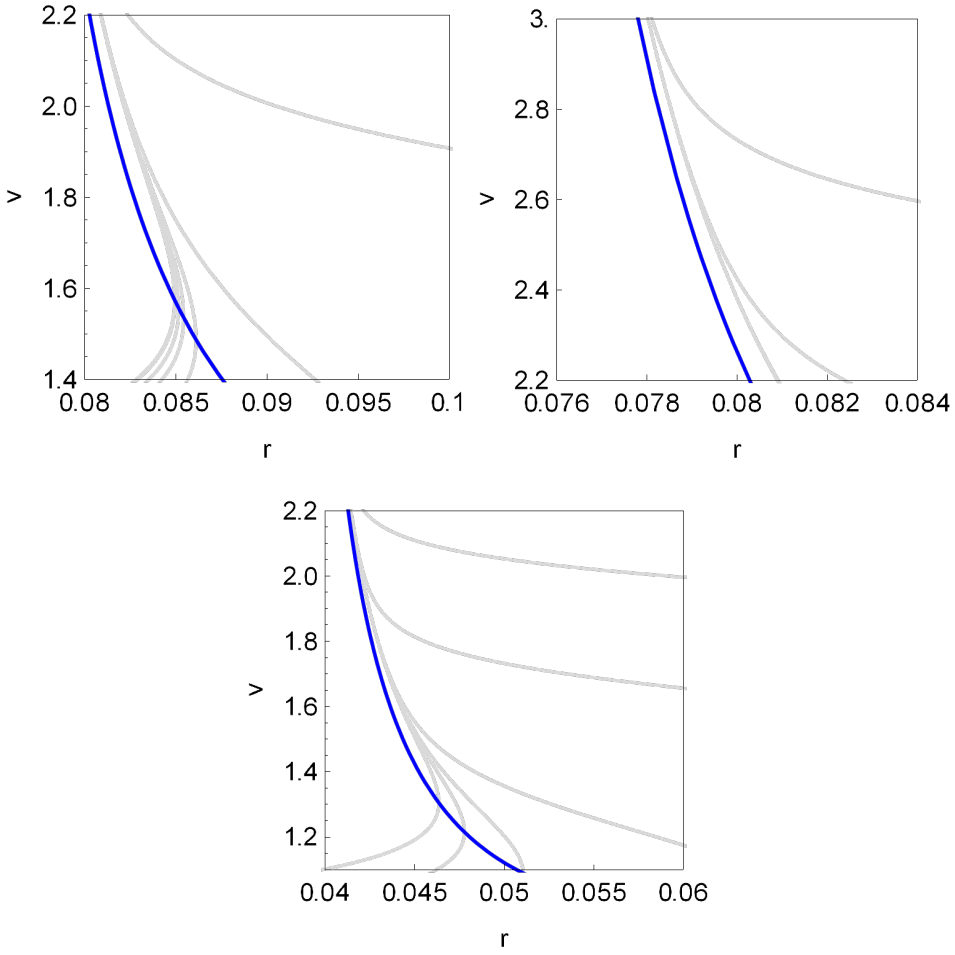

FIGURE 5.13: We show zoomed-in regions near $r = 0$ of (r, v) spacetime diagrams with $n = 1$ in the presence of an horizon, i.e. $r_{\mathrm{NP}} < \min\left(r_{\mathrm{NP,c}}(v)\right)$. Inner horizons are in blue. Top left panel: $G_0\mu = \frac{1}{10}$ and $1.4 \leq v \leq 2.2$. Top right panel: $G_0\mu = \frac{1}{10}$ and $2.2 \leq v \leq 3.0$. Bottom panel: $G_0\mu = \frac{1}{20}$ and $1.1 \leq v \leq 2.2$.

5.7 Conclusion and outlook

We first reviewed the VKP model, a simple classical GR model describing the gravitational collapse to a black hole of spherically symmetric, linearly accreting null dust. This model forms a subclass of the dynamical accreting Vaidya spacetimes which, in EF coordinates, have increasing mass functions $M(v)$. We pointed out that, as implied by the null version of the Penrose singularity theorem [Pen65], this model fulfiling the null energy condition is singular. The singularity of the VKP model manifests itself in three ways: divergent curvature invariants at the spacetime's centre $r = 0$, future-incomplete null geodesics, and the formation of a partially-naked singularity for low-enough accretion rates $\mu < \mu_{\mathrm{c}}$.

As the singular VKP model does not provide us with a viable description of the formation of astrophysical black holes, we briefly reported on a more general class of classical dynamical spacetimes: the generalised Vaidya spacetimes with mass functions $M(v, r)$. We then proposed two models of regular, upgraded dynamical spacetimes that are embedded into the generalised Vaidya spacetimes. Following the RG improvement method [EH22; Pla23], one model results from the upgrade of the

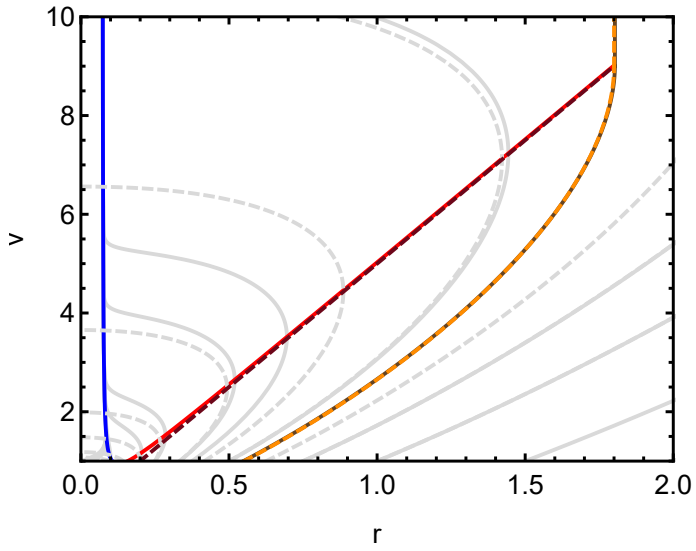

FIGURE 5.14: We show the (r, v) spacetime diagrams for null geodesics in the classical VKP model (dashed grey lines) and in the upgraded Vaidya model with $n = 1$ (continuous grey lines) in the presence of a horizon, i.e. $r_{\rm NP} < \min\left(r_{\rm NP,c}(v)\right)$. The classical event horizon is represented by a dashed orange curve and the classical apparent horizon by a dashed black line. The upgraded event horizon is represented by a brown curve, the upgraded apparent horizon by a red line and the upgraded inner horizon by a blue line.

Newton constant G_0 to a running coupling dictated by ASQG, and the identification of the RG scale with the square root of the first classical curvature invariant. An equivalent model is found by following the principled-parameterised approach [EH21b; EH21a; EHJ23], where the classical mass function $M(v)$ is upgraded to a mass function depending on v, r through a massless combination of the first classical (local) curvature invariant and a new-physics scale. The form of the latter mass function follows from the four physical principles implemented in the principled-parameterised approach which, among others, ensure regularity of the upgraded spacetime, as in the stationary case [EH21b; EH21a; EHJ23].

We verified that the regular upgraded spacetime fails to satisfy the null energy condition and documented the impact on null geodesics, particularly near the would-be classical curvature singularity. Although upgraded null (radial) geodesics are past-incomplete, they are no longer future-incomplete; instead, they are repelled from the core and lensed towards a marginally stable, inner photon surface which acts as an attractor. The latter attractor solves the predictivity problem of geodesics emanating at $(r = 0, v > 0)$ by capturing them, thus providing us with a "cosmic censorship of quantum gravity". However, it can trigger a potential instability due to the accumulation of the energy carried by trapped photons. Additionally, the upgraded spacetime is horizonless at small v for any accretion rate. Hence, for $\mu < \mu_{\rm c}$, the regularisation of the naked singularity and thus the – possibly quantum – modifications of GR may be visible to asymptotic observers.

5.7.1 Outlook

The analysis performed in this chapter motivates future work along the following lines.

First, within the modified Vaidya spacetime, it is interesting to explore timelike and null geodesics in more detail, without the restriction to radial null geodesics. Additionally, exploring geodesic motion at $r < 0$ can shed more light on the question of past and future geodesic completeness.

Second, we can extend the principled-parameterised approach to dynamical spacetimes with fewer symmetries, i.e. axisymmetric dynamical spacetimes such as the Kerr-Vaidya spacetime [ST15], and learn more about the universality of mass functions that render spacetimes with Killing vectors regular. However, this analysis might be complicated by the foliation-dependence of the apparent horizon in the Kerr-Vaidya spacetime [ST15; Dah21]. A possible generalisation, in which we start with a generalised Vaidya spacetime instead of a Vaidya spacetime, is sketched in Subsec. 5.7.1.

Furthermore, the question of the impact of backreaction on the stability of the upgraded spacetime remains open. This requires to understand the relevant timescales, to determine whether the upgraded spacetime we have explored may be viable despite the presence of an inner photon surface.

So far, we have extended the principled-parameterised approach to black-hole spacetimes beyond GR from the stationary case [EH21a; EH21b; EHJ23] to the time-dependent setting of gravitational collapse. We have focused on the simple VKP model and now sketch how the approach may also be employed in less simple models, e.g. in the generalised Vaidya spacetime. In other words, instead of considering a generalised Vaidya spacetime as the *endpoint* of the upgrade procedure, we determine whether it can be considered as a *starting point*.

To that end, we need to consider the non-derivative curvature invariants, because a suitable measure of local curvature is the key ingredient in the principled-parameterised approach.

Among the full set of the 17 ZM invariants in App. B.3 for the generalised Vaidya spacetime, eleven are non-zero. Most of those non-zero invariants cannot be written as powers of each other unless it is explicitly indicated how to do so in App. B.3. However, this does not mean that the remaining seven non-zero invariants are all algebraically independent of each other. Syzygies, which are polynomial relations between the curvature invariants, may be found. We do find a non-trivial syzygy, namely

$$\frac{I_{11}}{I_1} + \frac{I_5^2}{12} - \frac{I_6}{3} = 0, \tag{5.50}$$

which reduces the number of polynomially independent curvature invariants to at most six.

We postulate that, if the modulus of any of the non-zero, independent curvature invariants exceeds a critical value, modifications to the spacetime become sizeable. We thus construct a measure of the local curvature as follows: we take the absolute value of each classical curvature invariant to an appropriate power so that it has the same dimensionality as the Kretschmann scalar I_1. We then form the average of these quantities, i.e. the RMS of the sum of appropriate powers of the classical curvature invariants. By using the RMS, we avoid a bias with respect to the sign of the curvature, assuming that new physics kicks in at large positive or negative

curvatures. This amounts to considering a local curvature K of the general form

$$K = \frac{1}{N}\sqrt{\sum_{j=1}^{N} |I_j|^{\alpha_j}}, \quad \alpha_j \in \mathbb{Q}, \tag{5.51}$$

with I_j being the non-zero, polynomially independent, curvature invariants of the classical non-upgraded spacetime. This corresponds to the case (ii) in App. B.5.

Using only the independent curvature invariants, the local curvature scale of a generalised Vaidya spacetime takes the form

$$K = \frac{1}{6}\sqrt{|I_1| + |I_5|^2 + |I_6| + |I_7|^{\frac{2}{3}} + |I_8|^{\frac{1}{2}} + |I_{13}|^{\frac{2}{5}}}, \tag{5.52}$$

where the implicit dependence of K in $M(v,r)$ and its r-derivatives $M'(v,r)$, $M''(v,r)$ is hidden in the curvature invariants.

In practice, this expression is significantly more complicated than simply $K = \sqrt{I_1}$, which we could use for the Vaidya spacetime. As a result, the principled-parameterised approach should be applicable to a generalised Vaidya spacetime, but we expect the numerical analysis of the spacetime to be significantly more involved than starting from a Vaidya spacetime.

Chapter 6

Towards a general parameterisation of non-circular black-hole spacetimes

In this chapter, we discuss parameterisations of BH spacetimes which provide a theory-agnostic way of writing down deviations from GR and then testing them, c.f. the existing parameterisations [BF79; VH10; Vig10; VYS11; JP11; Joh13b; KRZ16; CY20]. We argue that more general parameterisations of BH spacetimes are needed to fully account for all potential deviations from the Kerr paradigm. Those parameterisations may possess fewer symmetries than those of GR and, in particular, should include non-circular spacetimes. There is indeed no reason to expect that circularity holds beyond GR, where spacetimes are no longer Ricci-flat. Additionally, the regular, spinning BH spacetimes proposed in [EH21b; EH21a] are non-circular and result in peculiar image features, namely cusps, a dent and an asymmetry in the photon rings surrounding the black-hole shadow.

We start by pointing out that BH parameterisations beyond GR that exist in the current literature make unnecessary additional symmetry assumptions which need not hold on general grounds: first, circularity; second, a hidden constant of motion. Then, we demonstrate that promoting the classical mass to a mass function can lead to families of regular black-hole spacetimes that break circularity, c.f. [EH21b; EH21a], while we show for the first time how a similar upgrade of the classical spin fails to regularise the curvature singularity, c.f. [DEH22]. This motivates us to go beyond upgrading classical mass and spin constants to particular functions and propose a more general, non-circular, stationary, axisymmetric and asymptotically flat parameterisation in two sets of coordinates, namely horizon-penetrating and Boyer-Lindquist coordinates. We explicitly check that this new parameterisation includes existing circular and non-circular BH spacetimes, and explain why horizon-penetrating coordinates may be more suitable to parameterise non-circular deviations from the Kerr geometry.

6.1 The parameterised approach to black holes beyond GR

The EHT results from the 2017 observation campaign show that both M87* and SgrA* are consistent with a Kerr BH within current nominal resolution and systematic uncertainties [Aki+19a; Aki+22a]. Hence, if M87* and SgrA* were to be different from s Kerr BH, their spacetime geometries would need to deviate only slightly from that of Kerr. Capturing deviations from the Kerr BH is the idea behind the *parameterised approach* to BHs beyond GR. Given the difficulty of obtaining stationary, axisymmetric, asymptotically flat BH solutions to theories beyond GR, the latter

parameterised approach aims to capture all possible deviations with respect to the Kerr (or Schwarzschild) BH in a theory-agnostic way.

The parameterised approach goes beyond promoting the classical mass and spin to particular functions which, although successfully leading to non-singular BH spacetimes for families of locality-based mass upgrades $M \to M(r,\chi) \equiv M(K \cdot l_{\rm NP}^4)$ depending on the local curvature scale K[1], c.f. Subsec. 6.2.1, fails to regularise spacetimes via a spin function, c.f. Subsec. 6.2.2.

Based on our work [DEH22], we first review that existing parameterisations of BH spacetimes beyond GR can be split into different symmetry classes, depicted in Fig. 6.1. We then review the main two symmetry classes existing parameterisations belong to, namely circular spacetimes with an additional hidden constant of motion in Subsec. 6.1.2 and circular spacetimes only in Subsec. 6.1.3. Next, we motivate and propose a more general parameterised spacetime that is non-circular in two relevant sets of coordinates, namely Horizon-Penetrating (HP) in Subsec. 6.3.2 and Boyer-Lindquist (BL) coordinates in Subsec. 6.3.5. Finally, we take a closer look at one example included in the newly proposed, non-circular parameterisation and conclude.

6.1.1 Symmetry classes of parameterised spacetimes beyond GR

The parameterised approach starts from a vacuum GR BH metric, either Kerr or its subcase Schwarzschild, and introduces a set of additional functions of the (non-Killing) coordinates parameterised by additional parameters. The latter additional functions are such that the parameterised metric reduces to Kerr (or Schwarzschild) for specific values of those functions, when appropriate limits are taken or when deviation parameters vanish. It thus follows a similar reasoning as the Parameterised Post-Newtonian (PPN) formalism, in which weak-field and low-velocity deviations with respect to Newtonian's gravity are introduced order by order in the Einstein's field equations (see [Hoh21] for a recent review on the PPN formalism). However, the parameterised approach contrasts with the PPN formalism in three ways:

- no systematic expansion in small parameters is performed;
- deviation parameters can be of order $\mathcal{O}(1)$;
- there is not always a one-to-one or direct connection between the newly added deviation parameters and their physical relevance.

In particular, it is generally not possible to relate a given deviation parameter in a parameterised metric to a single PPN parameter as was done in [Psa+21].

The various sets of possible deviation functions define classes of parameterisations that share similar features, in particular common symmetries, depicted in Fig. 6.1. Starting from the GR Schwarzschild metric, one may preserve staticity and spherical symmetry when parameterising deviations from it, to stay within the most symmetric class of circular, static, spherically symmetric metrics with a hidden constant of motion. If we relax the spherical symmetry to axisymmetry, we move on to the class of static and axisymmetric parameterisations which are based on the GR Weyl metrics

[1] Here, the symbol K appearing in the mass function does not correspond to the Kretschmann scalar, but to the local curvature scale expressed in terms of a suitable combination of curvature invariants, as defined in App. B.5.

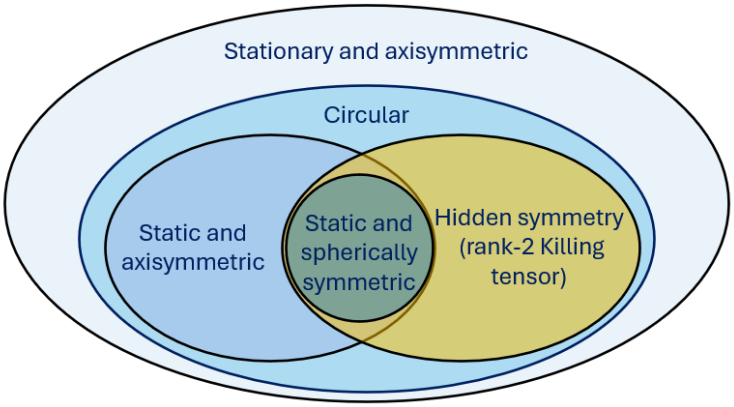

FIGURE 6.1: We depict subclasses of stationary and axisymmetric metrics according to their symmetries. "Circular" metrics refer to metrics satisfying the circularity conditions spelled out in Eqs. 6.3 and 6.4. A subclass of those circular metrics possess a hidden symmetry generated by a rank-2 Killing tensor, a generalisation of the Carter constant given in Eq. 2.13.

[Wey17a].[2] If we relax staticity, we end up in the orange box in Fig. 6.1 containing all circular, stationary, axisymmetric spacetimes with a hidden constant of motion, to which the Kerr solution belongs.

Indeed, while possessing fewer symmetries than the Schwarzschild spacetime which lies in the central box in Fig. 6.1, the Kerr spacetime is highly symmetric. Apart from its stationarity and its axisymmetry, it is circular in the sense that it fulfils the circularity conditions

$$\xi_1^{[\mu}\xi_2^{\nu}\nabla^{\kappa}\xi_1^{\lambda]} = 0 \text{ at at least one point,} \tag{6.1}$$

$$\xi_2^{[\mu}\xi_1^{\nu}\nabla^{\kappa}\xi_2^{\lambda]} = 0 \text{ at at least one point,} \tag{6.2}$$

$$\xi_1^{\mu}R_{\mu}^{\ [\nu}\xi_2^{\kappa}\xi_1^{\lambda]} = 0 \text{ everywhere,} \tag{6.3}$$

$$\xi_2^{\mu}R_{\mu}^{\ [\nu}\xi_1^{\kappa}\xi_2^{\lambda]} = 0 \text{ everywhere} \tag{6.4}$$

involving the two Killing vector fields ξ_1 and ξ_2, the Ricci tensor $R_{\mu\nu}$ and the covariant derivative ∇^{μ} of the Kerr spacetime.

Independently of the choice of coordinates, circularity imposes some restrictions on the Ricci tensor in the directions of the two Killing vectors, hence implying an isometry of the spacetime. In BL coordinates, where the Killing vectors are $\xi_t = \partial_t$ and $\xi_\phi = \partial_\phi$, circularity simplifies to the invariance under the simultaneous transformations $t \to -t$, $\phi \to -\phi$. As such, circularity is manifest in the Kerr metric Sec. 2.2, as the infinitesimal elements dt and $d\phi$ only appear with themselves or with each other.

Circularity also appears to be related to the existence of closed photon orbits. Indeed, every stationary, axisymmetric and asymptotically flat BH spacetime that is also circular must admit at least two planar closed photon orbits – one with (prograde) and one against (retrograde) the rotation of the BH [CH20; CHN24]. Whether the proof extends beyond circularity remains an open question, because the proof shows

[2] More detail on Weyl metrics is provided in App. C.3, but since metrics of that form are often unphysical, we will not discuss them further.

that circularity implies two planar closed photon orbits, but it is not clear whether circularity is a sufficient or necessary condition.

On top of circularity, the Kerr spacetime also possesses a hidden symmetry associated with the presence of a rank-2 Killing tensor (see Eq. 6.5 for the defining equation of Killing tensors). The latter hidden symmetry gives rise to a constant of motion, known as the Carter constant, c.f. Eq. 2.13. Killing tensors of rank $n \geq 2$ are manifest in the local dynamics of test particles. In particular, together with the other constant of motions, the Carter constant leads to the separability of Kerr's geodesic equation.

Starting from the GR Kerr metric, one may: (i) preserve all Kerr symmetries – thus staying in the orange box in Fig. 6.1 – or (ii) relax some of them – thus gaining in generality by gradually moving towards less and less symmetric spacetimes, i.e. towards the outer blue boxes in Fig. 6.1.

Constraints on the deviation parameters from observations allow us to quantify possible deviations from the no-hair theorem and from the vacuum GR symmetries (those of Schwarzschild, Weyl or Kerr spacetimes), and thus to select relevant classes of parameterised spacetimes, upon lifting the degeneracies that may occur among deviation parameters [Psa+21].

6.1.2 Circular parameterised spacetimes with an additional hidden constant of motion

Moving on to metrics beyond GR, stationary, axisymmetric and circular parameterised spacetimes may also contain an additional hidden constant of motion or *generalised Carter constant*. Those hidden constants of motion are associated to Killing tensors, the higher-rank generalisation of Killing vectors. The Killing equation $\nabla_{(\mu}\xi_{\nu)} = 0$ defining a Killing vector ξ_μ in fact generalises to a rank-n Killing tensor $K_{\mu_1\ldots\mu_n}$ as

$$\nabla_{(\mu}K_{\mu_1\ldots\mu_n)} = 0, \tag{6.5}$$

where round brackets denote complete symmetrisation. As such, a Killing vector is a rank-1 Killing tensor, and the metric is itself a rank-2 Killing tensor, as follows from the metric compatibility of the covariant derivative based on the Christoffel connection. However, metric compatibility does not generate constants of motion but rather ensures the absence of non-metricity d.o.f.

While Killing vectors encode an explicit isometry of the underlying spacetime, higher-rank Killing tensors manifest themselves in the local dynamics of tests particles: they imply a hidden constant of motion. Supplemented with sufficiently many other constants of motion, this leads to the separability of the geodesics equations. The existence of a hidden constant of motion along a geodesic parameterised by its proper time τ and with tangent vector $u^\mu = \frac{dx^\mu(\tau)}{d\tau}$ stems from the generalised Killing equation Eq. 6.5, which implies that $C = K_{\mu_1\ldots\mu_n}u^{\mu_1}\ldots u^{\mu_n}$ is conserved along a geodesic, i.e. $\frac{dC}{d\tau} = 0$.

The most general (inverse) metric with two independent Killing vectors and one non-trivial rank-2 Killing tensor takes the form [BF79]

$$g^{\mu\nu}\partial_\mu\partial_\nu = \frac{1}{S_1(x_1)+S_2(x_2)}\Big[\Big(G_1^{ij}(x_1)+G_2^{ij}(x_2)\Big)\partial x_i\partial x_j + \Delta_1(x_1)\partial x_1^2 + \Delta_2(x_2)\partial x_2^2\Big], \tag{6.6}$$

where i, j refer to the two Killing coordinates, and 1, 2 to the two non-Killing coordinates. While the form Eq. 6.6 seems to have more free functions than the four (or

five) free functions of circular metrics, c.f. Eq. 6.12, functions $S_1(x_1)$, $S_2(x_2)$, $G_1^{ij}(x_1)$, $G_2^{ij}(x_2)$, $\Delta_1(x_1)$ and $\Delta_2(x_2)$ only depend on one coordinate at a time, either x_1 or x_2. The resulting rank-2 Killing tensor $K^{\mu\nu}$ and the associated generalised Carter constant C are [BF79]

$$K^{\mu\nu}\partial_\mu\partial_\nu = \frac{1}{S_1(x_1)+S_2(x_2)}\Big[\Big(S_1(x_1)G_2^{ij}(x_2) - S_2(x_2)G_1^{ij}(x_1)\Big)\partial x_i\partial x_j - S_2(x_2)\Delta_1(x_1)\partial x_1^2 + S_1(x_1)\Delta_2(x_2)\partial x_2^2\Big], \tag{6.7}$$

$$C = K^{\mu\nu}u_\mu u_\nu, \tag{6.8}$$

with u_μ the 4-velocity of a test particle.

The parameterisation in Eq. 6.6 is fully equivalent to the one presented in [Joh13a, Eq. (10)], as explicitly demonstrated in App. C.2. While we have not verified the consistency of the parameterisation in Eq. 6.6 with the parameterisations in [VYS11, Eqs. (30) and (56)] because those parameterisations are implicitly given in terms of differential equations, the latter parameterisations are in fact built from a rank-2 Killing tensor for which [BF79] claims generality. We easily recognise that the Kerr metric is of the above form Eq. 6.6 in BL coordinates and that it has a hidden constant of motion, namely the Carter constant Eq. 2.13.

While [BF79] does not assume circularity, we have explicitly checked that all such metrics are circular. Due to their additional hidden constant of motion, they form a subclass of the most general circular parameterisation in Eq. 6.12 represented in orange in Fig. 6.1.

In principle, additional hidden constants of motion can occur when Killing tensors with a high-order rank, i.e. rank > 2, are present. We are not aware of a proof that precludes their existence, although searches for them have not been successful so far in 4D (see [OYW21] for a systematic order-by-order – in small spin-parameter and small beyond-GR coupling constant – search for Killing tensors up to rank 6 in two quadratic gravity theories). Hence, it is to the best of our knowledge not excluded that axisymmetric, stationary spacetimes with higher-rank (i.e. rank > 2) Killing tensors are non-circular, e.g. in dimensions higher than four [GK22].

6.1.3 Circular parameterised spacetimes

When relaxing the presence of a hidden symmetry leading to a hidden constant of motion, we end up in the more general class of stationary, axisymmetric and asymptotically flat spacetimes which are circular in the above sense of Subsec. 6.1.1.

Most existing parameterisations beyond GR belong to that subclass, as reviewed in [DEH22; HP23]: the Benenti-Francaviglia parameterisation [BF79], the bumpy-Kerr parameterisations [VH10; Vig10; VYS11], the Johannsen-Psaltis (JP) parameterisation [JP11; Joh13a] and the KRZ parameterisation [KRZ16]. Note that the bumpy-Kerr parameterisations in [VH10; Vig10] contain some non-circular spacetimes but are not exhaustive, because they only introduce two and three free functions, respectively. Moreover, the parameterisation in [Joh13a] as well as the implicitly defined spacetimes in [VYS11, Eqs. (30) and (56)] are circular but additionally assume the existence of a hidden constant of motion, thus falling into the category described in Subsec. 6.1.2.

The construction of a general metric that follows from circularity [Wey17b; Pap66; KT66], see also [Wal84, Sec. 7.1], proceeds as follows. A general stationary and axisymmetric metric $g_{\mu\nu}$ in 4D has ten non-vanishing and independent metric components to start.[3] These metric components are only functions of the two non-Killing coordinates since we impose that the Killing symmetries must be manifest. Because we are free to perform four coordinate transformations in 4D, we can always reduce the number of non-vanishing metric components to six in some well-chosen set of coordinates. As in [DEH22], we review how the symmetries of a circular, axisymmetric and stationary spacetime lead to only five non-vanishing metric components in one particular set of coordinates, and that those are all but one off-diagonal component.

To perform the explicit construction of a general circular metric, we work in BL coordinates (t, r, θ, ϕ), in which the two Killing vectors are $\xi_t = \partial_t$ and $\xi_\phi = \partial_\phi$.[4] Circularity imposes an additional isometry, by which metric components can be set to zero or become functions of one another [Pap66; KT66; Wal84]. Every axisymmetric and stationary spacetime possesses "surfaces of transitivity", labelled by constant values of r and θ, which are generated by ξ_t and ξ_ϕ in the sense that those are tangent to the surfaces of transitivity (except at the rotation axis where ξ_ϕ vanishes). If the spacetime is circular, then there is a family of 2D surfaces which are everywhere orthogonal to the surfaces of transitivity, dubbed *meridional surfaces*. The distinctive feature of circular spacetimes is not that those meridional surfaces exist, as they also appear in non-circular spacetimes, but that they exist globally [Pap66; KT66]. Circularity indeed implies an additional isometry, that is the invariance under the

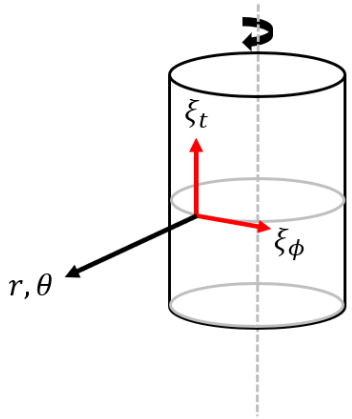

FIGURE 6.2: We depict 2D surfaces of transitivity of 4D stationary and axisymmetric spacetimes generated by its two Killing vectors ξ_t and ξ_ϕ (red arrows) in BL coordinates. The black arrow pointing out indicates the direction of the 2D orthogonal surfaces spanned by r and θ.

simultaneous transformation $t \to -t$ and $\phi \to -\phi$. At the level of the metric, it

[3] In full generality, an arbitrary rank-2 tensor in 4D has 16 non-vanishing components. However, a metric is a symmetric rank-2 tensor, thus reducing the number of potentially non-vanishing metric components to 10.

[4] This choice of coordinate is unique for spacetimes in which deviations from Kerr are small enough. In other words, spacetimes for which the Kerr limit can only be taken in a unique way. For larger deviations, unicity is lost and the Kerr spacetime can occur more than once in the resulting configuration space of metrics. This is similar to the Gribov ambiguity [Gri78] in non-Abelian gauge theories and also affects the gravitational configuration space [EPZ04].

imposes that four metric components vanish, namely

$$0 = g_{tr} = g_{t\theta} = g_{\phi r} = g_{\phi\theta}. \tag{6.9}$$

Hence, within BL coordinates, the most general circular, axisymmetric and stationary spacetime has at most six non-vanishing metric components.

However, we can perform two additional simplifications in the free functions entering these non-vanishing metric components. To show that, we focus on the 2D meridional surfaces, labelled by constant values of t and ϕ and spanned by ∂_r and ∂_θ. Since those surfaces exist globally thanks to circularity, we can write a global line element ds^2 for them. Given that every 2D metric is conformally flat, we can always transform BL coordinates (r, θ) to coordinates $(\tilde{r}, \tilde{\theta})$, in which the two-dimensional line element within the meridional surfaces can be written as

$$ds^2_{\text{mer}} = g_{\tilde{r}\tilde{r}} \left(d\tilde{r}^2 + \tilde{r}^2 d\tilde{\theta} \right), \tag{6.10}$$

with just one free function $g_{\tilde{r}\tilde{r}}$ multiplying the flat 2D line element in 2D spherical coordinates. Thus, $g_{\tilde{r}\tilde{\theta}} = 0$, reducing the number of non-vanishing metric components to five. Moreover, $g_{\tilde{\theta}\tilde{\theta}} = \tilde{r}^2 g_{\tilde{r}\tilde{r}}$ is parameterised by the same free function as $g_{\tilde{r}\tilde{r}}$. As a result, a general metric for circular, stationary and axisymmetric spacetimes has five non-vanishing metric components parameterised by four free functions. This is known as the Lewis-Papapetrou form of a circular metric [Pap66; KT66; Wal84].

As an example, the Kerr metric in the Lewis-Papapetrou form reads

$$\begin{aligned} ds^2 = &- dt^2 + \frac{4G_0 M\tilde{r}\left((G_0M+\tilde{r})^2 - a^2\right)}{\left(a^2 - (G_0M+\tilde{r})^2\right)^2 + 4a^2\tilde{r}^2\cos^2(\theta)} \left(dt - a\sin^2(\theta)d\phi\right)^2 \\ &+ \left(\frac{\left(a^2 - (G_0M+\tilde{r})^2\right)^2}{4\tilde{r}^2} + a^2 \right) \sin^2(\theta) d\phi^2 \\ &+ \frac{\left(\left(a^2 - (G_0M+\tilde{r})^2\right)^2 + 4a^2\tilde{r}^2\cos^2(\theta)\right)}{4\tilde{r}^4} \left(d\tilde{r}^2 + \tilde{r}^2 d\theta^2\right), \end{aligned} \tag{6.11}$$

with the transformation $r(\tilde{r})$ given by the condition $g_{\theta\theta} = \tilde{r}^2 g_{\tilde{r}\tilde{r}}$. More details on the derivation of Eq. 6.11 are provided in App. C.1. While it is possible to write the Kerr metric in Lewis-Papapetrou form, i.e. the most reduced form, the resulting coordinates are unconventional and unnecessarily complicated.

This highlights that it can be advantageous to work in a parameterisation in BL coordinates, where g_{rr} and $g_{\theta\theta}$ are two different free functions. Such a general parameterised, rotating, black-hole metric (i.e. axisymmetric, stationary and asymptotically flat metric) that respects circularity has been proposed in [KRZ16]. It takes the form

$$\begin{aligned} ds^2_{KRZ} = &- \frac{f(r,\theta) - \omega(r,\theta)^2 \sin^2\theta}{\kappa^2(r,\theta)} dt^2 - 2\omega(r,\theta) r \sin^2\theta dt d\phi + \kappa^2(r,\theta) r^2 \sin^2\theta d\phi^2 \\ &+ \sigma(r,\theta) \left(\frac{\beta^2(r,\theta)}{f(r,\theta)} dr^2 + r^2 d\theta^2 \right), \end{aligned} \tag{6.12}$$

with five free functions of the non-Killing coordinates $f(r,\theta)$, $\omega(r,\theta)$, $\kappa(r,\theta)$, $\sigma(r,\theta)$ and $\beta(r,\theta)$. Owing to the five free functions, this is not the most reduced form. Indeed, Eq. 6.12 makes only partial use of the coordinate freedom in the 2D surfaces of transitivity by setting $g_{r\theta} = 0$. We confirm that one of the five free functions in Eq. 6.12

is superfluous – meaning that it can be removed by a coordinate transformation – by explicitly checking that the circularity conditions Eqs. 6.3 and 6.4 hold for any choice of the five free functions.

So far, we have discussed existing stationary, axisymmetric and asymptotically flat parameterisations in view of their symmetry constraints, namely circularity and the existence of a hidden constant of motion [BF79; VH10; Vig10; VYS11; JP11; Joh13a; KRZ16]. While those parameterisations generally assume a non-vanishing (asymptotic) spin parameter a, spherical symmetry and staticity are usually imposed on them once used in specific applications, e.g. the derivation of QNMs [RZ14; Car+19; McM+19] or photon orbits [HGE19; KR20a; Tos22]. Due to those symmetry restrictions, the extent of the obtained results is limited and calls for more generality.

6.2 Promoting a classical hair to a "quantum hair"

The no-hair conjecture [MTW73] proposes that classical black holes should be well-described by the Kerr metric with asymptotic mass M and (reduced) spin a. Thus, promoting those classical hair to "quantum" hair in otherwise classical spacetime metrics might provide us with a test of the no-hair conjecture and the Kerr paradigm.

"Quantum" hair naturally arise within the principled-parameterised approach Sec. 5.4, in which regularisation of the central classical singularity occurs through a weakening of gravity. The latter effect is encoded in a coordinate-dependent "quantum" mass hair tied to the local curvature of the classical spacetime. Firstly, we show how families of locality-based, "quantum" mass hair functions in the principled-parameterised approach can cure the central curvature singularity. Secondly, we investigate for the first time, see [DEH22], whether a similar regularisation can occur for "quantum" spin hair functions.

6.2.1 Mass upgrade in the principled-parameterised approach

The principled-parameterised approach has been applied to stationary, axisymmetric and asymptotically flat spacetimes in [EH21b; EH21a]. It led to families of spacetime metrics in which the constant ADM mass parameter M was upgraded to a mass function depending only on the non-Killing coordinates r, χ in ingoing Kerr coordinates $(u, r, \chi \equiv \cos\theta, \phi)$, i.e. $M(r,\chi)$, in a specific way, by satisfying the four principles spelt out in Sec. 5.4: the regularity, locality and simplicity principles together with the Newtonian limit. This corresponds to modifying a classical hair to a "quantum" hair.

The line element associated with those metrics is part of the Kerr-Schild class [KS09] and corresponds to

$$\begin{aligned} ds_{\text{reg, local}} = &-\frac{r^2 - 2G_0M(r,\chi)r + a^2\chi^2}{r^2 + a^2\chi^2}du^2 + 2\,du\,dr - 4\frac{G_0M(r,\chi)ar}{r^2+a^2\chi^2}\left(1-\chi^2\right)du\,d\phi \\ &- 2a\left(1-\chi^2\right)dr\,d\phi + \frac{r^2+a^2\chi^2}{1-\chi^2}d\chi^2 \\ &+ \frac{1-\chi^2}{r^2+a^2\chi^2}\left(\left(a^2+r^2\right)^2 - a^2\left(r^2 - 2G_0M(r,\chi)r + a^2\right)\cdot\left(1-\chi^2\right)\right)d\phi^2, \end{aligned} \tag{6.13}$$

and fulfils the regularity, simplicity, and locality principles and has the correct Newtonian limit for $r \to \infty$. By choosing the exact form of $M(r,\chi)$, distinct families of spacetimes can be derived.

Metrics obtained within the principled-parameterised approach are such that the mass function depends on the coordinates r, χ only through the dimensionless product $K \cdot l_{\rm NP}^4$ involving a suitable choice of the classical local curvature K and a new-physics length scale $l_{\rm NP}$. The local curvature for Kerr can be approximated to

$$K \approx K_{\rm Kerr} = \sqrt{I_1^2 + I_2^2} = \frac{48 G_0^2 M^2}{(r^2 + a^2\chi^2)^3}, \tag{6.14}$$

with I_1 and I_2 the two classical, independent, non-zero, non-derivative curvature invariants of the Kerr spacetime, see Appendices B.1, B.2 and B.5 for more detail.

Hence, different choices of $M(r,\chi) = M(K \cdot l_{\rm NP}^4)$ define distinct families of spacetimes. Those can, for example, be [EH21b]

$$M(K \cdot l_{\rm NP}^4) = \frac{M}{1 + (K \cdot l_{\rm NP}^4)^{\frac{\beta}{2}}}, \ \beta > 1, \tag{6.15}$$

$$M(K \cdot l_{\rm NP}^4) = M e^{-(K \cdot l_{\rm NP}^4)^{\beta}}, \ \beta \geq \frac{1}{6}, \tag{6.16}$$

where the minimal value of β is set by the requirement of a well-defined geometry with neither singular (as prescribed by the regularity principle discussed in Subsec. 5.5.1) nor multi-valued curvature invariants. Note that a subset of spacetimes in Eq. 6.13 fulfil the circularity conditions Eqs. 6.3 and 6.4, namely those with mass functions $M(r)$ [DEH22].

The mass functions in Eqs. 6.15 and 6.16 have a fast enough fall-off at small r, which encodes a weakening of gravity that can be interpreted as an effective repulsive force produced by quantum gravity fluctuations. The line element Eq. 6.13 thus plays an important role in quantum-gravity scenarios where quantum gravity fluctuations are thought of regularising spacetime singularities and, accordingly, all non-derivative curvature invariants [BR00; RT06; Nic09; MN10; HR15; AOS18; HGE19; NSW19; Pla19; Con+20; EH21b; EH21a; EH22; Pla23].

6.2.2 Failure of a spin upgrade in and beyond the principled-parameterised approach

Building on the "quantum" mass hair, an interesting question to raise is: can an alternative variant of such a "quantum" hair be produced by upgrading the spin parameter a to a function $a(r,\chi)$, such that the resulting rotating black hole is non-singular? In other words, is the mass upgrade singled out by quantum gravity, or can another upgrade, e.g. spin upgrade, lead to non-singular rotating black holes?
If the answer to the first question is positive, then we should determine to which subclass of stationary and axisymmetric spacetimes the upgraded spacetime with "quantum" spin hair belongs, c.f. Fig. 6.1. If the answer is negative, it supports the special status of the "quantum" mass hair.

A rotating black hole (axisymmetric and stationary) can acquire a "quantum" spin hair by promoting the constant spin parameter a to a spin function $a(r,\chi)$, resulting

in the line element

$$ds^2 = -\left(1 - \frac{2G_0 M r}{r^2 + a(r,\chi)^2\chi^2}\right) du^2 + 2\,du\,dr - \frac{4G_0 M\, a(r,\chi)\, r}{r^2 + a(r,\chi)^2\chi^2}(1-\chi^2)\,du\,d\phi$$
$$- 2a\,(1-\chi^2)\,dr\,d\phi + \frac{r^2 + a(r,\chi)^2\chi^2}{1-\chi^2}d\chi^2 + \frac{1-\chi^2}{r^2 + a(r,\chi)^2\chi^2}\Big[(a(r,\chi)^2 + r^2)^2$$
$$- a(r,\chi)^2(r^2 - 2G_0 M r + a(r,\chi)^2)\cdot(1-\chi^2)\Big]\,d\phi^2. \tag{6.17}$$

Similarly to Subsec. 6.2.1, different choices of $a(r,\chi)$ lead to different families of spacetimes and circularity, see Eqs. 6.3 and 6.4, is recovered only for $a(r,\chi) \to a(r)$.

We first explore spin upgrades within the principled-parameterised approach, that is spin functions $a(r,\chi)$ which, among others, obey the locality principle and depend on r, χ only through the local curvature defined in Eq. 6.14.

We require that such locality-based spin functions $a(K \cdot l_{\rm NP}^4)$ satisfy the correct Newtonian limit to leading order, i.e.

$$a(K \cdot l_{\rm NP}^4) \overset{K\cdot l_{\rm NP}^4 \to 0}{\longrightarrow} a_\infty \equiv a = \text{const.} \tag{6.18}$$

Additionally, to fulfil the regularity principle, we demand that all non-derivative, upgraded curvature invariants are finite everywhere in spacetime, in particular at the location of the classical singularity $(r = 0, \chi = 0)$. Focusing first on the first invariant $I_1 = C_{\mu\nu\rho\sigma}C^{\mu\nu\rho\sigma}$, c.f. App. B.2, we require that

$$\lim_{r\to 0}\lim_{\chi\to 0} I_1 \overset{!}{=} \lim_{\chi\to 0}\lim_{r\to 0} I_1 < \infty, \tag{6.19}$$

since, away from the classical singularity $(r = 0, \chi = 0)$, no singularities can occur in any of the invariants as long as $a(K \cdot l_{\rm NP}^4)$ is itself regular. To evaluate this condition, we split I_1 into its "classical part" $I_{1,\rm c}$ – containing no derivatives of $a(K \cdot l_{\rm NP}^4)$ – and its "quantum" counterpart $I_{1,\rm d}$ – which depends on the derivatives of $a(K \cdot l_{\rm NP}^4)$ – such that $I_1 = I_{1,\rm c} + I_{1,\rm d}$. We further assume that the regularity condition Eq. 6.19 applies separately to $I_{1,\rm c}$ and $I_{1,\rm d}$, otherwise delicate cancellations of divergences would have to occur between $I_{1,\rm c}$ and $I_{1,\rm d}$. The "classical part" $I_{1,\rm c}$ is given by

$$I_{1,\rm c} = \frac{48G_0^2M^2\left(r^6 - 15\,a^2(K\cdot l_{\rm NP}^4)\,r^4\chi^2 + 15\,a^4(K\cdot l_{\rm NP}^4)\,r^2\chi^4 - a^6(K\cdot l_{\rm NP}^4)\,\chi^6\right)}{\left(r^2 + a^2(K\cdot l_{\rm NP}^4)\,\chi^2\right)^6}. \tag{6.20}$$

Following our assumption, if divergences occur in $I_{1,\rm c}$, those cannot be cancelled in $I_{1,\rm d}$ and, as such, make I_1 divergent. In the limit $r \to 0$, we get

$$\lim_{r\to 0} I_{1,\rm c} = -\frac{48G_0^2M^2}{a^6(K\cdot l_{\rm NP}^4\big|_{r=0})\chi^6}. \tag{6.21}$$

The limit $\chi \to 0$ of Eq. 6.21 is finite if the leading behaviour of $\lim_{\chi\to 0} a(K\cdot l_{\rm NP}^4\big|_{r=0})$ is of the form

$$\lim_{\chi\to 0} a(K\cdot l_{\rm NP}^4\big|_{r=0}) \sim \frac{1}{\chi^n},\ n \geq 1, \tag{6.22}$$

in other words, if $a(K\cdot l_{\rm NP}^4) \sim a_\infty \cdot (K\cdot l_{\rm NP}^4)^p,\ p \geq 1$.

In the limit $\chi \to 0$ and assuming that the spin function takes the form $a(K \cdot l_{\rm NP}^4) \sim a_\infty \cdot (K \cdot l_{\rm NP}^4)^p$, $p \geq 1$, we get

$$\lim_{\chi \to 0} I_{1,c} = \frac{48 G_0^2 M^2}{r^6}, \tag{6.23}$$

which clearly diverges in the limit $r \to 0$.

Hence, we conclude that under the assumptions specified above, a "quantum" spin hair $a(K \cdot l_{\rm NP}^4)$ derived within the principled-parameterised approach cannot lead to a resolution of the classical curvature singularity. This is intriguing, as it implies a certain degree of uniqueness to a "quantum" mass hair that consists in a mass function $M(K \cdot l_{\rm NP}^4)$. One can of course imagine scenarios in which both upgrades $M(K \cdot l_{\rm NP}^4)$ and $a(K \cdot l_{\rm NP}^4)$ are present simultaneously in regular black holes, but the upgrade $a(K \cdot l_{\rm NP}^4)$ is insufficient on its own if the locality principle is to simultaneously be satisfied.

This result suggests to generalise the above procedure. We thus abandon the locality principle encoded in the principled-parameterised approach to find regular, non-derivative curvature invariants, and look for less constrained spin functions $a(r, \chi)$ depending independently on r and χ.

Near the classical singularity $(r = 0, \chi = 0)$, i.e. for small r and χ, let us assume that $a(r, \chi)$ has a series expansion starting with $a(r, \chi) \sim r^\alpha \chi^\beta$, $\alpha, \beta \in \mathbb{Z}$. Then, the choice

$$a(r, \chi) = \chi^\beta, \ \beta \leq -3, \tag{6.24}$$

renders the full curvature invariant I_1 finite and single-valued in the limit $r, \chi \to 0$. This result relies on the absence of subleading terms in r. However, the form Eq. 6.24 contradicts Eq. 6.18, i.e. the Newtonian limit of a constant spin a at large r, and thus the choice $a(r, \chi) \sim \chi^\beta$, $\beta \leq -3$ cannot be a valid spin function.

This suggests to add an r-dependence to Eq. 6.24 without spoiling its behaviour in the leading-order expansion for small r and χ. We can, for instance, consider rational functions like

$$a(r, \chi) = a_\infty \frac{r}{r+1} + \frac{1}{\chi^4 (r^3 + 1)}, \tag{6.25}$$

with a_∞ the constant spin parameter obtained in the Newtonian limit. The latter spin function indeed satisfies both conditions Eqs. 6.18 and 6.24. Nonetheless, the sequence of limits $\lim_{r \to 0} \lim_{\chi \to 0}$ for the Ricci scalar and I_1 is either indeterminate or divergent, due to the presence of subleading terms in the series expansion around $r = 0$ which still depend on r.

Instead, we can consider a spin function with exponential suppression in r, such as, e.g.

$$a(r, \chi) = \frac{a_\infty}{e^{\frac{1}{r}}} \cdot \frac{r}{r+1} + \frac{1}{\chi^4} \left(1 - \frac{1}{e^{\frac{1}{r}}} \right). \tag{6.26}$$

For this spin function, we observe that subleading terms in r remain in the series expansion, rendering the invariants multi-valued and potentially divergent. Indeed, our tests of various functions (with even stronger suppression at small r than in Eq. 6.26) beyond those reported here suggest that any subleading dependence on r beyond the choice $a(r, \chi) = \chi^\beta$ renders some curvature invariants ill-defined.

To summarise, we do not find an example of a spin modification that renders non-derivative curvature invariants finite, neither within the principled-parameterised approach, nor when abandoning the locality principle. As we have not comprehensively explored the space of functions $a(r, \chi)$ that do not satisfy the locality principle, there may potentially be a choice of spin function that results in singularity resolution. However, we note that the spin function enters both denominators and numerators of different metric coefficients in Eq. 6.17 and of curvature invariants, hence rendering all non-derivative, curvature invariants finite seems unachievable.

6.3 Going beyond circularity, separability and spherical symmetry

To comprehensively understand how black holes beyond GR "look like", e.g. in terms of shadow images and properties, the *parameterised approach* of deviations from the Kerr metric is best used. But achieving comprehensiveness requires the parameterisations to be as general as necessary to include all relevant cases. First, stationary and axisymmetric parameterisations should be favoured over the simplistic static and spherically symmetric ones, as astrophysical black holes do rotate. Second, parameterisations that are "too symmetric", i.e. that make too many symmetry assumptions, should be replaced by more general – thus less symmetric – ones for two reasons. On purely theoretical grounds, we aim to be as general as necessary to capture all leading-order deviation effects from GR in parameterised metrics. Hence, parameterised black holes beyond GR need not be as symmetric as GR ones. On more pragmatic grounds, we aim to describe already-known spacetimes (solutions or not of a certain theory) and there are already examples of non-circular spacetimes, both within non-vacuum GR [IS03; IS04; BSM11; Ury+14; SG23] and beyond GR [HGE19; Min20; Ans+21; BA+20; EH21a; EH21b; Fer23].

6.3.1 Non-circular spacetimes

In vacuum GR, the Einstein field equations Eq. 2.1 give $R_{\mu\nu} = 0$. As the circularity conditions Eqs. 6.3 and 6.4 directly involve the Ricci tensor $R_{\mu\nu}$, circularity is trivially satisfied in vacuum GR, i.e. for the Kerr black hole. However, circularity needs not hold beyond vacuum GR. Indeed, the coexistence of toroidal magnetic fields and convective motion result in meridional flows and thus non-circular metrics for neutron stars [IS03; IS04; BSM11; Ury+14; SG23]. In addition to that, [Ver03] suggests that non-circular interior solutions for compact rotating bodies can be matched onto circular external solutions in GR.

Beyond GR, non-circular spinning black holes were obtained in various settings: first, as disformal solutions[5] to modified gravitational dynamics within scalar-tensor or vector-tensor theories [Min20; Ans+21; BA+20]; second, as black-hole spacetimes

[5]Disformal transformations [Bek93; BEF07; BL13] are used in ghost-free scalar-tensor and vector-tensor theories (e.g. Horndeski theories), as a way to obtain other ghost-free theories. Within scalar-tensor theories, a disformal transformation maps a pair $(g_{\mu\nu}, \phi)$ composed of a metric $g_{\mu\nu}$ and a scalar field ϕ to another pair $(\tilde{g}_{\mu\nu}, \phi)$, where $\tilde{g}_{\mu\nu} = A(\phi, X)g_{\mu\nu} + B(\phi, X)\nabla_\mu\phi\nabla_\nu\phi$ and $X \equiv g^{\mu\nu}\nabla_\mu\phi\nabla_\nu\phi$. It corresponds to a generalisation of a conformal transformation for which $B(\phi, X) = 0$. A disformal transformation is invertible as long as $A(\phi, X) \neq 0$, $A(\phi, X) + XB(\phi, X) \neq 0$ and $A(\phi, X) - X\partial_X A(\phi, X) - X^2\partial_X B(\phi, X) \neq 0$. Hence, an invertible disformal transformation maps a given action $S[g_{\mu\nu}, \phi]$ to a new action $\tilde{S}[g_{\mu\nu}, \phi] \equiv S[\tilde{g}_{\mu\nu}, \phi]$ without changing the number of physical d.o.f. However, once minimally-coupled matter fields are included, the two actions are no longer related by an invertible transformation in general, and hence they can be inequivalent.

inspired by ASQG [HGE19; EH21a]; third, in the framework of "bumpy Kerr metrics" in [VH10, Eq. (2.36)] and [Vig10, Eq. (1.5)]; fourth, as solutions in semiclassical gravity when well-known quantum gravitational effects are considered [Fer23]; finally, within a *principled-parameterised approach* developed in [EH21b; EH21a]. The latter non-circular, regular, rotating spacetimes fulfil the locality principle. As argued in [Hel21], any other regularisation that is circular would violate the locality principle, indicating a possible connection between the locality principle and non-circularity.

Non-circular spacetimes often exhibit peculiar GW and EM features. As for the EM signatures in "shadow" images, ASQG-inspired black holes can have a dent, cusps and a lack of reflection symmetry [EH21b; EH21a; DEH22], see Subsec. 4.2.1, while a "pedicel"-like structure [Lon+20] and cusp-like features [VGY18] can appear in disformal Kerr black holes. Peculiar non-circular signatures of a disformal Kerr background manifest in the motion of a S_2-like pulsar and on the associated time of arrival of emitted photons [Tak+21] as well as in the globally accumulated phase of an EMRI's gravitational waveform [Bab+24]. Those effects could in principle be detected by future EM (e.g. the Square Kilometre Array) and GW (e.g. LISA) missions.

6.3.2 Non-circular parameterisation in horizon-penetrating coordinates

Horizon-Penetrating (HP) coordinates can be used to set up black-hole parameterisations in and beyond circularity. There is a strong reason to favour HP coordinates such as ingoing Kerr coordinates (u, r, χ, ϕ), where u is a lightcone time. These coordinates make it easy to avoid accidental introductions of coordinate singularities at the horizon. The reason is that Kerr spacetime in HP coordinates

$$\begin{aligned} ds^2_{\rm HP} = &-\left(\frac{r^2 - 2G_0Mr + a^2\chi^2}{r^2 + a^2\chi^2}\right) du^2 + 2dudr - 4\frac{G_0Mar}{r^2 + a^2\chi^2}(1-\chi^2)dud\phi \\ &- 2a(1-\chi^2)drd\phi + \frac{r^2 + a^2\chi^2}{1-\chi^2}d\chi^2 \\ &+ \frac{1-\chi^2}{r^2 + a^2\chi^2}\left(\left(a^2 + r^2\right)^2 - a^2\left(r^2 - 2G_0Mr + a^2\right)\left(1-\chi^2\right)\right) d\phi^2 \end{aligned} \tag{6.27}$$

does not feature coordinate singularities at the horizons $r_\pm = G_0M \pm \sqrt{G_0^2M^2 - a^2}$. Therefore, a spacetime that parametrically deviates from the Kerr spacetime does not feature curvature singularities at the horizon, as long as the functions that encode these parameterised deviations are non-singular and invertible. In contrast, BL coordinates require additional non-trivial conditions on the metric coefficients to achieve the same, cf. [Joh13a; Joh13b; CPR14; Hel21].

To encode parametric deviations $\Delta_{\mathrm{HP,j}}(r,\chi)$, $i=1,\ldots,6$, from the Kerr spacetime in a more general, non-circular spacetime, we write

$$\begin{aligned} ds^2_{\mathrm{HP}} = &-\left(\frac{r^2-2G_0Mr+a^2\chi^2}{r^2+a^2\chi^2}\right)\left(1+\Delta_{\mathrm{HP},1}(r,\chi)\right)du^2+2\left(1+\Delta_{\mathrm{HP},2}(r,\chi)\right)dudr \\ &-4\frac{G_0Mar}{r^2+a^2\chi^2}(1-\chi^2)(1+\Delta_{\mathrm{HP},3}(r,\chi))dud\phi-2a(1-\chi^2)(1+\Delta_{\mathrm{HP},4}(r,\chi))drd\phi \\ &+\frac{r^2+a^2\chi^2}{1-\chi^2}(1+\Delta_{\mathrm{HP},5}(r,\chi))d\chi^2 \\ &+\frac{1-\chi^2}{r^2+a^2\chi^2}\left(\left(a^2+r^2\right)^2-a^2\left(r^2-2G_0Mr+a^2\right)\left(1-\chi^2\right)\right)(1+\Delta_{\mathrm{HP},6}(r,\chi))d\phi^2. \end{aligned} \tag{6.28}$$

In contrast to the circular parameterisations we have discussed in Sections 6.1.2 and 6.1.3, we write non-circular spacetimes in terms of deviations from the Kerr spacetime. The reason is phenomenological: there is currently – within the observational uncertainties – no indication for deviations of BHs from the Kerr solution, thus deviations are already constrained, see e.g. [HGE19; Koc+21] for constraints in the context of shadow images. Therefore, writing a parameterisation in terms of deviations from Kerr spacetime connects most directly to observations.

We first require that the spacetime is asymptotically flat. For $\Delta_{\mathrm{HP},i}=0$, $i=1,\ldots,6$, i.e. in the Kerr-limit, this is the case. To preserve this property for generic deviation functions, we demand that

$$\lim_{r\to\infty}\Delta_{\mathrm{HP},i}(r,\chi)=0. \tag{6.29}$$

Additionally, one may require that the $\mathcal{O}\left(\frac{1}{r}\right)$ terms agree with those of the Kerr spacetime, such that the Newtonian limit is preserved at leading order. To achieve this, the corrections arising from $\Delta_{\mathrm{HP},i}$, $i=1,\ldots,6$, must only set in at higher order, i.e.

$$\Delta_{\mathrm{HP},i}(r,\chi)\sim\mathcal{O}\left(\frac{1}{r^2}\right). \tag{6.30}$$

Similarly, if agreement with the PM expansion to higher orders is to be achieved, constraints may be pushed to higher orders in r.

Next, we consider the limit of flat Minkowski spacetime. For Kerr spacetime, this limit is reached for $G_0M\to 0$, which results in a Riemann tensor that is identically zero in all its components. For the metric Eq. 6.28, this is no longer the case. For instance, it suffices to set $\Delta_{\mathrm{HP},2}(r,\chi)\neq 0$, with all other $\Delta_{\mathrm{HP},i\neq 2}=0$, for the spacetime to no longer be Ricci flat and feature a non-vanishing Ricci scalar. To preserve the property that the spacetime is flat in the limit $M\to 0$, one may demand that $\Delta_{\mathrm{HP},i}\sim G_0M$. Alternatively, the compact objects described by Eq. 6.28 may be characterised by additional ("quantum") hair, such that even in the limit $G_0M\to 0$, a non-trivial spacetime geometry exists. Whether or not the parameter G_0M preserves its interpretation as the ADM mass of the compact object is left for future work.

Similarly, we consider the limit $a\to 0$, which results in spherical symmetry (i.e. Schwarzschild) in the case of Kerr spacetime. This is no longer the case for

Eq. 6.28 which, in that limit, reduces to

$$\lim_{a\to 0} ds^2_{\rm HP} = -\left(1-\frac{2G_0M}{r}\right)\left(1+\Delta_{{\rm HP},1}(r,\chi)\right)du^2 + 2\left(1+\Delta_{{\rm HP},2}(r,\chi)\right)dudr + \frac{r^2}{1-\chi^2}(1+\Delta_{{\rm HP},5}(r,\chi))d\chi^2 + \left(1-\chi^2\right)r^2(1+\Delta_{{\rm HP},6}(r,\chi))d\phi^2. \quad (6.31)$$

The remaining χ-dependence in g_{uu} and g_{ur} is a clear sign of the breaking of spherical symmetry, as is the deviation of the angular line element from its canonical form $ds^2_{\rm angular} = \frac{r^2}{1-\chi^2}d\chi^2 + (1-\chi^2)r^2d\phi^2$. One may object that four coordinate transformations can absorb the additional χ-dependence introduced by the four functions $\Delta_{{\rm HP},1,2,5,6}(r,\chi)$. However, these coordinate transformations can, in general, not be done without introducing new off-diagonal terms in the line element. This can be seen, for example, by inspecting the curvature invariants of Eq. 6.31. As an example, the Ricci scalar is non-vanishing and depends on χ and r explicitly, as well as through derivatives of $\Delta_{{\rm HP},1,2,5,6}(r,\chi)$. Therefore, curvature invariants in this limit are in general not spherically symmetric. Accordingly, there are two sources of breaking of spherical symmetry to axisymmetry: one is the presence of spin, a, the other is, broadly speaking, additional ("quantum") hair encoded in the χ-dependence of $\Delta_{{\rm HP},1,2,5,6}(r,\chi)$.

For arbitrary deviations $\Delta_{{\rm HP},i}(r,\chi)$, $i=1,\dots,6$, changes of the spacetime signature can occur. The metric determinant is given by

$$\begin{aligned}\det(g_{\rm HP}) =& \frac{1+\Delta_{{\rm HP},5}}{1-\chi^2}\Big[(1+\Delta_{{\rm HP},4})\,a^2\left(1-\chi^2\right)^2\Big(2(1+\Delta_{{\rm HP},2})(1+\Delta_{{\rm HP},3})G_0Mr \\ &+(1+\Delta_{{\rm HP},1})(1+\Delta_{{\rm HP},4})\left(-2G_0Mr+r^2+a^2\chi^2\right)\Big) \\ &+(1+\Delta_{{\rm HP},2})(1-\chi^2)\Big(2(1+\Delta_{{\rm HP},3})(1+\Delta_{{\rm HP},4})G_0Ma^2r(1-\chi^2) \\ &-(1+\Delta_{{\rm HP},2})(1+\Delta_{{\rm HP},6})\left(r^4+\chi^2a^2(1+r^2)+2G_0Mra^2(1-\chi^2)\right)\Big)\Big],\end{aligned} \quad (6.32)$$

such that the signature translates into conditions on the $\Delta_{{\rm HP},i}(r,\chi)$, $i=1,\dots,6$. If all $\Delta_{{\rm HP}\,i}(r,\chi)\sim\epsilon=$ const., $i=1,\dots,6$, the determinant Eq. 6.32 simplifies to $\det(g_{\rm HP}) = -(1+\epsilon)^4(r^2+a^2\chi^2)^2$, which means that the signature does not change as long as $\epsilon > -1$. In fact, the eigenvalues of the metric change sign at $\epsilon=-1$, such that the Lorentzian metric signature flips by a global minus sign from $(-,+,+,+)$ for $\epsilon>-1$ to $(+,-,-,-)$ for $\epsilon<-1$. This global sign flip is physically meaningless as it just turns the mostly-plus convention for Lorentzian metrics into the mostly-minus convention, and they are equivalent. We thus caution that the change in metric signature arising here differs from those which mark the transition between a Lorentzian and a Euclidean metric (and vice-versa) in QG settings, see e.g. [Sak84; MSV07; Amb+15; BB17; SX18].

The non-circular parameterisation in Eq. 6.28 reduces to a parameterisation of circular black holes if conditions on the $\Delta_{{\rm HP},i}(r,\chi)$, $i=1,\dots,6$ hold. The circularity conditions in Eqs. 6.3 and 6.4 amount to lengthy differential conditions that are not

straightforward to solve. The only two conditions that we find straightforward to solve are: i) $\Delta_{\mathrm{HP},5}(r,\chi)$ can deviate from zero while preserving circularity, if all other $\Delta_{\mathrm{HP},i\neq5}(r,\chi)=0$; ii) $\Delta_{\mathrm{HP},i}(r,\chi)=\epsilon=\text{const.}\ \forall\, i$ preserves circularity, but as soon as $\Delta_{\mathrm{HP},1}(r,\chi)$ is chosen to differ from the other deviation functions, circularity is broken. Accordingly, an explicit restriction to circular spacetimes appears to be quite non-trivial in HP coordinates. Instead, the parameterisation in Eq. 6.12 appears to be the preferred one for circular spacetimes, because circularity is straightforward to implement in BL coordinates.

6.3.3 From a non-circular parameterisation to a circular one

As it seems that non-circular and circular spacetime favour two different sets of coordinates, it is interesting to understand how the more general, non-circular parameterisation in Eq. 6.28 and the circular parameterisation in Eq. 6.12 are related.

An explicit transformation of Eq. 6.28 into the parameterisation of circular black-hole spacetimes in BL coordinates is challenging to provide. Instead, we use a counting argument to plausibilise the existence of such a coordinate transformation. To summarise, this counting argument adds all available free functions and subtracts the non-trivial conditions that must be satisfied either for the metric to be of the form Eq. 6.12 or for a coordinate transformation to exist.

There are 14 free functions to start with, out of which 6 are the deviation functions $\Delta_{\mathrm{HP},i}(r,\chi)$, $i=1,\dots,6$, in the parameterisation Eq. 6.28 and 8 are the free functions resulting from coordinate transformations which preserve the manifest Killing coordinates. These 14 free functions are subject to 9 constraints, namely 4 differential constraints on the 8 free functions from coordinate transformations, and 5 constraints arising from the vanishing of some metric components in the circular metric parameterisation in Eq. 6.12.

That four coordinate transformations, which preserve manifest Killing coordinates, provide 8 free functions, subject to 4 differential constraints, can be seen as follows. In 4D, a general coordinate transformation from coordinates x^μ to coordinates y^μ can be written as

$$dy^\mu = F^\mu_\nu dx^\nu. \tag{6.33}$$

The 16 functions F^μ_ν need to form exact differentials and, hence, are subject to the differential constraints $\partial_\alpha F^\mu_\nu = \partial_\nu F^\mu_\alpha$. Thus, there are 16 free functions subject to 6 differential constraints in this general case, i.e. one differential constraint per pair of indices (α,ν) with $\alpha,\nu\in\{1,2,3,4\}$ labelling coordinates $x^\mu=(x^1,x^2,x^3,x^4)$. To preserve manifest Killing coordinates, the transformations of r and χ must not involve the coordinates t and ϕ_{BL}. Indeed, if r and χ were functions of t and ϕ_{BL}, the metric components would depend on the two Killing coordinates, therefore the Killing symmetries would no longer be manifest in the metric. Further, it must hold that $du=dt+\dots$ and $d\phi=d\phi_{\mathrm{BL}}+\dots$, such that the transformation of u and ϕ only contains 2 free functions of r,χ each. Together, this reduces the 16 free functions from the general coordinate transformation to 8 free functions of the non-Killing coordinates, and the number of differential constraints from 6 to 4, cf. [GB93, Eq. (2.2)].

In addition, 6 free deviation functions $\Delta_{\mathrm{HP},i}(r,\chi)$, $i=1,\dots,6$ are given in the initial form of the metric and 5 constraints arise from the final form of the metric, namely the fact that all but one off-diagonal metric element in Eq. 6.12 vanishes.

As a result of 14 ($= 8 + 6$) free functions with 9 ($= 4 + 5$) constraints, at least 5 free functions remain (more if not all constraints are linearly independent) that solely depend on r and χ. Five free functions of r and χ are exactly what is needed to parameterise circular black holes in BL coordinates in the form Eq. 6.12, and are even one function too many if one does not insist on BL coordinates but want the Lewis-Papapetrou form, cf. Subsec. 6.1.3.

6.3.4 Example: a non-circular and regular spacetime through mass upgrade

We have discussed in Subsec. 6.2.1 families of regular spacetimes constructed in the principled-parameterised approach from an upgrade of the ADM mass parameter to a "quantum" mass hair. The regularisation of those spacetimes occurs through a weakening of gravity encoded in a locality-based mass function $M(r,\chi) \equiv M(K \cdot l_{\rm NP}^4)$. The resulting regular spacetime is non-circular for $M(r,\chi)$, and circular for $M(r)$.

We now explicitly show that these two families of regular black-hole spacetimes, given by the metric Eq. 6.13 with $M(r,\chi)$ and $M(r)$, are included in the more general, non-circular parameterisation in HP coordinates postulated in Eq. 6.28.

The correspondence between the general parameterisation Eq. 6.28 in HP coordinates and the non-circular, regular black-hole with "quantum" mass hair in Eq. 6.13, is given by

$$\Delta_{\rm HP,2} = 0, \tag{6.34}$$
$$\Delta_{\rm HP,4} = 0, \tag{6.35}$$
$$\Delta_{\rm HP,5} = 0, \tag{6.36}$$
$$\Delta_{\rm HP,1} = \frac{2rG_0\left(M - M(r,\chi)\right)}{r^2 + a^2\chi^2 - 2G_0Mr}, \tag{6.37}$$
$$\Delta_{\rm HP,3} = \frac{M(r,\chi) - M}{M}, \tag{6.38}$$
$$\Delta_{\rm HP,6} = -\frac{2a^2G_0\left(M(r,\chi) - M\right)r(\chi^2-1)}{r^4 + a^4\chi^2 + a^2r\left(2G_0M + r(r - 2G_0M)\chi^2\right)}. \tag{6.39}$$

The regular, rotating black holes in e.g. [RT06; Abd+16; Tor17; KSG20; KG21; He+20; SV22] can be brought into the general form Eq. 6.28 for the special case $M(r,\chi) = M(r)$ in Eqs. 6.34 to 6.39, followed by a coordinate transformation into BL coordinates (where for clarity we denote the azimuthal angle $\phi_{\rm BL}$ in BL coordinates) according to

$$\begin{aligned} t &= u - \int dr\, \frac{r^2 + a^2}{r^2 + a^2 - 2G_0M(r)r}, \\ \phi_{\rm BL} &= \phi - \int dr\, \frac{a}{r^2 + a^2 - 2G_0M(r)r}. \end{aligned} \tag{6.40}$$

The fact that the spacetime described by Eqs. 6.34 to 6.39 and $M(r,\chi) = M(r)$ is a very special choice in the general class Eq. 6.28 suggests that the regular black holes that have been discussed in the literature are a special subclass of a more general family of rotating regular black holes. Indeed, the black-hole spacetimes with $M(r,\chi) = M(r)$ all fulfill the circularity condition, and are thus all circular.

Despite having shown examples of non-circular black-hole spacetimes in the parameterisation Eq. 6.28, we do not provide a general proof that all non-circular black-hole spacetimes can be written in this form as it is beyond the scope of this

thesis. Instead, we motivate the non-circular parameterisation Eq. 6.28 by the following observations: (i) it contains the Kerr spacetime in the limit $\Delta_{\mathrm{HP},i}(r,\chi) \to 0$; (ii) it includes both circular and non-circular spacetimes, in particular those that have recently been motivated from a locality principle for new physics in a principled-parameterised approach [EH21b; EH21a].

We conjecture that the choice of six free functions in the non-vanishing metric components is sufficient to describe all axisymmetric, stationary and asymptotically flat black-hole spacetimes that can be reached as deformations of the Kerr spacetime. The argument underlying this conjecture is the following: from the initial ten metric components, four free functions can be removed by a change of spacetime coordinates, thus six free functions are enough to fully describe a given spacetime. This, however, assumes that the number of free functions corresponds to the number of non-vanishing metric components in HP coordinates.

An interesting example to test this conjecture is the non-circular black holes found in particular scalar-tensor or vector-tensor theories [Min20; Ans+21; BA+20]. While these non-circular black holes have been constructed in BL coordinates, they are transformed (by a combination of coordinate and disformal transformations) to a specific choice of HP coordinates with seven non-vanishing metric components, see [Ans+21, App. A].

It remains an open question whether other suitable coordinate transformations can be constructed which cast these non-circular black holes to the HP form in Eq. 6.28. If such a coordinate transformation cannot be found, then Eq. 6.28 needs to be generalised by adding the appropriate deviation function.

Despite this open question, we argue that Eqs. 6.34 to 6.39 with either $M(r,\chi)$ or $M(r)$ are particularly relevant from a quantum-gravity point of view, e.g. [BR00; RT06; Nic09; MN10; HR15; AOS18; Pla19; NSW19; Con+20; HGE19; EH21b; EH21a]. The latter metrics make three of the initial six deviation functions $\Delta_{\mathrm{HP},i}(r,\chi)$ irrelevant, thus highlighting that Eq. 6.28 does not require further generalisation to encode the effects of several quantum-gravity scenarios. The argument is based on the assumption that QG must regularise spacetime singularities and thus regularise all (non-derivative) curvature invariants. A priori, this could occur in distinct ways. One way which has been explored extensively is captured by Eqs. 6.34 to 6.39 and discussed in Subsec. 6.2.1: it relies on an effective weakening of gravity through a fast-enough fall-off of the mass function at small r. This can be interpreted as an effective repulsive force coming from quantum gravity. From the point of view of black-hole "hair", the constant mass parameter is modified to a function, i.e. the corresponding classical "hair" is modified.

6.3.5 Non-circular parameterisation in Boyer-Lindquist coordinates

BL coordinates are widely used in parameterisations of black-hole spacetimes, and they are well-suited to implement circularity (though not to prevent curvature singularities at the horizon). Therefore, we now explore how to describe non-circular spacetimes in BL coordinates instead of HP coordinates.

To describe non-circular black holes in BL coordinates, one has to go beyond the Boyer-Lindquist form of the metric, which means we need to allow some metric functions, which vanish for a Kerr black hole, to be non-zero. Because circularity implies the invariance under the simultaneous mapping $t \to -t$, $\phi_{\mathrm{BL}} \to -\phi_{\mathrm{BL}}$, breaking circularity can be achieved by allowing $g_{t\chi} \neq 0$, $g_{\chi\phi_{\mathrm{BL}}} \neq 0$, $g_{tr} \neq 0$ or

$g_{r\phi_{\rm BL}} \neq 0$. Adding these four free functions to the four free functions of circular, axisymmetric, stationary spacetime in the Lewis-Papapetrou form would provide eight free functions.

What also differs in non-circular spacetimes (compared to circular ones) is that meridional surfaces are only locally orthogonal to the surfaces of transitivity, but no longer guaranteed to be (globally) integrable. Thus, the argument used in Subsec. 6.1.3 that reduces the number of free functions in the meridional sector to just one no longer holds, and that sector has two additional free functions. Thus, in the most general case, we expect the more general, non-circular parameterisation to have ten free functions in BL coordinates. However, it might be possible to extend the local patch in which $ds^2_{\rm mer} = g_{\tilde{r}\tilde{r}}\left(d\tilde{r}^2 + \frac{\tilde{r}^2}{1-\chi^2}\,d\chi^2\right)$ holds far enough to cover the entire region of a spacetime that one is interested in.

Because we have the freedom to perform four coordinate transformations, we expect that a metric should never have more than six free functions in *some* set of coordinates. [ABCG07] states that there is indeed such a coordinate choice in which six free functions are enough. This choice of coordinates could in general depend on the chosen metric.

However, this argument does not take into account that one might want to work in coordinates in which the Killing symmetries are manifest in the metric. The latter condition limits the available coordinate transformations, or indeed fixes the coordinate system to be the BL one as we do here. Insisting on coordinates in which the Killing symmetries are manifest (and assuming an extension of the local patch, see above) leads to eight free functions, cf. [GB93] in the context of global hyperbolicity and a 3+1 decomposition.

As a result, we propose that such a non-circular spacetime in BL coordinates is described by the line element

$$\begin{aligned} ds^2 = &-\left(1-\frac{2G_0Mr}{r^2+a^2\chi^2}\right)(1+\delta_1(r,\chi))\,dt^2 + 2\delta_2(r,\chi)dt\,dr + 2\delta_3(r,\chi)dt\,d\chi \\ &- \frac{4G_0Mr\,a\,(1-\chi^2)}{r^2+a^2\chi^2}(1+\delta_4(r,\chi))dt\,d\phi_{\rm BL} + \frac{r^2+a^2\chi^2}{r^2-2G_0Mr+a^2}\,(1+\delta_5(r,\chi))\,dr^2 \\ &+ 2\gamma(r,\chi)dr\,d\chi + 2\delta_6(r,\chi)dr\,d\phi_{\rm BL} + \frac{r^2+a^2\chi^2}{1-\chi^2}(1+\delta_7(r,\chi))d\chi^2 \\ &+ 2\delta_8(r,\chi)d\chi d\phi_{\rm BL} + \left(r^2+a^2+\frac{2G_0Mr\,a^2(1-\chi^2)}{r^2+a^2\chi^2}\right)(1-\chi^2)(1+\delta_9(r,\chi))d\phi^2_{\rm BL}. \end{aligned} \tag{6.41}$$

with ten free functions given by $\delta_i(r,\chi)$, $i = 1,\ldots,9$ and $\gamma(r,\chi)$. If the choice $ds^2_{\rm mer} = g_{rr}\left(dr^2 + \frac{r^2-2G_0Mr+a^2}{1-\chi^2}\,d\chi^2\right)$, which is always possible locally, is available in a large enough patch of spacetime, then $\gamma(r,\chi) = 0$ and additionally $\delta_5(r,\chi)$ and $\delta_7(r,\chi)$ are related to each other, leaving a total of 8 free functions.

For $\delta_i(r,\chi) = 0\ \forall i$, the metric reduces to the Kerr metric in BL coordinates. Increasing values of $\delta_i(r,\chi)$, $i = 1,\ldots,9$, parameterise deviations from the Kerr spacetime.

To ensure that the spacetime remains asymptotically flat, we require

$$\lim_{r\to\infty}\delta_i(r,\chi) = 0. \tag{6.42}$$

Regularity imposes differential conditions on the $\delta_i(r,\chi)$, both at the classical location of the curvature singularity $r=0=\chi$ as well as at the event horizon $r=r_+$. Whereas conditions at $(r,\chi)=(0,0)$ might have been expected, conditions at finite $r=r_+$ are not immediately obvious. These arise because for $\delta_i(r,\chi)=0\ \forall i$, the metric Eq. 6.41 contains the well-known coordinate singularities of Kerr spacetime in BL coordinates, but these singularities cancel in curvature invariants. Because this cancellation requires that different metric functions are delicately balanced, arbitrary deformations of metric functions, i.e. arbitrary choices of $\delta_i(r,\chi)$, can easily introduce curvature singularities lying on the horizon. Those correspond to naked singularities [Joh13a; Joh13b; CPR14; Hel21].

We now show explicitly that the non-circular parameterisation Eq. 6.41 contains all circular black holes as subcases, and also several examples of non-circular black holes.

The more specialised parameterisation from [KRZ16], namely Eq. 6.12, that respects circularity is of course included in Eq. 6.41. This is easiest to see by switching from $\chi=\cos\theta$ back to θ. Then, the mapping between Eq. 6.12 and Eq. 6.41 is given by

$$
\begin{aligned}
\omega(r,\theta) =& \frac{2aG_0M\,(1+\delta_4(r,\theta))}{r^2+a^2\cos^2\theta},\\
\kappa^2(r,\theta) =& \frac{1+\delta_9(r,\theta)}{r^2}\left(a^2+r^2+\frac{2G_0M\,r\,a^2\sin^2\theta}{r^2+a^2\cos^2\theta}\right),\\
\sigma(r,\theta) =& \left(\frac{a^2\cos^2\theta}{r^2}+1\right)\cdot(1+\delta_7(r,\theta)),\\
f(r,\theta) =& \frac{1}{r^2\,(r^2+a^2\cos^2\theta)^2}\Bigg\{r^3(a^2+r^2)\,[r-2G_0M(1+\delta_1(r,\theta))]\,(1+\delta_9(r,\theta))\\
&+a^2\Bigg[a^2(a^2+r^2)(1+\delta_9(r,\theta))\cos^4\theta-r(1+\delta_9(r,\theta))\cos^2\theta\,\big[2r^2(G_0M-r\\
&+G_0M\delta_1(r,\theta))+a^2(G_0M-2r+2G_0M\delta_1(r,\theta))+a^2\cos(2\theta)G_0M\big]\\
&+2G_0Mr^2(r(1+\delta_9(r,\theta))-2G_0M\,\big[\delta_1(r,\theta)-2\delta_4(r,\theta)-\delta_4^2(r,\theta)+\delta_9(r,\theta)\\
&+\delta_1(r,\theta)\delta_9(r,\theta)\big]\sin^2\theta\Bigg]\Bigg\},\\
\beta^2(r,\theta) =& \frac{1+\delta_5(r,\theta)}{(a^2+r(r-2G_0M))(1+\delta_7(r,\theta))(r^2+a^2\cos^2\theta)^2}\\
&\cdot\Bigg\{r^3(r^2+a^2)\,[r-2G_0M(1+\delta_1(r,\theta))]\,(1+\delta_9(r,\theta))\\
&+a^2\Bigg[a^2(a^2+r^2)(1+\delta_9(r,\theta))\cos^4\theta-r(1+\delta_9(r,\theta))\cos^2\theta\,\big[2r^2(G_0M-r\\
&+G_0M\delta_1(r,\theta))+a^2(G_0M-2r+2G_0M\delta_1(r,\theta))+a^2G_0M\cos(2\theta)\big]\\
&+2G_0Mr^2(r(1+\delta_9(r,\theta))-2G_0M\,\big[\delta_1(r,\theta)-2\delta_4(r,\theta)\\
&-\delta_4^2(r,\theta)+\delta_9(r,\theta)+\delta_1(r,\theta)\delta_9(r,\theta)\big]\sin^2\theta\Bigg]\Bigg\},
\end{aligned}
\tag{6.43}
$$

with $\delta_{2,3,6,8}(r,\theta) = 0$.

Next, we consider the spacetime from [EH21b; EH21a] given by the metric Eq. 6.13. This spacetime cannot be represented in Boyer-Lindquist form (i.e. with five non-vanishing metric components) as in [KRZ16], because it is non-circular, as we have confirmed by an explicit calculation. Here, we show that it can be written in BL coordinates if $g_{t\chi} \neq 0$ and $g_{\chi\phi} \neq 0$ and that it is thus contained in Eq. 6.41. We first write an ansatz for a coordinate transformation

$$du = dt + F^u_r\, dr + F^u_\chi\, d\chi, \tag{6.44}$$

$$d\phi = d\phi_{\mathrm{BL}} + F^\phi_r\, dr + F^\phi_\chi\, d\chi, \tag{6.45}$$

from the HP coordinates (u, r, χ, ϕ) to BL coordinates $(t, r, \chi, \phi_{\mathrm{BL}})$. We then require that $g_{r\chi} = 0 = g_{r\phi_{\mathrm{BL}}}$, i.e. $\delta_6(r,\chi) = 0$ (in addition to $\gamma(r,\chi) = 0$). These conditions can be solved by requiring that

$$F^u_r = \frac{r^2 + a^2}{r^2 + a^2 - 2r\, G_0 M(r,\chi)}, \quad F^\phi_r = \frac{a}{r^2 + a^2 - 2r\, G_0 M(r,\chi)}. \tag{6.46}$$

Because F^u_χ and F^ϕ_χ are unrestricted, they can be chosen such that $\partial_r F^u_\chi = \partial_\chi F^u_r$ and $\partial_r F^\phi_\chi = \partial_\chi F^\phi_r$. This means that the differential forms in Eq. 6.45 are exact. However, this already fails in the case where we additionally require $g_{t\chi} = 0$, see [EH21a, App. A.5]. In our case, we can write the explicit coordinate transformation as

$$\begin{aligned} dt &= du - \frac{r^2 + a^2}{r^2 + a^2 - 2G_0 M(r,\chi) r} dr - 2G_0 a \left(\int dr \frac{r M^{(0,1)}(r,\chi)}{r^2 + a^2 - 2G_0 M(r,\chi) r} \right) d\chi, \\ d\phi_{\mathrm{BL}} &= d\phi - \frac{a}{r^2 + a^2 - 2G_0 M(r,\chi) r} dr - 2G_0 a \left(\int dr \frac{r M^{(0,1)}(r,\chi)}{r^2 + a^2 - 2G_0 M(r,\chi) r} \right) d\chi \end{aligned} \tag{6.47}$$

which, for the case $M(r,\chi) = M = \text{const.}$, reduces to the standard transformation between ingoing Kerr and BL coordinates and results in $g_{t\chi} = 0$. In addition, the coordinates $(t, r, \chi, \phi_{\mathrm{BL}})$ form the standard coordinate system of asymptotically flat spacetime in Boyer-Lindquist form, obtained by taking the limit $\lim_{r\to\infty} M(r,\chi) = M = \text{const.}$ Applying the explicit coordinate transformation Eq. 6.47, the non-circular,

locality-based black-hole spacetime in [EH21a] can thus be written as

$$
\begin{aligned}
ds^2_{\text{reg, local}} = &-\left[1-\frac{2G_0M(r,\chi)r}{\Sigma(r,\chi)}\right]dt^2+\left[\frac{\Sigma(r,\chi)}{\overline{\Delta}(r,\chi)}\right]dr^2+\left[\frac{4G_0M(r,\chi)\,r\,a(\chi^2-1)}{\Sigma(r,\chi)}\right]dtd\phi_{\text{BL}}\\
&+\left[-\frac{\Sigma(r,\chi)}{\chi^2-1}-\mathcal{M}_2(r,\chi)^2+\mathcal{M}_1(r,\chi)^2\,\left(r^2+a^2\right)(\chi^2-1)\right.\\
&\left.+\frac{2G_0M(r,\chi)r}{\Sigma(r,\chi)}\mathcal{M}(r,\chi)^2\right]d\chi^2\\
&+\left[\left(r^2+a^2\right)(\chi^2-1)-\frac{2G_0M(r,\chi)r\,a^2\left(\chi^2-1\right)^2}{\Sigma(r,\chi)}\right]d\phi^2_{\text{BL}}\\
&+\left[\frac{4G_0M(r,\chi)\,r\mathcal{M}(r,\chi)}{\Sigma(r,\chi)}-2\mathcal{M}_2(r,\chi)\right]dtd\chi\\
&+\left[\frac{4G_0M(r,\chi)\,r\,a\,\mathcal{M}(r,\chi)(\chi^2-1)}{\Sigma(r,\chi)}-2(\chi^2-1)(r^2+a^2)\mathcal{M}_1(r,\chi)\right]d\chi d\phi_{\text{BL}}.
\end{aligned}
\tag{6.48}
$$

with

$$
\Sigma(r,\chi)=(r^2+a^2\chi^2)\,,\qquad \mathcal{M}(r,\chi)=\mathcal{M}_2(r,\chi)+\mathcal{M}_1(r,\chi)(\chi^2-1)\,a\,,
$$

$$
\overline{\Delta}(r,\chi)=(r^2-2\,G_0M(r,\chi)\,r+a^2)\,,\qquad \mathcal{M}_1(r,\chi)=\frac{d}{d\chi}\int dr\,\frac{a}{r^2-2\,G_0M(r,\chi)\,r+a^2}\,,
$$

$$
\mathcal{M}_2(r,\chi)=\frac{d}{d\chi}\int dr\,\frac{r^2+a^2}{r^2-2\,G_0M(r,\chi)\,r+a^2}.
\tag{6.49}
$$

This form of the metric exemplifies that, to avoid the generation of curvature singularities at the event horizon, deviations from the Kerr spacetime have to take a somewhat intricate form in BL coordinates, because delicate cancellations are necessary. In comparison, the metric in HP coordinates, cf. Eq. 6.13, takes a much simpler form, therefore also enabling faster and more efficient manipulations such as the calculation of curvature invariants.

6.4 Conclusion and outlook

We reviewed parameterisations of axisymmetric, stationary and asymptotically flat black-hole spacetimes that exist in the literature and pointed out that many of those, e.g. [Joh13a; KRZ16], are circular and may possess an additional hidden constant of motion. Circular spacetimes, due to the additional isometry that is implied by circularity, parameterise black-hole spacetimes with just four free metric functions that occur in five non-vanishing metric components.

Because those symmetry assumptions need not hold in non-vacuum GR and beyond GR, we generalised to a parameterisation of black-hole spacetimes beyond circularity. We first wrote the metric in the preferred set of horizon-penetrating coordinates with just six metric functions, which allows to write deviations from the Kerr metric without introducing spurious coordinate singularities at the horizon. We

derived the correspondence between the proposed non-circular parameterisations and the existing circular parameterisations.

We discovered that the locality-based black-hole spacetimes introduced in [EH21a], which lead to a combination of three image features, are not circular and motivated a potential correspondence between the specific deviations from circularity and the image features discovered in [EH21b; EH21a]. Additionally, we explored for the first time an alternative to a popular class of modifications: instead of promoting the mass parameter to a mass function to regularise the curvature singularity as in [Bar68b; Dym92; BR00; Hay06; SV19b], we tested whether the same could be achieved by promoting the spin parameter to a spin function. We found indications that it fails, highlighting the special role played by regular black holes based on a mass function.

Finally, we provided a more general, non-circular parameterisation in Boyer-Lindquist coordinates containing, in general, ten non-zero metric components.

Several questions for future work follow from our investigations.
A first open question is: what is the minimal, general parameterisation of axisymmetric, stationary and asymptotically flat BH spacetimes? It is at present unclear, whether the parameterisation in terms of ten (or, under additional assumptions, eight) deviation functions that we presented in BL coordinates, overparameterises the configuration space of these spacetimes. Similarly, it is also unclear whether the parameterisation in terms of six deviation functions in HP coordinates we proposed is general enough to capture all such spacetimes. We gave a general counting argument that corroborates its generality, but it did not take consider that a given set of coordinates may not cover the full spacetime, but just a patch of it. However, we used as guiding rationale the necessity to find a parameterisation which can account for the BH spacetimes in [EH21b; EH21a].

A second open question is: how do the two parameterisations of non-circular spacetimes we have provided relate to each other? We provided parameterisations in both HP and BL coordinates, because those coordinates have both pros and cons. Circularity is best imposed in BL coordinates, but those introduce spurious coordinate singularities at the horizon which, in general, results in differential constraints on metric components. Those complications are absent in HP coordinates, but it is not straightfoward to express circular spacetimes in them. However, it was not possible to provide a general coordinate transformation relating the two parameterisations without specifying the deviation functions. Thus, we do not know how the six deviation functions in HP coordinates transform into the ten (or eight) deviation functions in BL coordinates, except in special cases.

A third open question is: may non-circular spacetimes have hidden constants of motion based on higher-rank, i.e. $n > 2$, Killing tensors? The presence of a rank-two Killing tensor automatically implies circularity as well as the separability of the geodesic equation of a test particle and, hence, its analytical solvability. Nonetheless, this may be different for rank higher than two. While the absence of separability might be viewed as a drawback from a calculational point of view, it does not imply that non-circular spacetimes are not phenomenologically relevant. Their phenomenology may just be more challenging to characterise.

Finally, on a phenomenological level, we do not know whether the connection between deviations from circularity and the dent- and cusp-like image features as well as the image asymmetry (cf. Fig. 4.11) is more general than just for the family of

non-circular spacetimes in [EH21b; EH21a]. Some circular spacetimes in the literature do exhibit one of these features, e.g. [CHR17; WCJ17; KLM21], but we are not aware of a circular spacetime having all three features in combination. It is thus relevant to understand whether or not the combination of all three image features is a marker of specific deviations from circularity. Apart from the particular non-circular cases in [EH21b; EH21a], first steps in this direction have recently been made in circular spacetime metrics which respect post-Newtonian constraints from observations in the solar-system [Wil14].

In [MPO20; YPO23; Ayz22; HP23], the authors obtained images of the black-hole shadow and photon rings with current EHT capabilities. In [YPO23; Ayz22], they provided models to account for astrophysical uncertainties linked to parameters in the accretion disk, and placed constraints on parameters characterising circular deviations from Kerr, accounting for astrophysical uncertainties linked to parameters of the accretion disk.

In [CANY20; SB22; DBB23; AKN24; GC24; Kum+24b], constraints on deviation parameters were derived using gravitational wave data from the LIGO-Virgo-KAGRA collaboration on the inspiral and ringdown phases of black-hole mergers.

Going forward, both approaches may be useful. However, it has to be kept in mind that constraints obtained from binary-black-hole mergers only constrain the metrics of supermassive black holes observed by the EHT if one assumes that a black-hole uniqueness theorem holds. In theories beyond GR, this may not be the case, see e.g. [Eic+23], thus constraints from both types of observations are valuable.

Chapter 7

Final remarks

The classical theory of gravity, GR, along with the framework of quantum field theory, QFT, is a cornerstone of modern theoretical physics. GR remarkably describes all observed gravitational phenomena so far to an exquisite precision, across a wide range of length (and thus curvature) scales [BCA24]. It also postulates that the most compact spinning objects, namely BHs, are surprisingly simply characterised by two parameters in vacuum, their mass M and (reduced) spin a, see Chapter 2. While the agreement of GR with observations was previously obtained in the weak-field regime, i.e. on laboratory, solar-system and cosmological scales, the picture changed with the advent of tests in the strong-field regime, first with the detection of transient GW signals by the LIGO-Virgo collaboration in 2015 [Abb+16a], second with the first shadow images of M87* produced by the EHT collaboration in 2019 [Aki+19a] and third with the compelling evidence for a Stochastic Gravitational Wave Background (SGWB) with Pulsar Timing Arrays (PTAs) [Aga+23]. Together with the future planned missions – ET [Mag+20], CE [Eva+23], LISA [Col+24b], DECIGO [Kaw23] and the Square Kilometer Array (SKA) [Ren+22] for GWs and BHEX [Joh+24], ngEHT [Ayz+23] for EM signals – these new observational capabilities offer the unprecedented possibility to test GR on higher curvature scales and for strong gravitational fields.

One can thus raise the question that S. Chandrasekhar addressed to C. Will: *"why do you spend so much time and energy testing GR? We know that the theory is right"* [Ber+15]. There are two answers to that question: on the observational side, the short answer is *because we now can*; on the theoretical side, the short answer is *because we should*.

Theoretically, it is indeed not a question of *whether* GR breaks down, but a question of *where* and *how* it does so. We discussed the failures of GR in the strong-field regime – especially in black holes – in Subsec. 3.1.2; to cite a few of them, GR black holes are plagued by curvature singularities at their centre, unstable inner (Cauchy) horizons and future-incomplete geodesics. Evading those singularities requires to go *beyond GR* by considering classical modified gravity theories which violate one or more assumptions of the Lovelock theorem [Lov71; Lov72]. Those may introduce undesirable components, such as ghosts (leading to non-unitarity) or a fifth force, c.f. Sec. 3.2. We can go further beyond GR by including quantum matter fields on a curved classical background as in semiclassical gravity, see Sec. 3.3, but this fails to provide a consistent picture of the interplay of quantum matter fields and spacetime geometry on all scales. Furthermore, applying the usual QFT quantisation method to GR is inadequate, as GR turns out not to be perturbatively renormalisable [GS87; Sho07]. Hence, we might shift our paradigm and require gravity to be *quantum in nature* so as to resolve all (or, at least, some) classical singularities, see Sec. 3.5. In particular, we may focus on QG theories that admit a QFT formulation and can make predictions that can be tested in the IR-regime, to connect with observations.

This is the case of the QG theory of asymptotic safety. In ASQG, UV-completion at transplanckian scales is achieved via non-perturbative renormalisability, in which quantum scale symmetry is realised at an interacting fixed point. Additionally, predictivity beyond the Planck scale is ensured by the presence of only a finite number of free couplings (or parameters) in the IR-regime whose values need to be fixed experimentally. The compelling evidence for an interacting UV fixed-point in gravity alone and in gravity with suitable matter content in 4D Euclidean signature [Per17a; Eic19; RS19b; Bon+20; ES22; Sau23; PR23] marks a significant step in the quest of consistent, UV-finite and predictive fundamental theories of quantum gravity.

Black holes lie at the core of testing GR in the strong-field regime, for multiple reasons that we exposit in the following.
Firstly, they are the most compact astrophysical objects in our Universe, meaning that they have the deepest gravitational potential wells. Secondly, GR postulates their existence, and in simple terms: spinning black holes are solely defined by their event horizon – the boundary of no-return – and their mass and spin. This apparent simplicity thus offers an ideal playground to test the validity of Birkhoff's uniqueness theorem [BL23] and the no-hair theorem [MTW73] up to near-horizon scales. Thirdly, they appear in different settings and we now have the ability to probe many of their facets: isolated and in their stationary regime as probed by the EHT or in binaries and in their dynamical regime as probed by LIGO-Virgo-KAGRA; through EM signals such as radio, X-rays and GRBs or through GW signals emitted during the inspiral, merger and ringdown phases of coalescing binaries; in the stellar-mass range with LIGO-Virgo-KAGRA or in the supermassive range with the EHT and PTAs.

When viewing black holes through the prism of beyond-GR theories, and especially QG theories like ASQG, both theoretical and observational challenges emerge.
On the theoretical side, we need to:

T1. find a consistent, UV-finite and predictive (quantum) gravity theory, c.f. Sec. 3.5 and Subsec. 3.5.1;

T2. make sure this theory contains viable BH solutions that accurately describe astrophysical BHs, see Chapters 5 and 6;

T3. adopt both top-down and bottom-up approaches and bridge the gap between them, due to the difficulty of finding BH solutions beyond GR, see Chapters 4 to 6.

On the observational side, we aim to:

O1. find manifest characteristic imprints, e.g. in shadow images, see Chapter 4, and symmetries of BHs in beyond-GR theories and approaches, c.f. Chapter 6;

O2. lift the degeneracies among beyond-GR parameters and features, see Chapter 4;

O3. increase both the resolution, sensitivity and noise mitigation of observational capabilities, c.f. Chapter 4;

O4. enhance synergies between different probes of the strong-gravity regime, namely GWs and EM signals, e.g. thanks to the future mission LISA (see Subsec. 4.4.2).

In this thesis, we embarked on a journey which combined theoretical and phenomenological approaches to gain deeper insights into BH spacetimes beyond GR. While the approaches we followed all assumed the existence of some new physics inspired

from or within QG theories, the nature of the latter could as well be classical.

We started this thesis by reviewing the properties and singularities of GR vacuum and non-vacuum BH solutions in Chapter 2.

In Chapter 3, we motivated the need to go *beyond GR*, from classical modified theories of gravity to QG theories by way of semiclassical gravity. We especially focused on ASQG, a QFT-based QG theory which postulates a new quantum scale symmetry ensuring both the non-perturbative renormalisability and predictivity of the theory. We then sketched three ways of approaching BHs beyond GR, from the *fundamental (top-down) approach* – to which ASQG belong – to the *parameterised approach (bottom-up)* by way of the *principled-parameterised approach*. Finally, we provided an overview of alternative objects to black holes, namely ECOs.

In Chapter 4, we recalled the notion of gravitational lensing near compact objects and discussed its role in BH imaging. Next, we outlined how the images of the supermassive BHs M87* and SgrA* were derived by the EHT thanks to VLBI. We introduced the notions of *shadow* and *photon rings* which play a key role in characterising the spacetime geometry and, thus, the nature of the imaged compact object. Based on the observation that spacetimes beyond GR exhibit peculiar imprints in their shadow boundary and photon rings, in particular an increased separation between consecutive photon rings, we assessed whether two thin, radially-symmetric photon rings in synthetic images could be told apart with current and future VLBI arrays. Using data from both visibility and closure amplitudes, we drew the following conclusions: (i) the EHT 2022 array cannot make the difference between one or two thin rings, unless (ii) super-resolution techniques are used on top of it; a ngEHT array can tell the rings apart, provided that (iii) the sensitivity of the whole array is largely increased and observations at 230 and 345 GHz are combined or (iv) a space-based station is added to it on a well-chosen orbit. Despite the limitations of our study – among others, the use of simple geometric ring models, the thin-ring assumption and the exclusion of foreground emission – we made one step forward in the aforementioned key directions **O1**, **O2** and **O3** on the observational side.

In Chapter 5, we made progress towards more astrophysical BHs beyond GR by exploring their dynamical formation, in line with the theoretical research objectives **T2** and **T3**. We first reviewed the VKP model, a particularly simple model of the classical Vaidya spacetime describing the formation of a spherically symmetric BH via linear accretion of shells of null dust. We highlighted the issues associated with such a simple model, that is the formation of curvature and naked singularities in combination with future-incomplete null geodesics. To regularise these classical singularities we performed two upgrades of the VKP model: one following the RG-improvement method, in which we promoted the Newton coupling constant in the metric to the running coupling derived in ASQG and identified the RG scale with the first classical curvature invariant; the other by following the principled-parameterised approach and upgrading the Misner-Sharp mass to a mass function depending on the spacetime coordinates through the first classical curvature invariant and a new-physics scale. The two upgrades were found to be equivalent upon a specific choice on the class of mass functions in the principled-parameterised approach. While the upgraded spacetimes were free of singularities by construction, we showed that radial null geodesics were all future-complete but not past-complete. Additionally, we found that modifications beyond GR translated into a repulsive gravitational force repelling null geodesics from the core which balanced out the standard attractive gravitational force at the external boundary of the region violating the NEC, yielding

a marginally stable attractor. We emphasised that this attractor could trigger mass-inflation instabilities within a horizon. Finally, we found that there were values of the new-physics scale for which the upgraded spacetimes were horizonless, thus not shielding beyond-GR modifications to asymptotic observers.

In Chapter 6, we adopted a more general – hence theory-agnostic – approach to BHs beyond GR to more comprehensively capture all possible BH spacetime geometries. It aimed to complement the more simple spherically symmetric upgrade carried out in Chapter 5 through RG improvement and the principled-parameterised approach, and thus fit within the research objectives **O1**, **T2** and **T3**. We first reviewed existing parameterisations and pointed out that they made unnecessary assumptions about two spacetime symmetries, namely circularity and an additional hidden constant of motion. Next, we determined whether promoting classical mass or spin hair to "quantum" hair – which naturally appear in QG theories – was sufficient to regularise classical singularities, and found that regularisation only occurred for a "quantum" mass hair. Since some non-vacuum GR and beyond-GR spacetimes do not satisfy circularity and hidden constant of motion, we put forward a more general, non-circular parameterisation in two sets of coordinates. We exemplified that connecting one to the other was difficult, because circular (non-circular) parameterisations favour one (the other) set of coordinates, respectively. Although this new, non-circular parameterisation accounts for significantly more general spacetime metrics with fewer symmetries, it is unknown whether it is minimal, and whether there is a clear link between the absence of circularity and the presence of the three image features presented in Subsec. 4.2.1.

We conclude this thesis by underlining how bright the future looks for finding and characterising compact objects beyond GR, and how promising the synergies between distinct QG and modified gravity theories are for constructing a consistent, UV-finite and predictive fundamental theory of gravity.

On the observational side, numerous missions are designed and planned in the coming years to better test GR in the strong-field regime with compact objects. The number of detections of GWs from stellar-mass coalescing binaries will be enhanced by a factor of nearly thousand with the third generation of ground-based laser interferometers [Cha+24a], namely advanced LIGO-Virgo-KAGRA [Abb+16b], ET [Mag+20] and CE [Eva+23], thanks to a ten-fold increase in sensitivity and a substantial improvement in noise mitigation. Equipped with such a network of ground-based GW detectors, we will be capable of detecting almost all binary BH mergers and half of binary NS mergers in the current observable Universe [BS22]. Simultaneously, LISA, a space-based laser interferometer will be launched in the mid-2030s [Col+24b] and will allow us, among others, to probe the dynamical regime of supermassive BH binaries [Bar+20] and, thus, compare with the EHT results. Regarding EM probes of dark compact objects, several proposals have been put forward to upgrade the current EHT array into an ngEHT array (most probably in two phases) with new sites, an increase in sensitivity for some of the existing sites and a combination of multiple observation frequencies [Joh+23; Ayz+23; Doe+23]. Furthermore, there are current incentives to place one or several VLBI antennas into space and combine them with the current EHT or an ngEHT array [Roe+19; Pes+19; Pal+19; Haw+19; FSA20; Gur+21; Shl+24; Joh+24]. Upon overcoming the underlined technical challenges, the boost in angular resolution with BHEX mission will enable us to probe down to the first photon ring of M87* and SgrA* [Lup+24; Gal+24], and sharpen our understanding of accretion physics [Kaw+24].

On the theoretical side, synergies are growing among different QG theories

[Boe+22]. This is best exemplified with the *Swampland program* [Vaf05; OV07], reviewed in [BCV17; Pal19; Bee+22; GnH21; Agm+22], whose goal is to identify and discard the consistent-looking EFTs that do not admit a UV-completion with the addition of gravity, i.e. those that can not be obtained from a quantum theory of gravity. The latter theories belong to the so-called "Swampland", while those that do admit such a UV-completion in QG are said to be part of the "Landscape". To identify the non-healthy theories, the Swampland program puts forward a set of criteria or conjectures motivated by ST and more basic physics such as unitarity, black-hole physics etc., such as the "no-global symmetries conjecture". However, there are different definitions of what the Swampland is, depending on the QG theory one is especially interested in. Those Swamplands may or may not, partially or fully overlap, see [Eic+24] for a discussion of Swamplands from the point of view of ASQG. Finding and comparing Swamplands within different QG theories can help to understand to what extent Swampland conjectures hold for any QG, or only for some sharing a similar UV framework.
Besides that, more and more progress is made on finding analytical BH-like solutions (or models) within (or inspired by) QG theories (see [Per17b] for LQG, [EH22; Pla23] for ASQG, [Ben+22] for ST) and in modified gravity theories (see [KK23], [BA+20] in DHOST theories, [Pod+20] for quadratic gravity and [Tor23] for regular rotating black holes), and determining whether theory-agnostic BH spacetimes could be solutions of some QG-motivated actions [KP22]. Thanks to the advances in numerical relativity, numerical rotating black hole solutions can also be obtained, see e.g. [SYS21; FM23; Gar+23; Gra24], and complement our understanding of the analytical derivations, which are often limited to spherical symmetry.

In closing, although falsifying QG theories and modified gravity theories through BH phenomenology remains a tremendously difficult task, studying – possibly quantum – modified gravitational effects and understanding their implications on observations can provide us with observational signatures of those theories. Equipped with such observational signatures, we might put constraints on the set of allowed theories and discriminate among them.

Appendix A

Disentangling photon rings with future radio telescope arrays

A.1 Gaussian profile

In order to check that, in the thin-ring regime, the type of flux density profiles has no impact on the detectability of a second ring (see Fig. A.1), we use another profile. This profile is Gaussian and based on the auxiliary function

$$\nu(r;d,\omega) = \frac{1}{N} e^{-(d-2r)^2/2\omega^2}, \tag{A.1}$$

normalised such that

$$\int_0^\infty dr\, 2\pi r \int_0^{2\pi} d\theta\, \nu(r;d,\omega) = 1, \tag{A.2}$$

which leads to the normalisation factor

$$N = \frac{\pi}{4}\left\{\sqrt{2\pi} d\omega \left[\mathrm{erf}\left(d/\sqrt{2}\omega\right)+1\right] + 2\omega^2 e^{-d^2/2\omega^2}\right\}, \tag{A.3}$$

where $\mathrm{erf}(x)$ is the error function.

The resulting total Gaussian flux density profile combines two Gaussian rings and is thus given by

$$F_{\mathrm{Gaussian}}(r) = \frac{F_{\mathrm{tot}}}{1+\Delta F}\nu(r;d_1,\omega_1) + \frac{F_{\mathrm{tot}}}{1+1/\Delta F}\nu(r;d_1-2s,\omega_2).$$

The total flux density is F_{tot}, and the total flux densities for the two rings correspond to the prefactors in Eq. (A.4), i.e.

$$F_1 = \frac{F_{\mathrm{tot}}}{1+\Delta F}, \quad F_2 = \frac{F_{\mathrm{tot}}}{1+1/\Delta F}. \tag{A.4}$$

A.2 Comparison of two profiles in a quantitative test of detectability

We still focus on synthetic data in the limit of relatively thin rings and use the same flat fitting profile as in Subsec. 4.3.1. However, we construct synthetic data with two different profiles, namely the crescent profile Eq. 4.16, and the Gaussian profile App. A.1, with or without a loose constraint on the width of the outer ring $\omega_1 \leq 10.5\,\mu$as in the fits, and for $\omega_1 = 2\,\mu$as (thin) or $\omega_1 = 8\,\mu$as (relatively thin). The detectability test for the 2022 EHT array at 230 GHz as a function of the separation is shown in Fig. A.1. As curves for the Gaussian and crescent profiles are superposed

for equal values of the parameters, we deduce that the type of profile does not matter within the thin ring assumption. Note that this assumption remains valid for a relatively thin outer ring, i.e. when $\omega_1 = 8\,\mu$as.

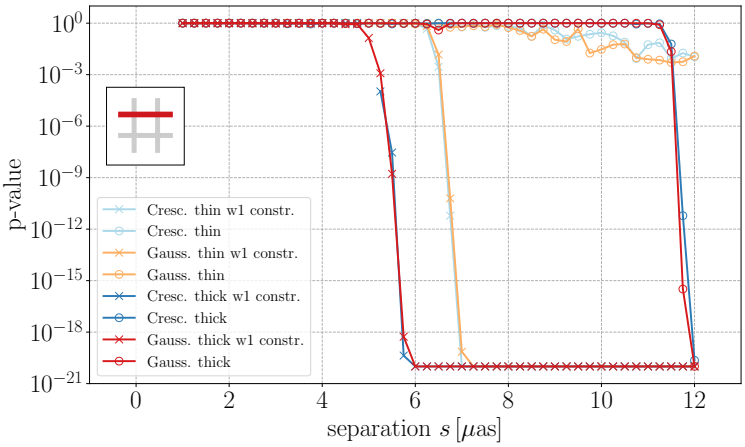

FIGURE A.1: We show the 2-ring detectability (according to the p-value test, cf. Subsec. 4.3.3) projected onto the ray $\Delta F = 0.5$, cf. Fig. 4.13, for the EHT 2022 array at 230 GHz. We vary the profile (either crescent or Gaussian), the width of the outer ring (either $\omega_1 = 2\,\mu$as or $8\,\mu$as) and the constraint on the width of the outer ring in the fits (either none or $\omega_1 \leq 10.5\,\mu$as). The remaining 2-ring parameter is chosen as $\omega_2 = 1\,\mu$as.

A.3 Array specifications

We provide details (see Tables A.1 to A.4) on the stations in the VLBI arrays considered in this work and summarised in Tab. 4.1.

Facility	Location	X[a](m)	Y[a](m)	Z[a](m)	SEFD[b] at 230 GHz (Jy)	SEFD[c] at 345 GHz (Jy)
ALMA	Chile	2225061.164	-5440057.37	-2481681.15	74	250
APEX	Chile	2225039.53	-5441197.63	-2479303.36	4700	8880
GLT	Greenland	541547.0	-1387978.6	6180982.0	5000	14390
JCMT	Hawaii, USA	-5464584.68	-2493001.17	2150653.98	10500	5780
KPNO	Arizona, US	-1995954.4	-5037389.4	3357044.3	13000	44970
LMT	Mexico	-768713.9637	-5988541.7982	2063275.9472	4500	2040
NOEMA	France	4524000.4	468042.1	4460309.8	700	1410
PV 30 m	Spain	5088967.9000	-301681.6000	3825015.8000	1900	3850
SMA	Hawaii, USA	-5464523.400	-2493147.080	2150611.750	6200	5730
SMT	Arizona, USA	-1828796.200	-5054406.800	3427865.200	17100	17190
SPT	Antarctica	0.01	0.01	-6359609.7	19300	25440

[a] Geocentric coordinates with X pointing to the Greenwich meridian, Y pointing 90° away in the equatorial plane (eastern longitudes have positive Y), and positive Z pointing in the direction of the North Pole.
[b] SEFD values at 230 GHz from [Aki+19b]
[c] SEFD values at 345 GHz from [Bro]

TABLE A.1: Array specifications for EHT 2022 at 230 and 345 GHz

Facility	Location	X[a](m)	Y[a](m)	Z[a](m)	SEFD[b] at 230 GHz (Jy)	SEFD[c] at 345 GHz (Jy)
ALMA	Chile	2225061.164	-5440057.37	-2481681.15	74	250
APEX	Chile	2225039.53	-5441197.63	-2479303.36	4700	8880
BAJA	Baja California, Mexico	-2352576.0	-4940331.0	3271508.0	74	250
CNI	La Palma, Canary Islands, Spain	5311000.0	-1725000.0	3075000.0	74	250
GAM	Gamsberg, Namibia	5627890.0	1637767.0	-2512493.0	74	250
GLT	Greenland	541647.0	-1388536.0	6180829.0	5000	14390
HAY	Masachussetts, USA	1521000.0	-4417000.0	4327000.0	74	250
JCMT	Hawaii, USA	-5464584.68	-2493001.17	2150653.98	10500	5780
KP 12 m	Arizona, USA	-1994314.0	-5037909.0	3357619.0	13000	44970
KVN-YS	Korea	-3042280.9137	4045902.7164	3867374.3544	74	250
LAS	Chile	1818163.826	-5280331.162	-3074870.820	74	250
LLAMA	Argentina	2325327.209	-5341469.111	-2599682.209	74	250
LMT	Mexico	-768713.9637	-5988541.7982	2063275.9472	4500	2040
NOEMA	France	4523998.40	468045.240	4460309.760	700	1410
OVRO	California, USA	-2409598.0	-4478348.0	3838607.0	74	250
PV 30 m	Spain	5088967.9000	-301681.6000	3825015.8000	1900	3850
SMA	Hawaii, USA	-5464523.400	-2493147.080	2150611.750	6200	5730
SMT	Arizona, USA	-1828796.200	-5054406.800	3427865.200	17100	17190
SPT	Antarctica	0.01	0.01	-6359609.7	19300	25440

[a] Geocentric coordinates with X pointing to the Greenwich meridian, Y pointing 90° away in the equatorial plane (eastern longitudes have positive Y), and positive Z pointing in the direction of the North Pole.
[b] SEFD values at 230 GHz from [Aki+19b] for EHT 2022 sites, and taken as ALMA's (lowest) SEFD value for ngEHT planned and phase-1 sites from [Joh+23]
[c] SEFD values at 345 GHz from [Bro] for EHT 2022 sites, and taken as ALMA's (lowest) SEFD value for ngEHT planned and phase-1 sites from [Joh+23]

TABLE A.2: Array specifications for ngEHT-low (low SEFD values) at 230 and 345 GHz.

Facility	Location	X[a](m)	Y[a](m)	Z[a](m)	SEFD[b] at 230 GHz (Jy)	SEFD[b] at 345 GHz (Jy)
ALMA	Chile	2225061.164	-5440057.37	-2481681.15	74	250
APEX	Chile	2225039.53	-5441197.63	-2479303.36	4700	8880
BAJA	Baja California, Mexico	-2352576.0	-4940331.0	3271508.0	19300	44970
CNI	La Palma, Canary Islands, Spain	5311000.0	-1725000.0	3075000.0	19300	44970
GAM	Gamsberg, Namibia	5627890.0	1637767.0	-2512493.0	19300	44970
GLT	Greenland	541647.0	-1388536.0	6180829.0	5000	14390
HAY	Masachussetts, USA	1521000.0	-4417000.0	4327000.0	19300	44970
JCMT	Hawaii, USA	-5464584.68	-2493001.17	2150653.98	10500	5780
KP 12 m	Arizona, USA	-1994314.0	-5037909.0	3357619.0	13000	44970
KVN-YS	Korea	-3042280.9137	4045902.7164	3867374.3544	19300	44970
LAS	Chile	1818163.826	-5280331.162	-3074870.820	19300	44970
LLAMA	Argentina	2325327.209	-5341469.111	-2599682.209	19300	44970
LMT	Mexico	-768713.9637	-5988541.7982	2063275.9472	4500	2040
NOEMA	France	4523998.40	468045.240	4460309.760	700	1410
OVRO	California, USA	-2409598.0	-4478348.0	3838607.0	19300	44970
PV 30 m	Spain	5088967.9000	-301681.6000	3825015.8000	1900	3850
SMA	Hawaii, USA	-5464523.400	-2493147.080	2150611.750	6200	5730
SMT	Arizona, USA	-1828796.200	-5054406.800	3427865.200	17100	17190
SPT	Antarctica	0.01	0.01	-6359609.7	19300	25440

[a] Geocentric coordinates with X pointing to the Greenwich meridian, Y pointing 90° away in the equatorial plane (eastern longitudes have positive Y), and positive Z pointing in the direction of the North Pole.
[b] SEFD values at 230 GHz from [Aki+19b] for EHT 2022 sites, and taken as SPT's (highest) SEFD value for ngEHT planned and phase-1 sites from [Joh+23]
[c] SEFD values at 345 GHz from [Bro] for EHT 2022 sites, and taken as KP's (highest) SEFD value for ngEHT planned and phase-1 sites from [Joh+23]

TABLE A.3: Array specifications for ngEHT-high (high SEFD values) at 230 and 345 GHz.

Facility	Location	X[a](m)	Y[a](m)	Z[a](m)	SEFD[b] at 230 GHz (Jy)	SEFD[b] at 345 GHz (Jy)
ALMA	Chile	2225061.164	-5440057.37	-2481681.15	74	250
APEX	Chile	2225039.53	-5441197.63	-2479303.36	4700	8880
BAJA	Baja California, Mexico	-2352576.0	-4940331.0	3271508.0	74	250
CNI	La Palma, Canary Islands, Spain	5311000.0	-1725000.0	3075000.0	74	250
GAM	Gamsberg, Namibia	5627890.0	1637767.0	-2512493.0	74	250
GLT	Greenland	541647.0	-1388536.0	6180829.0	5000	14390
HAY	Masachussetts, USA	1521000.0	-4417000.0	4327000.0	74	250
JCMT	Hawaii, USA	-5464584.68	-2493001.17	2150653.98	10500	5780
KP 12 m	Arizona, USA	-1994314.0	-5037909.0	3357619.0	13000	44970
KVN-YS	Korea	-3042280.9137	4045902.7164	3867374.3544	74	250
LAS	Chile	1818163.826	-5280331.162	-3074870.820	74	250
LLAMA	Argentina	2325327.209	-5341469.111	-2599682.209	74	250
LMT	Mexico	-768713.9637	-5988541.7982	2063275.9472	4500	2040
NOEMA	France	4523998.40	468045.240	4460309.760	700	1410
OVRO	California, USA	-2409598.0	-4478348.0	3838607.0	74	250
PV 30 m	Spain	5088967.9000	-301681.6000	3825015.8000	1900	3850
SMA	Hawaii, USA	-5464523.400	-2493147.080	2150611.750	6200	5730
SMT	Arizona, USA	-1828796.200	-5054406.800	3427865.200	17100	17190
SPT	Antarctica	0.01	0.01	-6359609.7	19300	25440
space-based[d]	Above Odense (Denmark) at 35786 km	23560747.282	4319365.430	34681814.518	36600	56000

[a] Geocentric coordinates with *X* pointing to the Greenwich meridian, *Y* pointing 90° away in the equatorial plane (eastern longitudes have positive Y), and positive *Z* pointing in the direction of the North Pole.
[b] SEFD values at 230 GHz from [Aki+19b] for EHT 2022 sites, and taken as ALMA's (lowest) SEFD value for ngEHT planned and phase-1 sites from [Joh+23]
[c] SEFD values at 345 GHz from [Bro] for EHT 2022 sites, and taken as ALMA's (lowest) SEFD value for ngEHT planned and phase-1 sites from [Joh+23]
[d] SEFD values for the space-based telescope at 230 and 345 GHz estimated from Tab. 1 in [Roe+19]

TABLE A.4: Array specifications for ngEHT-space (low SEFD values) at 230 and 345 GHz.

Appendix B

The principled-parameterised approach to gravitational collapse

B.1 Algebraically complete basis of non-derivative curvature invariants

The algebraically complete basis of non-derivative curvature invariants for arbitrary spacetimes is given by the 17 Zakhary-McIntosh (ZM) invariants [CM91; ZM97; CZ]. Those are constructed from the Weyl tensor $C_{\mu\nu\rho\sigma}$, its dual $\bar{C}_{\mu\nu\rho\sigma} = \frac{1}{2}\epsilon_{\mu\nu\alpha\beta}C^{\alpha\beta}{}_{\rho\sigma}$ with $\epsilon_{\mu\nu\alpha\beta}$ the totally antisymmetric Levi-Civita tensor, and the Ricci tensor $R_{\mu\nu}$. They form four real Weyl-invariants (solely built from the Weyl tensor) I_{1-4}, four Ricci-invariants I_{5-8} and nine real mixed Ricci-Weyl invariants I_{9-17}.

$$I_1 = C_{\mu\nu\rho\sigma}C^{\mu\nu\rho\sigma} \tag{B.1}$$

$$I_2 = C_{\mu\nu\rho\sigma}\overline{C}^{\mu\nu\rho\sigma} \tag{B.2}$$

$$I_3 = C_{\mu\nu}{}^{\rho\sigma}C_{\rho\sigma}{}^{\alpha\beta}C_{\alpha\beta}{}^{\mu\nu} \tag{B.3}$$

$$I_4 = \overline{C}_{\mu\nu}{}^{\rho\sigma}C_{\rho\sigma}{}^{\alpha\beta}C_{\alpha\beta}{}^{\mu\nu} \tag{B.4}$$

$$I_5 = R \tag{B.5}$$

$$I_6 = R_\mu{}^\nu R_\nu{}^\mu \tag{B.6}$$

$$I_7 = R_\mu{}^\nu R_\nu{}^\rho R_\rho{}^\mu \tag{B.7}$$

$$I_8 = R_\mu{}^\nu R_\nu{}^\rho R_\rho{}^\sigma R_\sigma{}^\mu \tag{B.8}$$

$$I_9 = R^{\mu\nu}R^{\rho\sigma}C_{\mu\rho\nu\sigma} \tag{B.9}$$

$$I_{10} = R^{\mu\nu}R^{\rho\sigma}\overline{C}_{\mu\rho\nu\sigma} \tag{B.10}$$

$$I_{11} = R^{\nu\rho}R_{\gamma\delta}\left(C_{\mu\nu\rho\sigma}C^{\mu\gamma\delta\sigma} - \overline{C}_{\mu\nu\rho\sigma}\overline{C}^{\mu\gamma\delta\sigma}\right) \tag{B.11}$$

$$I_{12} = 2R^{\nu\rho}R_{\gamma\delta}C_{\mu\nu\rho\sigma}\overline{C}^{\mu\gamma\delta\sigma} \tag{B.12}$$

$$I_{13} = R_\mu{}^\gamma R_\gamma{}^\rho R_\nu{}^\delta R_\delta{}^\sigma C^{\mu\nu}{}_{\rho\sigma} \tag{B.13}$$

$$I_{14} = R_\mu{}^\gamma R_\gamma{}^\rho R_\nu{}^\delta R_\delta{}^\sigma \overline{C}^{\mu\nu}{}_{\rho\sigma} \tag{B.14}$$

$$I_{15} = \frac{1}{16}R^{\nu\rho}R_{\gamma\delta}\left(C_{\mu\nu\rho\sigma}C^{\mu\gamma\delta\sigma} + \overline{C}_{\mu\nu\rho\sigma}\overline{C}^{\mu\gamma\delta\sigma}\right) \tag{B.15}$$

$$I_{16} = \frac{1}{32}R^{\rho\sigma}R^{\gamma\delta}C^{\mu\kappa\lambda\nu}\left(C_{\mu\rho\sigma\nu}C_{\kappa\gamma\delta\lambda} + \overline{C}_{\mu\rho\sigma\nu}\overline{C}_{\kappa\gamma\delta\lambda}\right) \tag{B.16}$$

$$I_{17} = \frac{1}{32}R^{\rho\sigma}R^{\gamma\delta}\overline{C}^{\mu\kappa\lambda\nu}\left(C_{\mu\rho\sigma\nu}C_{\kappa\gamma\delta\lambda} + \overline{C}_{\mu\rho\sigma\nu}\overline{C}_{\kappa\gamma\delta\lambda}\right). \tag{B.17}$$

B.2 Kerr algebraically complete basis of non-derivative curvature invariants

In the case of the Kerr spacetime, only the pure Weyl invariants I_{1-4} do not vanish, namely

$$I_1 = \frac{48M^2}{(r^2+a^2\chi^2)^6}\left(r^6 - 15r^4a^2\chi^2 + 15r^2a^4\chi^4 - a^6\chi^6\right) \tag{B.18}$$

$$I_2 = -\frac{96M^2}{(r^2+a^2\chi^2)^6}\left(3r^4 - 10r^2a^2\chi^2 + 3a^4\chi^4\right) \tag{B.19}$$

$$I_3 = \frac{96M^3}{(r^2+a^2\chi^2)^9}\left(r^9 - 36r^7a^2\chi^2 + 126r^5a^4\chi^4\right) \tag{B.20}$$

$$I_4 = -\frac{96M^3}{(r^2+a^2\chi^2)^9}\left(9r^8a\chi - 84r^6a^3\chi^3 + 126r^4a^5\chi^5 - 36r^2a^7\chi^7 + a^9\chi^9\right). \tag{B.21}$$

In fact, not all those four invariants are independent, because they obey the following polynomial relations called *syzygies*

$$I_1(I_1^2 - 3I_2^2) = 12(I_3^2 - I_4^2), \tag{B.22}$$

$$I_2(3I_1^2 - I_2^2) = 24I_3I_4, \tag{B.23}$$

which lower the number of independent, non-derivative curvature invariants to two. The two independent invariants can be chosen to be I_1 and I_2.

B.3 Algebraically complete basis of non-derivative curvature invariants in a generalised Vaidya spacetime

The 17 ZM polynomial curvature invariants of a generalised Vaidya spacetime in Eq. 5.23, containing a generalised mass function $M(v,r)$ with dependencies on both

advanced time and radial coordinates, correspond to

$$I_1 = \frac{4G_0^2}{3r^6}\left(6M(v,r) + r\left(-4M^{(0,1)}(v,r) + rM^{(0,2)}(v,r)\right)\right)^2, \tag{B.24}$$

$$I_2 = 0, \tag{B.25}$$

$$I_3 = \frac{4G_0^3}{9r^9}\left(6M(v,r) + r\left(-4M^{(0,1)}(v,r) + rM^{(0,2)}(v,r)\right)\right)^3 = \frac{1}{2\sqrt{3}}I_1^{3/2}, \tag{B.26}$$

$$I_4 = 0, \tag{B.27}$$

$$I_5 = G_0 \cdot \frac{4M^{(0,1)}(v,r) + 2r\,M^{(0,2)}(v,r)}{r^2}, \tag{B.28}$$

$$I_6 = G_0^2 \cdot \frac{8\left(M^{(0,1)}(v,r)\right)^2 + 2r^2\left(M^{(0,2)}(v,r)\right)^2}{r^4}, \tag{B.29}$$

$$I_7 = G_0^3 \cdot \frac{16\left(M^{(0,1)}(v,r)\right)^3 + 2r^3\left(M^{(0,2)}(v,r)\right)^3}{r^6}, \tag{B.30}$$

$$I_8 = G_0^4 \cdot \frac{32\left(M^{(0,1)}(v,r)\right)^4 + 2r^2\left(M^{(0,2)}(v,r)\right)^4}{r^8}, \tag{B.31}$$

$$I_9 = \frac{2G_0^3}{3r^7}\left(-2M^{(0,1)}(v,r) + rM^{(0,2)}(v,r)\right)^2 \cdot \tag{B.32}$$

$$\left(6M(v,r) + r\left(-4M^{(0,1)}(v,r) + rM^{(0,2)}(v,r)\right)\right), \tag{B.33}$$

$$I_{10} = 0, \tag{B.34}$$

$$I_{11} = \frac{G_0^4}{3r^4}\left(-2M^{(0,1)}(v,r) + rM^{(0,2)}(v,r)\right)^2 I_1 = \frac{I_9\sqrt{I_1}}{\sqrt{3}}, \tag{B.35}$$

$$I_{12} = 0, \tag{B.36}$$

$$I_{13} = \frac{G_0^5}{\sqrt{3}r^8}\left(-4\left(M^{(0,1)}(v,r)\right)^2 + r^2\left(M^{(0,2)}(v,r)\right)^2\right)^2\sqrt{I_1}, \tag{B.37}$$

$$I_{14} = 0, \tag{B.38}$$

$$I_{15} = \frac{1}{16}I_{11}, \tag{B.39}$$

$$I_{16} = \frac{1}{8\sqrt{3}}I_{11}\sqrt{I_1}, \tag{B.40}$$

$$I_{17} = 0, \tag{B.41}$$

where $M^{(0,n)}(v,r) = \frac{\partial^n M(v,r)}{\partial r^n}$ and no partial derivatives with respect to the advanced time v appear.

B.4 Defining equation for the apparent horizon in a generalised Vaidya spacetime

Here we derive the defining equation for the location of the apparent horizon in a generalised Vaidya spacetime Eq. 5.23 in two different ways and discuss its solutions.

In a first approach, we use the fact that an apparent horizon is a marginally trapped surface to find its location. Hence, the apparent horizon is determined by

finding the null outgoing Θ_{out} and null ingoing Θ_{in} expansions such that

$$\Theta_{\text{out}} = 0, \quad \Theta_{\text{in}} < 0. \tag{B.42}$$

It has been shown in [Dah21][1] that the null expansions in a generalised Vaidya spacetime take the form

$$\Theta_{\text{out}} = \frac{1}{r}\left(1 - \frac{2G_0 M(v,r)}{r}\right), \quad \Theta_{\text{in}} = -\frac{2}{r}. \tag{B.43}$$

Hence, finding the location of the apparent horizon through the conditions in Eq. B.42 amounts to satisfy

$$1 - \frac{2G_0 M(v,r)}{r} = 0, \quad r > 0. \tag{B.44}$$

We subsequently show how to arrive to the same conclusion following another method based on a change of coordinates at the level of the metric.
We start from the result derived in [NV06; Far13], where the authors argue that any spherically symmetric line element can be written in Painlevé-Gullstrand (PG) coordinates in the form[2]

$$\begin{aligned} ds^2_{\text{PG}} =& g_{\text{tt,PG}}\, dt^2 + 2g_{\text{tr,PG}}\, dt\, dr + dr^2 + r^2 d\Omega^2 \\ =& -\left(c(r,t)^2 - v_1(r,t)^2\right) dt^2 + 2v_1(r,t)\, dt\, dr + dr^2 + r^2 d\Omega^2. \end{aligned} \tag{B.45}$$

The apparent horizon is found from the expansions of the in- and outgoing radial null geodesics. In the above form of the line element, it is simple to see where both expansions vanish. Radial null geodesics fulfil the condition

$$0 = -\left(c(r,t)^2 - v_1(r,t)^2\right) dt^2 + 2v_1(r,t)\, dt\, dr + dr^2, \tag{B.46}$$

leading to

$$\frac{dr}{dt} = -v_1(r,t) \pm c(r,t). \tag{B.47}$$

For $c(r,t) < v_1(r,t)$, outgoing null geodesics are no longer moving towards larger r, such that the apparent horizon is defined by the condition

$$c(r,t) = v_1(r,t). \tag{B.48}$$

In turn, this condition can be rewritten in the form [Far13]

$$g^{rr}_{\text{PG}} = 0. \tag{B.49}$$

We now show that if a coordinate transformation into ingoing EF coordinates exists[3], then this condition implies $g^{rr}_{\text{EF}} = 0$. Starting from PG coordinates, we make the transformation

$$t = h(v,r), \tag{B.50}$$

[1] We recover the expansions of a generalised Vaidya spacetime by taking the limit $a \to 0$ of the null expansions in Kerr-Vaidya.

[2] We use $v_1(r,t)$ instead of the notation $v(r,t)$ in [NV06] to avoid confusion with the coordinate v.

[3] [NV06] argues that any spherically symmetric metric can be written in the form Eq. B.45. Accordingly, starting from a spherically symmetric metric in EF coordinates, the transformation must in principle exist, even if in practice it may take a form that is difficult to solve explicitly.

with a function $h(v,r)$ that is to be determined. We arrive at

$$\begin{aligned} ds^2 &= g_{\mathrm{tt,PG}}\left(h^{(1,0)}(v,r)\right)^2 dv^2 + \left(g_{\mathrm{tt,PG}}h^{(0,1)}(v,r) + 2g_{\mathrm{tr,PG}}h^{(0,1)}(v,r) + 1\right) dr^2 \\ &\quad + \left(2g_{\mathrm{tt,PG}}h^{(1,0)}(v,r)h^{(0,1)}(v,r) + 2g_{\mathrm{tr,PG}}h^{(1,0)}(v,r)\right) dr\, dv + r^2\, d\Omega^2, \end{aligned} \tag{B.51}$$

where $h^{(1,0)}(v,r) \equiv \frac{\partial h(v,r)}{\partial v}$ and similarly $h^{(0,1)}(v,r) \equiv \frac{\partial h(v,r)}{\partial r}$. To correspond to the form Eq. 5.1, we require

$$2 = 2g_{\mathrm{tt,PG}}h^{(1,0)}(v,r)h^{(0,1)}(v,r) + 2g_{\mathrm{tr,PG}}h^{(1,0)}(v,r), \tag{B.52}$$

$$0 = g_{\mathrm{tt,PG}}h^{(0,1)}(v,r) + 2g_{\mathrm{tr,PG}}h^{(0,1)}(v,r) + 1, \tag{B.53}$$

which, in turns, leads to

$$\begin{aligned} h^{(1,0)}(v,r) &= \frac{\partial h(v,r)}{\partial v} = \frac{g_{\mathrm{tt,PG}} + 2g_{\mathrm{tr,PG}}}{g_{\mathrm{tt,PG}}\left(g_{\mathrm{tr,PG}} - 1\right) + 2g_{\mathrm{tr,PG}}^2}, \\ h^{(0,1)}(v,r) &= \frac{\partial h(v,r)}{\partial r} = \frac{-1}{g_{\mathrm{tt,PG}} + 2g_{\mathrm{tr,PG}}}. \end{aligned} \tag{B.54}$$

Assuming that the two conditions can be solved to provide an $h(v,r)$, we can relate g^{rr}_{PG} to g^{rr}_{EF} by

$$g^{\mathrm{rr}}_{\mathrm{EF}} = -g_{\mathrm{tt,EF}} = -g_{\mathrm{tt,PG}}\left(h^{(1,0)}(v,r)\right)^2 = g^{\mathrm{rr}}_{\mathrm{PG}}\left(g_{\mathrm{tt,PG}} - g_{\mathrm{tr,PG}}\right)\left(h^{(1,0)}(v,r)\right)^2. \tag{B.55}$$

Accordingly, $g^{\mathrm{rr}}_{\mathrm{PG}} = 0$ implies $g^{\mathrm{rr}}_{\mathrm{EF}} = 0$.

We now evaluate the condition $g^{\mathrm{rr}}_{\mathrm{EF}} = 0$ for the generalised Vaidya metric in Eq. 5.23 with upgraded mass Eq. 5.27:

$$\begin{aligned} g^{rr}_{\mathrm{EF}} &= g_{\mathrm{vv,EF}}, \\ &= 1 - \frac{2G_0}{r}M(v,r), \\ &= 1 - \frac{2G_0}{r}M(v)f_{\mathrm{NP}}\left(I_1 r_{\mathrm{NP}}^4\right). \end{aligned} \tag{B.56}$$

As we have discussed in Subsec. 5.5.1, $f_{\mathrm{NP}} \leq 1$ holds for all r. This implies that the apparent horizon lies at smaller radii, i.e. the black hole is more compact.

Further, the condition $g^{rr}_{\mathrm{EF}} = 0$ generically has two real solutions. The first is the shifted apparent horizon; the second is a new, inner apparent horizon, which occurs because $f_{\mathrm{NP}} \to 0$ for small r. If r_{NP} is large enough, the two horizons merge; for larger r_{NP}, the spacetime is horizonless, because the solutions to $g^{rr} = 0$ are all complex in this regime.

These results mirror similar results in the stationary limit with a constant ADM mass M. This is because in the stationary case, $g^{rr} = 0$ is the condition for the event horizon. Upon the identification $M = \mu\bar{v}$, the two equations become identical and thus the time-dependent case must agree with the stationary case for each fixed value $\bar{v}$.

B.5 Construction of a local curvature

Stationary and axisymmetric spacetimes like Kerr have a lower degree of symmetry than static, spherically symmetric spacetimes like Schwarzschild. As a result, they possess several independent, non-zero, non-derivative curvature invariants, see e.g. App. B.2 for Kerr. These independent curvature invariants can be of different signs, and can change sign themselves since they are no longer monotonic functions of the radial coordinate r, unlike in the Schwarzschild case.

Following an EFT point of view, we expect deviations from GR to show up at large values of the local curvature K. In order for the latter to be coordinate-invariant, it must depend on coordinates only through the N independent, non-derivative curvature invariants of the classical spacetime we start with. Note that there exist both non-derivative curvature invariants (solely built from the Riemann tensor) and derivative curvature invariants (built from the Riemann tensor and its covariant derivatives). While the number of algebraically independent invariants is finite (as the set of ZM invariants is finite), the number of algebraically independent derivative invariants increases with the number of covariant derivatives, thus being infinite. This is why we restrict the local curvature scale to the independent, non-derivative curvature invariants. Since arbitrary axisymmetric and stationary spacetimes can have several independent, non-zero such invariants, and that those can change sign, we may define the local curvature in two ways: (i) either as the maximum of the absolute values of all independent curvature invariants I_j at a given spacetime point, or (ii) as the RMS of all independent curvature invariants I_j.

Case (i), used in [EH21a; EH21b; DEH22], amounts to write

$$K = \max_j \left(|I_j| \right), \; j = 1, \dots, N. \tag{B.57}$$

For Kerr, the local curvature $K = \max\left(|I_1|, |I_2|, \frac{1}{2}|I_3|, \frac{1}{2}|I_4|\right)$ is well approximated by the envelope function $K = \sqrt{I_1^2 + I_2^2}$, as only the invariants I_1, I_2 are independent.

Case (ii), used in [DE24], corresponds to

$$K = \frac{1}{N} \sqrt{\sum_{j=1}^{N} |I_j|^{\alpha_j}}, \; j = 1, \dots, N, \; \alpha_j \in \mathbb{Q}. \tag{B.58}$$

Appendix C

Towards a general parameterisation of non-circular black-hole spacetimes

C.1 Kerr metric in Lewis-Papapetrou form

We explicitly show that Kerr spacetime can be written in Lewis-Papapetrou form with coordinates $(t, \tilde{r}, \theta, \phi)$, i.e. no transformation is applied to θ. In particular, we demand that, besides the three non-vanishing metric components g_{tt}, $g_{t\phi}$ and $g_{\phi\pi}$, the line element on the meridional surfaces takes the form $ds^2_{\text{mer}} = g_{\tilde{r}\tilde{r}}\left(d\tilde{r}^2 + \tilde{r}^2 d\theta^2\right)$, with just one free function $g_{\tilde{r}\tilde{r}}$. The coordinates $(t, \tilde{r}, \theta, \phi)$ differ from the BL coordinates by the condition that relates the metric components $g_{\tilde{r}\tilde{r}}$ and $g_{\theta\theta}$, namely

$$g_{\theta\theta} = \tilde{r}^2 g_{\tilde{r}\tilde{r}}. \tag{C.1}$$

We start from the Kerr spacetime in BL coordinates and allow for an unknown coordinate transformation $r(\tilde{r})$ of the radial BL coordinate r. Under the transformation $r \to \tilde{r}$, the condition in Eq. C.1 translates into a differential equation for $r(\tilde{r})$, i.e.

$$\left(\frac{dr(\tilde{r})}{d\tilde{r}}\right)^2 = \frac{\Delta(r(\tilde{r}))}{\tilde{r}^2}, \tag{C.2}$$

with $\Delta(r(\tilde{r})) = r(\tilde{r})^2 - 2G_0 M r(\tilde{r}) + a^2$. Eq. C.2 admits two solutions, but only the following one is physical

$$r(\tilde{r}) = \frac{e^{-c_1}}{2\tilde{r}}\left(G_0^2 M^2 - a^2 + 2\,e^{c_1} G_0 M\,\tilde{r} + e^{2\,c_1}\tilde{r}^2\right), \tag{C.3}$$

with c_1 a constant of integration. Picking $c_1 = 0$ for simplicity in Eq. C.3, there are two possible inverse coordinate transformations $\tilde{r}(r)$, but only the following is invertible outside the event horizon,

$$\tilde{r}(r) = r - G_0 M + \sqrt{r^2 - 2G_0 M r + a^2} \tag{C.4}$$

$$-a^2 dr^2 = \frac{a^2 - G_0^2 M^2 + \tilde{r}^2}{2\tilde{r}^2} d\tilde{r}^2, \tag{C.5}$$

and explicitly relates BL coordinates (t, r, θ, ϕ) to coordinates $(t, \tilde{r}, \theta, \phi)$. Hence, App. C.1 enables us to write the Kerr metric in Lewis-Papapetrou form as

$$\begin{aligned} ds^2 = &- dt^2 + \frac{4G_0 M\tilde{r}\left((G_0M+\tilde{r})^2 - a^2\right)}{\left(a^2 - (G_0M+\tilde{r})^2\right)^2 + 4a^2\tilde{r}^2\cos^2(\theta)}\left(dt - a\sin^2(\theta)d\phi\right)^2 \\ &+ \left(\frac{\left(a^2-(G_0M+\tilde{r})^2\right)^2}{4\tilde{r}^2} + a^2\right)\sin^2(\theta)d\phi^2 \\ &+ \frac{\left(\left(a^2-(G_0M+\tilde{r})^2\right)^2 + 4a^2\tilde{r}^2\cos^2(\theta)\right)}{4\tilde{r}^4}\left(d\tilde{r}^2 + \tilde{r}^2 d\theta^2\right). \end{aligned} \tag{C.6}$$

C.2 Equivalence of parameterisations with a hidden constant of motion

We explicitly derive the correspondence between the most general parameterisation of circular, stationary, axisymmetric and asymptotically flat spacetimes with a hidden constant of motion, namely Eq. 6.6, and the one given in [Joh13a, Eq. (10)]. The latter parameterisation reads in BL coordinates

$$\begin{aligned} g^{\mu\nu}\partial_\mu\partial_\nu = &- \frac{1}{\Delta\tilde{\Sigma}}\left[(r^2+a^2)A_1(r)\partial_t + aA_2(r)\partial_\phi\right]^2 + \frac{\Delta}{\tilde{\Sigma}}A_5(r)\left(\partial_r\right)^2 + \frac{1}{\tilde{\Sigma}}A_6(\theta)\left(\partial_\theta\right)^2 \\ &+ \frac{1}{\tilde{\Sigma}\sin(\theta)^2}\left[A_3(\theta)\partial_\phi + a\sin(\theta)^2 A_4(\theta)\partial_t\right]^2 \end{aligned} \tag{C.7}$$

where $f(r)$, $g(\theta)$, $A_i(r)$, $i = 1,2,5$ and $A_j(\theta)$, $j = 3,4,6$ are functions of the two non-Killing coordinates only, i.e. r and θ. $\Delta(r) = r^2 - 2G_0Mr + a^2$ and $\Sigma(r,\theta) = r^2 + a^2\cos(\theta)^2$ denote the common functions appearing also in the Kerr metric in Boyer-Lindquist coordinates (with M and a the asymptotic black hole mass and spin, respectively) and $\tilde{\Sigma}(r,\theta) = \Sigma(r,\theta) + f(r) + g(\theta)$.

Identifying x_i, x_j with the two Killing coordinates t, ϕ and $(x_1, x_2) = (r, \theta)$, the relations

$$S_r(r) + S_\theta(\theta) = \tilde{\Sigma}(r,\theta) = \Sigma(r,\theta) + f(r) + g(\theta), \tag{C.8}$$
$$\Delta_r(r) = \Delta(r)\, A_5(r), \tag{C.9}$$
$$\Delta_\theta(\theta) = A_6(\theta), \tag{C.10}$$
$$G_r^{tt}(r) = -\frac{(r^2+a^2)^2 A_1(r)^2}{\Delta(r)}, \tag{C.11}$$
$$G_r^{t\phi}(r) = -\frac{(r^2+a^2)a\, A_1(r)\, A_2(r)}{\Delta(r)}, \tag{C.12}$$
$$G_r^{\phi\phi}(r) = -\frac{a^2\, A_2(r)^2}{\Delta(r)}, \tag{C.13}$$
$$G_\theta^{tt}(\theta) = a^2\, \sin(\theta)^2\, A_4(\theta)^2, \tag{C.14}$$
$$G_\theta^{t\phi}(\theta) = a\, A_3(\theta)\, A_4(\theta), \tag{C.15}$$
$$G_\theta^{\phi\phi}(\theta) = \frac{A_3(\theta)^2}{\sin(\theta)^2}, \tag{C.16}$$

establish the full equivalence of the two parameterisations.

C.3 Static and axisymmetric solutions in GR: Weyl metrics

The complete class of circular, static and axisymmetric GR solutions of the (non-vacuum, i.e. sourced) Einstein field equations Eq. 2.1 were derived in 1917 by H. Weyl [Wey17a]. Metrics belonging to that class are written in a well-suited set of coordinates (t, r, z, ϕ) as ([Wal84, Sec. 7.1])

$$ds^2 = -e^{2U(r,z)}dt^2 + e^{-2U(r,z)}\left(e^{2\gamma(r,z)}\left(dr^2 + dz^2\right) + r^2 d\phi^2\right). \tag{C.17}$$

The symmetries of those metrics are manifestly given by the two Killing vectors $\xi^t = \partial_t$ and $\xi^\phi = \partial_\phi$. Because the dt^2 component of the metric is strictly negative, thus timelike, and there are no cross-terms between the time coordinate t and the spatial coordinates (r, z, ϕ), the metric is indeed static.

The potential $U(r, z)$ is an arbitrary, axisymmetric solution of the ordinary Laplace equation $\Delta U(r, z) = 0$ in an unphysical 3D flat spacetime with metric $ds^2 = dr^2 + r^2 d\phi^2 + dz^2$. The other potential $\gamma(r, z)$ satisfies the partial differential equations

$$\begin{aligned} \frac{\partial\gamma(r,z)}{\partial r} &= r\left[\left(\frac{\partial U(r,z)}{\partial r}\right)^2 - \left(\frac{\partial U(r,z)}{\partial z}\right)^2\right] \\ \frac{\partial\gamma(r,z)}{\partial z} &= 2r\frac{\partial U(r,z)}{\partial r}\frac{\partial U(r,z)}{\partial z}. \end{aligned} \tag{C.18}$$

Finding direct solutions for $U(r, z)$ and $\gamma(r, z)$ is especially difficult, although two solutions were found in [Zip66] (in vacuum) and in [Cha83] in different coordinates than r, z. Moreover, most of the metrics of the Weyl-form are unphysical in the sense that they are not asymptotically flat or have naked curvature singularities on their axis of symmetry (z-axis). Nonetheless, the metric Eq. C.17 contains the Schwarzschild metric as a subcase, when $U(r, z)$ is the potential of a finite-length rod located on the z-axis, centered at the origin and with constant mass per unit length.

Bibliography

[AAR21] Ellery Ames, Håkan Andréasson, and Oliver Rinne. "Dynamics of gravitational collapse in the axisymmetric Einstein–Vlasov system". In: *Class. Quant. Grav.* 38.10 (2021), p. 105003. DOI: 10.1088/1361-6382/abdd0c. arXiv: 2010.15771 [gr-qc].

[AB21] Abhay Ashtekar and Eugenio Bianchi. "A short review of loop quantum gravity". In: *Rept. Prog. Phys.* 84.4 (2021), p. 042001. DOI: 10.1088/1361-6633/abed91. arXiv: 2104.04394 [gr-qc].

[AB+23] R. Alves Batista et al. "White Paper and Roadmap for Quantum Gravity Phenomenology in the Multi-Messenger Era". In: (Dec. 2023). arXiv: 2312.00409 [gr-qc].

[AB24] Dimitry Ayzenberg and Cosimo Bambi. "Tests of General Relativity Using Black Hole X-ray Data". In: *Handbook of X-ray and Gamma-ray Astrophysics*. Ed. by Cosimo Bambi and Andrea Santangelo. Singapore: Springer Nature Singapore, 2024, pp. 5269–5304. ISBN: 978-981-19-6960-7. DOI: 10.1007/978-981-19-6960-7_131. URL: https://doi.org/10.1007/978-981-19-6960-7_131.

[Aba+24] A. G. Abac et al. "Observation of Gravitational Waves from the Coalescence of a $2.5 - 4.5\ M_\odot$ Compact Object and a Neutron Star". In: (Apr. 2024). arXiv: 2404.04248 [astro-ph.HE].

[Abb+16a] B. P. Abbott et al. "Observation of Gravitational Waves from a Binary Black Hole Merger". In: *Phys. Rev. Lett.* 116.6 (2016), p. 061102. DOI: 10.1103/PhysRevLett.116.061102. arXiv: 1602.03837 [gr-qc].

[Abb+16b] B. P. Abbott et al. "Prospects for observing and localizing gravitational-wave transients with Advanced LIGO, Advanced Virgo and KAGRA". In: *Living Rev. Rel.* 19 (2016), p. 1. DOI: 10.1007/s41114-020-00026-9. arXiv: 1304.0670 [gr-qc].

[Abb+17a] B. P. Abbott et al. "Gravitational Waves and Gamma-rays from a Binary Neutron Star Merger: GW170817 and GRB 170817A". In: *Astrophys. J. Lett.* 848.2 (2017), p. L13. DOI: 10.3847/2041-8213/aa920c. arXiv: 1710.05834 [astro-ph.HE].

[Abb+17b] B. P. Abbott et al. "Multi-messenger Observations of a Binary Neutron Star Merger". In: *Astrophys. J. Lett.* 848.2 (2017), p. L12. DOI: 10.3847/2041-8213/aa91c9. arXiv: 1710.05833 [astro-ph.HE].

[Abb+20] R. Abbott et al. "GW190521: A Binary Black Hole Merger with a Total Mass of $150 M_\odot$". In: *Phys. Rev. Lett.* 125.10 (2020), p. 101102. DOI: 10.1103/PhysRevLett.125.101102. arXiv: 2009.01075 [gr-qc].

[Abb+22] T. M. C. Abbott et al. "Dark Energy Survey Year 3 results: Cosmological constraints from galaxy clustering and weak lensing". In: *Phys. Rev. D* 105.2 (2022), p. 023520. DOI: 10.1103/PhysRevD.105.023520. arXiv: 2105.13549 [astro-ph.CO].

[ABCG06] Eloy Ayon-Beato, Cuauhtemoc Campuzano, and Alberto Garcia. "Conformally flat noncircular spacetimes". In: *Phys. Rev. D* 74 (2006), p. 024014. DOI: 10.1103/PhysRevD.74.024014. arXiv: gr-qc/0506004.

[ABCG07] Eloy Ayon-Beato, Cuauhtemoc Campuzano, and Alberto Garcia. "A new derivation of the conformally flat stationary cyclic noncircular spacetimes". In: *J. Phys. Conf. Ser.* 91 (2007). Ed. by Miguel Alcubierre Moya, Hector H. Garcia-Compean, and Luis A. Urena-Lopez, p. 012006. DOI: 10.1088/1742-6596/91/1/012006.

[Abd+16] Ahmadjon Abdujabbarov et al. "Shadow of rotating regular black holes". In: *Phys. Rev. D* 93.10 (2016), p. 104004. DOI: 10.1103/PhysRevD.93.104004. arXiv: 1604.03809 [gr-qc].

[Abd+22] Elcio Abdalla et al. "Cosmology intertwined: A review of the particle physics, astrophysics, and cosmology associated with the cosmological tensions and anomalies". In: *JHEAp* 34 (2022), pp. 49–211. DOI: 10.1016/j.jheap.2022.04.002. arXiv: 2203.06142 [astro-ph.CO].

[Abr+12] A. Abramowski et al. "The 2010 very high energy gamma-ray flare & 10 years of multi-wavelength observations of M 87". In: *Astrophys. J.* 746 (2012), p. 151. DOI: 10.1088/0004-637X/746/2/151. arXiv: 1111.5341 [astro-ph.CO].

[Abu+23] R. Abuter et al. "Polarimetry and astrometry of NIR flares as event horizon scale, dynamical probes for the mass of Sgr A*". In: *Astron. Astrophys.* 677 (2023), p. L10. DOI: 10.1051/0004-6361/202347416. arXiv: 2307.11821 [astro-ph.GA].

[ADA17] Jahed Abedi, Hannah Dykaar, and Niayesh Afshordi. "Echoes from the Abyss: Tentative evidence for Planck-scale structure at black hole horizons". In: *Phys. Rev. D* 96.8 (2017), p. 082004. DOI: 10.1103/PhysRevD.96.082004. arXiv: 1612.00266 [gr-qc].

[Ada+24] A. G. Adame et al. "DESI 2024 VI: Cosmological Constraints from the Measurements of Baryon Acoustic Oscillations". In: (Apr. 2024). arXiv: 2404.03002 [astro-ph.CO].

[Add+22] A. Addazi et al. "Quantum gravity phenomenology at the dawn of the multi-messenger era—A review". In: *Prog. Part. Nucl. Phys.* 125 (2022), p. 103948. DOI: 10.1016/j.ppnp.2022.103948. arXiv: 2111.05659 [hep-ph].

[AF13] Marek A. Abramowicz and P. Chris Fragile. "Foundations of Black Hole Accretion Disk Theory". In: *Living Rev. Rel.* 16 (2013), p. 1. DOI: 10.12942/lrr-2013-1. arXiv: 1104.5499 [astro-ph.HE].

[Afz+23] Adeela Afzal et al. "The NANOGrav 15 yr Data Set: Search for Signals from New Physics". In: *Astrophys. J. Lett.* 951.1 (2023), p. L11. DOI: 10.3847/2041-8213/acdc91. arXiv: 2306.16219 [astro-ph.HE].

[Aga+23] Gabriella Agazie et al. "The NANOGrav 15 yr Data Set: Evidence for a Gravitational-wave Background". In: *Astrophys. J. Lett.* 951.1 (2023), p. L8. DOI: 10.3847/2041-8213/acdac6. arXiv: 2306.16213 [astro-ph.HE].

[Agh+20] N. Aghanim et al. "Planck 2018 results. VI. Cosmological parameters". In: *Astron. Astrophys.* 641 (2020). [Erratum: Astron.Astrophys. 652, C4 (2021)], A6. DOI: 10.1051/0004-6361/201833910. arXiv: 1807.06209 [astro-ph.CO].

[Agm+22] Nathan Benjamin Agmon et al. "Lectures on the string landscape and the Swampland". In: (Dec. 2022). arXiv: 2212.06187 [hep-th].

[AK04] Abhay Ashtekar and Badri Krishnan. "Isolated and dynamical horizons and their applications". In: *Living Rev. Rel.* 7 (2004), p. 10. DOI: 10.12942/lrr-2004-10. arXiv: gr-qc/0407042.

[Aki+19a] Kazunori Akiyama et al. "First M87 Event Horizon Telescope Results. I. The Shadow of the Supermassive Black Hole". In: *Astrophys. J. Lett.* 875 (2019), p. L1. DOI: 10.3847/2041-8213/ab0ec7. arXiv: 1906.11238 [astro-ph.GA].

[Aki+19b] Kazunori Akiyama et al. "First M87 Event Horizon Telescope Results. II. Array and Instrumentation". In: *Astrophys. J. Lett.* 875.1 (2019), p. L2. DOI: 10.3847/2041-8213/ab0c96. arXiv: 1906.11239 [astro-ph.IM].

[Aki+19c] Kazunori Akiyama et al. "First M87 Event Horizon Telescope Results. III. Data Processing and Calibration". In: *Astrophys. J. Lett.* 875.1 (2019), p. L3. DOI: 10.3847/2041-8213/ab0c57. arXiv: 1906.11240 [astro-ph.GA].

[Aki+19d] Kazunori Akiyama et al. "First M87 Event Horizon Telescope Results. IV. Imaging the Central Supermassive Black Hole". In: *Astrophys. J. Lett.* 875.1 (2019), p. L4. DOI: 10.3847/2041-8213/ab0e85. arXiv: 1906.11241 [astro-ph.GA].

[Aki+19e] Kazunori Akiyama et al. "First M87 Event Horizon Telescope Results. V. Physical Origin of the Asymmetric Ring". In: *Astrophys. J. Lett.* 875.1 (2019), p. L5. DOI: 10.3847/2041-8213/ab0f43. arXiv: 1906.11242 [astro-ph.GA].

[Aki+19f] Kazunori Akiyama et al. "First M87 Event Horizon Telescope Results. VI. The Shadow and Mass of the Central Black Hole". In: *Astrophys. J. Lett.* 875.1 (2019), p. L6. DOI: 10.3847/2041-8213/ab1141. arXiv: 1906.11243 [astro-ph.GA].

[Aki+21a] Kazunori Akiyama et al. "First M87 Event Horizon Telescope Results. VII. Polarization of the Ring". In: *Astrophys. J. Lett.* 910.1 (2021), p. L12. DOI: 10.3847/2041-8213/abe71d. arXiv: 2105.01169 [astro-ph.HE].

[Aki+21b] Kazunori Akiyama et al. "First M87 Event Horizon Telescope Results. VIII. Magnetic Field Structure near The Event Horizon". In: *Astrophys. J. Lett.* 910.1 (2021), p. L13. DOI: 10.3847/2041-8213/abe4de. arXiv: 2105.01173 [astro-ph.HE].

[Aki+22a] Kazunori Akiyama et al. "First Sagittarius A* Event Horizon Telescope Results. I. The Shadow of the Supermassive Black Hole in the Center of the Milky Way". In: *Astrophys. J. Lett.* 930.2 (2022), p. L12. DOI: 10.3847/2041-8213/ac6674. arXiv: 2311.08680 [astro-ph.HE].

[Aki+22b] Kazunori Akiyama et al. "First Sagittarius A* Event Horizon Telescope Results. II. EHT and Multiwavelength Observations, Data Processing, and Calibration". In: *Astrophys. J. Lett.* 930.2 (2022), p. L13. DOI: 10.3847/2041-8213/ac6675. arXiv: 2311.08679 [astro-ph.HE].

[Aki+22c] Kazunori Akiyama et al. "First Sagittarius A* Event Horizon Telescope Results. III. Imaging of the Galactic Center Supermassive Black Hole". In: *Astrophys. J. Lett.* 930.2 (2022), p. L14. DOI: 10.3847/2041-8213/ac6429. arXiv: 2311.09479 [astro-ph.HE].

[Aki+22d] Kazunori Akiyama et al. "First Sagittarius A* Event Horizon Telescope Results. IV. Variability, Morphology, and Black Hole Mass". In: *Astrophys. J. Lett.* 930.2 (2022), p. L15. DOI: 10.3847/2041-8213/ac6736. arXiv: 2311.08697 [astro-ph.HE].

[Aki+22e] Kazunori Akiyama et al. "First Sagittarius A* Event Horizon Telescope Results. V. Testing Astrophysical Models of the Galactic Center Black Hole". In: *Astrophys. J. Lett.* 930.2 (2022), p. L16. DOI: 10.3847/2041-8213/ac6672. arXiv: 2311.09478 [astro-ph.HE].

[Aki+22f] Kazunori Akiyama et al. "First Sagittarius A* Event Horizon Telescope Results. VI. Testing the Black Hole Metric". In: *Astrophys. J. Lett.* 930.2 (2022), p. L17. DOI: 10.3847/2041-8213/ac6756. arXiv: 2311.09484 [astro-ph.HE].

[Aki+23] Kazunori Akiyama et al. "First M87 Event Horizon Telescope Results. IX. Detection of Near-horizon Circular Polarization". In: *Astrophys. J. Lett.* 957.2 (2023), p. L20. DOI: 10.3847/2041-8213/acff70. arXiv: 2311.10976 [astro-ph.HE].

[Aki+24a] Kazunori Akiyama et al. "First Sagittarius A* Event Horizon Telescope Results. VII. Polarization of the Ring". In: *Astrophys. J. Lett.* 964.2 (2024), p. L25. DOI: 10.3847/2041-8213/ad2df0.

[Aki+24b] Kazunori Akiyama et al. "First Sagittarius A* Event Horizon Telescope Results. VIII. Physical Interpretation of the Polarized Ring". In: *Astrophys. J. Lett.* 964.2 (2024), p. L26. DOI: 10.3847/2041-8213/ad2df1.

[Aki+24c] Kazunori Akiyama et al. "Mid-Range Science Objectives for the Event Horizon Telescope". In: (Oct. 2024). arXiv: 2410.02986 [astro-ph.HE].

[Aki+24d] Kazunori Akiyama et al. "The persistent shadow of the supermassive black hole of M 87. I. Observations, calibration, imaging, and analysis". In: *Astron. Astrophys.* 681 (2024), A79. DOI: 10.1051/0004-6361/202347932.

[AKN24] Zaryab Ahmed, Shilpa Kastha, and Alex B. Nielsen. "Constraining parametric deviations from the Kerr spacetime using black hole ringdowns of GW150914 and GW190521". In: (Jan. 2024). arXiv: 2401.06049 [gr-qc].

[Akr+20] Y. Akrami et al. "Planck 2018 results. X. Constraints on inflation". In: *Astron. Astrophys.* 641 (2020), A10. DOI: 10.1051/0004-6361/201833887. arXiv: 1807.06211 [astro-ph.CO].

[AL19] Gwyneth Allwright and Luis Lehner. "Towards the nonlinear regime in extensions to GR: assessing possible options". In: *Class. Quant. Grav.* 36.8 (2019), p. 084001. DOI: 10.1088/1361-6382/ab0ee1. arXiv: 1808.07897 [gr-qc].

[Ale17] Tal Alexander. "Stellar Dynamics and Stellar Phenomena Near a Massive Black Hole". In: *Ann. Rev. Astron. Astrophys.* 55 (2017), pp. 17–57. DOI: 10.1146/annurev-astro-091916-055306. arXiv: 1701.04762 [astro-ph.GA].

[Alf42] Hannes Alfvén. "Existence of electromagnetic-hydrodynamic waves". In: *Nature* 150.3805 (1942), pp. 405–406.

[Alg+21] J. C. Algaba et al. "Broadband Multi-wavelength Properties of M87 during the 2017 Event Horizon Telescope Campaign". In: *Astrophys. J. Lett.* 911.1 (2021), p. L11. DOI: 10.3847/2041-8213/abef71. arXiv: 2104.06855 [astro-ph.HE].

[Alg+24] J. C. Algaba et al. "Broadband Multi-wavelength Properties of M87 during the 2018 EHT Campaign including a Very High Energy Flaring Episode". In: (Apr. 2024). arXiv: 2404.17623 [astro-ph.HE].

[Amb+15] Jan Ambjørn et al. "Signature Change of the Metric in CDT Quantum Gravity?" In: *JHEP* 08 (2015), p. 033. DOI: 10.1007/JHEP08(2015)033. arXiv: 1503.08580 [hep-th].

[Amb24] Jan Ambjorn. "Lattice Quantum Gravity: EDT and CDT". In: 2024. DOI: 10.1007/978-981-19-3079-9_84-1. arXiv: 2209.06555 [hep-lat].

[Ans+21] Timothy Anson et al. "Disforming the Kerr metric". In: *JHEP* 01 (2021), p. 018. DOI: 10.1007/JHEP01(2021)018. arXiv: 2006.06461 [gr-qc].

[Ant+22] D. Antypas et al. "New Horizons: Scalar and Vector Ultralight Dark Matter". In: (Mar. 2022). arXiv: 2203.14915 [hep-ex].

[Ant+24] J. Antoniadis et al. "The second data release from the European Pulsar Timing Array - IV. Implications for massive black holes, dark matter, and the early Universe". In: *Astron. Astrophys.* 685 (2024), A94. DOI: 10.1051/0004-6361/202347433. arXiv: 2306.16227 [astro-ph.CO].

[Ant+97] Ignatios Antoniadis et al. "R**4 couplings in M and type II theories on Calabi-Yau spaces". In: *Nucl. Phys. B* 507 (1997), pp. 571–588. DOI: 10.1016/S0550-3213(97)00572-5. arXiv: hep-th/9707013.

[AOS18] Abhay Ashtekar, Javier Olmedo, and Parampreet Singh. "Quantum Transfiguration of Kruskal Black Holes". In: *Phys. Rev. Lett.* 121.24 (2018), p. 241301. DOI: 10.1103/PhysRevLett.121.241301. arXiv: 1806.00648 [gr-qc].

[AP17] Abhay Ashtekar and Jorge Pullin, eds. *Loop Quantum Gravity: The First 30 Years*. Vol. 4. 100 Years of General Relativity. World Scientific, 2017. ISBN: 978-981-320-992-3, 978-981-322-001-0, 978-981-320-993-0. DOI: 10.1142/10445.

[ARMV23] E Albentosa-Ruiz and I Marti-Vidal. "Robust analysis of differential Faraday rotation based on interferometric closure observables". In: *Astronomy & Astrophysics* 672 (2023), A67.

[Arr+22] Julio Arrechea et al. "Semiclassical relativistic stars". In: *Sci. Rep.* 12.1 (2022), p. 15958. DOI: 10.1038/s41598-022-19836-8. arXiv: 2110.15808 [gr-qc].

[AS17] Ivan Agullo and Parampreet Singh. "Loop Quantum Cosmology". In: *Loop Quantum Gravity: The First 30 Years*. Ed. by Abhay Ashtekar and Jorge Pullin. WSP, 2017, pp. 183–240. DOI: 10.1142/9789813220003_0007. arXiv: 1612.01236 [gr-qc].

[AS68] Milton Abramowitz and Irene A Stegun. *Handbook of mathematical functions with formulas, graphs, and mathematical tables*. Vol. 55. US Government printing office, 1968.

[Asa+13] Keiichi Asada et al. "Discovery of Sub- to Superluminal Motions in the M87 Jet: An Implication of Acceleration from Sub-relativistic to Relativistic Speeds". In: *Astrophys. J. Lett.* 781 (2013), p. L2. DOI: 10.1088/2041-8205/781/1/L2. arXiv: 1311.5709 [astro-ph.HE].

[ASCF22] Llibert Aresté Saló, Katy Clough, and Pau Figueras. "Well-Posedness of the Four-Derivative Scalar-Tensor Theory of Gravity in Singularity Avoiding Coordinates". In: *Phys. Rev. Lett.* 129.26 (2022), p. 261104. DOI: 10.1103/PhysRevLett.129.261104. arXiv: 2208.14470 [gr-qc].

[ASHM10] Rene Andrae, Tim Schulze-Hartung, and Peter Melchior. "Dos and don'ts of reduced chi-squared". In: (Dec. 2010). arXiv: 1012.3754 [astro-ph.IM].

[ATP24] Fabio Aratore, Oleg Yu. Tsupko, and Volker Perlick. "Constraining spherically symmetric metrics by the gap between photon rings". In: *Phys. Rev. D* 109.12 (2024), p. 124057. DOI: 10.1103/PhysRevD.109.124057. arXiv: 2402.14733 [gr-qc].

[ATV08] Abhay Ashtekar, Victor Taveras, and Madhavan Varadarajan. "Information is Not Lost in the Evaporation of 2-dimensional Black Holes". In: *Phys. Rev. Lett.* 100 (2008), p. 211302. DOI: 10.1103/PhysRevLett.100.211302. arXiv: 0801.1811 [gr-qc].

[AY09] Stephon Alexander and Nicolas Yunes. "Chern-Simons Modified General Relativity". In: *Phys. Rept.* 480 (2009), pp. 1–55. DOI: 10.1016/j.physrep.2009.07.002. arXiv: 0907.2562 [hep-th].

[Ayz22] Dimitry Ayzenberg. "Testing gravity with black hole shadow subrings". In: *Class. Quant. Grav.* 39.10 (2022), p. 105009. DOI: 10.1088/1361-6382/ac655d. arXiv: 2202.02355 [gr-qc].

[Ayz+23] D. Ayzenberg et al. "Fundamental Physics Opportunities with the Next-Generation Event Horizon Telescope". In: (Dec. 2023). arXiv: 2312.02130 [astro-ph.HE].

[BA+20] Jibril Ben Achour et al. "On rotating black holes in DHOST theories". In: *JCAP* 11 (2020), p. 001. DOI: 10.1088/1475-7516/2020/11/001. arXiv: 2006.07245 [gr-qc].

[Bab+20] Eugeny Babichev et al. "Regular black holes via the Kerr-Schild construction in DHOST theories". In: *JCAP* 06 (2020), p. 049. DOI: 10.1088/1475-7516/2020/06/049. arXiv: 2004.00597 [hep-th].

[Bab+24] Eugeny Babichev et al. "Testing disformal non-circular deformation of Kerr black holes with LISA". In: *JCAP* 06 (2024), p. 065. DOI: 10.1088/1475-7516/2024/06/065. arXiv: 2403.16192 [gr-qc].

[Bak20] Athanasios Bakopoulos. "Black holes and wormholes in the Einstein-scalar-Gauss-Bonnet generalized theories of gravity". PhD thesis. Ioannina U., 2020. DOI: 10.12681/eadd/48145. arXiv: 2010.13189 [gr-qc].

[Bam11] Cosimo Bambi. "Testing the Kerr black hole hypothesis". In: *Mod. Phys. Lett. A* 26 (2011), pp. 2453–2468. DOI: 10.1142/S0217732311036929. arXiv: 1109.4256 [gr-qc].

[Bam23] Cosimo Bambi, ed. *Regular Black Holes. Towards a New Paradigm of Gravitational Collapse*. Springer Series in Astrophysics and Cosmology. Springer, 2023. ISBN: 978-981-99-1595-8, 978-981-99-1598-9, 978-981-99-1596-5. DOI: 10.1007/978-981-99-1596-5. arXiv: 2307.13249 [gr-qc].

[Ban+24] Indranil Banik et al. "Strong constraints on the gravitational law from *Gaia* DR3 wide binaries". In: *Mon. Not. Roy. Astron. Soc.* 527.3 (2024), pp. 4573–4615. DOI: 10.1093/mnras/stad3393. arXiv: 2311.03436 [astro-ph.SR].

[Bar+20] Enrico Barausse et al. "Prospects for Fundamental Physics with LISA". In: *Gen. Rel. Grav.* 52.8 (2020), p. 81. DOI: 10.1007/s10714-020-02691-1. arXiv: 2001.09793 [gr-qc].

[Bar68a] James Bardeen. "Non-singular general relativistic gravitational collapse". In: *Proceedings of the 5th International Conference on Gravitation and the Theory of Relativity*. 1968, p. 87.

[Bar68b] JM Bardeen. "Conference Proceedings of GR5, Tbilisi, USSR". In: (1968).

[Bas+23] Ajay Bassi et al. "Cosmological evolution in bimetric gravity: observational constraints and LSS signatures". In: *Eur. Phys. J. C* 83.6 (2023), p. 525. DOI: 10.1140/epjc/s10052-023-11707-4. arXiv: 2301.11000 [astro-ph.CO].

[BB17] Martin Bojowald and Suddhasattwa Brahma. "Signature change in loop quantum gravity: Two-dimensional midisuperspace models and dilaton gravity". In: *Phys. Rev. D* 95.12 (2017), p. 124014. DOI: 10.1103/PhysRevD.95.124014. arXiv: 1610.08840 [gr-qc].

[BC12] Dario Benedetti and Francesco Caravelli. "The Local potential approximation in quantum gravity". In: *JHEP* 06 (2012). [Erratum: JHEP 10, 157 (2012)], p. 017. DOI: 10.1007/JHEP06(2012)017. arXiv: 1204.3541 [hep-th].

[BC88] John D. Barrow and S. Cotsakis. "Inflation and the Conformal Structure of Higher Order Gravity Theories". In: *Phys. Lett. B* 214 (1988), pp. 515–518. DOI: 10.1016/0370-2693(88)90110-4.

[BC95] Patrick R. Brady and Chris M. Chambers. "Nonlinear instability of Kerr type Cauchy horizons". In: *Phys. Rev. D* 51 (1995), pp. 4177–4186. DOI: 10.1103/PhysRevD.51.4177. arXiv: gr-qc/9501025.

[BCA24] Cosimo Bambi and Alejandro Cardenas-Avendano, eds. *Recent Progress on Gravity Tests. Challenges and Future Perspectives*. Springer Series in Astrophysics and Cosmology. Springer, 2024. ISBN: 978-981–972870-1, 978-981–972873-2, 978-981–972871-8. DOI: 10.1007/978-981-97-2871-8.

[BCL16] Eugeny Babichev, Christos Charmousis, and Antoine Lehébel. "Black holes and stars in Horndeski theory". In: *Class. Quant. Grav.* 33.15 (2016), p. 154002. DOI: 10.1088/0264-9381/33/15/154002. arXiv: 1604.06402 [gr-qc].

[BCR22] Arnau Bas i Beneito, Gianluca Calcagni, and Lesław Rachwał. "Classical and quantum nonlocal gravity". In: (Nov. 2022). arXiv: 2211.05606 [hep-th].

[BCV17] T. Daniel Brennan, Federico Carta, and Cumrun Vafa. "The String Landscape, the Swampland, and the Missing Corner". In: *PoS* TASI2017 (2017), p. 015. DOI: 10.22323/1.305.0015. arXiv: 1711.00864 [hep-th].

[Bee+22] Marieke van Beest et al. "Lectures on the Swampland Program in String Compactifications". In: *Phys. Rept.* 989 (2022), pp. 1–50. DOI: 10.1016/j.physrep.2022.09.002. arXiv: 2102.01111 [hep-th].

[BEF07] Jean-Philippe Bruneton and Gilles Esposito-Farese. "Field-theoretical formulations of MOND-like gravity". In: *Phys. Rev. D* 76 (2007). [Erratum: Phys.Rev.D 76, 129902 (2007)], p. 124012. DOI: 10.1103/PhysRevD.76.129902. arXiv: 0705.4043 [gr-qc].

[Bei12] M. Beilicke. "VERITAS Observations of M 87 in 2011/2012". In: *AIP Conf. Proc.* 1505.1 (2012). Ed. by Felix A. Aharonian, Werner Hofmann, and Frank M. Rieger, pp. 586–589. DOI: 10.1063/1.4772328. arXiv: 1210.7830 [astro-ph.HE].

[Bek72] J. D. Bekenstein. "Black holes and the second law". In: *Lett. Nuovo Cim.* 4 (1972), pp. 737–740. DOI: 10.1007/BF02757029.

[Bek73] Jacob D. Bekenstein. "Black holes and entropy". In: *Phys. Rev. D* 7 (1973), pp. 2333–2346. DOI: 10.1103/PhysRevD.7.2333.

[Bek75] J. D. Bekenstein. "Nonsingular General Relativistic Cosmologies". In: *Phys. Rev. D* 11 (1975), pp. 2072–2075. DOI: 10.1103/PhysRevD.11.2072.

[Bek93] Jacob D. Bekenstein. "The Relation between physical and gravitational geometry". In: *Phys. Rev. D* 48 (1993), pp. 3641–3647. DOI: 10.1103/PhysRevD.48.3641. arXiv: gr-qc/9211017.

[Ben+22] Iosif Bena et al. "Fuzzballs and Microstate Geometries: Black-Hole Structure in String Theory". In: (Apr. 2022). arXiv: 2204.13113 [hep-th].

[Ber+15] Emanuele Berti et al. "Testing General Relativity with Present and Future Astrophysical Observations". In: *Class. Quant. Grav.* 32 (2015), p. 243001. DOI: 10.1088/0264-9381/32/24/243001. arXiv: 1501.07274 [gr-qc].

[Ber19] Emanuele Berti. "Topical Collection: Testing the Kerr spacetime with gravitational-wave and electromagnetic observations". In: *Gen. Rel. Grav.* 51 (2019), p. 140. DOI: 10.1007/s10714-019-2622-2. arXiv: 1911.00541 [gr-qc].

[Bez+21] Miguel Bezares et al. "Kinetic screening in nonlinear stellar oscillations and gravitational collapse". In: *Phys. Rev. D* 104.4 (2021), p. 044022. DOI: 10.1103/PhysRevD.104.044022. arXiv: 2105.13992 [gr-qc].

[Bez+22] Miguel Bezares et al. "No Evidence of Kinetic Screening in Simulations of Merging Binary Neutron Stars beyond General Relativity". In: *Phys. Rev. Lett.* 128.9 (2022), p. 091103. DOI: 10.1103/PhysRevLett.128.091103. arXiv: 2107.05648 [gr-qc].

[BF79] S. Benenti and M. Francaviglia. "Remarks on certain separability structures and their applications to general relativity". In: *Gen. Rel. Grav.* 10.1 (1979), pp. 79–92. DOI: 10.1007/bf00757025.

[BH17] C. G. Böhmer and P. A. Hogan. "A Vaidya-type generalization of Kerr spacetime". In: *Mod. Phys. Lett. A* 32.35 (2017), p. 1750189. DOI: 10.1142/S0217732317501899. arXiv: 1710.01059 [gr-qc].

[BH91] Steven A. Balbus and John F. Hawley. "A powerful local shear instability in weakly magnetized disks. 1. Linear analysis. 2. Nonlinear evolution". In: *Astrophys. J.* 376 (1991), pp. 214–233. DOI: 10.1086/170270.

[BH98] Steven A. Balbus and John F. Hawley. "Instability, turbulence, and enhanced transport in accretion disks". In: *Rev. Mod. Phys.* 70 (1998), pp. 1–53. DOI: 10.1103/RevModPhys.70.1.

[BHA23] Johanna N. Borissova, Aaron Held, and Niayesh Afshordi. "Scale-invariance at the core of quantum black holes". In: *Class. Quant. Grav.* 40.7 (2023), p. 075011. DOI: 10.1088/1361-6382/acbc60. arXiv: 2203.02559 [gr-qc].

[BIT03] B. Bertotti, L. Iess, and P. Tortora. "A test of general relativity using radio links with the Cassini spacecraft". In: *Nature* 425 (2003), pp. 374–376. DOI: 10.1038/nature01997.

[BKP17] Alfio Bonanno, Benjamin Koch, and Alessia Platania. "Cosmic Censorship in Quantum Einstein Gravity". In: *Class. Quant. Grav.* 34.9 (2017), p. 095012. DOI: 10.1088/1361-6382/aa6788. arXiv: 1610.05299 [gr-qc].

[BKP18] Alfio Bonanno, Benjamin Koch, and Alessia Platania. "Gravitational collapse in Quantum Einstein Gravity". In: *Found. Phys.* 48.10 (2018), pp. 1393–1406. DOI: 10.1007/s10701-018-0195-7. arXiv: 1710.10845 [gr-qc].

[BL13] Dario Bettoni and Stefano Liberati. "Disformal invariance of second order scalar-tensor theories: Framing the Horndeski action". In: *Phys. Rev. D* 88 (2013), p. 084020. DOI: 10.1103/PhysRevD.88.084020. arXiv: 1306.6724 [gr-qc].

[BL23] G.D. Birkhoff and R.E. Langer. *Relativity and Modern Physics*. Harvard University Press, 1923. URL: https://books.google.dk/books?id=NEpAAAAAIAAJ.

[Bla+20] Lindy Blackburn et al. "Closure statistics in interferometric data". In: *The Astrophysical Journal* 894.1 (2020), p. 31.

[BM23] Ram Brustein and A. J. M. Medved. "Sourcing the Kerr geometry". In: (Oct. 2023). arXiv: 2310.16467 [gr-qc].

[BMB22] Tamara Bogdanovic, M. Coleman Miller, and Laura Blecha. "Electromagnetic counterparts to massive black-hole mergers". In: *Living Rev. Rel.* 25.1 (2022), p. 3. DOI: 10.1007/s41114-022-00037-8. arXiv: 2109.03262 [astro-ph.HE].

[BMS09] Dario Benedetti, Pedro F. Machado, and Frank Saueressig. "Asymptotic safety in higher-derivative gravity". In: *Mod. Phys. Lett. A* 24 (2009), pp. 2233–2241. DOI: 10.1142/S0217732309031521. arXiv: 0901.2984 [hep-th].

[BMS10] Dario Benedetti, Pedro F. Machado, and Frank Saueressig. "Taming perturbative divergences in asymptotically safe gravity". In: *Nucl. Phys. B* 824 (2010), pp. 168–191. DOI: 10.1016/j.nuclphysb.2009.08.023. arXiv: 0902.4630 [hep-th].

[BN22] Rudrajit Banerjee and Max Niedermaier. "The spatial Functional Renormalization Group and Hadamard states on cosmological spacetimes". In: *Nucl. Phys. B* 980 (2022), p. 115814. DOI: 10.1016/j.nuclphysb.2022.115814. arXiv: 2201.02575 [hep-th].

[Boe+22] Jan de Boer et al. "Frontiers of Quantum Gravity: shared challenges, converging directions". In: (July 2022). arXiv: 2207.10618 [hep-th].

[Boj20] Martin Bojowald. "Black-Hole Models in Loop Quantum Gravity". In: *Universe* 6.8 (2020), p. 125. DOI: 10.3390/universe6080125. arXiv: 2009.13565 [gr-qc].

[Bon+20] Alfio Bonanno et al. "Critical reflections on asymptotically safe gravity". In: *Front. in Phys.* 8 (2020), p. 269. DOI: 10.3389/fphy.2020.00269. arXiv: 2004.06810 [gr-qc].

[Bon47] H. Bondi. "Spherically symmetrical models in general relativity". In: *Mon. Not. Roy. Astron. Soc.* 107 (1947), pp. 410–425. DOI: 10.1093/mnras/107.5-6.410.

[Boo05] Ivan Booth. "Black hole boundaries". In: *Can. J. Phys.* 83 (2005), pp. 1073–1099. DOI: 10.1139/p05-063. arXiv: gr-qc/0508107.

[BORG17] Cecilia Bejarano, Gonzalo J. Olmo, and Diego Rubiera-Garcia. "What is a singular black hole beyond General Relativity?" In: *Phys. Rev. D* 95.6 (2017), p. 064043. DOI: 10.1103/PhysRevD.95.064043. arXiv: 1702.01292 [hep-th].

[BP20] Avery E Broderick and Dominic W Pesce. "Closure traces: Novel calibration-insensitive quantities for radio astronomy". In: *The Astrophysical Journal* 904.2 (2020), p. 126.

[BP23] Johanna N. Borissova and Alessia Platania. "Formation and evaporation of quantum black holes from the decoupling mechanism in quantum gravity". In: *JHEP* 03 (2023), p. 046. DOI: 10.1007/JHEP03(2023)046. arXiv: 2210.01138 [gr-qc].

[BP82] R. D. Blandford and D. G. Payne. "Hydromagnetic flows from accretion discs and the production of radio jets". In: *Mon. Not. Roy. Astron. Soc.* 199.4 (1982), pp. 883–903. DOI: 10.1093/mnras/199.4.883.

[BPS15] Tessa Baker, Dimitrios Psaltis, and Constantinos Skordis. "Linking Tests of Gravity On All Scales: from the Strong-Field Regime to Cosmology". In: *Astrophys. J.* 802 (2015), p. 63. DOI: 10.1088/0004-637X/802/1/63. arXiv: 1412.3455 [astro-ph.CO].

[BR00] Alfio Bonanno and Martin Reuter. "Renormalization group improved black hole space-times". In: *Phys. Rev. D* 62 (2000), p. 043008. DOI: 10.1103/PhysRevD.62.043008. arXiv: hep-th/0002196.

[BR16] Nigel T. Bishop and Luciano Rezzolla. "Extraction of Gravitational Waves in Numerical Relativity". In: *Living Rev. Rel.* 19 (2016), p. 2. DOI: 10.1007/s41114-016-0001-9. arXiv: 1606.02532 [gr-qc].

[BR89] E. A. Bergshoeff and M. de Roo. "The Quartic Effective Action of the Heterotic String and Supersymmetry". In: *Nucl. Phys. B* 328 (1989), pp. 439–468. DOI: 10.1016/0550-3213(89)90336-2.

[BR99] Alfio Bonanno and Martin Reuter. "Quantum gravity effects near the null black hole singularity". In: *Phys. Rev. D* 60 (1999), p. 084011. DOI: 10.1103/PhysRevD.60.084011. arXiv: gr-qc/9811026.

[Bra+23] Jens Braun et al. "Renormalised spectral flows". In: *SciPost Phys. Core* 6 (2023), p. 061. DOI: 10.21468/SciPostPhysCore.6.3.061. arXiv: 2206.10232 [hep-th].

[Bro] Avery Broderick. *ngEHTexplorer*. URL: https://github.com/aeb/ngEHTexplorer.

[Bro+20] Avery E. Broderick et al. "Hybrid Very Long Baseline Interferometry Imaging and Modeling with themis". In: *Astrophys. J.* 898.1 (2020), p. 9. DOI: 10.3847/1538-4357/ab9c1f. arXiv: 2208.09003 [astro-ph.IM].

[Bro+22a] Avery E. Broderick et al. "Measuring Spin from Relative Photon-ring Sizes". In: *Astrophys. J.* 927.1 (2022), p. 6. DOI: 10.3847/1538-4357/ac4970. arXiv: 2105.09962 [astro-ph.HE].

[Bro+22b] Avery E. Broderick et al. "The Photon Ring in M87*". In: *Astrophys. J.* 935 (2022), p. 61. DOI: 10.3847/1538-4357/ac7c1d. arXiv: 2208.09004 [astro-ph.HE].

[BS+16] Jose Luis Blázquez-Salcedo et al. "Black holes in Einstein-Gauß-Bonnet-dilaton theory". In: *IAU Symp.* 324 (2016). Ed. by Andreja Gomboc, pp. 265–272. DOI: 10.1017/S1743921316012965. arXiv: 1610.09214 [gr-qc].

[BS21] Cosimo Bambi and Dejan Stojkovic. "Astrophysical Wormholes". In: *Universe* 7.5 (2021), p. 136. DOI: 10.3390/universe7050136. arXiv: 2105.00881 [gr-qc].

[BS22] Ssohrab Borhanian and B. S. Sathyaprakash. "Listening to the Universe with Next Generation Ground-Based Gravitational-Wave Detectors". In: (Feb. 2022). arXiv: 2202.11048 [gr-qc].

[BS23] Kirill A. Bronnikov and Sergey V. Sushkov. "Current problems and recent advances in wormhole physics". In: *Universe* 9 (2023), p. 81. arXiv: 2301.11390 [gr-qc].

[BSG23] Avery E. Broderick, Kiana Salehi, and Boris Georgiev. "Shadow Implications: What Does Measuring the Photon Ring Imply for Gravity?" In: *Astrophys. J.* 958.2 (2023), p. 114. DOI: 10.3847/1538-4357/acf9f6. arXiv: 2307.15120 [astro-ph.HE].

[BSG24] Miguel Bezares and Nicolas Sanchis-Gual. "Exotic compact objects: a recent numerical-relativity perspective". In: (June 2024). arXiv: 2406.04901 [gr-qc].

[BSM11] Reiner Birkl, Nikolaos Stergioulas, and Ewald Muller. "Stationary, Axisymmetric Neutron Stars with Meridional Circulation in General Relativity". In: *Phys. Rev. D* 84 (2011), p. 023003. DOI: 10.1103/PhysRevD.84.023003. arXiv: 1011.5475 [gr-qc].

[BSM99] J. A. Biretta, W. B. Sparks, and F. Macchetto. "HUBBLE SPACE TELESCOPE Observations of Superluminal Motion in the M87 Jet". In: *The Astrophysical Journal* 520.2 (Aug. 1999), p. 621. DOI: 10.1086/307499. URL: https://dx.doi.org/10.1086/307499.

[Buc59] Hans A. Buchdahl. "General Relativistic Fluid Spheres". In: *Phys. Rev.* 116 (1959), p. 1027. DOI: 10.1103/PhysRev.116.1027.

[Bul+16] Philip Bull et al. "Beyond ΛCDM: Problems, solutions, and the road ahead". In: *Phys. Dark Univ.* 12 (2016), pp. 56–99. DOI: 10.1016/j.dark.2016.02.001. arXiv: 1512.05356 [astro-ph.CO].

[Bur+03] Marta Burgay et al. "An Increased estimate of the merger rate of double neutron stars from observations of a highly relativistic system". In: *Nature* 426 (2003), pp. 531–533. DOI: 10.1038/nature02124. arXiv: astro-ph/0312071.

[Bur+23] Clare Burrage et al. "Spinning black holes with axion hair". In: *Class. Quant. Grav.* 40.20 (2023), p. 205021. DOI: 10.1088/1361-6382/acf9d6. arXiv: 2306.03662 [gr-qc].

[BV00] Carlos Barcelo and Matt Visser. "Scalar fields, energy conditions, and traversable wormholes". In: *Class. Quant. Grav.* 17 (2000), pp. 3843–3864. DOI: 10.1088/0264-9381/17/18/318. arXiv: gr-qc/0003025.

[BV02] Carlos Barcelo and Matt Visser. "Twilight for the energy conditions?" In: *Int. J. Mod. Phys. D* 11 (2002), pp. 1553–1560. DOI: 10.1142/S0218271802002888. arXiv: gr-qc/0205066.

[BZ77] R. D. Blandford and R. L. Znajek. "Electromagnetic extractions of energy from Kerr black holes". In: *Mon. Not. Roy. Astron. Soc.* 179 (1977), pp. 433–456. DOI: 10.1093/mnras/179.3.433.

[CAnKL24] Alejandro Cárdenas-Avendaño, Lennox Keeble, and Alexandru Lupsasca. "Assessing the impact of instrument noise and astrophysical fluctuations on measurements of the first black hole photon ring". In: *Phys. Rev. D* 109.12 (2024), p. 124052. DOI: 10.1103/PhysRevD.109.124052. arXiv: 2404.01083 [gr-qc].

[CAnL23] Alejandro Cárdenas-Avendaño and Alexandru Lupsasca. "Prediction for the interferometric shape of the first black hole photon ring". In: *Phys. Rev. D* 108.6 (2023), p. 064043. DOI: 10.1103/PhysRevD.108.064043. arXiv: 2305.12956 [gr-qc].

[CANY20] Alejandro Cardenas-Avendano, Sourabh Nampalliwar, and Nicolas Yunes. "Gravitational-wave versus X-ray tests of strong-field gravity". In: *Class. Quant. Grav.* 37.13 (2020), p. 135008. DOI: 10.1088/1361-6382/ab8f64. arXiv: 1912.08062 [gr-qc].

[Car00] Bernard J. Carr. "A Classification of spherically symmetric self-similar dust models". In: *Phys. Rev. D* 62 (2000), p. 044022. DOI: 10.1103/PhysRevD.62.044022. arXiv: gr-qc/0003007.

[Car+09] Vitor Cardoso et al. "Geodesic stability, Lyapunov exponents and quasinormal modes". In: *Phys. Rev. D* 79.6 (2009), p. 064016. DOI: 10.1103/PhysRevD.79.064016. arXiv: 0812.1806 [hep-th].

[Car14] S. Carlip. "Black Hole Thermodynamics". In: *Int. J. Mod. Phys. D* 23 (2014), p. 1430023. DOI: 10.1142/S0218271814300237. arXiv: 1410.1486 [gr-qc].

[Car+18] Vitor Cardoso et al. "Black Holes in an Effective Field Theory Extension of General Relativity". In: *Phys. Rev. Lett.* 121.25 (2018). [Erratum: Phys.Rev.Lett. 131, 109903 (2023)], p. 251105. DOI: 10.1103/PhysRevLett.121.251105. arXiv: 1808.08962 [gr-qc].

[Car+19] Vitor Cardoso et al. "Parametrized black hole quasinormal ringdown: Decoupled equations for nonrotating black holes". In: *Phys. Rev. D* 99.10 (2019), p. 104077. DOI: 10.1103/PhysRevD.99.104077. arXiv: 1901.01265 [gr-qc].

[Car19] Sean M. Carroll. *Spacetime and Geometry: An Introduction to General Relativity*. Cambridge University Press, July 2019. ISBN: 978-0-8053-8732-2, 978-1-108-48839-6, 978-1-108-77555-7. DOI: 10.1017/9781108770385.

[Car70] Brandon Carter. "The commutation property of a stationary, axisymmetric system". In: *Commun. Math. Phys.* 17 (1970), pp. 233–238. DOI: 10.1007/BF01647092.

[Car71] B. Carter. "Axisymmetric Black Hole Has Only Two Degrees of Freedom". In: *Phys. Rev. Lett.* 26 (1971), pp. 331–333. DOI: 10.1103/PhysRevLett.26.331.

[Car73] B. Carter. "Black holes equilibrium states". In: *Les Houches Summer School of Theoretical Physics: Black Holes*. 1973, pp. 57–214.

[Cas18] Pablo Antonio Moreno Casares. "A review on Loop Quantum Gravity". In: (Aug. 2018). arXiv: 1808.01252 [gr-qc].

[CBG69] Y. Choquet-Bruhat and Robert P. Geroch. "Global aspects of the Cauchy problem in general relativity". In: *Commun. Math. Phys.* 14 (1969), pp. 329–335. DOI: 10.1007/BF01645389.

[CD24] Pablo A. Cano and Marina David. "Isospectrality in Effective Field Theory Extensions of General Relativity". In: (July 2024). arXiv: 2407.12080 [hep-th].

[CDL15] Salvatore Capozziello and Mariafelicia De Laurentis. "Extended Gravity: State of the Art and Perspectives". In: *13th Marcel Grossmann Meeting on Recent Developments in Theoretical and Experimental General Relativity, Astrophysics, and Relativistic Field Theories*. 2015, pp. 1097–1112. DOI: 10.1142/9789814623995_0092. arXiv: 1307.4523 [gr-qc].

[CDY24] Pablo A. Cano, Alexander Deich, and Nicolás Yunes. "Accuracy of the slow-rotation approximation for black holes in modified gravity in light of astrophysical observables". In: *Phys. Rev. D* 109.2 (2024), p. 024048. DOI: 10.1103/PhysRevD.109.024048. arXiv: 2305.15341 [gr-qc].

[CG24] Federico Cattorini and Bruno Giacomazzo. "GRMHD study of accreting massive black hole binaries in astrophysical environment: A review". In: *Astropart. Phys.* 154 (2024), p. 102892. DOI: 10.1016/j.astropartphys.2023.102892. arXiv: 2401.02521 [astro-ph.HE].

[CH20] Pedro V. P. Cunha and Carlos A. R. Herdeiro. "Stationary black holes and light rings". In: *Phys. Rev. Lett.* 124.18 (2020), p. 181101. DOI: 10.1103/PhysRevLett.124.181101. arXiv: 2003.06445 [gr-qc].

[Cha+18] Andrew A. Chael et al. "Interferometric Imaging Directly with Closure Phases and Closure Amplitudes". In: *Astrophys. J.* 857.1 (2018), p. 23. DOI: 10.3847/1538-4357/aab6a8. arXiv: 1803.07088 [astro-ph.IM].

[Cha+19] Christos Charmousis et al. "Rotating Black Holes in Higher Order Gravity". In: *Phys. Rev. D* 100.8 (2019), p. 084020. DOI: 10.1103/PhysRevD.100.084020. arXiv: 1903.05519 [hep-th].

[Cha22] Andrew Chael. *eht-imaging*. Version 1.2.6. May 2022. DOI: 10.5281/zenodo.7226661. URL: https://github.com/achael/eht-imaging.

[Cha+23] Andrew Chael et al. "Multifrequency Black Hole Imaging for the Next-generation Event Horizon Telescope". In: *Astrophys. J.* 945.1 (2023), p. 40. DOI: 10.3847/1538-4357/acb7e4. arXiv: 2210.12226 [astro-ph.HE].

[Cha+24a] K. Chatziioannou et al. "Compact binary coalescences: gravitational-wave astronomy with ground-based detectors". In: (Sept. 2024). arXiv: 2409.02037 [gr-qc].

[Cha+24b] Erandi Chavez et al. "Prospects of Detecting a Jet in Sagittarius A* with VLBI". In: (May 2024). arXiv: 2405.06029 [astro-ph.HE].

[Cha83] Subrahmanyan Chandrasekhar. "On stars, their evolution and their stability". In: (Dec. 1983).

[Che+18] Pisin Chen et al. "Pre-Hawking radiation cannot prevent the formation of apparent horizon". In: *Phys. Rev. D* 97.6 (2018), p. 064045. DOI: 10.1103/PhysRevD.97.064045. arXiv: 1710.01533 [gr-qc].

[CHM11] Roberto Casadio, Stephen D. H. Hsu, and Behrouz Mirza. "Asymptotic Safety, Singularities, and Gravitational Collapse". In: *Phys. Lett. B* 695 (2011), pp. 317–319. DOI: 10.1016/j.physletb.2010.10.060. arXiv: 1008.2768 [gr-qc].

[CHN24] Pedro V. P. Cunha, Carlos A. R. Herdeiro, and João P. A. Novo. "Light rings on stationary axisymmetric spacetimes: Blind to the topology and able to coexist". In: *Phys. Rev. D* 109.6 (2024), p. 064050. DOI: 10.1103/PhysRevD.109.064050. arXiv: 2401.05495 [gr-qc].

[CHP09] Alan Coley, Sigbjorn Hervik, and Nicos Pelavas. "Spacetimes characterized by their scalar curvature invariants". In: *Class. Quant. Grav.* 26 (2009), p. 025013. DOI: 10.1088/0264-9381/26/2/025013. arXiv: 0901.0791 [gr-qc].

[CHR17] Pedro V. P. Cunha, Carlos A. R. Herdeiro, and Eugen Radu. "Fundamental photon orbits: black hole shadows and spacetime instabilities". In: *Phys. Rev. D* 96.2 (2017), p. 024039. DOI: 10.1103/PhysRevD.96.024039. arXiv: 1705.05461 [gr-qc].

[Ciu+19] Ignazio Ciufolini et al. "An Improved Test of the General Relativistic Effect of Frame-Dragging Using the LARES and LAGEOS Satellites". In: *Eur. Phys. J. C* 79.10 (2019), p. 872. DOI: 10.1140/epjc/s10052-019-7386-z. arXiv: 1910.09908 [gr-qc].

[Ciu24] Ignazio Ciufolini. "The General Theory of Relativity and Its Tests in the Solar System". In: *Recent Progress on Gravity Tests: Challenges and Future Perspectives*. Ed. by Cosimo Bambi and Alejandro Cárdenas-Avendaño. Singapore: Springer Nature Singapore, 2024, pp. 27–59. ISBN: 978-981-97-2871-8. DOI: 10.1007/978-981-97-2871-8_2. URL: https://doi.org/10.1007/978-981-97-2871-8_2.

[CK24] Anton Chudaykin and Martin Kunz. "Modified gravity interpretation of the evolving dark energy in light of DESI data". In: (July 2024). arXiv: 2407.02558 [astro-ph.CO].

[CL20] Ramiro Cayuso and Luis Lehner. "Nonlinear, noniterative treatment of EFT-motivated gravity". In: *Phys. Rev. D* 102.8 (2020), p. 084008. DOI: 10.1103/PhysRevD.102.084008. arXiv: 2005.13720 [gr-qc].

[Cli+12] Timothy Clifton et al. "Modified Gravity and Cosmology". In: *Phys. Rept.* 513 (2012), pp. 1–189. DOI: 10.1016/j.physrep.2012.01.001. arXiv: 1106.2476 [astro-ph.CO].

[CM24] Andreas Crivellin and Bruce Mellado. "Anomalies in particle physics and their implications for physics beyond the standard model". In: *Nature Rev. Phys.* 6.5 (2024), pp. 294–309. DOI: 10.1038/s42254-024-00703-6. arXiv: 2309.03870 [hep-ph].

[CM91] J. Carminati and R. G. McLenaghan. "Algebraic invariants of the Riemann tensor in a four-dimensional Lorentzian space". In: *J. Math. Phys.* 32.11 (1991), pp. 3135–3140. DOI: 10.1063/1.529470.

[Col+05] Shaun Cole et al. "The 2dF Galaxy Redshift Survey: Power-spectrum analysis of the final dataset and cosmological implications". In: *Mon. Not. Roy. Astron. Soc.* 362 (2005), pp. 505–534. DOI: 10.1111/j.1365-2966.2005.09318.x. arXiv: astro-ph/0501174.

[COL17] Juan Cayuso, Néstor Ortiz, and Luis Lehner. "Fixing extensions to general relativity in the nonlinear regime". In: *Phys. Rev. D* 96.8 (2017), p. 084043. DOI: 10.1103/PhysRevD.96.084043. arXiv: 1706.07421 [gr-qc].

[Col+24a] The Event Horizon Telescope Collaboration et al. "First Sagittarius A* Event Horizon Telescope Results. VIII. Physical Interpretation of the Polarized Ring". In: *Astrophys. J. Lett.* 964.2 (2024), p. L26. DOI: 10.3847/2041-8213/ad2df1.

[Col+24b] Monica Colpi et al. "LISA Definition Study Report". In: (Feb. 2024). arXiv: 2402.07571 [astro-ph.CO].

[Con+20] Ernesto Contreras et al. "Black hole shadow of a rotating scale–dependent black hole". In: *Phys. Rev. D* 101.6 (2020), p. 064053. DOI: 10.1103/PhysRevD.101.064053. arXiv: 1906.06990 [gr-qc].

[Cor+24] Maxence Corman et al. "Nonlinear studies of modifications to general relativity: Comparing different approaches". In: (May 2024). arXiv: 2405.15581 [gr-qc].

[CP06] Alessandro Codello and Roberto Percacci. "Fixed points of higher derivative gravity". In: *Phys. Rev. Lett.* 97 (2006), p. 221301. DOI: 10.1103/PhysRevLett.97.221301. arXiv: hep-th/0607128.

[CP19] Vitor Cardoso and Paolo Pani. "Testing the nature of dark compact objects: a status report". In: *Living Rev. Rel.* 22.1 (2019), p. 4. DOI: 10.1007/s41114-019-0020-4. arXiv: 1904.05363 [gr-qc].

[CPR08] Alessandro Codello, Roberto Percacci, and Christoph Rahmede. "Ultraviolet properties of f(R)-gravity". In: *Int. J. Mod. Phys. A* 23 (2008), pp. 143–150. DOI: 10.1142/S0217751X08038135. arXiv: 0705.1769 [hep-th].

[CPR09] Alessandro Codello, Roberto Percacci, and Christoph Rahmede. "Investigating the Ultraviolet Properties of Gravity with a Wilsonian Renormalization Group Equation". In: *Annals Phys.* 324 (2009), pp. 414–469. DOI: 10.1016/j.aop.2008.08.008. arXiv: 0805.2909 [hep-th].

[CPR14] Vitor Cardoso, Paolo Pani, and Joao Rico. "On generic parametrizations of spinning black-hole geometries". In: *Phys. Rev. D* 89 (2014), p. 064007. DOI: 10.1103/PhysRevD.89.064007. arXiv: 1401.0528 [gr-qc].

[CR+18] Raúl Carballo-Rubio et al. "Phenomenological aspects of black holes beyond general relativity". In: *Phys. Rev. D* 98.12 (2018), p. 124009. DOI: 10.1103/PhysRevD.98.124009. arXiv: 1809.08238 [gr-qc].

[CR+20] Raúl Carballo-Rubio et al. "Geodesically complete black holes". In: *Phys. Rev. D* 101 (2020), p. 084047. DOI: 10.1103/PhysRevD.101.084047. arXiv: 1911.11200 [gr-qc].

[CR+23a] Raúl Carballo-Rubio et al. "A connection between regular black holes and horizonless ultracompact stars". In: *JHEP* 08 (2023), p. 046. DOI: 10.1007/JHEP08(2023)046. arXiv: 2211.05817 [gr-qc].

[CR+23b] Raúl Carballo-Rubio et al. "Singularity-free gravitational collapse: From regular black holes to horizonless objects". In: (Jan. 2023). arXiv: 2302.00028 [gr-qc].

[CR+24] Raúl Carballo-Rubio et al. "Disentangling photon rings beyond General Relativity with future radio-telescope arrays". In: *JCAP* 05 (2024), p. 103. DOI: 10.1088/1475-7516/2024/05/103. arXiv: 2312.11351 [gr-qc].

[CRCY22] Raúl Carballo-Rubio, Vitor Cardoso, and Ziri Younsi. "Toward very large baseline interferometry observations of black hole structure". In: *Phys. Rev. D* 106.8 (2022), p. 084038. DOI: 10.1103/PhysRevD.106.084038. arXiv: 2208.00704 [gr-qc].

[CRE24] Raúl Carballo-Rubio and Astrid Eichhorn. "Black hole horizons must be veiled by photon spheres". In: (May 2024). arXiv: 2405.08872 [gr-qc].

[CT23] W. W. Campbell and R. Trumpler. "OBSERVATIONS ON THE DEFLECTION OF LIGHT IN PASSING THROUGH THE SUN'S GRAVITATIONAL FIELD, MADE DURING THE TOTAL SOLAR ECLIPSE OF SEPTEMBER 21, 1923". In: *Publications of the Astronomical Society of the Pacific* 35.205 (June 1923), p. 158. DOI: 10.1088/123292a. URL: https://dx.doi.org/10.1088/123292a.

[Cun+17] Pedro V. P. Cunha et al. "Lensing and dynamics of ultracompact bosonic stars". In: *Phys. Rev. D* 96.10 (2017), p. 104040. DOI: 10.1103/PhysRevD.96.104040. arXiv: 1709.06118 [gr-qc].

[Cur17] Erik Curiel. "A Primer on Energy Conditions". In: *Einstein Stud.* 13 (2017), pp. 43–104. DOI: 10.1007/978-1-4939-3210-8_3. arXiv: 1405.0403 [physics.hist-ph].

[CVE01] Clarissa-Marie Claudel, K. S. Virbhadra, and G. F. R. Ellis. "The Geometry of photon surfaces". In: *J. Math. Phys.* 42 (2001), pp. 818–838. DOI: 10.1063/1.1308507. arXiv: gr-qc/0005050.

[Cve+22] Mirjam Cvetic et al. "Snowmass White Paper: String Theory and Particle Physics". In: (Apr. 2022). arXiv: 2204.01742 [hep-th].

[CW73] Sidney R. Coleman and Erick J. Weinberg. "Radiative Corrections as the Origin of Spontaneous Symmetry Breaking". In: *Phys. Rev. D* 7 (1973), pp. 1888–1910. DOI: 10.1103/PhysRevD.7.1888.

[CY20] Zack Carson and Kent Yagi. "Asymptotically flat, parameterized black hole metric preserving Kerr symmetries". In: *Phys. Rev. D* 101.8 (2020), p. 084030. DOI: 10.1103/PhysRevD.101.084030. arXiv: 2002.01028 [gr-qc].

[CY22] Zack Carson and Kent Yagi. "Testing General Relativity with Gravitational Waves". In: *Handbook of Gravitational Wave Astronomy*. Ed. by Cosimo Bambi, Stavros Katsanevas, and Konstantinos D. Kokkotas. Singapore: Springer Nature Singapore, 2022, pp. 1591–1623. ISBN: 978-981-16-4306-4. DOI: 10.1007/978-981-16-4306-4_41. URL: https://doi.org/10.1007/978-981-16-4306-4_41.

[CZ] J. CARMINATI and E. ZAKHARY. "ALGEBRAIC COMPLETENESS FOR THE INVARIANTS OF THE RIEMANN TENSOR". In: *The Ninth Marcel Grossmann Meeting*, pp. 831–834. DOI: 10.1142/9789812777386_0081. eprint: https://www.worldscientific.com/doi/pdf/10.1142/9789812777386_0081. URL: https://www.worldscientific.com/doi/abs/10.1142/9789812777386_0081.

[CZ02] J Carminati and E Zakhary. "Algebraic Completeness for the Invariants of the Riemann Tensor". In: *The Ninth Marcel Grossmann Meeting: On Recent Developments in Theoretical and Experimental General Relativity, Gravitation and Relativistic Field Theories (In 3 Volumes)*. World Scientific. 2002, pp. 831–834.

[D'A24] Edoardo D'Angelo. "Asymptotic safety in Lorentzian quantum gravity". In: *Phys. Rev. D* 109.6 (2024), p. 066012. DOI: 10.1103/PhysRevD.109.066012. arXiv: 2310.20603 [hep-th].

[D'A+24] Edoardo D'Angelo et al. "An Algebraic QFT Approach to the Wetterich Equation on Lorentzian Manifolds". In: *Annales Henri Poincare* 25.4 (2024), pp. 2295–2352. DOI: 10.1007/s00023-023-01348-4. arXiv: 2202.07580 [math-ph].

[Daa+23] Jesse Daas et al. "Probing quadratic gravity with the Event Horizon Telescope". In: *Astron. Astrophys.* 673 (2023), A53. DOI: 10.1051/0004-6361/202244080. arXiv: 2204.08480 [gr-qc].

[Dah21] Pravin Kumar Dahal. "Trapped region in Kerr–Vaidya space–time". In: *J. Astrophys. Astron.* 42.2 (2021), p. 48. DOI: 10.1007/s12036-021-09741-3. arXiv: 2101.02057 [gr-qc].

[Dal+24] Neal Dalal et al. "Probing H0 and resolving AGN disks with ultra-fast photon counters". In: *Phys. Rev. D* 109.12 (2024), p. 123029. DOI: 10.1103/PhysRevD.109.123029. arXiv: 2403.15903 [astro-ph.CO].

[Dat38a] B Datt. "About a Class of Solutions of the Gravitational Equations of Relativity". In: *Zeitschrift fur Physik* 108.5-6 (1938), pp. 314–321.

[Dat38b] B Datt. "Über eine klasse von Lösungen der gravitationsgleichungen der relativität". In: *Zeitschrift für Physik* 108 (1938), pp. 314–321.

[Dav75] P. C. W. Davies. "Scalar particle production in Schwarzschild and Rindler metrics". In: *J. Phys. A* 8 (1975), pp. 609–616. DOI: 10.1088/0305-4470/8/4/022.

[DBB23] Kallol Dey, Enrico Barausse, and Soumen Basak. "Measuring deviations from the Kerr geometry with black hole ringdown". In: *Phys. Rev. D* 108.2 (2023), p. 024064. DOI: 10.1103/PhysRevD.108.024064. arXiv: 2212.10725 [gr-qc].

[DE24] Héloïse Delaporte and Astrid Eichhorn. "The principled-parameterized approach to gravitational collapse". In: (July 2024). arXiv: 2407.07862 [gr-qc].

[DED20] F. W. Dyson, A. S. Eddington, and C. Davidson. "A Determination of the Deflection of Light by the Sun's Gravitational Field, from Observations Made at the Total Eclipse of May 29, 1919". In: *Phil. Trans. Roy. Soc. Lond. A* 220 (1920), pp. 291–333. DOI: 10.1098/rsta.1920.0009.

[DEH22] Héloïse Delaporte, Astrid Eichhorn, and Aaron Held. "Parameterizations of black-hole spacetimes beyond circularity". In: *Class. Quant. Grav.* 39.13 (2022), p. 134002. DOI: 10.1088/1361-6382/ac7027. arXiv: 2203.00105 [gr-qc].

[Des84] Stanley Deser. "Improvement Versus Stability in Gravity Scalar Coupling". In: *Phys. Lett. B* 134 (1984), pp. 419–421. DOI: 10.1016/0370-2693(84)91375-3.

[DF+22] Francesco Di Filippo et al. "On the Inner Horizon Instability of Non-Singular Black Holes". In: *Universe* 8.4 (2022), p. 204. DOI: 10.3390/universe8040204. arXiv: 2203.14516 [gr-qc].

[DFT10] Antonio De Felice and Shinji Tsujikawa. "f(R) theories". In: *Living Rev. Rel.* 13 (2010), p. 3. DOI: 10.12942/lrr-2010-3. arXiv: 1002.4928 [gr-qc].

[DG+23] Loris Del Grosso et al. "Fermion soliton stars". In: *Phys. Rev. D* 108.4 (2023), p. 044024. DOI: 10.1103/PhysRevD.108.044024. arXiv: 2301.08709 [gr-qc].

[DHR20] Jorge F. M. Delgado, Carlos A. R. Herdeiro, and Eugen Radu. "Spinning black holes in shift-symmetric Horndeski theory". In: *JHEP* 04 (2020), p. 180. DOI: 10.1007/JHEP04(2020)180. arXiv: 2002.05012 [gr-qc].

[Dim+20] Alexandru Dima et al. "Spin-induced black hole spontaneous scalarization". In: *Phys. Rev. Lett.* 125.23 (2020), p. 231101. DOI: 10.1103/PhysRevLett.125.231101. arXiv: 2006.03095 [gr-qc].

[DJ92] I H Dwivedi and P S Joshi. "Cosmic censorship violation in non-self-similar Tolman-Bondi models". In: *Classical and Quantum Gravity* 9.7 (July 1992), p. L69. DOI: 10.1088/0264-9381/9/7/001. URL: https://dx.doi.org/10.1088/0264-9381/9/7/001.

[DJ94] I. H. Dwivedi and P. S. Joshi. "On the occurrence of naked singularity in spherically symmetric gravitational collapse". In: *Commun. Math. Phys.* 166 (1994), pp. 117–128. DOI: 10.1007/BF02099303. arXiv: gr-qc/9405049.

[DM13] Juergen A. Dietz and Tim R. Morris. "Asymptotic safety in the f(R) approximation". In: *JHEP* 01 (2013), p. 108. DOI: 10.1007/JHEP01(2013)108. arXiv: 1211.0955 [hep-th].

[DM22] John F. Donoghue and Gabriel Menezes. "On quadratic gravity". In: *Nuovo Cim. C* 45.2 (2022), p. 26. DOI: 10.1393/ncc/i2022-22026-7. arXiv: 2112.01974 [hep-th].

[DMDMRG23] I. De Martino, R. Della Monica, and D. Rubiera-Garcia. "Optical appearance of a nonsingular de Sitter core black hole geometry under several thin disk emissions". In: *Phys. Rev. D* 108.12 (2023), p. 124054. DOI: 10.1103/PhysRevD.108.124054. arXiv: 2310.11039 [gr-qc].

[Doe+01] S. S. Doeleman et al. "Structure of sagittarius a* at 86 ghz using vlbi closure quantities". In: *Astron. J.* 121 (2001), p. 2610. DOI: 10.1086/320376. arXiv: astro-ph/0102232.

[Doe+23] Sheperd S. Doeleman et al. "Reference Array and Design Consideration for the Next-Generation Event Horizon Telescope". In: *Galaxies* 11.5 (2023), p. 107. DOI: 10.3390/galaxies11050107. arXiv: 2306.08787 [astro-ph.IM].

[Don20] John F. Donoghue. "A Critique of the Asymptotic Safety Program". In: *Front. in Phys.* 8 (2020), p. 56. DOI: 10.3389/fphy.2020.00056. arXiv: 1911.02967 [hep-th].

[Don23] John F. Donoghue. "Quantum General Relativity and Effective Field Theory". In: 2023. DOI: 10.1007/978-981-19-3079-9_1-1. arXiv: 2211.09902 [hep-th].

[Don+24] Daniela D. Doneva et al. "Spontaneous scalarization". In: *Rev. Mod. Phys.* 96.1 (2024), p. 015004. DOI: 10.1103/RevModPhys.96.015004. arXiv: 2211.01766 [gr-qc].

[Don95] John F. Donoghue. "Introduction to the effective field theory description of gravity". In: *Advanced School on Effective Theories*. June 1995. arXiv: gr-qc/9512024.

[DP19] Deniz O. Devecioglu and Mu-In Park. "Birkhoff's theorem in Hořava gravity". In: *Phys. Rev. D* 99.10 (2019), p. 104068. DOI: 10.1103/PhysRevD.99.104068. arXiv: 1804.05698 [hep-th].

[DS91] Thibault Damour and Gerhard Schaefer. "New tests of the strong equivalence principle using binary pulsar data". In: *Phys. Rev. Lett.* 66 (1991), pp. 2549–2552. DOI: 10.1103/PhysRevLett.66.2549.

[DSZ15] Maximilian Demmel, Frank Saueressig, and Omar Zanusso. "A proper fixed functional for four-dimensional Quantum Einstein Gravity". In: *JHEP* 08 (2015), p. 113. DOI: 10.1007/JHEP08(2015)113. arXiv: 1504.07656 [hep-th].

[DT20a] Pravin Kumar Dahal and Daniel R. Terno. "Kerr-Vaidya black holes". In: *Phys. Rev. D* 102 (2020), p. 124032. DOI: 10.1103/PhysRevD.102.124032. arXiv: 2008.13370 [gr-qc].

[DT20b] Shane W. Davis and Alexander Tchekhovskoy. "Magnetohydrodynamics Simulations of Active Galactic Nucleus Disks and Jets". In: *Ann. Rev. Astron. Astrophys.* 58 (2020), pp. 407–439. DOI: 10.1146/annurev-astro-081817-051905. arXiv: 2101.08839 [astro-ph.HE].

[Dup+21] N. Dupuis et al. "The nonperturbative functional renormalization group and its applications". In: *Phys. Rept.* 910 (2021), pp. 1–114. DOI: 10.1016/j.physrep.2021.01.001. arXiv: 2006.04853 [cond-mat.stat-mech].

[DY18] Daniela D. Doneva and Stoytcho S. Yazadjiev. "New Gauss-Bonnet Black Holes with Curvature-Induced Scalarization in Extended Scalar-Tensor Theories". In: *Phys. Rev. Lett.* 120.13 (2018), p. 131103. DOI: 10.1103/PhysRevLett.120.131103. arXiv: 1711.01187 [gr-qc].

[Dym92] I. Dymnikova. "Vacuum nonsingular black hole". In: *Gen. Rel. Grav.* 24 (1992), pp. 235–242. DOI: 10.1007/BF00760226.

[DZ+24] Luca Del Zanna et al. "A GPU-Accelerated Modern Fortran Version of the ECHO Code for Relativistic Magnetohydrodynamics". In: (Jan. 2024). arXiv: 2401.03008 [astro-ph.HE].

[EGH23] Astrid Eichhorn, Roman Gold, and Aaron Held. "Horizonless Spacetimes As Seen by Present and Next-generation Event Horizon Telescope Arrays". In: *Astrophys. J.* 950.2 (2023), p. 117. DOI: 10.3847/1538-4357/accced. arXiv: 2205.14883 [astro-ph.HE].

[EGJ65] H. Epstein, V. Glaser, and A. Jaffe. "Nonpositivity of energy density in Quantized field theories". In: *Nuovo Cim.* 36 (1965), p. 1016. DOI: 10.1007/BF02749799.

[EH21a] Astrid Eichhorn and Aaron Held. "From a locality-principle for new physics to image features of regular spinning black holes with disks". In: *JCAP* 05 (2021), p. 073. DOI: 10.1088/1475-7516/2021/05/073. arXiv: 2103.13163 [gr-qc].

[EH21b] Astrid Eichhorn and Aaron Held. "Image features of spinning regular black holes based on a locality principle". In: *Eur. Phys. J. C* 81.10 (2021), p. 933. DOI: 10.1140/epjc/s10052-021-09716-2. arXiv: 2103.07473 [gr-qc].

[EH22] Astrid Eichhorn and Aaron Held. "Black holes in asymptotically safe gravity and beyond". In: (Dec. 2022). arXiv: 2212.09495 [gr-qc].

[EH23] Astrid Eichhorn and Aaron Held. "Quantum gravity lights up spinning black holes". In: *JCAP* 01 (2023), p. 032. DOI: 10.1088/1475-7516/2023/01/032. arXiv: 2206.11152 [gr-qc].

[EHJ23] Astrid Eichhorn, Aaron Held, and Philipp-Vincent Johannsen. "Universal signatures of singularity-resolving physics in photon rings of black holes and horizonless objects". In: *JCAP* 01 (2023), p. 043. DOI: 10.1088/1475-7516/2023/01/043. arXiv: 2204.02429 [gr-qc].

[Eic19] Astrid Eichhorn. "An asymptotically safe guide to quantum gravity and matter". In: *Front. Astron. Space Sci.* 5 (2019), p. 47. DOI: 10.3389/fspas.2018.00047. arXiv: 1810.07615 [hep-th].

[Eic+23] Astrid Eichhorn et al. "Breaking black-hole uniqueness at supermassive scales". In: (Dec. 2023). arXiv: 2312.11430 [gr-qc].

[Eic+24] Astrid Eichhorn et al. "The Absolute Swampland". In: (May 2024). arXiv: 2405.20386 [hep-th].

[Ein05] Albert Einstein. "On the electrodynamics of moving bodies". In: *Annalen Phys.* 17 (1905), pp. 891–921. DOI: 10.1002/andp.200590006.

[Ein15a] Albert Einstein. "Explanation of the Perihelion Motion of Mercury from the General Theory of Relativity". In: *Sitzungsber. Preuss. Akad. Wiss. Berlin (Math. Phys.)* 1915 (1915), pp. 831–839.

[Ein15b] Albert Einstein. "The Field Equations of Gravitation". In: *Sitzungsber. Preuss. Akad. Wiss. Berlin (Math. Phys.)* 1915 (1915), pp. 844–847.

[Ein16] Albert Einstein. "The foundation of the general theory of relativity." In: *Annalen Phys.* 49.7 (1916). Ed. by Jong-Ping Hsu and D. Fine, pp. 769–822. DOI: 10.1002/andp.19163540702.

[Eis+05] Daniel J. Eisenstein et al. "Detection of the Baryon Acoustic Peak in the Large-Scale Correlation Function of SDSS Luminous Red Galaxies". In: *Astrophys. J.* 633 (2005), pp. 560–574. DOI: 10.1086/466512. arXiv: astro-ph/0501171.

[Ell94] Ulrich Ellwanger. "FLow equations for N point functions and bound states". In: *Z. Phys. C* 62 (1994). Ed. by B. Geyer and E. M. Ilgenfritz, pp. 503–510. DOI: 10.1007/BF01555911. arXiv: hep-ph/9308260.

[End+17] Solomon Endlich et al. "An effective formalism for testing extensions to General Relativity with gravitational waves". In: *JHEP* 09 (2017), p. 122. DOI: 10.1007/JHEP09(2017)122. arXiv: 1704.01590 [gr-qc].

[EP22] William E. East and Frans Pretorius. "Binary neutron star mergers in Einstein-scalar-Gauss-Bonnet gravity". In: *Phys. Rev. D* 106.10 (2022), p. 104055. DOI: 10.1103/PhysRevD.106.104055. arXiv: 2208.09488 [gr-qc].

[EPZ04] Giampiero Esposito, Diego N. Pelliccia, and Francesco Zaccaria. "Gribov problem for gauge theories: A Pedagogical introduction". In: *Int. J. Geom. Meth. Mod. Phys.* 1 (2004), pp. 423–441. DOI: 10.1142/S0219887804000216. arXiv: hep-th/0404240.

[ER21a] William E. East and Justin L. Ripley. "Dynamics of Spontaneous Black Hole Scalarization and Mergers in Einstein-Scalar-Gauss-Bonnet Gravity". In: *Phys. Rev. Lett.* 127.10 (2021), p. 101102. DOI: 10.1103/PhysRevLett.127.101102. arXiv: 2105.08571 [gr-qc].

[ER21b] William E. East and Justin L. Ripley. "Evolution of Einstein-scalar-Gauss-Bonnet gravity using a modified harmonic formulation". In: *Phys. Rev. D* 103.4 (2021), p. 044040. DOI: 10.1103/PhysRevD.103.044040. arXiv: 2011.03547 [gr-qc].

[ER24] Astrid Eichhorn and Shouryya Ray. "Suppression of proton decay in quantum gravity". In: *Phys. Lett. B* 850 (2024), p. 138529. DOI: 10.1016/j.physletb.2024.138529. arXiv: 2304.06759 [hep-ph].

[ER35] Albert Einstein and N. Rosen. "The Particle Problem in the General Theory of Relativity". In: *Phys. Rev.* 48 (1935), pp. 73–77. DOI: 10.1103/PhysRev.48.73.

[ES22] Astrid Eichhorn and Marc Schiffer. "Asymptotic safety of gravity with matter". In: (Dec. 2022). arXiv: 2212.07456 [hep-th].

[ES23] Jonathan Engle and Simone Speziale. "Spin Foams: Foundations". In: 2023. DOI: 10.1007/978-981-19-3079-9_99-1. arXiv: 2310.20147 [gr-qc].

[Eva+23] Matthew Evans et al. "Cosmic Explorer: A Submission to the NSF MPSAC ngGW Subcommittee". In: (June 2023). arXiv: 2306.13745 [astro-ph.IM].

[Fal+13] K. Falls et al. "A bootstrap towards asymptotic safety". In: (Jan. 2013). arXiv: 1301.4191 [hep-th].

[Fal+16] Kevin Falls et al. "Further evidence for asymptotic safety of quantum gravity". In: *Phys. Rev. D* 93.10 (2016), p. 104022. DOI: 10.1103/PhysRevD.93.104022. arXiv: 1410.4815 [hep-th].

[Fal+18] Kevin Falls et al. "Asymptotic safety of quantum gravity beyond Ricci scalars". In: *Phys. Rev. D* 97.8 (2018), p. 086006. DOI: 10.1103/PhysRevD.97.086006. arXiv: 1801.00162 [hep-th].

[Far13] Valerio Faraoni. "Evolving black hole horizons in General Relativity and alternative gravity". In: *Galaxies* 1.3 (2013), pp. 114–179. DOI: 10.3390/galaxies1030114. arXiv: 1309.4915 [gr-qc].

[Feh+23] Jannik Fehre et al. "Lorentzian Quantum Gravity and the Graviton Spectral Function". In: *Phys. Rev. Lett.* 130.8 (2023), p. 081501. DOI: 10.1103/PhysRevLett.130.081501. arXiv: 2111.13232 [hep-th].

[Fer+22] Pedro G. S. Fernandes et al. "The 4D Einstein–Gauss–Bonnet theory of gravity: a review". In: *Class. Quant. Grav.* 39.6 (2022), p. 063001. DOI: 10.1088/1361-6382/ac500a. arXiv: 2202.13908 [gr-qc].

[Fer23] Pedro G. S. Fernandes. "Rotating black holes in semiclassical gravity". In: *Phys. Rev. D* 108.6 (2023), p. L061502. DOI: 10.1103/PhysRevD.108.L061502. arXiv: 2305.10382 [gr-qc].

[FHK24] Pau Figueras, Aaron Held, and Áron D. Kovács. "Well-posed initial value formulation of general effective field theories of gravity". In: (July 2024). arXiv: 2407.08775 [gr-qc].

[Fis+16] Vincent L. Fish et al. "Persistent Asymmetric Structure of Sagittarius A* on Event Horizon Scales". In: *Astrophys. J.* 820.2 (2016), p. 90. DOI: 10.3847/0004-637X/820/2/90. arXiv: 1602.05527 [astro-ph.GA].

[FKM96] Sergio Ferrara, Ramzi R. Khuri, and Ruben Minasian. "M theory on a Calabi-Yau manifold". In: *Phys. Lett. B* 375 (1996), pp. 81–88. DOI: 10.1016/0370-2693(96)00270-5. arXiv: hep-th/9602102.

[FLR12] Kevin Falls, Daniel F. Litim, and Aarti Raghuraman. "Black Holes and Asymptotically Safe Gravity". In: *Int. J. Mod. Phys. A* 27 (2012), p. 1250019. DOI: 10.1142/S0217751X12500194. arXiv: 1002.0260 [hep-th].

[FLS19] Kevin G. Falls, Daniel F. Litim, and Jan Schröder. "Aspects of asymptotic safety for quantum gravity". In: *Phys. Rev. D* 99.12 (2019), p. 126015. DOI: 10.1103/PhysRevD.99.126015. arXiv: 1810.08550 [gr-qc].

[FM12] Benoit Famaey and Stacy McGaugh. "Modified Newtonian Dynamics (MOND): Observational Phenomenology and Relativistic Extensions". In: *Living Rev. Rel.* 15 (2012), p. 10. DOI: 10.12942/lrr-2012-10. arXiv: 1112.3960 [astro-ph.CO].

[FM13] H. Falcke and S. B. Markoff. "Toward the event horizon—the supermassive black hole in the Galactic Center". In: *Class. Quant. Grav.* 30 (2013), p. 244003. DOI: 10.1088/0264-9381/30/24/244003. arXiv: 1311.1841 [astro-ph.HE].

[FM23] Pedro G. S. Fernandes and David J. Mulryne. "A new approach and code for spinning black holes in modified gravity". In: *Class. Quant. Grav.* 40.16 (2023), p. 165001. DOI: 10.1088/1361-6382/ace232. arXiv: 2212.07293 [gr-qc].

[FMA00] Heino Falcke, Fulvio Melia, and Eric Agol. "Viewing the shadow of the black hole at the galactic center". In: *Astrophys. J. Lett.* 528 (2000), p. L13. DOI: 10.1086/312423. arXiv: astro-ph/9912263.

[FOP20] Kevin Falls, Nobuyoshi Ohta, and Roberto Percacci. "Towards the determination of the dimension of the critical surface in asymptotically safe gravity". In: *Phys. Lett. B* 810 (2020), p. 135773. DOI: 10.1016/j.physletb.2020.135773. arXiv: 2004.04126 [hep-th].

[FP67] L. D. Faddeev and V. N. Popov. "Feynman Diagrams for the Yang-Mills Field". In: *Phys. Lett. B* 25 (1967). Ed. by Jong-Ping Hsu and D. Fine, pp. 29–30. DOI: 10.1016/0370-2693(67)90067-6.

[Fra+22] Nicola Franchini et al. "Fixing the dynamical evolution in scalar-Gauss-Bonnet gravity". In: *Phys. Rev. D* 106.6 (2022), p. 064061. DOI: 10.1103/PhysRevD.106.064061. arXiv: 2206.00014 [gr-qc].

[FSA20] Vincent L. Fish, Maura Shea, and Kazunori Akiyama. "Imaging black holes and jets with a VLBI array including multiple space-based telescopes". In: *Adv. Space Res.* 65 (2020), pp. 821–830. DOI: 10.1016/j.asr.2019.03.029. arXiv: 1903.09539 [astro-ph.IM].

[FTH08] Joshua Frieman, Michael Turner, and Dragan Huterer. "Dark Energy and the Accelerating Universe". In: *Ann. Rev. Astron. Astrophys.* 46 (2008), pp. 385–432. DOI: 10.1146/annurev.astro.46.060407.145243. arXiv: 0803.0982 [astro-ph].

[Ful73] Stephen A. Fulling. "Nonuniqueness of canonical field quantization in Riemannian space-time". In: *Phys. Rev. D* 7 (1973), pp. 2850–2862. DOI: 10.1103/PhysRevD.7.2850.

[FW24] Paulo C. C. Freire and Norbert Wex. "Gravity experiments with radio pulsars". In: *Living Rev. Rel.* 27.1 (2024), p. 5. DOI: 10.1007/s41114-024-00051-y. arXiv: 2407.16540 [gr-qc].

[FW96] Eanna E. Flanagan and Robert M. Wald. "Does back reaction enforce the averaged null energy condition in semiclassical gravity?" In: *Phys. Rev. D* 54 (1996), pp. 6233–6283. DOI: 10.1103/PhysRevD.54.6233. arXiv: gr-qc/9602052.

[Gal+23] Lluís Galbany et al. "An updated measurement of the Hubble constant from near-infrared observations of Type Ia supernovae". In: *Astron. Astrophys.* 679 (2023), A95. DOI: 10.1051/0004-6361/202244893. arXiv: 2209.02546 [astro-ph.CO].

[Gal+24] Peter Galison et al. "The Black Hole Explorer: Using the Photon Ring to Visualize Spacetime Around the Black Hole". In: (June 2024). arXiv: 2406.11671 [gr-qc].

[Gar+23] Gustavo García et al. "High precision numerical sequences of rotating hairy black holes". In: *Phys. Rev. D* 107.8 (2023), p. 084047. DOI: 10.1103/PhysRevD.107.084047. arXiv: 2302.06659 [gr-qc].

[GB93] Eric Gourgoulhon and Silvano Bonazzola. "Noncircular axisymmetric stationary spacetimes". In: *Phys. Rev. D* 48 (6 Sept. 1993), pp. 2635–2652. DOI: 10.1103/PhysRevD.48.2635. URL: https://link.aps.org/doi/10.1103/PhysRevD.48.2635.

[GC24] Rajes Ghosh and Kabir Chakravarti. "Parameterized Non-circular Deviation from the Kerr Paradigm and Its Observational Signatures: Extreme Mass Ratio Inspirals and Lense-Thirring Effect". In: (June 2024). arXiv: 2406.02454 [gr-qc].

[GEG10] Reinhard Genzel, Frank Eisenhauer, and Stefan Gillessen. "The Galactic Center Massive Black Hole and Nuclear Star Cluster". In: *Rev. Mod. Phys.* 82 (2010), pp. 3121–3195. DOI: 10.1103/RevModPhys.82.3121. arXiv: 1006.0064 [astro-ph.GA].

[Gen+00] R. Genzel et al. "Stellar dynamics in the Galactic centre: Proper motions and anisotropy". In: *Mon. Not. Roy. Astron. Soc.* 317 (2000), p. 348. DOI: 10.1046/j.1365-8711.2000.03582.x. arXiv: astro-ph/0001428.

[Gen22] Reinhard Genzel. "Nobel Lecture: A forty-year journey". In: *Reviews of Modern Physics* 94.2 (2022), p. 020501.

[Gen+97] R. Genzel et al. "On the nature of the dark mass in the centre of the Milky Way". In: *Mon. Not. Roy. Astron. Soc.* 291 (1997), pp. 219–234. DOI: 10.1093/mnras/291.1.219.

[Ger+22] Mary Gerhardinger et al. "Well-posed UV completion for simulating scalar Galileons". In: *Phys. Rev. D* 106.4 (2022), p. 043522. DOI: 10.1103/PhysRevD.106.043522. arXiv: 2205.05697 [hep-th].

[Ger68] Robert P. Geroch. "What is a singularity in general relativity?" In: *Annals Phys.* 48 (1968), pp. 526–540. DOI: 10.1016/0003-4916(68)90144-9.

[GGS22] Thomas D. Galley, Flaminia Giacomini, and John H. Selby. "A no-go theorem on the nature of the gravitational field beyond quantum theory". In: *Quantum* 6 (2022), p. 779. DOI: 10.22331/q-2022-08-17-779. arXiv: 2012.01441 [quant-ph].

[Ghe+98] A. M. Ghez et al. "High proper motion stars in the vicinity of Sgr A*: Evidence for a supermassive black hole at the center of our galaxy". In: *Astrophys. J.* 509 (1998), pp. 678–686. DOI: 10.1086/306528. arXiv: astro-ph/9807210.

[Gie+16] Holger Gies et al. "Gravitational Two-Loop Counterterm Is Asymptotically Safe". In: *Phys. Rev. Lett.* 116.21 (2016), p. 211302. DOI: 10.1103/PhysRevLett.116.211302. arXiv: 1601.01800 [hep-th].

[Gil+09] S. Gillessen et al. "Monitoring stellar orbits around the Massive Black Hole in the Galactic Center". In: *Astrophys. J.* 692 (2009), pp. 1075–1109. DOI: 10.1088/0004-637X/692/2/1075. arXiv: 0810.4674 [astro-ph].

[GJ08] Eric Gourgoulhon and Jose Luis Jaramillo. "New theoretical approaches to black holes". In: *New Astron. Rev.* 51 (2008), pp. 791–798. DOI: 10.1016/j.newar.2008.03.026. arXiv: 0803.2944 [astro-ph].

[GK22] Finnian Gray and David Kubiznak. "Slowly rotating black holes with exact Killing tensor symmetries". In: *Phys. Rev. D* 105.6 (2022), p. 064017. DOI: 10.1103/PhysRevD.105.064017. arXiv: 2110.14671 [gr-qc].

[Gla61] S. L. Glashow. "Partial Symmetries of Weak Interactions". In: *Nucl. Phys.* 22 (1961), pp. 579–588. DOI: 10.1016/0029-5582(61)90469-2.

[GnH21] Mariana Graña and Alvaro Herráez. "The Swampland Conjectures: A Bridge from Quantum Gravity to Particle Physics". In: *Universe* 7.8 (2021), p. 273. DOI: 10.3390/universe7080273. arXiv: 2107.00087 [hep-th].

[Gol+17] A. Goldstein et al. "Fermi Observations of the LIGO Event GW170104". In: *Astrophys. J. Lett.* 846.1 (2017), p. L5. DOI: 10.3847/2041-8213/aa8319. arXiv: 1706.00199 [astro-ph.HE].

[Gol19] Roman Gold. "Relativistic Aspects of Accreting Supermassive Black-Hole Binaries in Their Natural Habitat: A Review". In: *Galaxies* 7.2 (2019), p. 63. DOI: 10.3390/galaxies7020063.

[Gol+20] Roman Gold et al. "Verification of Radiative Transfer Schemes for the EHT". In: *Astrophys. J.* 897.2 (2020), p. 148. DOI: 10.3847/1538-4357/ab96c6.

[GP09] Jerry B. Griffiths and Jiri Podolsky. *Exact Space-Times in Einstein's General Relativity*. Cambridge Monographs on Mathematical Physics. Cambridge: Cambridge University Press, 2009. ISBN: 978-1-139-48116-8. DOI: 10.1017/CBO9780511635397.

[Gra24] Philippe Grandclément. "Fully consistent rotating black holes in the cubic Galileon theory". In: *Class. Quant. Grav.* 41.2 (2024), p. 025012. DOI: 10.1088/1361-6382/ad17f1. arXiv: 2308.11245 [gr-qc].

[Gre22] Anne M. Green. "Dark matter in astrophysics/cosmology". In: *SciPost Phys. Lect. Notes* 37 (2022), p. 1. DOI: 10.21468/SciPostPhysLectNotes.37. arXiv: 2109.05854 [hep-ph].

[Gri78] V. N. Gribov. "Quantization of Nonabelian Gauge Theories". In: *Nucl. Phys. B* 139 (1978). Ed. by J. Nyiri, p. 1. DOI: 10.1016/0550-3213(78)90175-X.

[Gru+24] Andrzej Grudka et al. "Renormalisation of postquantum-classical gravity". In: (Feb. 2024). arXiv: 2402.17844 [hep-th].

[GS86] Marc H. Goroff and Augusto Sagnotti. "The Ultraviolet Behavior of Einstein Gravity". In: *Nucl. Phys. B* 266 (1986), pp. 709–736. DOI: 10.1016/0550-3213(86)90193-8.

[GS87] David J. Gross and John H. Sloan. "The Quartic Effective Action for the Heterotic String". In: *Nucl. Phys. B* 291 (1987), pp. 41–89. DOI: 10.1016/0550-3213(87)90465-2.

[GSH20] Jenny E. Greene, Jay Strader, and Luis C. Ho. "Intermediate-Mass Black Holes". In: *Ann. Rev. Astron. Astrophys.* 58 (2020), pp. 257–312. DOI: 10.1146/annurev-astro-032620-021835. arXiv: 1911.09678 [astro-ph.GA].

[Gue+22a] Merce Guerrero et al. "Light ring images of double photon spheres in black hole and wormhole spacetimes". In: *Phys. Rev. D* 105.8 (2022), p. 084057. DOI: 10.1103/PhysRevD.105.084057. arXiv: 2202.03809 [gr-qc].

[Gue+22b] Merce Guerrero et al. "Multiring images of thin accretion disk of a regular naked compact object". In: *Phys. Rev. D* 106.4 (2022), p. 044070. DOI: 10.1103/PhysRevD.106.044070. arXiv: 2205.12147 [gr-qc].

[Guo+23] Sen Guo et al. "Unveiling the unconventional optical signatures of regular black holes within accretion disk". In: *Eur. Phys. J. C* 83.11 (2023), p. 1059. DOI: 10.1140/epjc/s10052-023-12208-0. arXiv: 2310.20523 [gr-qc].

[Gur20] Leonid I. Gurvits. "Space VLBI: from first ideas to operational missions". In: *Advances in Space Research* 65.2 (2020). High-resolution space-borne radio astronomy, pp. 868–876. ISSN: 0273-1177. DOI: https://doi.org/10.1016/j.asr.2019.05.042. URL: https://www.sciencedirect.com/science/article/pii/S0273117719303886.

[Gur+21] Leonid I. Gurvits et al. "THEZA: TeraHertz Exploration and Zooming-in for Astrophysics: An ESA Voyage 2050 White Paper". In: *Exper. Astron.* 51.3 (2021), pp. 559–594. DOI: 10.1007/s10686-021-09714-y. arXiv: 1908.10767 [astro-ph.IM].

[Gur23] Leonid I Gurvits. "A Brief History of Space VLBI". In: *2023 8th IEEE History of Electrotechnology Conference (HISTELCON)*. IEEE. 2023, pp. 171–174.

[Gut81] Alan H. Guth. "The Inflationary Universe: A Possible Solution to the Horizon and Flatness Problems". In: *Phys. Rev. D* 23 (1981). Ed. by Li-Zhi Fang and R. Ruffini, pp. 347–356. DOI: 10.1103/PhysRevD.23.347.

[Gyu+20] Galin Gyulchev et al. "Observational signatures of strongly naked singularities: image of the thin accretion disk". In: *Eur. Phys. J. C* 80.11 (2020), p. 1017. DOI: 10.1140/epjc/s10052-020-08575-7. arXiv: 2003.06943 [gr-qc].

[Gyu+21] Galin Gyulchev et al. "Image of the thin accretion disk around compact objects in the Einstein–Gauss–Bonnet gravity". In: *Eur. Phys. J. C* 81.10 (2021), p. 885. DOI: 10.1140/epjc/s10052-021-09624-5. arXiv: 2106.14697 [gr-qc].

[HA24] Chris M. Harrison and Cristina Ramos Almeida. "Observational Tests of Active Galactic Nuclei Feedback: An Overview of Approaches and Interpretation". In: *Galaxies* 12.2 (2024), p. 17. DOI: 10.3390/galaxies12020017. arXiv: 2404.08050 [astro-ph.GA].

[Häb+24] Maximilian Häberle et al. "Fast-moving stars around an intermediate-mass black hole in ω Centauri". In: *Nature* 631.8020 (2024), pp. 285–288.

[Had+13] Kazuhiro Hada et al. "Innermost collimation structure of the M87 jet down to ~ten Schwarzschild radii". In: *Astrophys. J.* 775 (2013), p. 70. DOI: 10.1088/0004-637X/775/1/70. arXiv: 1308.1411 [astro-ph.CO].

[Har+22] Daniel Harlow et al. "TF1 Snowmass Report: Quantum gravity, string theory, and black holes". In: (Oct. 2022). arXiv: 2210.01737 [hep-th].

[Haw+19] Kari Haworth et al. "Studying black holes on horizon scales with space-VLBI". In: (Sept. 2019). arXiv: 1909.01405 [astro-ph.IM].

[Haw74] S. W. Hawking. "Black hole explosions". In: *Nature* 248 (1974), pp. 30–31. DOI: 10.1038/248030a0.

[Haw75] S. W. Hawking. "Particle Creation by Black Holes". In: *Commun. Math. Phys.* 43 (1975). Ed. by G. W. Gibbons and S. W. Hawking. [Erratum: Commun.Math.Phys. 46, 206 (1976)], pp. 199–220. DOI: 10.1007/BF02345020.

[Haw76] S. W. Hawking. "Breakdown of Predictability in Gravitational Collapse". In: *Phys. Rev. D* 14 (1976), pp. 2460–2473. DOI: 10.1103/PhysRevD.14.2460.

[Hay06] Sean A. Hayward. "Formation and evaporation of regular black holes". In: *Phys. Rev. Lett.* 96 (2006), p. 031103. DOI: 10.1103/PhysRevLett.96.031103. arXiv: gr-qc/0506126.

[HB24] J. E. Herrera and Y. Bonder. "Unimodular gravity as an initial value problem". In: *Phys. Rev. D* 109.10 (2024), p. 104025. DOI: 10.1103/PhysRevD.109.104025. arXiv: 2402.00141 [gr-qc].

[HBT54] R. Hanbury Brown and R. Q. Twiss. "A New type of interferometer for use in radio astronomy". In: *Phil. Mag. Ser. 7* 45 (1954), pp. 663–682. DOI: 10.1080/14786440708520475.

[HD83] R. w. Hellings and G. s. Downs. "UPPER LIMITS ON THE ISOTROPIC GRAVITATIONAL RADIATION BACKGROUND FROM PULSAR TIMING ANALYSIS". In: *Astrophys. J. Lett.* 265 (1983), pp. L39–L42. DOI: 10.1086/183954.

[He+20] Peng-Zhang He et al. "Shadows of rotating Hayward–de Sitter black holes with astrometric observables". In: *Eur. Phys. J. C* 80.12 (2020), p. 1195. DOI: 10.1140/epjc/s10052-020-08707-z. arXiv: 2009.06705 [gr-qc].

[HE23] Stephen W. Hawking and George F. R. Ellis. *The Large Scale Structure of Space-Time*. Cambridge Monographs on Mathematical Physics. Cambridge University Press, Feb. 2023. ISBN: 978-1-009-25316-1, 978-1-009-25315-4, 978-0-521-20016-5, 978-0-521-09906-6, 978-0-511-82630-6, 978-0-521-09906-6. DOI: 10.1017/9781009253161.

[Hel21] Aaron Held. "Invariant Renormalization-Group improvement". In: (May 2021). arXiv: 2105.11458 [gr-qc].

[Her+21] Carlos A. R. Herdeiro et al. "Spin-induced scalarized black holes". In: *Phys. Rev. Lett.* 126.1 (2021), p. 011103. DOI: 10.1103/PhysRevLett.126.011103. arXiv: 2009.03904 [gr-qc].

[Her80] Eduard Herlt. "Kerr-Schild-Vaidya fields with axial symmetry". In: *General Relativity and Gravitation* 12 (1980), pp. 1–7.

[HGE19] Aaron Held, Roman Gold, and Astrid Eichhorn. "Asymptotic safety casts its shadow". In: *JCAP* 06 (2019), p. 029. DOI: 10.1088/1475-7516/2019/06/029. arXiv: 1904.07133 [gr-qc].

[Him+20] Elizabeth Himwich et al. "Universal polarimetric signatures of the black hole photon ring". In: *Phys. Rev. D* 101.8 (2020), p. 084020. DOI: 10.1103/PhysRevD.101.084020. arXiv: 2001.08750 [gr-qc].

[HKM24] Hyat Huang, Jutta Kunz, and Deeshani Mitra. "Shadow images of compact objects in beyond Horndeski theory". In: *JCAP* 05 (2024), p. 007. DOI: 10.1088/1475-7516/2024/05/007. arXiv: 2401.15249 [gr-qc].

[Hod13] Shahar Hod. "Upper bound on the radii of black-hole photonspheres". In: *Phys. Lett. B* 727 (2013), pp. 345–348. DOI: 10.1016/j.physletb.2013.10.047. arXiv: 1701.06587 [gr-qc].

[Hoh21] Manuel Hohmann. "Parametrized Post-Newtonian Formalism". In: *Modified Gravity and Cosmology: An Update by the CANTATA Network*. Ed. by Emmanuel N. Saridakis et al. Cham: Springer International Publishing, 2021, pp. 357–373. ISBN: 978-3-030-83715-0. DOI: 10.1007/978-3-030-83715-0_24. URL: https://doi.org/10.1007/978-3-030-83715-0_24.

[Hol22] Bob Holdom. "2-2-holes simplified". In: *Phys. Lett. B* 830 (2022), p. 137142. DOI: 10.1016/j.physletb.2022.137142. arXiv: 2202.08442 [gr-qc].

[Hos05] Golam Mortuza Hossain. "On energy conditions and stability in effective loop quantum cosmology". In: *Class. Quant. Grav.* 22 (2005), pp. 2653–2670. DOI: 10.1088/0264-9381/22/13/009. arXiv: gr-qc/0503065.

[Hou+23] Jiamin Hou et al. "Cosmological Probes of Structure Growth and Tests of Gravity". In: *Universe* 9.7 (2023), p. 302. DOI: 10.3390/universe9070302. arXiv: 2306.13726 [gr-qc].

[HP02] Wolfgang Hasse and Volker Perlick. "Gravitational lensing in spherically symmetric static space-times with centrifugal force reversal". In: *Gen. Rel. Grav.* 34 (2002), pp. 415–433. DOI: 10.1023/A:1015384604371. arXiv: gr-qc/0108002.

[HP23] Dirk Heumann and Dimitrios Psaltis. "Identifying the event horizons of parametrically deformed black-hole metrics". In: *Phys. Rev. D* 107.4 (2023), p. 044015. DOI: 10.1103/PhysRevD.107.044015. arXiv: 2205.12994 [gr-qc].

[HR15] Hal M. Haggard and Carlo Rovelli. "Quantum-gravity effects outside the horizon spark black to white hole tunneling". In: *Phys. Rev. D* 92.10 (2015), p. 104020. DOI: 10.1103/PhysRevD.92.104020. arXiv: 1407.0989 [gr-qc].

[HR17] Bob Holdom and Jing Ren. "Not quite a black hole". In: *Phys. Rev. D* 95.8 (2017), p. 084034. DOI: 10.1103/PhysRevD.95.084034. arXiv: 1612.04889 [gr-qc].

[HS24] Gregory W. Horndeski and Alessandra Silvestri. "50 Years of Horndeski Gravity: Past, Present and Future". In: *Int. J. Theor. Phys.* 63.2 (2024), p. 38. DOI: 10.1007/s10773-024-05558-2. arXiv: 2402.07538 [gr-qc].

[Hub29] Edwin Hubble. "A relation between distance and radial velocity among extra-galactic nebulae". In: *Proc. Nat. Acad. Sci.* 15 (1929), pp. 168–173. DOI: 10.1073/pnas.15.3.168.

[Hug71] Lane P. Hughston. "Generalized Vaidya metrics". In: *International Journal of Theoretical Physics* 4.4 (Aug. 1971), pp. 267–271. DOI: 10.1007/BF00674279.

[Hul94] Russell A. Hulse. "The discovery of the binary pulsar". In: *Rev. Mod. Phys.* 66 (1994), pp. 699–710. DOI: 10.1103/RevModPhys.66.699.

[HZ23] Aaron Held and Jun Zhang. "Instability of spherically symmetric black holes in quadratic gravity". In: *Phys. Rev. D* 107.6 (2023), p. 064060. DOI: 10.1103/PhysRevD.107.064060. arXiv: 2209.01867 [gr-qc].

[IS03] Kunihito Ioka and Misao Sasaki. "Grad-Shafranov equation in non-circular stationary axisymmetric space-times". In: *Phys. Rev. D* 67 (2003), p. 124026. DOI: 10.1103/PhysRevD.67.124026. arXiv: gr-qc/0302106.

[IS04] Kunihito Ioka and Misao Sasaki. "Relativistic stars with poloidal and toroidal magnetic fields and meridional flow". In: *Astrophys. J.* 600 (2004), pp. 296–316. DOI: 10.1086/379650. arXiv: astro-ph/0305352.

[Isb+22] Jacob W Isbell et al. "The dusty heart of Circinus-I. Imaging the circumnuclear dust in N-band". In: *Astronomy & Astrophysics* 663 (2022), A35.

[Isl+23] Shafqat Ul Islam et al. "Investigating Loop Quantum Gravity with Event Horizon Telescope Observations of the Effects of Rotating Black Holes". In: *Astrophys. J.* 943.1 (2023), p. 22. DOI: 10.3847/1538-4357/aca411. arXiv: 2211.06653 [gr-qc].

[Isr67] Werner Israel. "Event horizons in static vacuum space-times". In: *Phys. Rev.* 164 (1967), pp. 1776–1779. DOI: 10.1103/PhysRev.164.1776.

[Isr85] Werner Israel. "General relativity: progress, problems, and prospects". In: *Canadian journal of physics* 63.1 (1985), pp. 34–43.

[Isr86] Werner Israel. "The formation of black holes in nonspherical collapse and cosmic censorship". In: *Canadian journal of Physics* 64.2 (1986), pp. 120–127.

[Iss+23] Sara Issaoun et al. "Enabling transformational ngEHT science via the inclusion of 86 GHz capabilities". In: *Galaxies* 11.1 (2023), p. 28.

[IWW24] Gino Isidori, Felix Wilsch, and Daniel Wyler. "The standard model effective field theory at work". In: *Rev. Mod. Phys.* 96.1 (2024), p. 015006. DOI: 10.1103/RevModPhys.96.015006. arXiv: 2303.16922 [hep-ph].

[JD92] P. S. Joshi and I. H. Dwivedi. "The Structure of Naked Singularity in Self-Similar Gravitational Collapse". In: *Commun. Math. Phys.* 146 (1992), pp. 333–342. DOI: 10.1007/BF02102631.

[JD93] P. S. Joshi and I. H. Dwivedi. "The Structure of naked singularity in selfsimilar gravitational collapse. 2." In: *Lett. Math. Phys.* 27 (1993), p. 235. DOI: 10.1007/BF00739581. arXiv: gr-qc/9302008.

[JD99] P. S. Joshi and I. H. Dwivedi. "Initial data and the end state of spherically symmetric gravitational collapse". In: *Class. Quant. Grav.* 16 (1999), pp. 41–59. DOI: 10.1088/0264-9381/16/1/003. arXiv: gr-qc/9804075.

[Jeb05] Jørg T Jebsen. "On the general spherically symmetric solutions of Einstein's gravitational equations in vacuo". In: *General Relativity and Gravitation* 37.12 (2005), pp. 2253–2259.

[Jeb21] Jørg Tofte Jebsen. *Über die allgemeinen kugelsymmetrischen Lösungen der Einstein'schen Gravitationsgleichungen im Vakuum*. Almqvist & Wiksell, 1921.

[Jef21] George Barker Jeffery. "The field of an electron on Einstein's theory of gravitation". In: *Proceedings of the Royal Society of London. Series A, Containing Papers of a Mathematical and Physical Character* 99.697 (1921), pp. 123–134.

[Jen58] RC Jennison. "A phase sensitive interferometer technique for the measurement of the Fourier transforms of spatial brightness distributions of small angular extent". In: *Monthly Notices of the Royal Astronomical Society* 118.3 (1958), pp. 276–284.

[Jia+19] Yan-Fei Jiang et al. "Global Radiation Magneto-hydrodynamic Simulations of Sub-Eddington Accretion Disks around Supermassive Black Holes". In: (Apr. 2019). DOI: 10.3847/1538-4357/ab4a00. arXiv: 1904.01674 [astro-ph.HE].

[Jia+24] He Jia et al. "Photon Ring Interferometric Signatures Beyond The Universal Regime". In: (May 2024). arXiv: 2405.08804 [astro-ph.HE].

[JM11] Pankaj S. Joshi and Daniele Malafarina. "Recent developments in gravitational collapse and spacetime singularities". In: *Int. J. Mod. Phys. D* 20 (2011), pp. 2641–2729. DOI: 10.1142/S0218271811020792. arXiv: 1201.3660 [gr-qc].

[Joh13a] Tim Johannsen. "Regular Black Hole Metric with Three Constants of Motion". In: *Phys. Rev. D* 88.4 (2013), p. 044002. DOI: 10.1103/PhysRevD.88.044002. arXiv: 1501.02809 [gr-qc].

[Joh13b] Tim Johannsen. "Systematic Study of Event Horizons and Pathologies of Parametrically Deformed Kerr Spacetimes". In: *Phys. Rev. D* 87.12 (2013), p. 124017. DOI: 10.1103/PhysRevD.87.124017. arXiv: 1304.7786 [gr-qc].

[Joh+20] Michael D. Johnson et al. "Universal interferometric signatures of a black hole's photon ring". In: *Sci. Adv.* 6.12 (2020), eaaz1310. DOI: 10.1126/sciadv.aaz1310. arXiv: 1907.04329 [astro-ph.IM].

[Joh+23] Michael D. Johnson et al. "Key Science Goals for the Next-Generation Event Horizon Telescope". In: *Galaxies* 11.3 (2023), p. 61. DOI: 10.3390/galaxies11030061. arXiv: 2304.11188 [astro-ph.HE].

[Joh+24] Michael D. Johnson et al. "The Black Hole Explorer: Motivation and Vision". In: June 2024. arXiv: 2406.12917 [astro-ph.IM].

[JP11] Tim Johannsen and Dimitrios Psaltis. "A Metric for Rapidly Spinning Black Holes Suitable for Strong-Field Tests of the No-Hair Theorem". In: *Phys. Rev. D* 83 (2011), p. 124015. DOI: 10.1103/PhysRevD.83.124015. arXiv: 1105.3191 [gr-qc].

[Kaw23] S. Kawamura. "Space gravitational wave antenna DECIGO and B-DECIGO". In: *16th Marcel Grossmann Meeting on Recent Developments in Theoretical and Experimental General Relativity, Astrophysics and Relativistic Field Theories*. 2023. DOI: 10.1142/9789811269776_0267.

[Kaw+24] Tomohisa Kawashima et al. "Black hole spacetime and properties of accretion flows and jets probed by Black Hole Explorer: science cases proposed by BHEX Japan team". In: *Proc. SPIE Int. Soc. Opt. Eng.* 13092 (2024), p. 130926X. DOI: 10.1117/12.3018053. arXiv: 2406.09995 [astro-ph.HE].

[Kay23] Bernard S. Kay. "Quantum Field Theory in Curved Spacetime (2nd Edition)". In: (Aug. 2023). arXiv: 2308.14517 [gr-qc].

[KB21] Jitendra Kumar and Puja Bharti. "The classification of interior solutions of anisotropic fluid configurations". In: (Dec. 2021). arXiv: 2112.12518 [gr-qc].

[KBP22] Panagiota Kanti, Athanasios Bakopoulos, and Nikolaos Pappas. "Scalar-Gauss-Bonnet theories: Evasion of no-hair theorems and novel black-hole solutions". In: *15th Marcel Grossmann Meeting on Recent Developments in Theoretical and Experimental General Relativity, Astrophysics, and Relativistic Field Theories*. 2022. DOI: 10.1142/9789811258251_0080.

[KC20] Folkert Kuipers and Xavier Calmet. "Singularity theorems in the effective field theory for quantum gravity at second order in curvature". In: *Universe* 6.10 (2020), p. 171. DOI: 10.3390/universe6100171. arXiv: 1911.05571 [gr-qc].

[KD13] Ayman Bin Kamruddin and Jason Dexter. "A geometric crescent model for black hole images". In: *Mon. Not. Roy. Astron. Soc.* 434 (2013), p. 765. DOI: 10.1093/mnras/stt1068. arXiv: 1306.3226 [astro-ph.HE].

[Ker63] Roy P. Kerr. "Gravitational field of a spinning mass as an example of algebraically special metrics". In: *Phys. Rev. Lett.* 11 (1963), pp. 237–238. DOI: 10.1103/PhysRevLett.11.237.

[KG21] Rahul Kumar and Sushant G. Ghosh. "Photon ring structure of rotating regular black holes and no-horizon spacetimes". In: *Class. Quant. Grav.* 38.8 (2021), p. 8. DOI: 10.1088/1361-6382/abdd48. arXiv: 2004.07501 [gr-qc].

[KK23] B. Kleihaus and J. Kunz. "Black Holes in Alternative Theories of Gravity". In: *Astron. Rep.* 67.Suppl 2 (2023), S108–S114. DOI: 10.1134/S106377292314010X.

[KKPM21] Polychronis S. Koliogiannis, Alkiviadis Kanakis-Pegios, and Charalampos C. Moustakidis. "Neutron Stars and Gravitational Waves: The Key Role of Nuclear Equation of State". In: *Foundations* 1.2 (2021), pp. 217–255. DOI: 10.3390/foundations1020017. arXiv: 2110.13557 [nucl-th].

[KKR11] Burkhard Kleihaus, Jutta Kunz, and Eugen Radu. "Rotating Black Holes in Dilatonic Einstein-Gauss-Bonnet Theory". In: *Phys. Rev. Lett.* 106 (2011), p. 151104. DOI: 10.1103/PhysRevLett.106.151104. arXiv: 1101.2868 [gr-qc].

[KKS97] Anne J Kox, Martin J Klein, and Robert Schulmann. "The collected papers of albert einstein; volume 6 the berlin years: Writings 1914-1917". In: *European Journal of Physics* 18.1 (1997), p. 52.

[Kle+16] Burkhard Kleihaus et al. "Spinning black holes in Einstein–Gauss-Bonnet–dilaton theory: Nonperturbative solutions". In: *Phys. Rev. D* 93.4 (2016), p. 044047. DOI: 10.1103/PhysRevD.93.044047. arXiv: 1511.05513 [gr-qc].

[Kle+23] Joost de Kleuver et al. "Testing the Existence of Event Horizons against Rotating Reflecting Surfaces". In: (Nov. 2023). arXiv: 2311.05555 [gr-qc].

[KLM21] Mohsen Khodadi, Gaetano Lambiase, and David F. Mota. "No-hair theorem in the wake of Event Horizon Telescope". In: *JCAP* 09 (2021), p. 028. DOI: 10.1088/1475-7516/2021/09/028. arXiv: 2107.00834 [gr-qc].

[Kob19] Tsutomu Kobayashi. "Horndeski theory and beyond: a review". In: *Rept. Prog. Phys.* 82.8 (2019), p. 086901. DOI: 10.1088/1361-6633/ab2429. arXiv: 1901.07183 [gr-qc].

[Koc+21] Prashant Kocherlakota et al. "Constraints on black-hole charges with the 2017 EHT observations of M87*". In: *Phys. Rev. D* 103.10 (2021), p. 104047. DOI: 10.1103/PhysRevD.103.104047. arXiv: 2105.09343 [gr-qc].

[Koc+23] Prashant Kocherlakota et al. "Toward General Relativistic Magnetohydrodynamics Simulations in Stationary Nonvacuum Spacetimes". In: *Astrophys. J. Lett.* 956.1 (2023), p. L11. DOI: 10.3847/2041-8213/acfd1f. arXiv: 2307.15140 [astro-ph.HE].

[Koc+24] Prashant Kocherlakota et al. "Prospects for future experimental tests of gravity with black hole imaging: Spherical symmetry". In: *Phys. Rev. D* 109.6 (2024), p. 064064. DOI: 10.1103/PhysRevD.109.064064. arXiv: 2307.16841 [gr-qc].

[Kog+22] Yasutaka Koga et al. "Dynamical photon sphere and time evolving shadow around black holes with temporal accretion". In: *Phys. Rev. D* 105.10 (2022), p. 104040. DOI: 10.1103/PhysRevD.105.104040. arXiv: 2202.00201 [gr-qc].

[Kov+02] John Kovac et al. "Detection of polarization in the cosmic microwave background using DASI". In: *Nature* 420 (2002), pp. 772–787. DOI: 10.1038/nature01269. arXiv: astro-ph/0209478.

[Kov+07] Y. Y. Kovalev et al. "The Inner Jet of the Radio Galaxy M87". In: *Astrophys. J. Lett.* 668 (2007), p. L27. DOI: 10.1086/522603. arXiv: 0708.2695 [astro-ph].

[Kov19] Áron D. Kovács. "Well-posedness of cubic Horndeski theories". In: *Phys. Rev. D* 100.2 (2019), p. 024005. DOI: 10.1103/PhysRevD.100.024005. arXiv: 1904.00963 [gr-qc].

[KP22] Benjamin Knorr and Alessia Platania. "Sifting quantum black holes through the principle of least action". In: *Phys. Rev. D* 106.2 (2022), p. L021901. DOI: 10.1103/PhysRevD.106.L021901. arXiv: 2202.01216 [hep-th].

[KR20a] Prashant Kocherlakota and Luciano Rezzolla. "Accurate mapping of spherically symmetric black holes in a parameterised framework". In: *Phys. Rev. D* 102.6 (2020), p. 064058. DOI: 10.1103/PhysRevD.102.064058. arXiv: 2007.15593 [gr-qc].

[KR20b] Áron D. Kovács and Harvey S. Reall. "Well-posed formulation of Lovelock and Horndeski theories". In: *Phys. Rev. D* 101.12 (2020), p. 124003. DOI: 10.1103/PhysRevD.101.124003. arXiv: 2003.08398 [gr-qc].

[KR22] Prashant Kocherlakota and Luciano Rezzolla. "Distinguishing gravitational and emission physics in black hole imaging: spherical symmetry". In: *Mon. Not. Roy. Astron. Soc.* 513.1 (2022), pp. 1229–1243. DOI: 10.1093/mnras/stac891. arXiv: 2201.05641 [gr-qc].

[Kra+21] M. Kramer et al. "Strong-Field Gravity Tests with the Double Pulsar". In: *Phys. Rev. X* 11.4 (2021), p. 041050. DOI: 10.1103/PhysRevX.11.041050. arXiv: 2112.06795 [astro-ph.HE].

[KRZ16] Roman Konoplya, Luciano Rezzolla, and Alexander Zhidenko. "General parametrization of axisymmetric black holes in metric theories of gravity". In: *Phys. Rev. D* 93.6 (2016), p. 064015. DOI: 10.1103/PhysRevD.93.064015. arXiv: 1602.02378 [gr-qc].

[KS09] R. P. Kerr and A. Schild. "Republication of: A new class of vacuum solutions of the Einstein field equations". In: *Gen. Rel. Grav.* 41.10 (2009), pp. 2485–2499. DOI: 10.1007/s10714-009-0857-z.

[KS20] Eleni-Alexandra Kontou and Ko Sanders. "Energy conditions in general relativity and quantum field theory". In: *Class. Quant. Grav.* 37.19 (2020), p. 193001. DOI: 10.1088/1361-6382/ab8fcf. arXiv: 2003.01815 [gr-qc].

[KSG20] Rahul Kumar, Balendra Pratap Singh, and Sushant G. Ghosh. "Shadow and deflection angle of rotating black hole in asymptotically safe gravity". In: *Annals Phys.* 420 (2020), p. 168252. DOI: 10.1016/j.aop.2020.168252. arXiv: 1904.07652 [gr-qc].

[KT66] Wolfgang Kundt and M. Trumper. "Orthogonal decomposition of axi-symmetric stationary spacetimes". In: *Z. Phys.* 192 (1966), pp. 419–422. DOI: 10.1007/BF01325677.

[Kum+24a] Rajesh Kumar et al. "Theoretical and experimental constraints for the equation of state of dense and hot matter". In: *Living Rev. Rel.* 27.1 (2024), p. 3. DOI: 10.1007/s41114-024-00049-6. arXiv: 2303.17021 [nucl-th].

[Kum+24b] Shailesh Kumar et al. "Exploring waveforms with non-GR deviations for extreme mass-ratio inspirals". In: (May 2024). arXiv: 2405.18508 [gr-qc].

[Kur84a] Yuhji Kuroda. "NAKED SINGULARITIES IN THE VAIDYA SPACETIME". In: (Jan. 1984).

[Kur84b] Yuhji Kuroda. "Naked singularities in the Vaidya spacetime". In: *Progress of theoretical physics* 72.1 (1984), pp. 63–72.

[KW23] Rahul Kumar Walia. "Observational predictions of LQG motivated polymerized black holes and constraints from Sgr A* and M87*". In: *JCAP* 03 (2023), p. 029. DOI: 10.1088/1475-7516/2023/03/029. arXiv: 2207.02106 [gr-qc].

[KWGM22] Rahul Kumar Walia, Sushant G. Ghosh, and Sunil D. Maharaj. "Testing Rotating Regular Metrics with EHT Results of Sgr A*". In: *Astrophys. J.* 939.2 (2022), p. 77. DOI: 10.3847/1538-4357/ac9623. arXiv: 2207.00078 [gr-qc].

[L+15] H. Lü et al. "Spherically Symmetric Solutions in Higher-Derivative Gravity". In: *Phys. Rev. D* 92.12 (2015), p. 124019. DOI: 10.1103/PhysRevD.92.124019. arXiv: 1508.00010 [hep-th].

[Lai+17] J. Laiho et al. "Recent results in Euclidean dynamical triangulations". In: *Acta Phys. Polon. Supp.* 10 (2017), pp. 317–320. DOI: 10.5506/APhysPolBSupp.10.317. arXiv: 1701.06829 [hep-th].

[Lak91] Kayll Lake. "Naked singularities in gravitational collapse which is not self-similar". In: *Phys. Rev. D* 43.4 (1991), p. 1416. DOI: 10.1103/PhysRevD.43.1416.

[Lak92] Kayll Lake. "Precursory singularities in spherical gravitational collapse". In: *Phys. Rev. Lett.* 68 (1992), pp. 3129–3132. DOI: 10.1103/PhysRevLett.68.3129.

[Lam+18] Frédéric Lamy et al. "Imaging a non-singular rotating black hole at the center of the Galaxy". In: *Class. Quant. Grav.* 35.11 (2018), p. 115009. DOI: 10.1088/1361-6382/aabd97. arXiv: 1802.01635 [gr-qc].

[Lan22] Klaas Landsman. "Penrose's 1965 singularity theorem: from geodesic incompleteness to cosmic censorship". In: *Gen. Rel. Grav.* 54.10 (2022), p. 115. DOI: 10.1007/s10714-022-02973-w. arXiv: 2205.01680 [physics.hist-ph].

[Lan+23] Chen Lan et al. "Regular Black Holes: A Short Topic Review". In: *Int. J. Theor. Phys.* 62.9 (2023), p. 202. DOI: 10.1007/s10773-023-05454-1. arXiv: 2303.11696 [gr-qc].

[Lan91] A Lannes. "Phase and amplitude calibration in aperture synthesis. Algebraic structures". In: *Inverse Problems* 7.2 (1991), p. 261.

[Lap17] Amos Lapidoth. *A foundation in digital communication*. Cambridge University Press, 2017.

[Lat12] James M. Lattimer. "The nuclear equation of state and neutron star masses". In: *Ann. Rev. Nucl. Part. Sci.* 62 (2012), pp. 485–515. DOI: 10.1146/annurev-nucl-102711-095018. arXiv: 1305.3510 [nucl-th].

[Lat21] J. M. Lattimer. "Neutron Stars and the Nuclear Matter Equation of State". In: *Ann. Rev. Nucl. Part. Sci.* 71 (2021), pp. 433–464. DOI: 10.1146/annurev-nucl-102419-124827.

[Law00] Peter Lawson. *Principles of long baseline stellar interferometry*. JPL, 2000.

[LBB22] Guillermo Lara, Miguel Bezares, and Enrico Barausse. "UV completions, fixing the equations, and nonlinearities in k-essence". In: *Phys. Rev. D* 105.6 (2022), p. 064058. DOI: 10.1103/PhysRevD.105.064058. arXiv: 2112.09186 [gr-qc].

[Lee+20] J. G. Lee et al. "New Test of the Gravitational $1/r^2$ Law at Separations down to 52 μm". In: *Phys. Rev. Lett.* 124.10 (2020), p. 101101. DOI: 10.1103/PhysRevLett.124.101101. arXiv: 2002.11761 [hep-ex].

[Lem33] G. Lemaitre. "The expanding universe". In: *Annales Soc. Sci. Bruxelles A* 53 (1933), pp. 51–85. DOI: 10.1023/A:1018855621348.

[LG21] Will Lockhart and Samuel E. Gralla. "How narrow is the M87* ring? I. The choice of closure likelihood function". In: *Mon. Not. Roy. Astron. Soc.* 509.3 (2021), pp. 3643–3659. DOI: 10.1093/mnras/stab3204. arXiv: 2107.06948 [astro-ph.HE].

[LG22] Will Lockhart and Samuel E. Gralla. "How narrow is the M87* ring – II. A new geometric model". In: *Mon. Not. Roy. Astron. Soc.* 517.2 (2022), pp. 2462–2470. DOI: 10.1093/mnras/stac2743. arXiv: 2208.09989 [astro-ph.HE].

[Lin+15] Nan Lin et al. "A parametrization to test black hole candidates with the spectrum of thin disks". In: *Eur. Phys. J. C* 75.12 (2015), p. 599. DOI: 10.1140/epjc/s10052-015-3837-3. arXiv: 1512.00724 [gr-qc].

[Lit01] Daniel F. Litim. "Optimized renormalization group flows". In: *Phys. Rev. D* 64 (2001), p. 105007. DOI: 10.1103/PhysRevD.64.105007. arXiv: hep-th/0103195.

[Liu+20] K. Liu et al. "A revisit of PSR J1909−3744 with 15-yr high-precision timing". In: *Mon. Not. Roy. Astron. Soc.* 499.2 (2020), pp. 2276–2291. DOI: 10.1093/mnras/staa2993. arXiv: 2009.12544 [astro-ph.HE].

[LLZ21] Gaoping Long, Yunlong Liu, and Xiangdong Zhang. "Energy conditions in the new model of loop quantum cosmology". In: *Chin. Phys. C* 45.11 (2021), p. 115102. DOI: 10.1088/1674-1137/ac1e83. arXiv: 2011.07712 [gr-qc].

[LN14] Daniel F. Litim and Konstantinos Nikolakopoulos. "Quantum gravity effects in Myers-Perry space-times". In: *JHEP* 04 (2014), p. 021. DOI: 10.1007/JHEP04(2014)021. arXiv: 1308.5630 [hep-th].

[Lol20] R. Loll. "Quantum Gravity from Causal Dynamical Triangulations: A Review". In: *Class. Quant. Grav.* 37.1 (2020), p. 013002. DOI: 10.1088/1361-6382/ab57c7. arXiv: 1905.08669 [hep-th].

[Lon+20] Fen Long et al. "Shadow of a disformal Kerr black hole in quadratic degenerate higher-order scalar–tensor theories". In: *Eur. Phys. J. C* 80.12 (2020), p. 1180. DOI: 10.1140/epjc/s10052-020-08744-8. arXiv: 2009.07508 [gr-qc].

[Lop03] Michael C. Lopresto. "Some Simple Black Hole Thermodynamics". In: *Phys. Teacher* 41 (2003), pp. 299–301. DOI: 10.1119/1.1571268.

[Lor+52] H.A. Lorentz et al. *The Principle of Relativity: A Collection of Original Memoirs on the Special and General Theory of Relativity*. Dover Books on Physics and Mathematical Physics. Dover, 1952. ISBN: 9780486600819. URL: https://books.google.dk/books?id=S1dmLWLhdqAC.

[Lov71] D. Lovelock. "The Einstein tensor and its generalizations". In: *J. Math. Phys.* 12 (1971), pp. 498–501. DOI: 10.1063/1.1665613.

[Lov72] D. Lovelock. "The four-dimensionality of space and the einstein tensor". In: *J. Math. Phys.* 13 (1972), pp. 874–876. DOI: 10.1063/1.1666069.

[LQ22] B. F. Liu and Erlin Qiao. "Accretion around black holes: The geometry and spectra". In: (Jan. 2022). arXiv: 2201.06198 [astro-ph.HE].

[LR02] O. Lauscher and M. Reuter. "Flow equation of quantum Einstein gravity in a higher derivative truncation". In: *Phys. Rev. D* 66 (2002), p. 025026. DOI: 10.1103/PhysRevD.66.025026. arXiv: hep-th/0205062.

[LT18] Josef Lense and Hans Thirring. "Ueber den Einfluss der Eigenrotation der Zentralkoerper auf die Bewegung der Planeten und Monde nach der Einsteinschen Gravitationstheorie". In: *Phys. Z.* 19 (1918), pp. 156–163.

[Lu+15] H. Lu et al. "Black Holes in Higher-Derivative Gravity". In: *Phys. Rev. Lett.* 114.17 (2015), p. 171601. DOI: 10.1103/PhysRevLett.114.171601. arXiv: 1502.01028 [hep-th].

[Lum79] J. P. Luminet. "Image of a spherical black hole with thin accretion disk". In: *Astron. Astrophys.* 75 (1979), pp. 228–235.

[Lup+24] Alexandru Lupsasca et al. "The Black Hole Explorer: Photon Ring Science, Detection and Shape Measurement". In: (June 2024). arXiv: 2406.09498 [gr-qc].

[LV59] Urbain Le Verrier. "Lettre de M. Le Verrier à M. Faye sur la théorie de Mercure et sur le mouvement du périhélie de cette planète". In: *Comptes rendus hebdomadaires des séances de l'Académie des sciences* 49 (1859), pp. 379–383.

[LVB21] Guillermo Lara, Sebastian H. Völkel, and Enrico Barausse. "Separating astrophysics and geometry in black hole images". In: *Phys. Rev. D* 104.12 (2021), p. 124041. DOI: 10.1103/PhysRevD.104.124041. arXiv: 2110.00026 [gr-qc].

[LW22] Yi Ling and Meng-He Wu. "The Shadows of Regular Black Holes with Asymptotic Minkowski Cores". In: *Symmetry* 14.11 (2022), p. 2415. DOI: 10.3390/sym14112415. arXiv: 2205.08919 [gr-qc].

[LWJ07] Chun Ly, R. Craig Walker, and William Junor. "High Frequency VLBI Imaging of the Jet Base of M87". In: *Astrophys. J.* 660 (2007), pp. 200–205. DOI: 10.1086/512846. arXiv: astro-ph/0701511.

[Lyn+04] A. G. Lyne et al. "A Double - pulsar system - A Rare laboratory for relativistic gravity and plasma physics". In: *Science* 303 (2004), pp. 1153–1157. DOI: 10.1126/science.1094645. arXiv: astro-ph/0401086.

[LZG18] Tianbo Liu, Zhiwen Zhao, and Haiyan Gao. "Experimental constraint on quark electric dipole moments". In: *Phys. Rev. D* 97.7 (2018), p. 074018. DOI: 10.1103/PhysRevD.97.074018. arXiv: 1704.00113 [hep-ph].

[M+23] Johannes Münch et al. "Generic features of a polymer quantum black hole". In: *Class. Quant. Grav.* 40.13 (2023), p. 135003. DOI: 10.1088/1361-6382/accccd. arXiv: 2212.06708 [gr-qc].

[Mag+20] Michele Maggiore et al. "Science Case for the Einstein Telescope". In: *JCAP* 03 (2020), p. 050. DOI: 10.1088/1475-7516/2020/03/050. arXiv: 1912.02622 [astro-ph.CO].

[Mag23] Elisa Maggio. "Probing the Horizon of Black Holes with Gravitational Waves". In: *Lect. Notes Phys.* 1017 (2023), pp. 333–346. DOI: 10.1007/978-3-031-31520-6_9. arXiv: 2310.07368 [gr-qc].

[Mal96] Juan Martin Maldacena. "Black holes in string theory". PhD thesis. Princeton U., 1996. arXiv: hep-th/9607235.

[Mar+02] Herman L. Marshall et al. "A High resolution x-ray image of the jet in M87". In: *Astrophys. J.* 564 (2002), p. 683. DOI: 10.1086/324396. arXiv: astro-ph/0109160.

[Mar17] Donald Marolf. "The Black Hole information problem: past, present, and future". In: *Rept. Prog. Phys.* 80.9 (2017), p. 092001. DOI: 10.1088/1361-6633/aa77cc. arXiv: 1703.02143 [gr-qc].

[Mat05] Samir D. Mathur. "The Fuzzball proposal for black holes: An Elementary review". In: *Fortsch. Phys.* 53 (2005). Ed. by E. Kiritsis, pp. 793–827. DOI: 10.1002/prop.200410203. arXiv: hep-th/0502050.

[May20] Daniel R. Mayerson. "Fuzzballs and Observations". In: *Gen. Rel. Grav.* 52.12 (2020), p. 115. DOI: 10.1007/s10714-020-02769-w. arXiv: 2010.09736 [hep-th].

[Maz82] P. O. Mazur. "PROOF OF UNIQUENESS OF THE KERR-NEWMAN BLACK HOLE SOLUTION". In: *J. Phys. A* 15 (1982), pp. 3173–3180. DOI: 10.1088/0305-4470/15/10/021.

[McM+19] Ryan McManus et al. "Parametrized black hole quasinormal ringdown. II. Coupled equations and quadratic corrections for nonrotating black holes". In: *Phys. Rev. D* 100.4 (2019), p. 044061. DOI: 10.1103/PhysRevD.100.044061. arXiv: 1906.05155 [gr-qc].

[MCS19] Akash K. Mishra, Sumanta Chakraborty, and Sudipta Sarkar. "Understanding photon sphere and black hole shadow in dynamically evolving spacetimes". In: *Phys. Rev. D* 99.10 (2019), p. 104080. DOI: 10.1103/PhysRevD.99.104080. arXiv: 1903.06376 [gr-qc].

[Mel+24] Y. Mellier et al. "Euclid. I. Overview of the Euclid mission". In: (May 2024). arXiv: 2405.13491 [astro-ph.CO].

[MEM24] David J. E. Marsh, David Ellis, and Viraf M. Mehta. *Dark Matter: Evidence, Theory, and Constraints*. Princeton University Press, Sept. 2024. ISBN: 978-0-691-24952-0.

[MFL21] Jacopo Mazza, Edgardo Franzin, and Stefano Liberati. "A novel family of rotating black hole mimickers". In: *JCAP* 04 (2021), p. 082. DOI: 10.1088/1475-7516/2021/04/082. arXiv: 2102.01105 [gr-qc].

[MGM14] Maombi D. Mkenyeleye, Rituparno Goswami, and Sunil D. Maharaj. "Gravitational collapse of generalized Vaidya spacetime". In: *Phys. Rev. D* 90.6 (2014), p. 064034. DOI: 10.1103/PhysRevD.90.064034. arXiv: 1407.4309 [gr-qc].

[Mil22] Mordehai Milgrom. "Broader view of bimetric MOND". In: *Phys. Rev. D* 106.8 (2022), p. 084010. DOI: 10.1103/PhysRevD.106.084010. arXiv: 2208.10882 [gr-qc].

[Min20] Masato Minamitsuji. "Disformal transformation of stationary and axisymmetric solutions in modified gravity". In: *Phys. Rev. D* 102.12 (2020), p. 124017. DOI: 10.1103/PhysRevD.102.124017. arXiv: 2012.13526 [gr-qc].

[Miz+18] Yosuke Mizuno et al. "The Current Ability to Test Theories of Gravity with Black Hole Shadows". In: *Nature Astron.* 2.7 (2018), pp. 585–590. DOI: 10.1038/s41550-018-0449-5. arXiv: 1804.05812 [astro-ph.GA].

[Miz22] Yosuke Mizuno. "GRMHD Simulations and Modeling for Jet Formation and Acceleration Region in AGNs". In: *Universe* 8.2 (2022), p. 85. DOI: 10.3390/universe8020085. arXiv: 2201.12608 [astro-ph.HE].

[MN10] Leonardo Modesto and Piero Nicolini. "Charged rotating noncommutative black holes". In: *Phys. Rev. D* 82 (2010), p. 104035. DOI: 10.1103/PhysRevD.82.104035. arXiv: 1005.5605 [gr-qc].

[Mor94] Tim R. Morris. "The Exact renormalization group and approximate solutions". In: *Int. J. Mod. Phys. A* 9 (1994), pp. 2411–2450. DOI: 10.1142/S0217751X94000972. arXiv: hep-ph/9308265.

[MPO20] Lia Medeiros, Dimitrios Psaltis, and Feryal Özel. "A Parametric model for the shapes of black-hole shadows in non-Kerr spacetimes". In: *Astrophys. J.* 896.1 (2020), p. 7. DOI: 10.3847/1538-4357/ab8bd1. arXiv: 1907.12575 [astro-ph.HE].

[MS08] Pedro F. Machado and Frank Saueressig. "On the renormalization group flow of f(R)-gravity". In: *Phys. Rev. D* 77 (2008), p. 124045. DOI: 10.1103/PhysRevD.77.124045. arXiv: 0712.0445 [hep-th].

[MS16] Grzegorz (Greg) Madejski and Marek Sikora. "Gamma-Ray Observations of Active Galactic Nuclei". In: *Ann. Rev. Astron. Astrophys.* 54 (2016), pp. 725–760. DOI: 10.1146/annurev-astro-081913-040044.

[MS24] Sebastian Murk and Ioannis Soranidis. "Light rings and causality for nonsingular ultracompact objects sourced by nonlinear electrodynamics". In: (June 2024). arXiv: 2406.07957 [gr-qc].

[MSV07] Marc Mars, Jose M. M. Senovilla, and Raul Vera. "Lorentzian and signature changing branes". In: *Phys. Rev. D* 76 (2007), p. 044029. DOI: 10.1103/PhysRevD.76.044029. arXiv: 0705.3380 [hep-th].

[MT70] M. Murenbeeld and J. R. Trollope. "Slowly Rotating Radiating Sphere and a Kerr-Vaidya Metric". In: *Phys. Rev. D* 1 (1970), pp. 3220–3223. DOI: 10.1103/PhysRevD.1.3220.

[MTC91] M Massi, G Tofani, and G Comoretto. "Baseline errors on VLBI measurements. I-Analytic description". In: *Astronomy and Astrophysics (ISSN 0004-6361), vol. 251, no. 2, Nov. 1991, p. 732-736.* 251 (1991), pp. 732–736.

[MTW73] Charles W. Misner, K. S. Thorne, and J. A. Wheeler. *Gravitation*. San Francisco: W. H. Freeman, 1973. ISBN: 978-0-7167-0344-0, 978-0-691-17779-3.

[Muk11] Sunil Mukhi. "String theory: a perspective over the last 25 years". In: *Class. Quant. Grav.* 28 (2011), p. 153001. DOI: 10.1088/0264-9381/28/15/153001. arXiv: 1110.2569 [physics.pop-ph].

[MV17] Chiara Marletto and Vlatko Vedral. "Why we need to quantise everything, including gravity". In: *npj Quantum Inf.* 3 (2017), p. 29. DOI: 10.1038/s41534-017-0028-0. arXiv: 1703.04325 [quant-ph].

[Mü24] Hendrik Müller. "Prospects of using closure traces directly for imaging in Very Long Baseline Interferometry". In: (July 2024). arXiv: 2407.20190 [astro-ph.IM].

[Nag+18] S. Nagy et al. "Regulator dependence of fixed points in quantum Einstein gravity with R^2 truncation". In: *Class. Quant. Grav.* 35.5 (2018), p. 055001. DOI: 10.1088/1361-6382/aaa6ee. arXiv: 1707.04934 [hep-th].

[Nar+12] Ramesh Narayan et al. "GRMHD Simulations of Magnetized Advection-Dominated Accretion on a Non-Spinning Black Hole: Role of Outflows". In: *Mon. Not. Roy. Astron. Soc.* 426 (2012), p. 3241. DOI: 10.1111/j.1365-2966.2012.22002.x. arXiv: 1206.1213 [astro-ph.HE].

[Nav+24] S. Navas et al. "Review of particle physics". In: *Phys. Rev. D* 110.3 (2024), p. 030001. DOI: 10.1103/PhysRevD.110.030001.

[NC19] Gamal G. L. Nashed and Salvatore Capozziello. "Charged spherically symmetric black holes in $f(R)$ gravity and their stability analysis". In: *Phys. Rev. D* 99.10 (2019), p. 104018. DOI: 10.1103/PhysRevD.99.104018. arXiv: 1902.06783 [gr-qc].

[NC23] G. G. L. Nashed and S. Capozziello. "Spinning (A)dS black holes with slow-rotation approximation in dynamical Chern-Simons modified gravity". In: *Phys. Rev. D* 107.6 (2023), p. 063008. DOI: 10.1103/PhysRevD.107.063008. arXiv: 2303.03159 [gr-qc].

[New+16] Matthew Newville et al. "LMFIT: Non-linear least-square minimization and curve-fitting for Python". In: *Astrophysics Source Code Library* (2016), ascl–1606.

[New+65] E T. Newman et al. "Metric of a Rotating, Charged Mass". In: *J. Math. Phys.* 6 (1965), pp. 918–919. DOI: 10.1063/1.1704351.

[New87] Isaac Newton. *Philosophiæ Naturalis Principia Mathematica*. England, 1687.

[NIA03] Ramesh Narayan, Igor V. Igumenshchev, and Marek A. Abramowicz. "Magnetically arrested disk: an energetically efficient accretion flow". In: *Publ. Astron. Soc. Jap.* 55 (2003), p. L69. DOI: 10.1093/pasj/55.6.L69. arXiv: astro-ph/0305029.

[Nic09] Piero Nicolini. "Noncommutative Black Holes, The Final Appeal To Quantum Gravity: A Review". In: *Int. J. Mod. Phys. A* 24 (2009), pp. 1229–1308. DOI: 10.1142/S0217751X09043353. arXiv: 0807.1939 [hep-th].

[NJ65] E. T. Newman and A. I. Janis. "Note on the Kerr spinning particle metric". In: *J. Math. Phys.* 6 (1965), pp. 915–917. DOI: 10.1063/1.1704350.

[Nor18] Gunnar Nordström. "On the energy of the gravitation field in Einstein's theory". In: *Koninklijke Nederlandse Akademie van Wetenschappen Proceedings Series B Physical Sciences* 20 (1918), pp. 1238–1245.

[NPP23] Mário Raia Neto, Daniela Pérez, and Joaquín Pelle. "The shadow of charged traversable wormholes". In: *Int. J. Mod. Phys. D* 32.02 (2023), p. 2250137. DOI: 10.1142/S0218271822501371. arXiv: 2210.14106 [gr-qc].

[NSW19] Piero Nicolini, Euro Spallucci, and Michael F. Wondrak. "Quantum Corrected Black Holes from String T-Duality". In: *Phys. Lett. B* 797 (2019), p. 134888. DOI: 10.1016/j.physletb.2019.134888. arXiv: 1902.11242 [gr-qc].

[NV06] Alex B. Nielsen and Matt Visser. "Production and decay of evolving horizons". In: *Class. Quant. Grav.* 23 (2006), pp. 4637–4658. DOI: 10.1088/0264-9381/23/14/006. arXiv: gr-qc/0510083.

[NYK22] Sourabh Nampalliwar, Aristomenis I. Yfantis, and Kostas D. Kokkotas. "GRMHD beyond Kerr: An extension of the HARM code for thin disks to non-Kerr spacetimes". In: (June 2022). arXiv: 2206.10474 [astro-ph.HE].

[Odi+23] Sergei D. Odintsov et al. "Recent Advances in Inflation". In: *Symmetry* 15.9 (2023), p. 1701. DOI: 10.3390/sym15091701. arXiv: 2307.16308 [gr-qc].

[OEK00] F. N. Owen, J. a Eilek, and N. E. Kassim. "M87 at 90cm: a different picture". In: *Astrophys. J.* 543 (2000), p. 611. DOI: 10.1086/317151. arXiv: astro-ph/0006150.

[OF16] Feryal Özel and Paulo Freire. "Masses, Radii, and the Equation of State of Neutron Stars". In: *Ann. Rev. Astron. Astrophys.* 54 (2016), pp. 401–440. DOI: 10.1146/annurev-astro-081915-023322. arXiv: 1603.02698 [astro-ph.HE].

[O'H24] Ciaran A. J. O'Hare. "Cosmology of axion dark matter". In: *PoS* COSMICWISPers (2024), p. 040. DOI: 10.22323/1.454.0040. arXiv: 2403.17697 [hep-ph].

[Oko+17] Maria Okounkova et al. "Numerical binary black hole mergers in dynamical Chern-Simons gravity: Scalar field". In: *Phys. Rev. D* 96.4 (2017), p. 044020. DOI: 10.1103/PhysRevD.96.044020. arXiv: 1705.07924 [gr-qc].

[Oko+19] Maria Okounkova et al. "Numerical binary black hole collisions in dynamical Chern-Simons gravity". In: *Phys. Rev. D* 100.10 (2019), p. 104026. DOI: 10.1103/PhysRevD.100.104026. arXiv: 1906.08789 [gr-qc].

[Oko20] Maria Okounkova. "Numerical relativity simulation of GW150914 in Einstein dilaton Gauss-Bonnet gravity". In: *Phys. Rev. D* 102.8 (2020), p. 084046. DOI: 10.1103/PhysRevD.102.084046. arXiv: 2001.03571 [gr-qc].

[Oko+20] Maria Okounkova et al. "Numerical relativity simulation of GW150914 beyond general relativity". In: *Phys. Rev. D* 101.10 (2020), p. 104016. DOI: 10.1103/PhysRevD.101.104016. arXiv: 1911.02588 [gr-qc].

[Olm+23] Gonzalo J. Olmo et al. "Shadows and photon rings of regular black holes and geonic horizonless compact objects". In: *Class. Quant. Grav.* 40.17 (2023), p. 174002. DOI: 10.1088/1361-6382/aceacd. arXiv: 2302.12064 [gr-qc].

[Ong20] Yen Chin Ong. "Space–time singularities and cosmic censorship conjecture: A Review with some thoughts". In: *Int. J. Mod. Phys. A* 35.14 (2020), p. 14. DOI: 10.1142/S0217751X20300070. arXiv: 2005.07032 [gr-qc].

[OP14] Nobuyoshi Ohta and Roberto Percacci. "Higher Derivative Gravity and Asymptotic Safety in Diverse Dimensions". In: *Class. Quant. Grav.* 31 (2014), p. 015024. DOI: 10.1088/0264-9381/31/1/015024. arXiv: 1308.3398 [hep-th].

[Opp23] Jonathan Oppenheim. "A Postquantum Theory of Classical Gravity?" In: *Phys. Rev. X* 13.4 (2023), p. 041040. DOI: 10.1103/PhysRevX.13.041040. arXiv: 1811.03116 [hep-th].

[OPV15] Nobuyoshi Ohta, Roberto Percacci, and Gian Paolo Vacca. "Flow equation for $f(R)$ gravity and some of its exact solutions". In: *Phys. Rev. D* 92.6 (2015), p. 061501. DOI: 10.1103/PhysRevD.92.061501. arXiv: 1507.00968 [hep-th].

[OPY22] Feryal Ozel, Dimitrios Psaltis, and Ziri Younsi. "Black Hole Images as Tests of General Relativity: Effects of Plasma Physics". In: *Astrophys. J.* 941.1 (2022), p. 88. DOI: 10.3847/1538-4357/ac9fcb. arXiv: 2111.01123 [astro-ph.HE].

[OR24] Jonathan Oppenheim and Andrea Russo. "Anomalous contribution to galactic rotation curves due to stochastic spacetime". In: (Feb. 2024). arXiv: 2402.19459 [gr-qc].

[ORGG22] Gonzalo J. Olmo, Diego Rubiera-Garcia, and Diego Sáez-Chillón Gómez. "New light rings from multiple critical curves as observational signatures of black hole mimickers". In: *Phys. Lett. B* 829 (2022), p. 137045. DOI: 10.1016/j.physletb.2022.137045. arXiv: 2110.10002 [gr-qc].

[Ori09] Daniele Oriti. "The Group field theory approach to quantum gravity: Some recent results". In: *AIP Conf. Proc.* 1196.1 (2009). Ed. by Jerzy Kowalski-Glikman, R. Durka, and M. Szczachor, pp. 209–218. DOI: 10.1063/1.3284386. arXiv: 0912.2441 [hep-th].

[OS39] J. R. Oppenheimer and H. Snyder. "On Continued gravitational contraction". In: *Phys. Rev.* 56 (1939), pp. 455–459. DOI: 10.1103/PhysRev.56.455.

[Ost50] M. Ostrogradsky. "Mémoires sur les équations différentielles, relatives au problème des isopérimètres". In: *Mem. Acad. St. Petersbourg* 6.4 (1850), pp. 385–517.

[OV07] Hirosi Ooguri and Cumrun Vafa. "On the Geometry of the String Landscape and the Swampland". In: *Nucl. Phys. B* 766 (2007), pp. 21–33. DOI: 10.1016/j.nuclphysb.2006.10.033. arXiv: hep-th/0605264.

[OYW21] Caroline B. Owen, Nicolás Yunes, and Helvi Witek. "Petrov type, principal null directions, and Killing tensors of slowly rotating black holes in quadratic gravity". In: *Phys. Rev. D* 103.12 (2021), p. 124057. DOI: 10.1103/PhysRevD.103.124057. arXiv: 2103.15891 [gr-qc].

[Pag05] Don N. Page. "Hawking radiation and black hole thermodynamics". In: *New J. Phys.* 7 (2005), p. 203. DOI: 10.1088/1367-2630/7/1/203. arXiv: hep-th/0409024.

[Pal19] Eran Palti. "The Swampland: Introduction and Review". In: *Fortsch. Phys.* 67.6 (2019), p. 1900037. DOI: 10.1002/prop.201900037. arXiv: 1903.06239 [hep-th].

[Pal+19] Daniel CM Palumbo et al. "Metrics and motivations for Earth–space VLBI: Time-resolving Sgr A* with the Event Horizon Telescope". In: *The Astrophysical Journal* 881.1 (2019), p. 62.

[Pal+23] Daniel C. M. Palumbo et al. "Demonstrating Photon Ring Existence with Single-baseline Polarimetry". In: *Astrophys. J. Lett.* 952.2 (2023), p. L31. DOI: 10.3847/2041-8213/ace630. arXiv: 2307.05293 [astro-ph.HE].

[Pan+10] Paolo Pani et al. "Gravitational instabilities of superspinars". In: *Phys. Rev. D* 82 (2010), p. 044009. DOI: 10.1103/PhysRevD.82.044009. arXiv: 1006.1863 [gr-qc].

[Pan+11] Paolo Pani et al. "Slowly rotating black holes in alternative theories of gravity". In: *Phys. Rev. D* 84 (2011), p. 087501. DOI: 10.1103/PhysRevD.84.087501. arXiv: 1109.3996 [gr-qc].

[Pap66] Achille Papapetrou. "Champs gravitationnels stationnaires a symetrie axiale". In: *Ann. Inst. H. Poincare Phys. Theor.* 4 (1966), pp. 83–105.

[Pap85a] A Papapetrou. "Formation of a singularity and causality." In: *A random walk in relativity and cosmology* (1985), pp. 184–191.

[Pap85b] A Papapetrou. "Formation of a singularity and causality." In: *A random walk in relativity and cosmology* (1985), pp. 184–191.

[Pau+22] Hadrien Paugnat et al. "Photon ring test of the Kerr hypothesis: Variation in the ring shape". In: *Astron. Astrophys.* 668 (2022), A11. DOI: 10.1051/0004-6361/202244216. arXiv: 2206.02781 [astro-ph.HE].

[Pen65] Roger Penrose. "Gravitational collapse and space-time singularities". In: *Phys. Rev. Lett.* 14 (1965), pp. 57–59. DOI: 10.1103/PhysRevLett.14.57.

[Pen69] R. Penrose. "Gravitational collapse: The role of general relativity". In: *Riv. Nuovo Cim.* 1 (1969), pp. 252–276. DOI: 10.1023/A:1016578408204.

[Per04] V. Perlick. "Gravitational lensing from a spacetime perspective". In: *Living Rev. Rel.* 7 (2004), p. 9. DOI: 10.12942/lrr-2004-9.

[Per07] Roberto Percacci. "Asymptotic Safety". In: (Sept. 2007), pp. 111–128. arXiv: 0709.3851 [hep-th].

[Per17a] Robert Percacci. *An Introduction to Covariant Quantum Gravity and Asymptotic Safety*. Vol. 3. 100 Years of General Relativity. World Scientific, 2017. ISBN: 978-981-320-717-2, 978-981-320-719-6. DOI: 10.1142/10369.

[Per17b] Alejandro Perez. "Black Holes in Loop Quantum Gravity". In: *Rept. Prog. Phys.* 80.12 (2017), p. 126901. DOI: 10.1088/1361-6633/aa7e14. arXiv: 1703.09149 [gr-qc].

[Per+99a] Eric S. Perlman et al. "Optical and radio polarimetry of the m87 jet at 0.2′ resolution". In: *Astron. J.* 117 (1999), p. 2185. DOI: 10.1086/300844. arXiv: astro-ph/9901176.

[Per+99b] S. Perlmutter et al. "Measurements of Ω and Λ from 42 High Redshift Supernovae". In: *Astrophys. J.* 517 (1999), pp. 565–586. DOI: 10.1086/307221. arXiv: astro-ph/9812133.

[Pes+19] Dominic W. Pesce et al. "Extremely long baseline interferometry with Origins Space Telescope". In: (Sept. 2019). arXiv: 1909.01408 [astro-ph.IM].

[PF73] Leonard Parker and S. A. Fulling. "Quantized matter fields and the avoidance of singularities in general relativity". In: *Phys. Rev. D* 7 (1973), pp. 2357–2374. DOI: 10.1103/PhysRevD.7.2357.

[PI89] Eric Poisson and W. Israel. "Inner-horizon instability and mass inflation in black holes". In: *Phys. Rev. Lett.* 63 (1989), pp. 1663–1666. DOI: 10.1103/PhysRevLett.63.1663.

[PI90] Eric Poisson and W. Israel. "Internal structure of black holes". In: *Phys. Rev. D* 41 (1990), pp. 1796–1809. DOI: 10.1103/PhysRevD.41.1796.

[PK18] Georgios O. Papadopoulos and Kostas D. Kokkotas. "Preserving Kerr symmetries in deformed spacetimes". In: *Class. Quant. Grav.* 35.18 (2018), p. 185014. DOI: 10.1088/1361-6382/aad7f4. arXiv: 1807.08594 [gr-qc].

[Pla19] Alessia Platania. "Dynamical renormalization of black-hole spacetimes". In: *Eur. Phys. J. C* 79.6 (2019), p. 470. DOI: 10.1140/epjc/s10052-019-6990-2. arXiv: 1903.10411 [gr-qc].

[Pla23] Alessia Platania. "Black Holes in Asymptotically Safe Gravity". In: 2023. DOI: 10.1007/978-981-19-3079-9_24-1. arXiv: 2302.04272 [gr-qc].

[PM21] D. Pugliese and G. Montani. "Aspects of GRMHD in high-energy astrophysics: geometrically thick disks and tori agglomerates around spinning black holes". In: *Gen. Rel. Grav.* 53.5 (2021), p. 51. DOI: 10.1007/s10714-021-02820-4. arXiv: 2005.03900 [astro-ph.HE].

[PMM03] G Perrin, F Malbet, and JD Monnier. "Astrophysics with closure phases". In: *European Astronomical Society Publications Series* 6 (2003), pp. 213–213.

[Pod+20] Jiri Podolský et al. "Black holes and other exact spherical solutions in Quadratic Gravity". In: *Phys. Rev. D* 101.2 (2020), p. 024027. DOI: 10.1103/PhysRevD.101.024027. arXiv: 1907.00046 [gr-qc].

[Pog24] Rosa Poggiani. "The new world discovered with the detection of Gravitational Waves". In: *PoS* MULTIF2023 (2024), p. 021. DOI: 10.22323/1.447.0021.

[Pop54] Daniel M Popper. "Red Shift in the Spectrum of 40 Eridani B." In: *Astrophysical Journal, vol. 120, p. 316* 120 (1954), p. 316.

[PR23] Jan M. Pawlowski and Manuel Reichert. "Quantum Gravity from dynamical metric fluctuations". In: (Sept. 2023). arXiv: 2309.10785 [hep-th].

[Pre06] Frans Pretorius. "Simulation of binary black hole spacetimes with a harmonic evolution scheme". In: *Class. Quant. Grav.* 23 (2006), S529–S552. DOI: 10.1088/0264-9381/23/16/S13. arXiv: gr-qc/0602115.

[PS18] Jan M. Pawlowski and Dennis Stock. "Quantum-improved Schwarzschild-(A)dS and Kerr-(A)dS spacetimes". In: *Phys. Rev. D* 98.10 (2018), p. 106008. DOI: 10.1103/PhysRevD.98.106008. arXiv: 1807.10512 [hep-th].

[PS22] Leandros Perivolaropoulos and Foteini Skara. "Challenges for ΛCDM: An update". In: *New Astron. Rev.* 95 (2022), p. 101659. DOI: 10.1016/j.newar.2022.101659. arXiv: 2105.05208 [astro-ph.CO].

[Psa08] Dimitrios Psaltis. "Probes and Tests of Strong-Field Gravity with Observations in the Electromagnetic Spectrum". In: *Living Rev. Rel.* 11 (2008), p. 9. DOI: 10.12942/lrr-2008-9. arXiv: 0806.1531 [astro-ph].

[Psa19] Dimitrios Psaltis. "Testing General Relativity with the Event Horizon Telescope". In: *Gen. Rel. Grav.* 51.10 (2019), p. 137. DOI: 10.1007/s10714-019-2611-5. arXiv: 1806.09740 [astro-ph.HE].

[Psa+21] Dimitrios Psaltis et al. "Probing the Black Hole Metric. I. Black Hole Shadows and Binary Black-Hole Inspirals". In: *Phys. Rev. D* 103 (2021), p. 104036. DOI: 10.1103/PhysRevD.103.104036. arXiv: 2012.02117 [gr-qc].

[PU50] A. Pais and G. E. Uhlenbeck. "On Field theories with nonlocalized action". In: *Phys. Rev.* 79 (1950), pp. 145–165. DOI: 10.1103/PhysRev.79.145.

[Qui19] Israel Quiros. "Selected topics in scalar–tensor theories and beyond". In: *Int. J. Mod. Phys. D* 28.07 (2019), p. 1930012. DOI: 10.1142/S021827181930012X. arXiv: 1901.08690 [gr-qc].

[QWF24] Zhi-Shuo Qu, Towe Wang, and Chao-Jun Feng. "Images of nonsingular nonrotating black holes in conformal gravity". In: *Annals Phys.* 464 (2024), p. 169642. DOI: 10.1016/j.aop.2024.169642. arXiv: 2301.07326 [gr-qc].

[Ray+24] Alexander W. Raymond et al. "First Very Long Baseline Interferometry Detections at 870μm". In: (Oct. 2024). DOI: 10.3847/1538-3881/ad5bdb. arXiv: 2410.07453 [astro-ph.IM].

[Rea+80] ACS Readhead et al. "Mapping radio sources with uncalibrated visibility data". In: *Nature* 285.5761 (1980), pp. 137–140.

[Rei16] H. Reissner. "Über die Eigengravitation des elektrischen Feldes nach der Einsteinschen Theorie". In: *Annalen Phys.* 355.9 (1916), pp. 106–120. DOI: 10.1002/andp.19163550905.

[Ren02] Alan D. Rendall. "The Einstein-Vlasov system". In: *50 Years of the Cauchy Problem in General Relativity: Summer School on Mathematical Relativity and Global Properties of Solutions of Einstein's Equations*. Aug. 2002. arXiv: gr-qc/0208082.

[Ren06] Alan D. Rendall. "Dynamics of k-essence". In: *Class. Quant. Grav.* 23 (2006), pp. 1557–1570. DOI: 10.1088/0264-9381/23/5/008. arXiv: gr-qc/0511158.

[Ren+22] Arianna I. Renzini et al. "Stochastic Gravitational-Wave Backgrounds: Current Detection Efforts and Future Prospects". In: *Galaxies* 10.1 (2022), p. 34. DOI: 10.3390/galaxies10010034. arXiv: 2202.00178 [gr-qc].

[Reu00] Martin Reuter. "Newton's constant isn't constant". In: Dec. 2000. arXiv: hep-th/0012069.

[Reu98] M. Reuter. "Nonperturbative evolution equation for quantum gravity". In: *Phys. Rev. D* 57 (1998), pp. 971–985. DOI: 10.1103/PhysRevD.57.971. arXiv: hep-th/9605030.

[Rha14] Claudia de Rham. "Massive Gravity". In: *Living Rev. Rel.* 17 (2014), p. 7. DOI: 10.12942/lrr-2014-7. arXiv: 1401.4173 [hep-th].

[Rie+24] Adam G. Riess et al. "JWST Observations Reject Unrecognized Crowding of Cepheid Photometry as an Explanation for the Hubble Tension at 8σ Confidence". In: *Astrophys. J. Lett.* 962.1 (2024), p. L17. DOI: 10.3847/2041-8213/ad1ddd. arXiv: 2401.04773 [astro-ph.CO].

[Rie+98] Adam G. Riess et al. "Observational evidence from supernovae for an accelerating universe and a cosmological constant". In: *Astron. J.* 116 (1998), pp. 1009–1038. DOI: 10.1086/300499. arXiv: astro-ph/9805201.

[Rob75] D. C. Robinson. "Uniqueness of the Kerr black hole". In: *Phys. Rev. Lett.* 34 (1975), pp. 905–906. DOI: 10.1103/PhysRevLett.34.905.

[Roe+19] Freek Roelofs et al. "Simulations of imaging the event horizon of Sagittarius A* from space". In: *Astron. Astrophys.* 625 (2019), A124. DOI: 10.1051/0004-6361/201732423. arXiv: 1904.04934 [astro-ph.HE].

[Rog+74] AEE Rogers et al. "The structure of radio sources 3C 273B and 3C 84 deduced from the'closure'phases and visibility amplitudes observed with three-element interferometers". In: *Astrophysical Journal, vol. 193, Oct. 15, 1974, pt. 1, p. 293-301.* 193 (1974), pp. 293–301.

[Rom04] Thomas A. Roman. "Some thoughts on energy conditions and wormholes". In: *10th Marcel Grossmann Meeting on Recent Developments in Theoretical and Experimental General Relativity, Gravitation and Relativistic Field Theories (MG X MMIII)*. Sept. 2004, pp. 1909–1922. DOI: 10.1142/9789812704030_0236. arXiv: gr-qc/0409090.

[Rom86] T. A. Roman. "Quantum Stress Energy Tensors and the Weak Energy Condition". In: *Phys. Rev. D* 33 (1986), pp. 3526–3533. DOI: 10.1103/PhysRevD.33.3526.

[Rov08] Carlo Rovelli. "Loop quantum gravity". In: *Living Rev. Rel.* 11 (2008), p. 5. DOI: 10.12942/lrr-2008-5.

[RRY23] Abhishek Hegade K. R, Justin L. Ripley, and Nicolás Yunes. "Where and why does Einstein-scalar-Gauss-Bonnet theory break down?" In: *Phys. Rev. D* 107.4 (2023), p. 044044. DOI: 10.1103/PhysRevD.107.044044. arXiv: 2211.08477 [gr-qc].

[RS02] M. Reuter and Frank Saueressig. "Renormalization group flow of quantum gravity in the Einstein-Hilbert truncation". In: *Phys. Rev. D* 65 (2002), p. 065016. DOI: 10.1103/PhysRevD.65.065016. arXiv: hep-th/0110054.

[RS19a] Suvrat Raju and Pushkal Shrivastava. "Critique of the fuzzball program". In: *Phys. Rev. D* 99.6 (2019), p. 066009. DOI: 10.1103/PhysRevD.99.066009. arXiv: 1804.10616 [hep-th].

[RS19b] Martin Reuter and Frank Saueressig. *Quantum Gravity and the Functional Renormalization Group: The Road towards Asymptotic Safety*. Cambridge University Press, Jan. 2019. ISBN: 978-1-107-10732-8, 978-1-108-67074-6.

[RSN20] Saibal Ray, Rikpratik Sengupta, and Himanshu Nimesh. "Gravastar: An alternative to black hole". In: *Int. J. Mod. Phys. D* 29.05 (2020), p. 2030004. DOI: 10.1142/S0218271820300049.

[RSW20] Maximilian Ruhdorfer, Javi Serra, and Andreas Weiler. "Effective Field Theory of Gravity to All Orders". In: *JHEP* 05 (2020), p. 083. DOI: 10.1007/JHEP05(2020)083. arXiv: 1908.08050 [hep-ph].

[RT06] M. Reuter and E. Tuiran. "Quantum Gravity Effects in Rotating Black Holes". In: *11th Marcel Grossmann Meeting on General Relativity*. Dec. 2006, pp. 2608–2610. DOI: 10.1142/9789812834300_0473. arXiv: hep-th/0612037.

[RT11] M. Reuter and E. Tuiran. "Quantum Gravity Effects in the Kerr Spacetime". In: *Phys. Rev. D* 83 (2011), p. 044041. DOI: 10.1103/PhysRevD.83.044041. arXiv: 1009.3528 [hep-th].

[RTF80] V. C. Rubin, N. Thonnard, and W. K. Ford Jr. "Rotational properties of 21 SC galaxies with a large range of luminosities and radii, from NGC 4605 /R = 4kpc/ to UGC 2885 /R = 122 kpc/". In: *Astrophys. J.* 238 (1980), p. 471. DOI: 10.1086/158003.

[RW04] M. Reuter and H. Weyer. "Renormalization group improved gravitational actions: A Brans-Dicke approach". In: *Phys. Rev. D* 69 (2004), p. 104022. DOI: 10.1103/PhysRevD.69.104022. arXiv: hep-th/0311196.

[RZ14] Luciano Rezzolla and Alexander Zhidenko. "New parametrization for spherically symmetric black holes in metric theories of gravity". In: *Phys. Rev. D* 90.8 (2014), p. 084009. DOI: 10.1103/PhysRevD.90.084009. arXiv: 1407.3086 [gr-qc].

[Sai24] Dhananjay Saikumar. "Exploring the Frontiers: Challenges and Theories Beyond the Standard Model". In: (Feb. 2024). arXiv: 2404.03666 [hep-ph].

[Sak84] A. D. Sakharov. "Cosmological Transitions With a Change in Metric Signature". In: *Sov. Phys. JETP* 60 (1984), pp. 214–218. DOI: 10.1070/PU1991v034n05ABEH002502.

[Sal06] Marcelo Salgado. "The Cauchy problem of scalar tensor theories of gravity". In: *Class. Quant. Grav.* 23 (2006), pp. 4719–4742. DOI: 10.1088/0264-9381/23/14/010. arXiv: gr-qc/0509001.

[Sal68] Abdus Salam. "Weak and Electromagnetic Interactions". In: *Conf. Proc. C* 680519 (1968), pp. 367–377. DOI: 10.1142/9789812795915_0034.

[Sat+22] Kaushik Satapathy et al. "The Variability of the Black Hole Image in M87 at the Dynamical Timescale". In: *Astrophys. J.* 925.1 (2022), p. 13. DOI: 10.3847/1538-4357/ac332e. arXiv: 2111.01317 [astro-ph.HE].

[Sau23] Frank Saueressig. "The Functional Renormalization Group in Quantum Gravity". In: 2023. DOI: 10.1007/978-981-19-3079-9_16-1. arXiv: 2302.14152 [hep-th].

[SB22] Swarnim Shashank and Cosimo Bambi. "Constraining the Konoplya-Rezzolla-Zhidenko deformation parameters III: Limits from stellar-mass black holes using gravitational-wave observations". In: *Phys. Rev. D* 105.10 (2022), p. 104004. DOI: 10.1103/PhysRevD.105.104004. arXiv: 2112.05388 [gr-qc].

[SBG24] Kiana Salehi, Avery E. Broderick, and Boris Georgiev. "Photon Rings and Shadow Size for General Axisymmetric and Stationary Integrable Spacetimes". In: *Astrophys. J.* 966.1 (2024), p. 143. DOI: 10.3847/1538-4357/ad37fa. arXiv: 2311.01495 [gr-qc].

[SBPL19] Olivier Sarbach, Enrico Barausse, and Jorge A. Preciado-López. "Well-posed Cauchy formulation for Einstein-æther theory". In: *Class. Quant. Grav.* 36.16 (2019), p. 165007. DOI: 10.1088/1361-6382/ab2e13. arXiv: 1902.05130 [gr-qc].

[Sch14] Matthew D. Schwartz. *Quantum Field Theory and the Standard Model*. Cambridge University Press, Mar. 2014. ISBN: 978-1-107-03473-0, 978-1-107-03473-0.

[Sch16] Karl Schwarzschild. "Über das gravitationsfeld eines massenpunktes nach der einsteinschen theorie". In: *Sitzungsberichte der königlich preussischen Akademie der Wissenschaften* (1916), pp. 189–196.

[Sch19] Maximilian Schlosshauer. "Quantum decoherence". In: *Phys. Rept.* 831 (2019), pp. 1–57. DOI: 10.1016/j.physrep.2019.10.001. arXiv: 1911.06282 [quant-ph].

[Sch60] L. I. Schiff. "Possible New Experimental Test of General Relativity Theory". In: *Phys. Rev. Lett.* 4 (1960), pp. 215–217. DOI: 10.1103/PhysRevLett.4.215.

[Sen+23] Ivo Sengo et al. "Kerr black holes with synchronised Proca hair: lensing, shadows and EHT constraints". In: *JCAP* 01 (2023), p. 047. DOI: 10.1088/1475-7516/2023/01/047. arXiv: 2209.06237 [gr-qc].

[SG23] Arthur G. Suvorov and Kostas Glampedakis. "Magnetic equilibria of relativistic axisymmetric stars: The impact of flow constants". In: *Phys. Rev. D* 108.8 (2023), p. 084006. DOI: 10.1103/PhysRevD.108.084006. arXiv: 2309.08071 [gr-qc].

[Sha+13] Lijing Shao et al. "A new limit on local Lorentz invariance violation of gravity from solitary pulsars". In: *Class. Quant. Grav.* 30 (2013), p. 165019. DOI: 10.1088/0264-9381/30/16/165019. arXiv: 1307.2552 [gr-qc].

[Sha+19] Rajibul Shaikh et al. "Shadows of spherically symmetric black holes and naked singularities". In: *Mon. Not. Roy. Astron. Soc.* 482.1 (2019), pp. 52–64. DOI: 10.1093/mnras/sty2624. arXiv: 1802.08060 [astro-ph.HE].

[Sha+24] Hasrat Hussain Shah et al. "Study of Gravastar in Einstein-Gauss-Bonnet Gravity: Gravastar in EGB theory". In: *Int. J. Theor. Phys.* 63.10 (2024), p. 247. DOI: 10.1007/s10773-024-05747-z.

[Shl+24] Anastasia Shlentsova et al. "Imaging the event horizon of M87* from space on different timescales". In: *Astron. Astrophys.* 686 (2024), A154. DOI: 10.1051/0004-6361/202347214. arXiv: 2403.03327 [astro-ph.HE].

[Sho07] Assaf Shomer. "A Pedagogical explanation for the non-renormalizability of gravity". In: (Sept. 2007). arXiv: 0709.3555 [hep-th].

[SJ22] S. Shankaranarayanan and Joseph P. Johnson. "Modified theories of gravity: Why, how and what?" In: *Gen. Rel. Grav.* 54.5 (2022), p. 44. DOI: 10.1007/s10714-022-02927-2. arXiv: 2204.06533 [gr-qc].

[SNT22] Joseph Samuel, Rajaram Nityananda, and Nithyanandan Thyagarajan. "Invariants in Polarimetric Interferometry: A Non-Abelian Gauge Theory". In: *Phys. Rev. Lett.* 128.9 (2022), p. 091101. DOI: 10.1103/PhysRevLett.128.091101. arXiv: 2108.11400 [gr-qc].

[SP22] Jay Solanki and Volker Perlick. "Photon sphere and shadow of a time-dependent black hole described by a Vaidya metric". In: *Phys. Rev. D* 105.6 (2022), p. 064056. DOI: 10.1103/PhysRevD.105.064056. arXiv: 2201.03274 [gr-qc].

[SP24] Kaitlyn M. Shavelle and Daniel C. M. Palumbo. "Prospects for the Detection of the Sgr A* Photon Ring with Next-generation Event Horizon Telescope Polarimetry". In: *Astrophys. J. Lett.* 970.1 (2024), p. L24. DOI: 10.3847/2041-8213/ad6000. arXiv: 2407.09750 [astro-ph.HE].

[SP73] M. Simpson and R. Penrose. "Internal instability in a Reissner-Nordstrom black hole". In: *Int. J. Theor. Phys.* 7 (1973), pp. 183–197. DOI: 10.1007/BF00792069.

[ST15] José M. M. Senovilla and Ramón Torres. "Particle production from marginally trapped surfaces of general spacetimes". In: *Class. Quant. Grav.* 32.8 (2015). [Erratum: Class.Quant.Grav. 32, 189501 (2015)], p. 085004. DOI: 10.1088/0264-9381/32/8/085004. arXiv: 1409.6044 [gr-qc].

[Sta+23] Seppe Staelens et al. "Black hole photon rings beyond general relativity". In: *Phys. Rev. D* 107.12 (2023), p. 124026. DOI: 10.1103/PhysRevD.107.124026. arXiv: 2303.02111 [gr-qc].

[Sta80] Alexei A. Starobinsky. "A New Type of Isotropic Cosmological Models Without Singularity". In: *Phys. Lett. B* 91 (1980). Ed. by I. M. Khalatnikov and V. P. Mineev, pp. 99–102. DOI: 10.1016/0370-2693(80)90670-X.

[Ste17] K. S. Stelle. "Abdus Salam and Quadratic Curvature Gravity: Classical Solutions". In: *Int. J. Mod. Phys. A* 32.09 (2017). Ed. by Lars Brink, Michael Duff, and Kok Khoo Phua, p. 1741012. DOI: 10.1142/S0217751X17410123.

[Ste77] K. S. Stelle. "Renormalization of Higher Derivative Quantum Gravity". In: *Phys. Rev. D* 16 (1977), pp. 953–969. DOI: 10.1103/PhysRevD.16.953.

[Sur19] Sumati Surya. "The causal set approach to quantum gravity". In: *Living Rev. Rel.* 22.1 (2019), p. 5. DOI: 10.1007/s41114-019-0023-1. arXiv: 1903.11544 [gr-qc].

[SV19a] Alex Simpson and Matt Visser. "Black-bounce to traversable wormhole". In: *JCAP* 02 (2019), p. 042. DOI: 10.1088/1475-7516/2019/02/042. arXiv: 1812.07114 [gr-qc].

[SV19b] Alex Simpson and Matt Visser. "Regular black holes with asymptotically Minkowski cores". In: *Universe* 6.1 (2019), p. 8. DOI: 10.3390/universe6010008. arXiv: 1911.01020 [gr-qc].

[SV22] Alex Simpson and Matt Visser. "The eye of the storm: a regular Kerr black hole". In: *JCAP* 03.03 (2022), p. 011. DOI: 10.1088/1475-7516/2022/03/011. arXiv: 2111.12329 [gr-qc].

[SW12] Lijing Shao and Norbert Wex. "New tests of local Lorentz invariance of gravity with small-eccentricity binary pulsars". In: *Class. Quant. Grav.* 29 (2012), p. 215018. DOI: 10.1088/0264-9381/29/21/215018. arXiv: 1209.4503 [gr-qc].

[SW64] Abdus Salam and John Clive Ward. "Electromagnetic and weak interactions". In: *Phys. Lett.* 13 (1964), pp. 168–171. DOI: 10.1016/0031-9163(64)90711-5.

[SX18] A. Stern and Chuang Xu. "Signature change in matrix model solutions". In: *Phys. Rev. D* 98.8 (2018), p. 086015. DOI: 10.1103/PhysRevD.98.086015. arXiv: 1808.07963 [hep-th].

[SYS21] Andrew Sullivan, Nicolás Yunes, and Thomas P. Sotiriou. "Numerical black hole solutions in modified gravity theories: Axial symmetry case". In: *Phys. Rev. D* 103.12 (2021), p. 124058. DOI: 10.1103/PhysRevD.103.124058. arXiv: 2009.10614 [gr-qc].

[Tak+21] Yohsuke Takamori et al. "Testing the Non-circularity of the Spacetime around Sagittarius A* with Orbiting Pulsars". In: (Aug. 2021). DOI: 10.1093/pasj/psac003. arXiv: 2108.13026 [gr-qc].

[TCL60] RQ Twiss, AWL Carter, and AG Little. "Brightness distribution over some strong radio sources at 1427 Mc/s". In: *The Observatory, Vol. 80, p. 153-159 (1960)* 80 (1960), pp. 153–159.

[TF14] R. Torres and F. Fayos. "Singularity free gravitational collapse in an effective dynamical quantum spacetime". In: *Phys. Lett. B* 733 (2014), pp. 169–175. DOI: 10.1016/j.physletb.2014.04.038. arXiv: 1405.7922 [gr-qc].

[TF15] Ramon Torres and Francesc Fayos. "On the quantum corrected gravitational collapse". In: *Phys. Lett. B* 747 (2015), pp. 245–250. DOI: 10.1016/j.physletb.2015.05.078. arXiv: 1503.07407 [gr-qc].

[Tie+22] Paul Tiede et al. "Measuring Photon Rings with the ngEHT". In: *Galaxies* 10.6 (2022), p. 111. DOI: 10.3390/galaxies10060111. arXiv: 2210.13498 [astro-ph.HE].

[Tin+20] G. M. Tino et al. "Precision Gravity Tests and the Einstein Equivalence Principle". In: *Prog. Part. Nucl. Phys.* 112 (2020), p. 103772. DOI: 10.1016/j.ppnp.2020.103772. arXiv: 2002.02907 [gr-qc].

[TMS17] A Richard Thompson, James M Moran, and George W Swenson. *Interferometry and synthesis in radio astronomy*. Springer Nature, 2017.

[TNS22] Nithyanandan Thyagarajan, Rajaram Nityananda, and Joseph Samuel. "Invariants in copolar interferometry: An Abelian gauge theory". In: *Phys. Rev. D* 105.4 (2022), p. 043019. DOI: 10.1103/PhysRevD.105.043019. arXiv: 2108.11399 [astro-ph.IM].

[Tol34] Richard C. Tolman. "Effect of imhomogeneity on cosmological models". In: *Proc. Nat. Acad. Sci.* 20 (1934), pp. 169–176. DOI: 10.1073/pnas.20.3.169.

[Tor14] Ramón Torres. "Singularity-free gravitational collapse and asymptotic safety". In: *Phys. Lett. B* 733 (2014), pp. 21–24. DOI: 10.1016/j.physletb.2014.04.010. arXiv: 1404.7655 [gr-qc].

[Tor17] R. Torres. "Non-singular quantum improved rotating black holes and their maximal extension". In: *Gen. Rel. Grav.* 49.6 (2017), p. 74. DOI: 10.1007/s10714-017-2236-5. arXiv: 1702.03567 [gr-qc].

[Tor22] Ramón Torres. "Regular Rotating Black Holes: A Review". In: (Aug. 2022). arXiv: 2208.12713 [gr-qc].

[Tor+23] Pablo Torne et al. "A Search for Pulsars around Sgr A* in the First Event Horizon Telescope Data Set". In: *Astrophys. J.* 959.1 (2023), p. 14. DOI: 10.3847/1538-4357/acf4f2. arXiv: 2308.15381 [astro-ph.HE].

[Tor23] Ramón Torres. "Regular Rotating Black Holes". In: *Regular Black Holes: Towards a New Paradigm of Gravitational Collapse*. Ed. by Cosimo Bambi. Singapore: Springer Nature Singapore, 2023, pp. 421–446. ISBN: 978-981-99-1596-5. DOI: 10.1007/978-981-99-1596-5_11. URL: https://doi.org/10.1007/978-981-99-1596-5_11.

[Tor24] Ramon Torres. "Observational and theoretical aspects of Superspinars". In: (July 2024). arXiv: 2407.14851 [gr-qc].

[Tos22] Bobir Toshmatov. "Circular orbits of particles around parameterized black hole". In: *Phys. Dark Univ.* 35 (2022), p. 100992. DOI: 10.1016/j.dark.2022.100992.

[Tot16] Toth, V. T. *Hawking radiation calculator*. 2016. URL: {https://www.vttoth.com/CMS/physics-notes/311-hawking-radiation-calculator} (visited on 07/12/2024).

[Tri24] Oem Trivedi. "Recent Advances in Cosmological Singularities". In: *Symmetry* 16.3 (2024), p. 298. DOI: 10.3390/sym16030298. arXiv: 2309.08954 [gr-qc].

[TWV90] J. A. Tyson, R. A. Wenk, and F. Valdes. "Detection of systematic gravitational lens galaxy image alignments - Mapping dark matter in galaxy clusters". In: *Astrophys. J. Lett.* 349 (1990), pp. L1–L4. DOI: 10.1086/185636.

[Unr76] W. G. Unruh. "Notes on black hole evaporation". In: *Phys. Rev. D* 14 (1976), p. 870. DOI: 10.1103/PhysRevD.14.870.

[Ury+14] Koji Uryu et al. "Equilibrium solutions of relativistic rotating stars with mixed poloidal and toroidal magnetic fields". In: *Phys. Rev. D* 90.10 (2014), p. 101501. DOI: 10.1103/PhysRevD.90.101501. arXiv: 1410.3913 [astro-ph.HE].

[Vaf05] Cumrun Vafa. "The String landscape and the swampland". In: (Sept. 2005). arXiv: hep-th/0509212.

[Vai51] P. C. Vaidya. "The gravitational field of a radiating star". In: *Proc. Indian Acad. Sci. A* 33.5 (1951), p. 264. DOI: 10.1007/BF03173260.

[Vai66] P. C. Vaidya. "An Analytical Solution for Gravitational Collapse with Radiation". In: *Astrophys. J.* 144 (1966), p. 943. DOI: 10.1086/148692.

[Ven92] A. E. M. van de Ven. "Two loop quantum gravity". In: *Nucl. Phys. B* 378 (1992), pp. 309–366. DOI: 10.1016/0550-3213(92)90011-Y.

[Ver03] Raul Vera. "Influence of general convective motions on the exterior of isolated rotating bodies in equilibrium". In: *Class. Quant. Grav.* 20 (2003), pp. 2785–2792. DOI: 10.1088/0264-9381/20/13/324. arXiv: gr-qc/0305108.

[VGY18] Tsvetan Vetsov, Galin Gyulchev, and Stoytcho Yazadjiev. "Shadows of Black Holes in Vector-Tensor Galileons Modified Gravity". In: (Jan. 2018). arXiv: 1801.04592 [gr-qc].

[VH10] Sarah J. Vigeland and Scott A. Hughes. "Spacetime and orbits of bumpy black holes". In: *Phys. Rev. D* 81 (2010), p. 024030. DOI: 10.1103/PhysRevD.81.024030. arXiv: 0911.1756 [gr-qc].

[Vig10] Sarah J. Vigeland. "Multipole moments of bumpy black holes". In: *Phys. Rev. D* 82 (2010), p. 104041. DOI: 10.1103/PhysRevD.82.104041. arXiv: 1008.1278 [gr-qc].

[Vin+16] F. H. Vincent et al. "Imaging a boson star at the Galactic center". In: *Class. Quant. Grav.* 33.10 (2016), p. 105015. DOI: 10.1088/0264-9381/33/10/105015. arXiv: 1510.04170 [gr-qc].

[Vin+21] F. H. Vincent et al. "Geometric modeling of M87* as a Kerr black hole or a non-Kerr compact object". In: *Astron. Astrophys.* 646 (2021), A37. DOI: 10.1051/0004-6361/202037787. arXiv: 2002.09226 [gr-qc].

[Vin+22] Frederic H. Vincent et al. "Images and photon ring signatures of thick disks around black holes". In: *Astron. Astrophys.* 667 (2022), A170. DOI: 10.1051/0004-6361/202244339. arXiv: 2206.12066 [astro-ph.HE].

[Vis07] Matt Visser. "The Kerr spacetime: A Brief introduction". In: *Kerr Fest: Black Holes in Astrophysics, General Relativity and Quantum Gravity*. June 2007. arXiv: 0706.0622 [gr-qc].

[Vis14] Matt Visser. "Physical observability of horizons". In: *Phys. Rev. D* 90.12 (2014), p. 127502. DOI: 10.1103/PhysRevD.90.127502. arXiv: 1407.7295 [gr-qc].

[Vis21] Luca Visinelli. "Boson stars and oscillatons: A review". In: *Int. J. Mod. Phys. D* 30.15 (2021), p. 2130006. DOI: 10.1142/S0218271821300068. arXiv: 2109.05481 [gr-qc].

[Vis95] Matt Visser. *Lorentzian wormholes: From Einstein to Hawking*. 1995. ISBN: 978-1-56396-653-8.

[Vis96a] Matt Visser. "Gravitational vacuum polarization. 1: Energy conditions in the Hartle-Hawking vacuum". In: *Phys. Rev. D* 54 (1996), pp. 5103–5115. DOI: 10.1103/PhysRevD.54.5103. arXiv: gr-qc/9604007.

[Vis96b] Matt Visser. "Gravitational vacuum polarization. 2: Energy conditions in the Boulware vacuum". In: *Phys. Rev. D* 54 (1996), pp. 5116–5122. DOI: 10.1103/PhysRevD.54.5116. arXiv: gr-qc/9604008.

[Vis97] Matt Visser. "Gravitational vacuum polarization. 4: Energy conditions in the Unruh vacuum". In: *Phys. Rev. D* 56 (1997), pp. 936–952. DOI: 10.1103/PhysRevD.56.936. arXiv: gr-qc/9703001.

[Vlb] *European Southern Observatory (ESO) public outreach*. https://www.eso.org/public/outreach/first-picture-of-a-black-hole/blog/. Accessed: 2024-08-13.

[VYS11] Sarah Vigeland, Nicolas Yunes, and Leo Stein. "Bumpy Black Holes in Alternate Theories of Gravity". In: *Phys. Rev. D* 83 (2011), p. 104027. DOI: 10.1103/PhysRevD.83.104027. arXiv: 1102.3706 [gr-qc].

[Wal84] Robert M. Wald. *General Relativity*. Chicago, USA: Chicago Univ. Pr., 1984. DOI: 10.7208/chicago/9780226870373.001.0001.

[Wal97] Robert M. Wald. "Gravitational collapse and cosmic censorship". In: Oct. 1997, pp. 69–85. DOI: 10.1007/978-94-017-0934-7_5. arXiv: gr-qc/9710068.

[Wan+24] Jade Wang et al. "High data rate laser communications for the Black Hole Explorer". In: *Space Telescopes and Instrumentation 2024: Optical, Infrared, and Millimeter Wave*. Vol. 13092. SPIE. 2024, pp. 2249–2255.

[WCJ17] Mingzhi Wang, Songbai Chen, and Jiliang Jing. "Shadow casted by a Konoplya-Zhidenko rotating non-Kerr black hole". In: *JCAP* 10 (2017), p. 051. DOI: 10.1088/1475-7516/2017/10/051. arXiv: 1707.09451 [gr-qc].

[Wea23] James Owen Weatherall. "Where Does General Relativity Break Down?" In: *Phil. Sci.* 90.5 (2023), pp. 1342–1351. DOI: 10.1017/psa.2022.98. arXiv: 2204.03869 [physics.hist-ph].

[Wei00] Steven Weinberg. "The Cosmological constant problems". In: *4th International Symposium on Sources and Detection of Dark Matter in the Universe (DM 2000)*. Feb. 2000, pp. 18–26. arXiv: astro-ph/0005265.

[Wei+13] David H. Weinberg et al. "Observational Probes of Cosmic Acceleration". In: *Phys. Rept.* 530 (2013), pp. 87–255. DOI: 10.1016/j.physrep.2013.05.001. arXiv: 1201.2434 [astro-ph.CO].

[Wei67] Steven Weinberg. "A Model of Leptons". In: *Phys. Rev. Lett.* 19 (1967), pp. 1264–1266. DOI: 10.1103/PhysRevLett.19.1264.

[Wei80] Steven Weinberg. "ULTRAVIOLET DIVERGENCES IN QUANTUM THEORIES OF GRAVITATION". In: *General Relativity: An Einstein Centenary Survey*. 1980, pp. 790–831.

[Wes+18] Julian Westerweck et al. "Low significance of evidence for black hole echoes in gravitational wave data". In: *Phys. Rev. D* 97.12 (2018), p. 124037. DOI: 10.1103/PhysRevD.97.124037. arXiv: 1712.09966 [gr-qc].

[Wet93] Christof Wetterich. "Exact evolution equation for the effective potential". In: *Phys. Lett. B* 301 (1993), pp. 90–94. DOI: 10.1016/0370-2693(93)90726-X. arXiv: 1710.05815 [hep-th].

[Wex14] Norbert Wex. "Testing Relativistic Gravity with Radio Pulsars". In: (Feb. 2014). arXiv: 1402.5594 [gr-qc].

[Wex16] Norbert Wex. "Neutron Stars as Probes for General Relativity and Gravitational Waves". In: *Handbook of Supernovae*. Springer International Publishing, 2016, pp. 1–24.

[Wey17a] H. Weyl. "The theory of gravitation". In: *Annalen Phys.* 54 (1917), pp. 117–145. DOI: 10.1007/s10714-011-1310-7.

[Wey17b] Hermann Weyl. "Zur Gravitationstheorie". In: *Annalen Phys.* 359.18 (1917), pp. 117–145. DOI: 10.1002/andp.19173591804.

[Wie21] Maciek Wielgus. "Photon rings of spherically symmetric black holes and robust tests of non-Kerr metrics". In: *Phys. Rev. D* 104.12 (2021), p. 124058. DOI: 10.1103/PhysRevD.104.124058. arXiv: 2109.10840 [gr-qc].

[Wie+22] Maciek Wielgus et al. "Millimeter Light Curves of Sagittarius A* Observed during the 2017 Event Horizon Telescope Campaign". In: *Astrophys. J. Lett.* 930.2 (2022), p. L19. DOI: 10.3847/2041-8213/ac6428. arXiv: 2207.06829 [astro-ph.HE].

[Wil14] Clifford M. Will. "The Confrontation between General Relativity and Experiment". In: *Living Rev. Rel.* 17 (2014), p. 4. DOI: 10.12942/lrr-2014-4. arXiv: 1403.7377 [gr-qc].

[Wil16] Clifford M. Will. "Gravity: Newtonian, Post-Newtonian, and General Relativistic". In: *Gravity: Where Do We Stand?* Ed. by Roberto Peron et al. 2016, pp. 9–72. DOI: 10.1007/978-3-319-20224-2_2.

[Win19] Himawan Winarto. "Review of Progress in Magnetorotational Instability". In: *Journal of Physics: Conference Series*. Vol. 1204. 1. IOP Publishing. 2019, p. 012097.

[WK74] K. G. Wilson and John B. Kogut. "The Renormalization group and the epsilon expansion". In: *Phys. Rept.* 12 (1974), pp. 75–199. DOI: 10.1016/0370-1573(74)90023-4.

[WN72] Clifford M. Will and Kenneth Nordtvedt Jr. "Conservation Laws and Preferred Frames in Relativistic Gravity. I. Preferred-Frame Theories and an Extended PPN Formalism". In: *Astrophys. J.* 177 (1972), p. 757. DOI: 10.1086/151754.

[Woo07] Richard P. Woodard. "Avoiding dark energy with 1/r modifications of gravity". In: *Lect. Notes Phys.* 720 (2007). Ed. by Lefteris Papantonopoulos, pp. 403–433. DOI: 10.1007/978-3-540-71013-4_14. arXiv: astro-ph/0601672.

[Woo15] Richard P. Woodard. "Ostrogradsky's theorem on Hamiltonian instability". In: *Scholarpedia* 10.8 (2015), p. 32243. DOI: 10.4249/scholarpedia.32243. arXiv: 1506.02210 [hep-th].

[WOR20] Lukas R. Weih, Hector Olivares, and Luciano Rezzolla. "Two-moment scheme for general-relativistic radiation hydrodynamics: a systematic description and new applications". In: *Mon. Not. Roy. Astron. Soc.* 495.2 (2020), pp. 2285–2304. DOI: 10.1093/mnras/staa1297. arXiv: 2003.13580 [gr-qc].

[Wor+22] R. L. Workman et al. "Review of Particle Physics". In: *PTEP* 2022 (2022), p. 083C01. DOI: 10.1093/ptep/ptac097.

[WR24] Steven Weinstein and Dean Rickles. "Quantum Gravity". In: *The Stanford Encyclopedia of Philosophy*. Ed. by Edward N. Zalta and Uri Nodelman. Spring 2024. Metaphysics Research Lab, Stanford University, 2024.

[Xie+21] Yiqi Xie et al. "Square Peg in a Circular Hole: Choosing the Right Ansatz for Isolated Black Holes in Generic Gravitational Theories". In: *Phys. Rev. Lett.* 126.24 (2021), p. 241104. DOI: 10.1103/PhysRevLett.126.241104. arXiv: 2103.03925 [gr-qc].

[XMS20] Semin Xavier, Jose Mathew, and S. Shankaranarayanan. "Infinitely degenerate exact Ricci-flat solutions in f(R) gravity". In: *Class. Quant. Grav.* 37.22 (2020), p. 225006. DOI: 10.1088/1361-6382/abbd0f. arXiv: 2003.05139 [gr-qc].

[Yan21] Huan Yang. "Relating Black Hole Shadow to Quasinormal Modes for Rotating Black Holes". In: *Phys. Rev. D* 103.8 (2021), p. 084010. DOI: 10.1103/PhysRevD.103.084010. arXiv: 2101.11129 [gr-qc].

[YP09] Nicolas Yunes and Frans Pretorius. "Dynamical Chern-Simons Modified Gravity. I. Spinning Black Holes in the Slow-Rotation Approximation". In: *Phys. Rev. D* 79 (2009), p. 084043. DOI: 10.1103/PhysRevD.79.084043. arXiv: 0902.4669 [gr-qc].

[YPO23] Ziri Younsi, Dimitrios Psaltis, and Feryal Özel. "Black Hole Images as Tests of General Relativity: Effects of Spacetime Geometry". In: *Astrophys. J.* 942.1 (2023), p. 47. DOI: 10.3847/1538-4357/aca58a. arXiv: 2111.01752 [astro-ph.HE].

[Zar+24] Soroush Zare et al. "Shadows, rings and optical appearance of a magnetically charged regular black hole illuminated by various accretion disks". In: (June 2024). arXiv: 2406.07300 [astro-ph.HE].

[Zho+24] Lihang Zhou et al. "Forward Ray Tracing and Hot Spots in Kerr Spacetime". In: (Aug. 2024). arXiv: 2408.16049 [gr-qc].

[Zip66] David M. Zipoy. "Topology of Some Spheroidal Metrics". In: *J. Math. Phys.* 7.6 (1966), p. 1137. DOI: 10.1063/1.1705005.

[ZM23] Tian Zhou and Leonardo Modesto. "Geodesic incompleteness of some popular regular black holes". In: *Phys. Rev. D* 107.4 (2023), p. 044016. DOI: 10.1103/PhysRevD.107.044016. arXiv: 2208.02557 [gr-qc].

[ZM97] E. Zakhary and C. B. G. Mcintosh. "A Complete Set of Riemann Invariants". In: *Gen. Rel. Grav.* 29.5 (1997), pp. 539–581. DOI: 10.1023/a:1018851201784.

[ZP71] Ya. B. Zeldovič and L. P. Pitaevskiĭ. "On the possibility of the creation of particles by a classical gravitational field". In: *Commun. Math. Phys.* 23 (1971), pp. 185–188. DOI: 10.1007/BF01877740.

[Zwi85] Barton Zwiebach. "Curvature Squared Terms and String Theories". In: *Phys. Lett. B* 156 (1985), pp. 315–317. DOI: 10.1016/0370-2693(85)91616-8.